

ALKENE, HYDRIDO(ALLYL) AND METAL-METAL BONDED
DERIVATIVES OF RHENIUM

by

Jun-Ming Zhuang

B.Sc., Fudan University, Shanghai, China, 1982

M.Sc., Shanghai Institute of Organic Chemistry,

Academia Sinia, 1984

THESIS SUBMITTED IN PARTIAL FULFILLMENT OF
THE REQUIREMENTS FOR THE DEGREE OF
DOCTOR OF PHILOSOPHY
in the Department
of
Chemistry

© Jun-Ming Zhuang 1990

SIMON FRASER UNIVERSITY

June, 1990

All rights reserved. This work may not be reproduced in whole or in part, by photocopy or other means, without permission of the author.

APPROVAL

Name: Jun-Ming Zhuang
Degree: DOCTOR OF PHILOSOPHY
Title of Thesis: Alkene, Hydrido(allyl) and Metal-Metal Bonded Derivatives of Rhenium

Examining Committee:

Chairman: Dr. P. W. Percival

Dr. D. Sutton, Senior Supervisor

Dr. F. W. B. Einstein, Supervisory Committee

Dr. A. C. Oehlschlager, Supervisory Committee

Dr. L. K. Peterson, Internal Examiner

Dr. P. M. Boorman, External Examiner
Department of Chemistry
University of Calgary

Date Approved: 28 September 1990

PARTIAL COPYRIGHT LICENSE

I hereby grant to Simon Fraser University the right to lend my thesis, project or extended essay (the title of which is shown below) to users of the Simon Fraser University Library, and to make partial or single copies only for such users or in response to a request from the library of any other university, or other educational institution, on its own behalf or for one of its users. I further agree that permission for multiple copying of this work for scholarly purposes may be granted by me or the Dean of Graduate Studies. It is understood that copying or publication of this work for financial gain shall not be allowed without my written permission.

Title of Thesis/Project/Extended Essay

ALKENE, HYDRIDO(ALLYL) AND METAL-METAL BONDED DERIVATIVES

OF RHENIUM.

Author:

(signature)

Jun-Ming Zhuang

(name)

3 October 1990

(date)

ABSTRACT

This thesis describes an investigation of the chemical reactions displayed by the 16e- active intermediate $[\text{Cp}^*\text{Re}(\text{CO})_2]$ with linear or cyclic alkenes, and the neutral electron-donor complex $\text{Cp}^*\text{Ir}(\text{CO})_2$. The relevant new reactions and derivatives have been determined as illustrated by the following:

The new alkene rhenium complexes of general formula $\text{Cp}^*\text{Re}(\text{CO})(\text{alkene})\text{L}_1$ ($\text{L}_1 = \text{CO}, \text{PMe}_3$; alkene = ethene, propene, 2-pentene, 1-octene, *cis*-2-octene, cyclohexene, 4-methylcyclohexene, cyclooctene, allene, 1,3-cyclohexadiene, 1,4-cyclohexadiene) have been synthesized by several different methods: (1) the photochemical reactions of $\text{Cp}^*\text{Re}(\text{CO})\text{L}_1\text{L}_2$ ($\text{L}_1 = \text{CO}, \text{PMe}_3$; $\text{L}_2 = \text{CO}, \text{N}_2$) with alkenes; (2) the thermal reaction of $\text{Cp}^*\text{Re}(\text{CO})_2(\text{THF})$ with allene; (3) the reaction of the cationic η^3 -allyl complexes with sodium borohydride or sodium methoxide. The allene rotation and 1,2-shift (from one double bond to the other) in the complex $\text{Cp}^*\text{Re}(\text{CO})_2(\eta^2\text{-allene})$ have been investigated. The activation parameters for the η^2 -allene rotation determined by temperature-dependent ^1H NMR experiments are: $\Delta G^\ddagger = 9.9 \pm 0.2$ kcal/mol (-50°C), $\Delta H^\ddagger = 10.9 \pm 0.3$ kcal/mol and $\Delta S^\ddagger = 4.7 \pm 1.4$ cal/K.mol. Saturation-transfer experiments at 100°C indicated that the 1,2-shift occurs with a large activation barrier.

The photochemical C-H activation of the coordinated alkenes

in $\text{Cp}^*\text{Re}(\text{CO})_2(\eta^2\text{-alkene})$ complexes has been investigated for a range of linear and cyclic alkenes. Two types of photochemical C-H activation of alkenes in Cp^*Re systems have been discovered: (1) the intramolecular allylic C-H activation of linear alkenes to give rhenium allyl hydride complexes; (2) the photochemical double C-H activation of coordinated cyclohexene, and the formation of $\text{Cp}^*\text{Re}(\text{CO})_2(\eta^2\text{-1,3-cyclohexadiene})$.

Photolysis of the propene complex $\text{Cp}^*\text{Re}(\text{CO})_2(\eta^2\text{-propene})$ produced two isomers *exo* and *endo* $\text{Cp}^*\text{Re}(\text{CO})(\text{H})(\eta^3\text{-allyl})$. An irreversible conversion from *exo* to *endo* occurs under thermal conditions, and the estimate of the Arrhenius activation energy gives a value $E_a = 28.9 \pm 3.2 \text{ kcal.mol}^{-1}$. Irradiation favours the reverse conversion from *endo* to *exo*.

The η^3 -allylalkane cationic complexes of general formula $[\text{Cp}^*\text{Re}(\text{CO})_2(\eta^3\text{-allylalkane})][\text{BF}_4]$ were produced by three different routes: (1) the allylic hydrogen of the η^2 -alkene complexes was abstracted by $[\text{Ph}_3\text{C}][\text{BF}_4]$; (2) the η^2 -diene complex was protonated by HBF_4 ; (3) the η^2 -3-methoxyalkene complex was protonated by HBF_4 . Fast *exo-endo* interconversion between two isomers *exo* and *endo* $[\text{Cp}^*\text{Re}(\text{CO})_2(\eta^3\text{-C}_3\text{H}_5)]^+$ was observed by magnetization-transfer experiments.

Three heterobinuclear complexes $\text{Cp}^*(\text{CO})\text{Re}(\mu_2\text{-CO})_2\text{Ir}(\text{CO})\text{Cp}^*$, $\text{Cp}(\text{CO})\text{Re}(\mu_2\text{-CO})_2\text{Ir}(\text{CO})\text{Cp}^*$ and $\text{Cp}^*(\text{CO})\text{Mn}(\mu_2\text{-CO})_2\text{Ir}(\text{CO})\text{Cp}^*$ have been synthesized and fully characterized.

To my parents

and

To my wife (Jun-Xue) and son (Wei-Wei)

庄俊明

ACKNOWLEDGEMENTS

The author would like to express his sincere gratitude to his supervisor, Professor D. Sutton, for his continued guidance, advice and encouragement throughout the course of this work.

The author expresses his sincere thanks to:

Professor F.W.B. Einstein, Dr. R.J. Batchelor and Dr. R.H. Jones for the crystal structure determinations involved in this thesis;

Dr. L. Peterson for his helpful discussions;

Dr. A. Tracey and Mrs. M. Tracey for their collaboration in the NMR studies; and

Dr. N. Lowe for proof reading this thesis.

The author also wishes to thank Mr. Greg Owen and Mr. Miki Yang for all their extra time, and Mr. Ramzi Hader for assistance with heterobimetallic complex syntheses.

TABLE OF CONTENTS

	Page
Title	i
Approval	ii
Abstract	iii
Dedication	v
Acknowledgements	vi
Table of Contents	vii
Abbreviations	x
List of Figures	xi
List of Tables	xiv
Chapter I Review of Carbon Hydrogen Activation by Organometallic Complexes	1
1.1. Introduction	1
1.2. Nature of Transition-Metal Systems Activating C-H Bonds	3
1.3. An Outline of C-H Activation in Organometallic Chemistry	8
1.4. Advances in the Study of C-H Activation	12
(i) C-H Activation by Oxidative Addition	12
(ii) Selectivity of C-H Activation	16
(iii) η^2 -Arene Intermediate	19
(iv) Functionalization of C-H Bonds by Transition- Metal Systems	21
Chapter II Synthesis and Characterization of Pentamethyl-	24

cyclopentadienyl(alkene) Complexes of Rhenium	
2.1.	Introduction 24
2.2.	Synthesis 27
2.3.	Characterization 39
2.4.	Chemical Reactions 41
2.5.	Discussion 52
2.5.1.	¹ H NMR Spectroscopy 52
2.5.2.	Mass Spectra 66
(i)	Linear Alkene Complexes 66
(ii)	Cyclic Alkene Complexes 77
(iii)	Diene Complexes 78
(iv)	Others 81
(v)	Summary 88
2.6.	Conclusion 96
2.7.	Experimental Section 99
Chapter III	Photochemical Allylic C-H Activation in a Cp*Re System 108
3.1.	Introduction 108
3.2.	Synthesis 110
3.3.	Characterization 118
3.4.	Chemical Reactions 140
3.5.	Discussion 150
3.5.1.	X-ray Structures of [15a] <i>exo</i> and [15b] <i>endo</i> 150
3.5.2.	IR Spectroscopy 151
3.5.3.	¹ H NMR Spectroscopy 155
3.5.4.	Mass Spectroscopy 167

3.5.5.	<i>Exo-endo</i> Interconversion of η^3 -Allyl Group	171
3.5.6.	Chemical Reactions	176
3.6.	Conclusion	186
3.7.	Experimental Section	188
Chapter IV	Syntheses, Characterizations and Reactions of Cationic η^3 -Allyl Complexes of Rhenium	199
4.1.	Introduction	199
4.2.	Synthesis	200
4.3.	Characterization	206
4.4.	Chemical Reactions	211
4.5.	Discussion	219
4.5.1.	^1H NMR Spectra	219
4.5.2.	Syntheses and Reactions	231
4.6.	Conclusion	236
4.7.	Experimental Section	237
Chapter V	Synthesis and Characterization of Hetero- bimetallic, Metal-Metal Bonded Complexes	243
5.1.	Introduction	243
5.2.	Synthesis and Characterization	244
5.3.	Discussion	251
5.3.1.	Synthesis	251
5.3.2.	Characterization	252
5.3.3.	X-ray Structure of Compound [26]	256
5.4.	Experimental Section	259
References		263

ABBREVIATIONS

Ar	aryl
ⁿ Bu	butyl, C ₄ H ₉
Cp	η^5 -cyclopentadienyl (η -C ₅ H ₅)
Cp*	η^5 -pentamethylcyclopentadienyl (η -C ₅ Me ₅)
Cy	cyclohexyl (C ₆ H ₁₁)
Et	ethyl, C ₂ H ₅
FAB	fast atom bombardment
GC	gas chromatography
IR	infrared
M	metal
Me	methyl, CH ₃
MS	mass spectra
NMR	nuclear magnetic resonance
NOE	nuclear Overhauser effect
OMe	methoxy, OCH ₃
Ph	phenyl, C ₆ H ₅
R	alkyl
THF	tetrahydrofuran

LIST OF FIGURES

Figure		Page
1	Three Geometric Configurations of Complexes	7
2	Transition State of C-H Activation	19
3	¹ H NMR Spectrum of the Complex [2]	46
4	¹ H NMR Spectrum of the Complex [12]	46
5	¹ H NMR Spectrum of the Complex [5]	47
6	¹ H NMR Spectrum of the Complex [4]	47
7	¹ H NMR Spectrum of the Complex [6]	48
8	¹ H NMR Spectrum of the Complex [8]	48
9	¹ H NMR Spectrum of the Complex [10]	49
10	¹ H NMR Spectrum of the Complex [11]	49
11	Decoupling Experiments on the Complex [9]	50
12	NOE Experiments on the Complex [9]	51
13	η^2 -Allene Rotation and 1,2-Shift in [9]	58
14	Variable-temperature ¹ H NMR Experiments on the Complex [9]	59
15	A Plot of the ΔG^* Values vs. (-T)	63
16	Saturation Transfer Experiments on [9]	64
17	Mass Spectra for the Complexes Shown	67
18	Computed Isotopic Abundance Patterns	82
19	Isotopic Abundance Pattern of [15]	87
20	400MHz ¹ H NMR (C ₆ D ₆) Spectrum in Metal-Hydride Region for Isomers [16c,d,e,f,k]	112

21	¹ H NMR Spectrum of the Complex [15a]exo	120
22	¹ H NMR Spectrum of the Complex [15b]endo	120
23	Perspective View of Isomers of [15](exo, endo)	121
24	Computer Simulation of ¹ H NMR Spectrum of the Complex [15a]exo	122
25	Computer Simulation of ¹ H NMR Spectrum of the Complex [15b]endo	122
26	Computer Simulation of ¹ H NMR Spectrum of the Complex [17b]exo	123
27	¹ H NMR Spectrum of the Complex [17b]exo	123
28	A Plot of the lnk Values vs. -(1/T)	139
29	IR spectrum ($\nu(\text{CO})$, hexane) (eq.61)	146
30	IR spectrum ($\nu(\text{CO})$, hexane) (eq.62)	146
31	IR spectrum ($\nu(\text{CO})$, hexane) (eq.63)	147
32	IR spectrum ($\nu(\text{CO})$, hexane) (eq.64)	147
33	NOE Experiments on [15a]exo	152
34	NOE Experiments on [15b]endo	153
35	Advantageous Transition State	162
36	Disadvantageous Transition State	162
37	¹ H NMR Spectrum of the Complex [18]	165
38	NOE Experiments on the Complex [18]	166
39	Dihydride Intermediates	169
40	Intramolecular Allylic C-H Activation through $d-\pi^*-\sigma^*$ Interaction	179
41	Intramolecular Allylic C-H Activation Mechanisms	181
42	View of the Cationic Complex in [19]	207

43	Perspective View of the Complex [21]	208
44	^1H NMR (CD_2Cl_2) Spectrum of the Complex [19]	214
45	^1H NMR (CDCl_3) Spectrum of the Complex [19]	215
46	^1H NMR Spectrum of the Complex [21]	216
47	^1H NMR Spectrum of the Complex [22]	217
48	^1H NMR Spectrum of the Complex [23]	218
49	Decoupling Experiments on [19]	220
50	NOE Experiments on [19]	222
51	Proton Abstraction by ^-OMe	235
52	Heterobinuclear Complexes [24]-[26]	244
53	Perspective View of the Complex [26]	248
54	^1H NMR Spectrum of the Complex [24]	249
55	^1H NMR Spectrum of the Complex [26]	249
56	^1H NMR Spectrum of the Complex [25]	250
57	Mass Spectra for the Complexes [24]-[26]	253
58	Isotopic Abundance Pattern for [25] and [26]	254

LIST OF TABLES

Table		Page
1	C-H Bond Dissociation Energies	1
2	Relative Rates of Reaction of $\text{Cp}^*\text{M}(\text{PMe}_3)\text{H}_2$ with Various Hydrocarbons on Photolysis	18
3	Structures of New Olefin Complexes [1]-[13]	29
4	Some Spectroscopic Parameters of the Olefin Complexes [1]-[13]	42
5	Proton Chemical Shifts and Coupling Constants for Ligands of Compounds [1]-[13]	43
6	Data for k and ΔG^\ddagger for the Complex [9]	61
7	Structures of Monocarbonyl η^3 -Allyl Complexes [15]-[18]	113
8	Some Spectroscopic Parameters of the Complexes [15]-[18]	126
9	Experimentally Observed Chemical Shifts for the Complexes [15]-[18]	127
10	Coupling Constants from Experimental ^1H NMR Spectra of Complexes [15]-[18]	128
11	The Calculated Coupling Constants for Complexes [15](<i>exo</i> , <i>endo</i>) and [17b] <i>exo</i>	129
12	Kinetic Data for <i>exo</i> \rightarrow <i>endo</i> Conversion of [15]	137
13	NMR Data for Complexes $\text{Pt}(\eta^3\text{-C}_3\text{H}_5)\text{Cl}(\text{L})$	156
14	Data for the Ratio of [15a] <i>exo</i> to [15b] <i>endo</i>	193

15	Structures of Complexes [19]-[23]	202
16	Some Spectroscopic Parameters of the Complexes [19]-[23]	203
17	Proton Chemical Shifts and Coupling Constants for Ligands of Compounds [19]-[23]	204
18	¹ H NMR Parameters for the Complex [19] and Related Allyl Complexes	227
19	Some Spectroscopic Parameters of the Heterobimetallic Complexes [24]-26]	246
20	¹³ C NMR Data for the Heterobimetallic Complexes [24]-[26]	247

Chapter I

Review of Carbon Hydrogen Activation by Organometallic Complexes

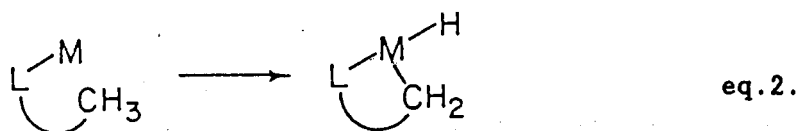
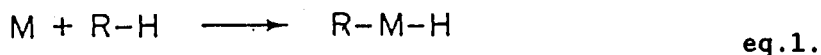
1.1. Introduction

Among the many interesting developments of organometallic chemistry, one of the most intriguing goals of homogeneous organometallic chemistry has been the use of transition-metal complexes to activate carbon-hydrogen bonds in very unreactive saturated and unsaturated hydrocarbons. Hydrocarbons are among the most abundant and unreactive of all organic compounds. Usually, the chemical stability of C-H bonds in unreactive hydrocarbons is ascribed to high C-H bond energies.

Table 1. C-H Bond Dissociation Energies¹

Bond	Energy(kcal.mol ⁻¹)
Ph-H	110
vinyl-H	108
Me-H	104
Et-H	98
Pr ⁱ -H	95
Bu ^t -H	91
allyl-H	87
PhCH ₂ -H	87

The data listed in Table 1 show the C-H bond strengths for a variety of saturated and unsaturated hydrocarbons. Although many chemical reactions of the C-H bonds of hydrocarbons have been discovered in organic chemistry, the control of chemoselectivity in these organic reactions has proved difficult to achieve.² Thus, a specific goal has interested inorganic chemists: exploring possible ways for an appropriate organometallic complex to insert directly a metal centre into a C-H bond in unreactive hydrocarbons.



The transformation represented in eq.1 (or eq.2) is referred to as "oxidative addition" because the metal centre is formally oxidized by two units in its conversion from a d^n electron species in the starting complex to a d^{n-2} electron species in the insertion product. There are two situations: one is the intramolecular C-H oxidative addition involving the metal centre and a ligand (eq.2), the other is intermolecular C-H oxidative addition involving the metal centre and a hydrocarbon molecule (eq.1). During

the past decade, it has been discovered that some organotransition-metal systems^{3,4} are capable of intra- or intermolecular oxidative addition to single C-H bonds in unreactive hydrocarbons.

1.2. Nature of Transition-Metal Systems Activating C-H Bonds

The catalytic activity of transition-metal complexes is generally thought to be due to the partially filled *d* orbitals of the transition-metal centre. It is believed that the partially filled *d* orbitals are able to interact with the σ and σ^* orbitals of C-H bonds leading to the C-H activation.

Crabtree⁵ has pointed out three possible ways in which the C-H bond can be activated by a transition-metal system: (1) by donating electron density to the C-H σ^* -orbital; (2) by abstracting C-H σ -bonding electrons; or (3) by doing both at once.

Consequently, C-H activation should be facilitated by electron rich metal centres which activate C-H bonds by donating electron density to the σ^* -orbital of the C-H bond, thereby decreasing the electron density on the metal centre. To date, the transition-metal atoms found to be capable of activating sp^2 and sp^3 C-H bonds usually have d^n ($n = 2-8$) electron configurations. In

particular, transition-metal complexes with d^8 electron configurations at the metal are involved in numerous synthetic and catalytic processes.⁶ The transition-metal atoms having a d^8 electron species in a complex (e.g., Ir and Rh) have also been shown to have a greater ability to activate C-H bonds. In this respect, the second-row and especially the third-row metals are preferred because of their stronger M-C and M-H bonds.⁷

A further requirement for C-H activation is that the transition-metal system usually needs to lose one ligand in order to generate a coordinatively unsaturated metal centre, which will effectively abstract σ -bonding electrons of the C-H bond to approach the stable 18-electron configuration. Dihydrogen⁸ and dinitrogen⁹ are generally considered to be the best leaving groups which quickly form coordinatively unsaturated metal centres.

In practice, the two pathways of C-H activation ((1) and (2)) described by Crabtree are found to operate simultaneously and, experimentally, it is difficult to determine the predominant route. For example, on the basis of studying a Mn/CH₄ system, Ozin¹⁰ discovered that a Mn 4s electron in the $3d^5 4s^2$ ground state is promoted to a spatially diffuse 4p orbital in the $3d^5 4s^1 4p^1$ excited state under photolysis at low temperature (10-12K). The singly occupied 4s and 4p metal orbitals are then available for bonding with the σ -bonding and σ^* -antibonding molecular orbitals of CH₄. The

combined interactions of $M^*(3d/4s) + CH_4(\sigma)$ and $M^*(3d/4p) + CH_4(\sigma^*)$ will lead to a weakening of the C-H bonds of methane.

Nevertheless, during the process of C-H activation by a transition-metal system, the metal centre will usually undergo changes in oxidation state, stereochemistry and coordination number. These changes can lead to the instability of organometallic complexes. Consequently, a common side-reaction is the decomposition of the organometallic complexes, especially when a coordinately unsaturated metal centre is being formed. Therefore, organometallic complexes normally need to bear some stabilizing ligands. These ligands are strongly bonded to the metal centre, producing transition-metal systems which can undergo such changes. Obviously, the pentamethylcyclopentadiene (Cp^*) group is an ideal ligand for this purpose. The fragmentations of a series of complexes $Cp^*Re(CO)L_1L_2$ ($L_1 = CO, PMe_3, L_2 = \eta^2$ -alkene; or $L_1 = H, Br, L_2 = \eta^3$ -allyl) in mass spectroscopy clearly demonstrate that Cp^* remains bonded to rhenium until all other ligands are completely lost (see Chapter II, section 2.5.2), indicating that a strong bond is present between Cp^* and rhenium.

Ligands may also exert electronic effects to aid the C-H activation step at a transition-metal centre, or influence the course of the C-H activation by their steric interactions with the

incoming substrates. In general, the Cp* ligand is considered to be a strongly electron-donating group which is also strongly bonded to the transition-metal centre. These are definite advantages for the C-H activation at a transition-metal centre, but are not the key factors.

For example, of the d^8 cobalt, rhodium and iridium complexes of the form Cp*M(CO)₂ (M = Co, Rh or Ir), only Rh and Ir complexes are able to activate the C-H bonds of hydrocarbons, not the Co complexes.³ Lichtenberger¹¹ has compared the differences in electronic structure and bonding characteristics between Cp*Co(CO)₂ and Cp*Rh(CO)₂. He discovered that the ionization energy of the Rh complex is about three times that of the Co complex. This is probably due to the ground-state bonding differences in these two complexes.^{6d}

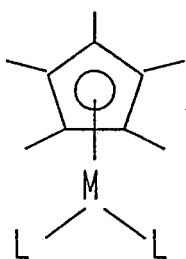
In 1985, Crabtree and Holt^{12a} pointed out the fact that C-H bond activation systems containing PMe₃, Cp*, and even PPh₃ work well. The cyclometalation product is not observed, which is a surprising feature of this chemistry. Why this preference for inter- over intramolecular reaction is observed for these systems is a major unsolved question in C-H activation studies.

In general, the preference for inter- over intramolecular reaction is a feature of these systems involving PMe₃, C₅Me₅ and even PPh₃, although the cyclometalation products have been observed in Bergman's¹³ and Sutton's⁹ work.

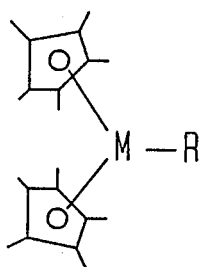
If it is assumed that the role of the phosphine ligand in a transition-metal system is to act as a catalyst, then the following questions suggest themselves: what is the catalytic role of the phosphine ligand? Can the phosphorus atom use its empty d -orbitals to facilitate interactions between d orbitals of the transition-metal atom and σ or σ^* orbitals of the C-H bond? The solutions to these challenging problems are still to be found.

The following three geometric configurations are usually seen in practical transition-metal systems which are able to activate C-H bonds. These structures allow substrates to approach the transition-metal centre readily.

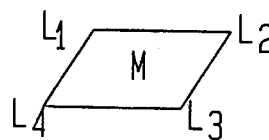
Fig.1. Three Geometric Configurations of Complexes



[I] half-sandwich



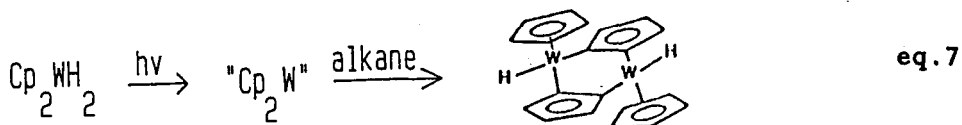
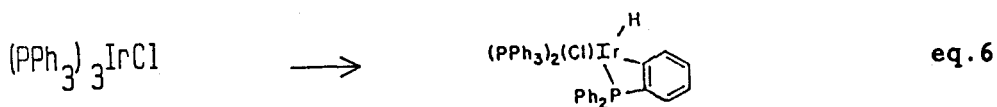
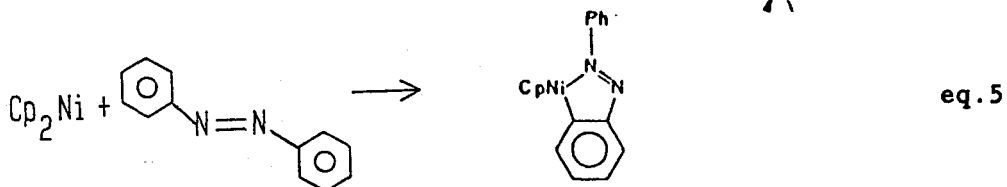
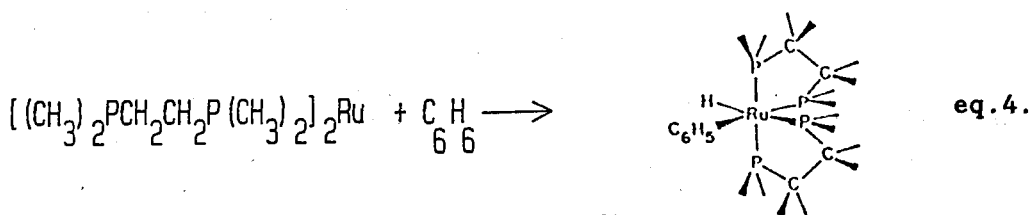
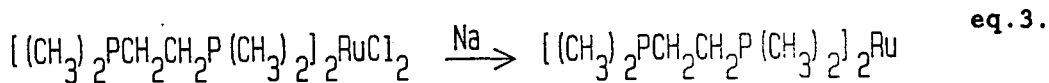
[II] bent sandwich

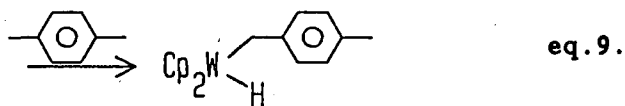
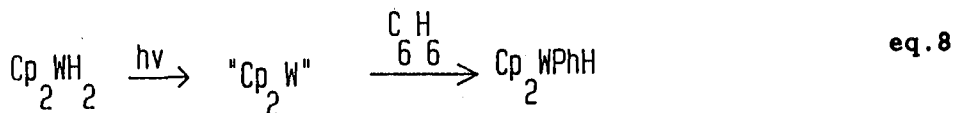


[III] square plane

1.3. An Outline of C-H Activation in Organometallic Chemistry

The first explicit description of C-H oxidative addition to a metal centre in a transition-metal complex was by Chatt and Davidson in 1965.¹⁴ Reduction of the octahedral bis(1,2-dimethylphosphinoethane) ruthenium dichloride complex in the presence of naphthalene or benzene gave the *cis*-*b*-naphthyl or phenyl ruthenium hydride complex (eqs. 3 and 4).





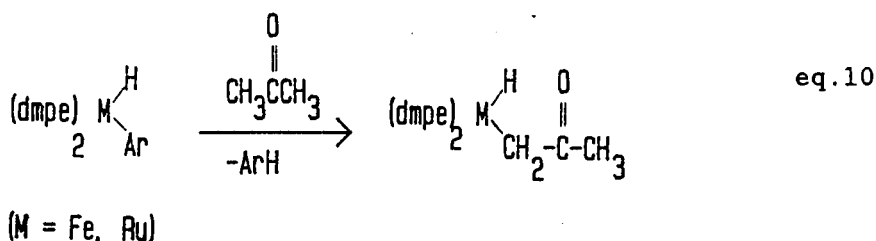
This reaction was remarkable because the strongest type of C-H bond had been cleaved and because it comprised the reaction of an initially free hydrocarbon with a molecular metal complex. Reaction may have been facilitated by an intermediate in which the arene molecule was co-ordinated, in some (productive) fashion, to the presumed zero-valent sixteen-electron ruthenium intermediate complex.¹⁴

Following the original Chatt-Davidson report,¹⁴ an enormous number of C-H activation reactions were discovered for mononuclear transition-metal complexes.¹⁵⁻¹⁷ The majority of reported C-H activations were intramolecular C-H oxidative additions, and were supposed to involve co-ordinately unsaturated complexes. A C-H bond associated with one of the ligands could approach closely, or be forced by electrostatic interaction to approach closely, the metal atom, so promoting this facile internal oxidative addition reaction.

Some specific examples of this process are illustrated in eqs.5-9. Eq.5 is the first example¹⁸ to be explicitly observed for the intramolecular oxidative addition of a ligand C-H bond to the metal centre. Eq.6² is an example of the large group, which involves

the so-called orthometallation process, in which insertion takes place into the ortho C-H bond of an aromatic ring attached to an atom directly bonded to the metal.

In attempts to extend these reactions to intermolecular cases, a few reactions have been found in which metal centers that are relatively electron-rich react with organic compounds having C-H bonds with low bond energy or high acidity (eq.10).¹⁹

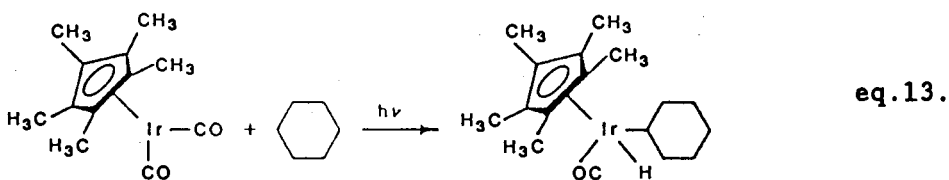
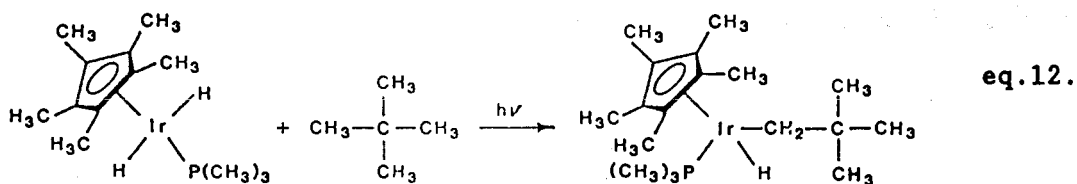
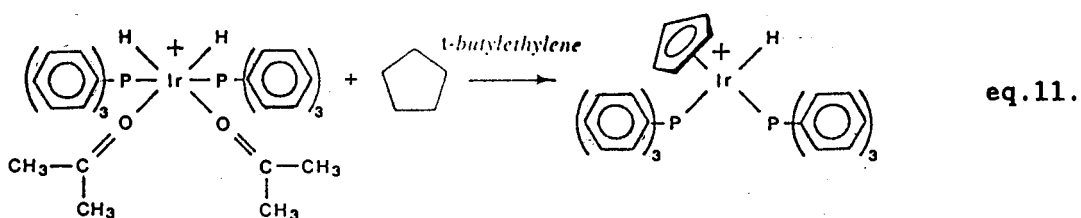


Green²⁰ made important early contributions in this area by discovering the photoextrusion of H₂ from a metal dihydride, (C₅H₅)₂WH₂. He used this reaction to activate C-H bonds in a number of molecules, e.g., eqs.7-9.

In 1979, Crabtree²¹ reported the first example of intermolecular C-H activation of saturated hydrocarbons, in which a diacetone iridium complex could stoichiometrically dehydrogenate cyclooctene to a cyclooctadiene complex, cyclopentane to a cyclopentadienyl complex, and other olefins to diolefin complexes (see eq.11).

In 1982, Bergman²² used an iridium complex (C₅Me₅)Ir(PMe₃)₂, dissolved in a potential substrate, such as neopentane.

When this complex was irradiated with UV light, it eliminated H_2 to become coordinately unsaturated. This intermediate then inserted into a C-H bond of the solvent to form a new complex (see eq.12). At about the same time, but independently, Graham²³ achieved similar results with an analogous iridium complex $(C_5Me_5)Ir(CO)_2$ (see eq.13).



After these publications by the groups of Bergman and Graham, C-H activation by transition-metal systems has become a very active area of current research.³

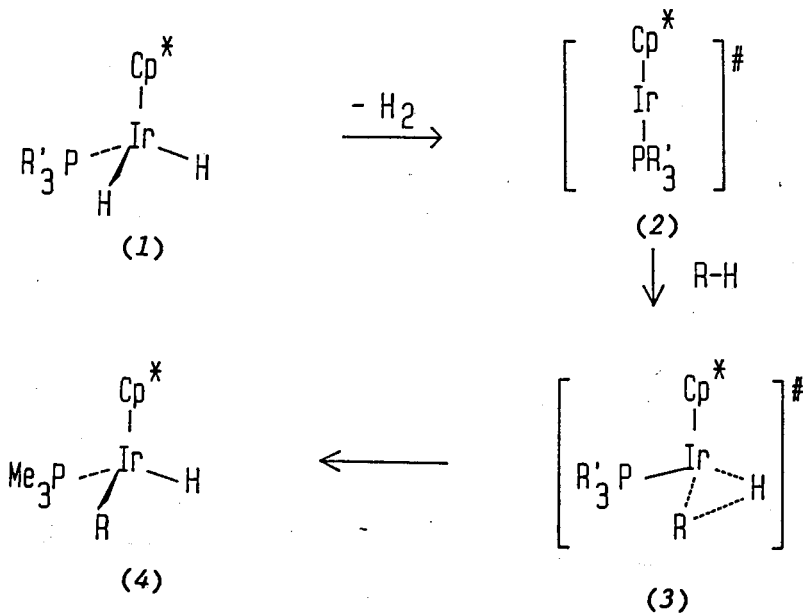
1.4. Advances in the Study of C-H Activation

Many exciting developments have been made in this research area with significant advances appearing in the literature over the past few years. Here, discussion is limited to the brief introduction of the major progress made in some relevant areas.

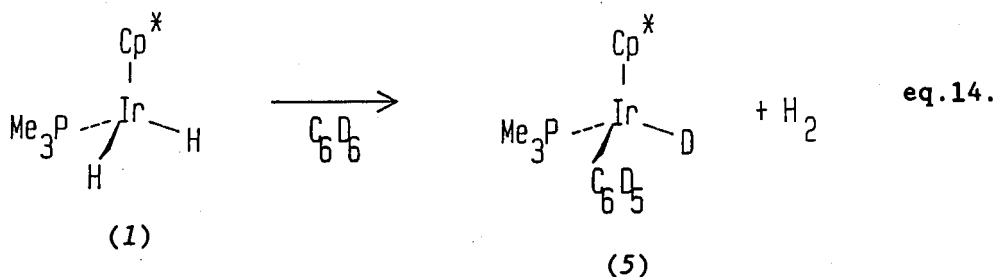
(1) C-H Activation by Oxidative Addition

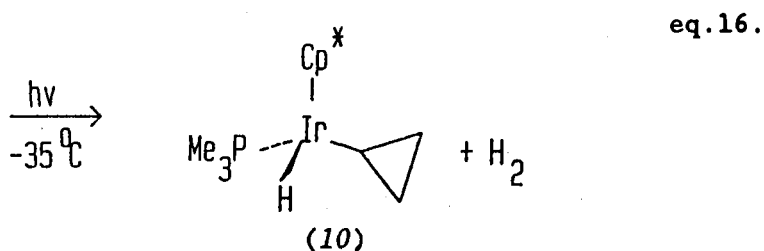
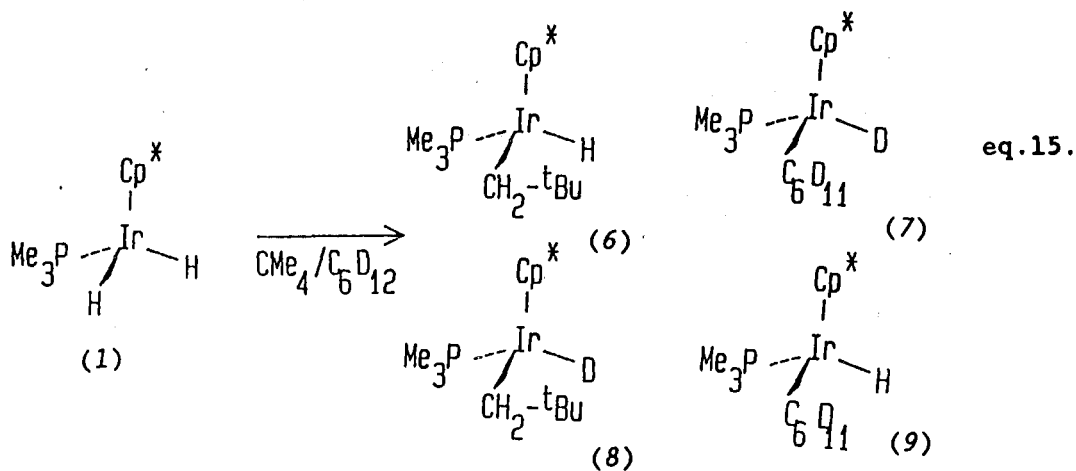
In 1982, the work of Bergman^{22,24} and Janowicz clearly showed the mechanism of the C-H bond oxidative addition (Scheme 1).

Scheme 1.



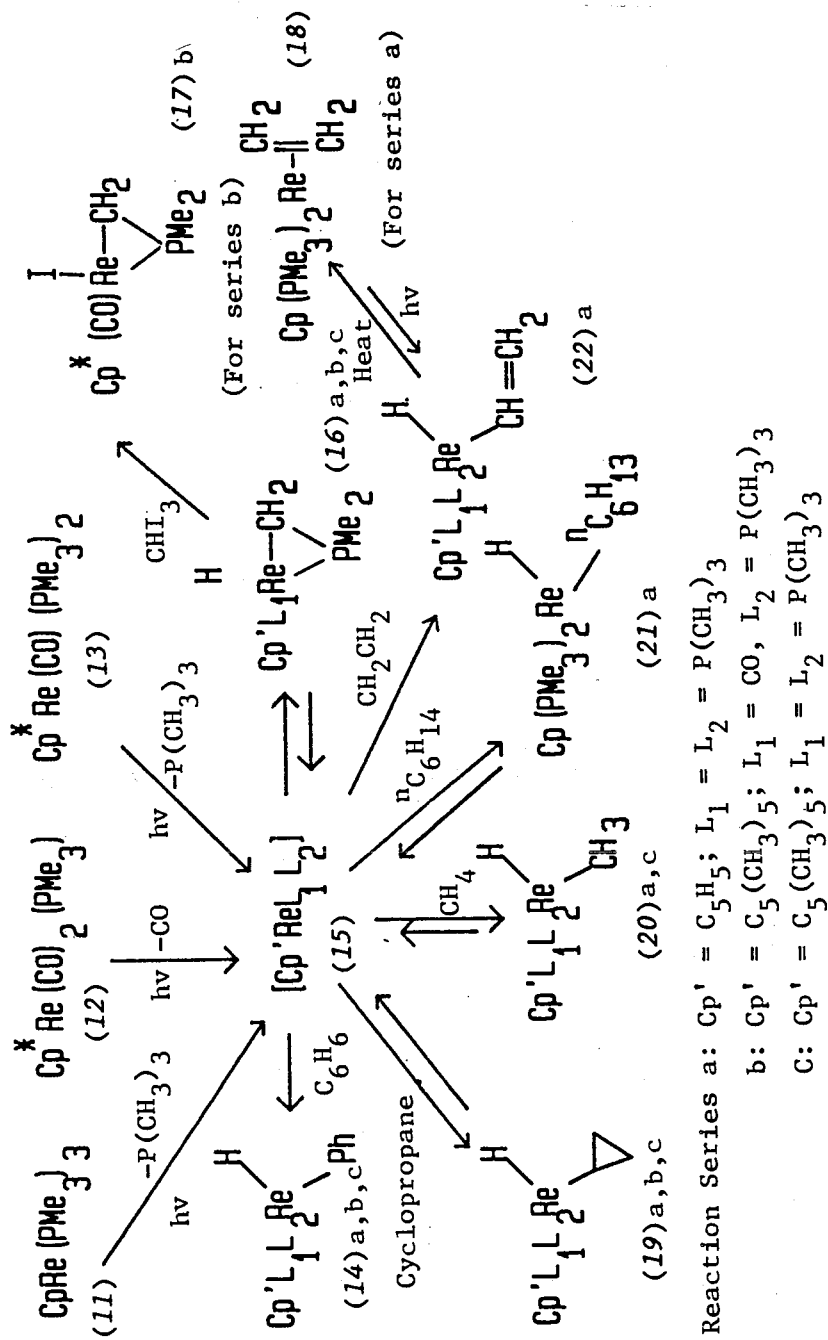
Upon photolysis or thermolysis, the dihydride iridium complex (1) loses H₂ to form an unsaturated, very reactive intermediate (2). This reacts with the C-H bonds of hydrocarbons, through the transition state (3), to give the corresponding alkyl hydride adducts (4). This mechanism of the C-H bond oxidative addition was confirmed by the following experimental results.^{22,24} Photolysis of Cp*Ir(PMe₃)(H)₂ in C₆D₆ (eq.14) gave only Cp*Ir(PMe₃)(D)(C₆D₅) (5) and H₂ without H/D exchange. This rules out the possibility of releasing a single H atom during the photolysis. Photolysis of Cp*Ir(PMe₃)(H)₂ in a solvent mixture of CMe₄ and C₆D₁₂ (ratio: CMe₄/C₆D₁₂ = 1/1) gave the major products (6) and (7), but (8) and (9) in a very small amount (eq.15). Radical mechanisms are ruled out by eq.15, because, if the free radical R[·] was present in the reaction, we would expect a mixture of four products (6-9) to be formed.





However, it is still possible that a solvent-caged radical pair could be present in the reaction process. To solve this problem, cyclopropane was chosen as a substrate, since its C-H bonding energy (106 kcal/mol) is large, due to the large amount of s character in these bonds, and its C-C bonding energy is relatively weak, due to ring strain. Photolysis of $\text{Cp}^*\text{Ir}(\text{PMe}_3)(\text{H})_2$ in liquid cyclopropane at -35°C only gave the hydrido cyclopropyl complex (10), formed by C-H insertion, rather than any product formed by inserting into C-C bonds of cyclopropane. The results are in sharp contrast to those which would be predicted for a radical-like species. Thus, it is believed that the C-H oxidative addition of the complex $\text{Cp}^*\text{Ir}(\text{PR}_3)(\text{H})_2$ involves the following processes: (1) H_2 loss; (2) 16 e- intermediate directly inserting into the C-H bond.

Scheme 2.



This mechanism involving a coordinately unsaturated intermediate has been generally accepted to explain the process of the C-H activation by a transition-metal system.

The examples shown in Scheme 2, reported by Bergman,¹³ show that the coordinately unsaturated rhenium centres of these complexes are able to insert into the unreactive C-H bonds of hydrocarbons with a high selectivity with respect to different alkanes despite lowered inter/intra selectivity. Bergman believed that suitable electron-donating ligands, attached to the metal centre, could promote both intra- and intermolecular C-H activation by Cp and Cp* rhenium complexes. Thus, the driving force for these C-H oxidative additions would seem to be the stronger interaction of a more negative metal centre with the C-H bonds of alkanes.

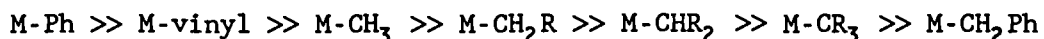
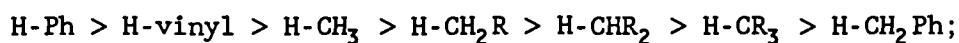
(ii) Selectivity of C-H Activation

Bergman and his co-workers^{22,25} have measured the selectivities of the rhodium and iridium intermediates [Cp*ML] (M - Rh, Ir; L - PMe₃). They showed that photolysis of Cp*MLH₂ in a wide variety of alkanes gives the corresponding alkyl hydride adducts with H₂ loss. The relative rates of different types of C-H bond activation by the intermediates [Cp*ML] were determined (see Table 2). The rhodium complex apparently favors primary C-H bond

insertion, while the iridium complex shows poor selectivity and inserts into both primary and secondary C-H bonds.

In addition, comparable studies have shown that Cp*Re and CpRe complexes (see Scheme 2) exhibit a high selectivity with respect to different alkanes.¹³ The active unsaturated species [CpRe(PMe₃)(CO)] and [CpRe(PMe₃)₂] only insert into primary C-H bonds of linear alkanes or the secondary C-H bonds of cyclopropane.

In general, the selectivity of C-H activation appears to be a consequence of both thermodynamic and kinetic factors. It is believed that the thermodynamic factor depends on the M-C bond strength. The trends of M-C and C-H bond strengths are shown as follows:³



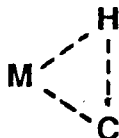
The kinetic factor depends on the steric hindrance in the transition-state.¹² On the basis of the analysis of 17 organometallic structures showing C-H...M interactions, Crabtree^{12a} has concluded that as the C-H bond approaches the metal centre, a large M...H-C angle will be reduced, leading to the carbon atom becoming close to the metal centre.

Table 2. Relative Rates of Reaction of $\text{Cp}^*\text{M}(\text{PMe}_3)_2$
with Various Hydrocarbons on Photolysis^{22,25}

Hydrocarbon	rel rate/C-H bond ^a	
	M - Ir	M - Rh
benzene	3.5	19.5
cyclopropane	2.1	10.4
n-hexane(1 ⁰)	2.7	5.9
n-hexane(2 ⁰)	0.2	0.0
propane(1 ⁰)	1.5	2.6
propane(2 ⁰)	0.3	0.0
cyclopentane	1.1	1.8
neopentane	1.14	
cyclohexane	1.0	1.0
cyclodecane	0.23	
cyclooctane	0.09	

^aData on a per hydrogen basis.

Fig.2. Transition State of C-H Activation



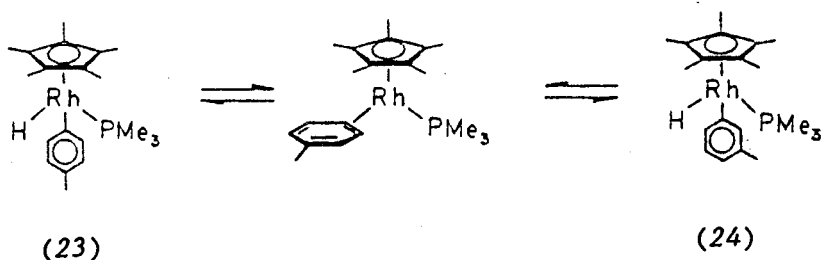
In this transition state (Fig.2), substituents on the carbon atom are therefore likely to interfere with the interaction between the metal centre and the carbon atom. That is why the kinetic factor is advantageous to the primary C-H bond oxidative addition to the metal centre because of less steric hindrance.

(iii) η^2 -Arene Intermediate²⁶

Jones^{26c} reported chemical evidence for the intermediacy of an η^2 -arene complex in the activation of aromatic C-H bonds by Cp^*Rh system. The tolyl ligand in the complex (23) isomerizes to give (24) under mild conditions without dissociation of the toluene. Thus, it was suggested that this isomerisation proceeds via an intermediate in which the toluene remains coordinated to the metal in an η^2 fashion.

More recently, Jones^{26b} studied isotope effects in C-H bond oxidative additions of the same rhodium system. Based on the following two experiments, Jones arrived at the same conclusion of the intermediacy of η^2 -arene (Scheme 3).

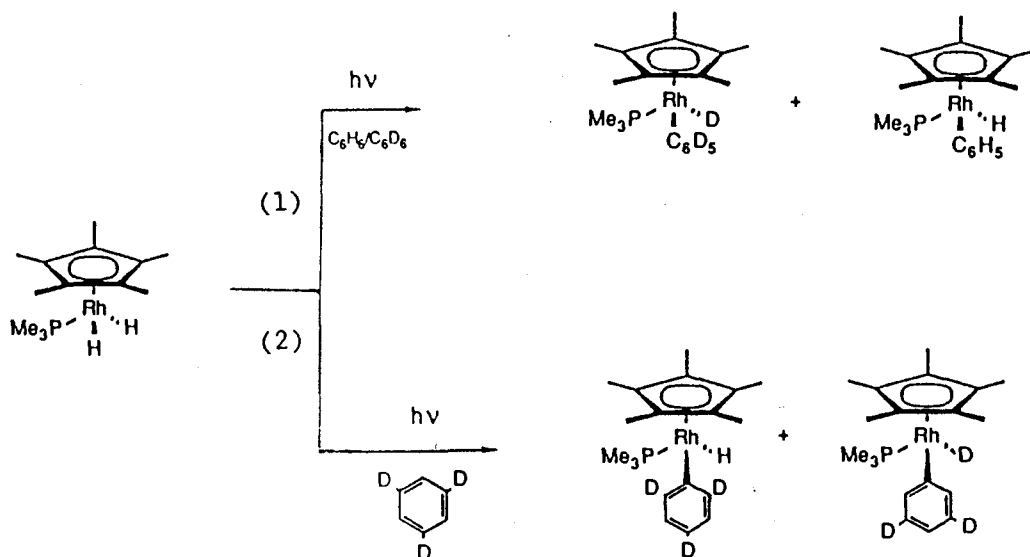
Scheme 3.



(1) Irradiation of $\text{Cp}^*\text{Rh}(\text{PMe}_3)\text{H}_2$ at 10°C in a 1:1 mixture of $\text{C}_6\text{H}_6/\text{C}_6\text{D}_6$ gave a $k_{\text{H}}/k_{\text{D}}$ ratio of 1.06 (± 0.05). This kinetic isotopic effect for $\text{Cp}^*\text{Rh}(\text{PMe}_3)$ selectivity corresponds to the intermolecular competition between C_6H_6 and C_6D_6 , and the value was small, indicating that the key step is not the C-H oxidative addition to the rhodium atom.

(2) Photolysis of $\text{Cp}^*\text{Rh}(\text{PMe}_3)\text{H}_2$ at -40°C in a solution of 1,3,5- $\text{C}_6\text{H}_3\text{D}_3$ showed a ratio of the complexes $\text{Cp}^*\text{Rh}(\text{PMe}_3)(2,4,6\text{-C}_6\text{D}_3\text{H}_2)\text{H}$ to $\text{Cp}^*\text{Rh}(\text{PMe}_3)(3,5\text{-C}_6\text{D}_2\text{H}_3)\text{D} \approx 1.4:1$. This result corresponds to the intramolecular competition between C-H and C-D bonds. The value of the isotope effect is larger than that in case (1), indicating that the C-H oxidative addition plays an important role in the key step.

Scheme 4.

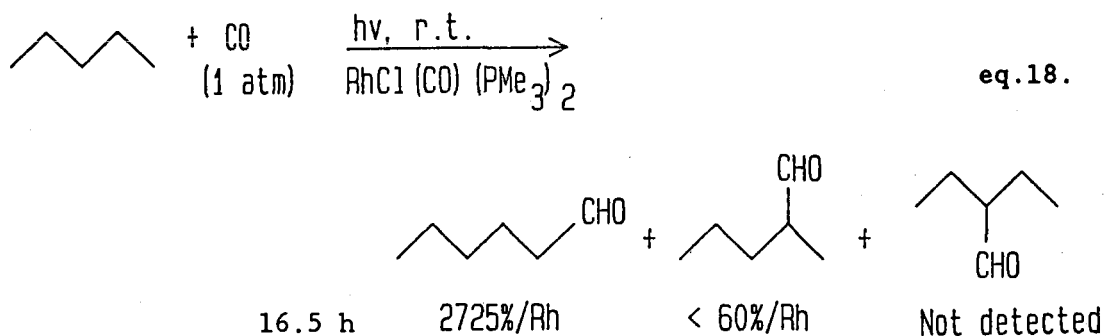
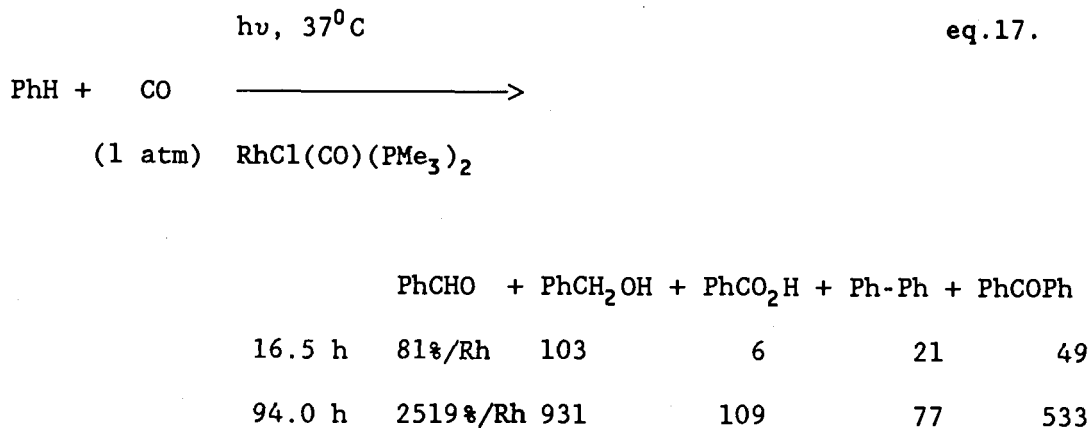


Therefore, the intermediacy of an η^2 -benzene complex in C-H bond activation of arenes by $[\text{Cp}^*\text{Rh}(\text{PMe}_3)]$ has been reasonably well established, and can completely explain all the above experimental results.

(iv) Functionalization of C-H bonds by Transition-Metal Systems

The ultimate goal in this research area is the development of new methods of functionalizing unreactive alkanes. However, only a few homogeneous catalytic reactions^{27,28} involving C-H bond activation have been attained. Among these, the rhodium complex

$\text{RhCl}(\text{CO})(\text{PPh}_3)_2$ has been shown to catalyze efficiently the carbonylation of C-H bonds of benzene^{28a} and, in particular, the regioselective carbonylation of the terminal methyl group of n-pentane.^{28b}



Eq.17 shows the time dependency of the carbonylation reaction catalyzed by $\text{RhCl}(\text{CO})(\text{PMe}_3)_2$. The total turnover number for the Ph group reached 47.8 [$= 25.19 + 9.31 + 1.09 + 2(0.77 + 5.33)$]

after 94 h. Also, the ratio of the other products (PhCH_2OH , PhCOPh and PhCO_2H) to PhCHO decreased clearly as the reaction proceeded.

Eq.18 shows a highly regioselective carbonylation by $\text{RhCl}(\text{CO})(\text{PMe}_3)_2$. The n-pentane afforded n-hexanal in a yield of 2725%/Rh after 16.5 h, while the yield of 2-methylpentanal was less than 60%/Rh and 2-ethylbutanal was not detected.

In summary, it is believed that there is considerable potential for the activation and functionalization of hydrocarbons catalyzed by organometallic complexes, particularly in view of the mild reaction conditions, the remarkable selectivity, and the abundance of the raw materials. Many challenging questions still await the chemists' solution.

CHAPTER II

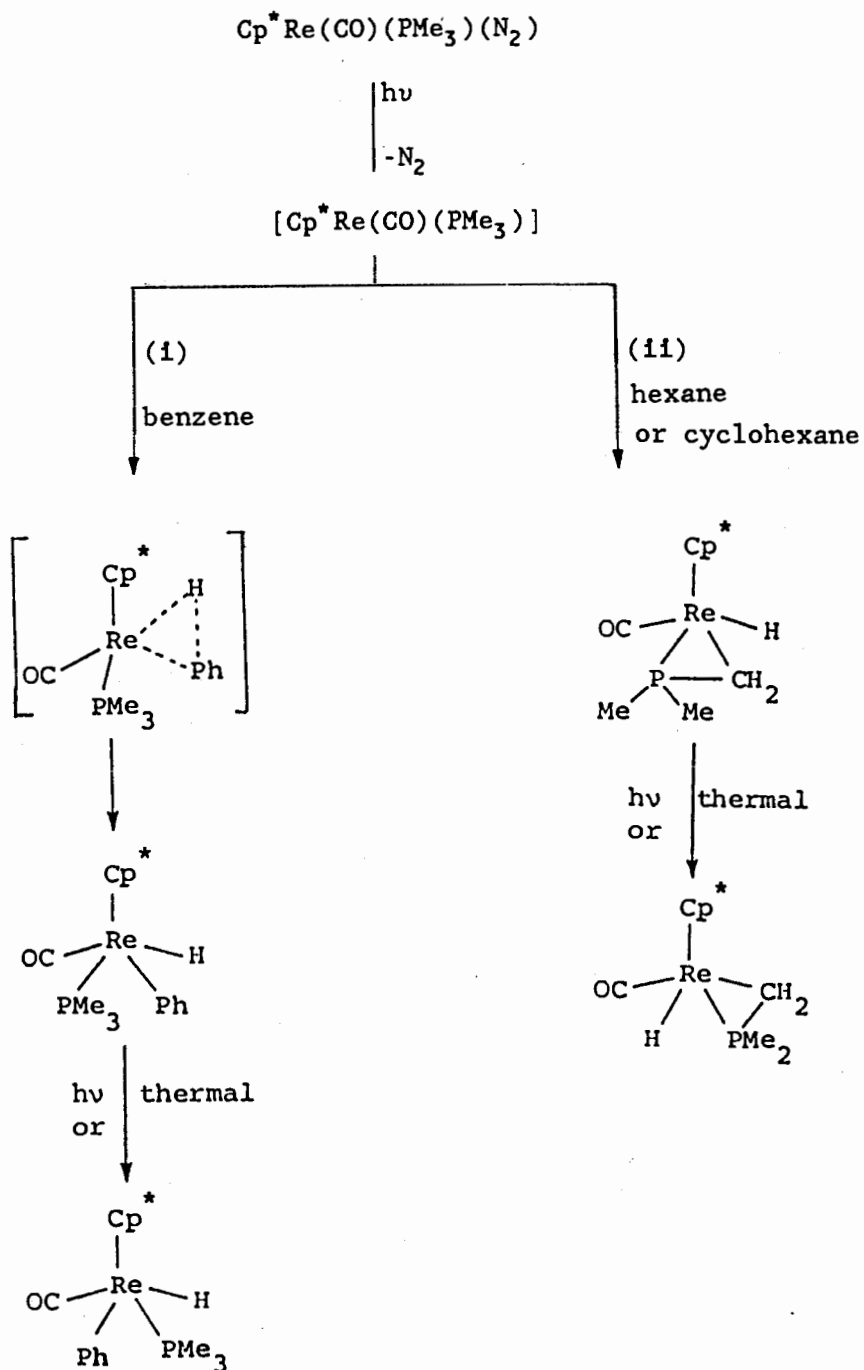
Synthesis and Characterization of Pentamethylcyclopentadienyl (olefin) Complexes of Rhenium

2.1. Introduction

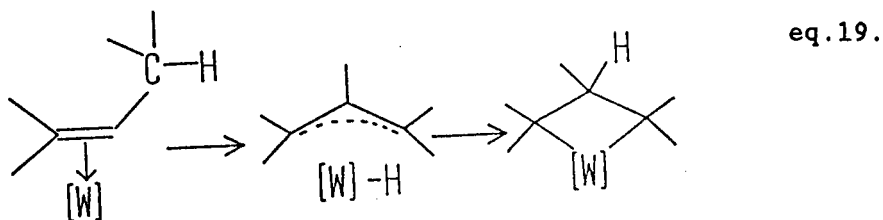
In recent years, the most comprehensive studies in the field of C-H activation involving iridium, rhodium and rhenium complexes have been carried out by Bergman,^{13,25,29} Crabtree,^{5,12,30} Graham^{23,31} and Jones.²⁶ In 1985, Bergman and his co-workers demonstrated that the rhenium complexes $\text{CpRe}(\text{PMe}_3)_3$, $\text{Cp}^*\text{Re}(\text{CO})_2(\text{PMe}_3)$ and $\text{Cp}^*\text{Re}(\text{CO})(\text{PMe}_3)_2$ can be used as photochemical precursors in intra- and intermolecular C-H activation reactions^{13a} (see Scheme 2). In our laboratory,⁹ the potential of dinitrogen complexes in carbon hydrogen activation has been studied in the photochemical reactions of the trimethylphosphine(dinitrogen) complex $\text{Cp}^*\text{Re}(\text{CO})(\text{PMe}_3)(\text{N}_2)$ in saturated and unsaturated hydrocarbons. Some of these reactions are shown in Scheme 5.

To continue our study of C-H activation, we were interested in attempting to observe whether C-H activation occurred for alkenes in rhenium systems. It is a well-known fact that the allylic C-H bond energy (≈ 87 kcal/mol) is the lowest bond energy of all

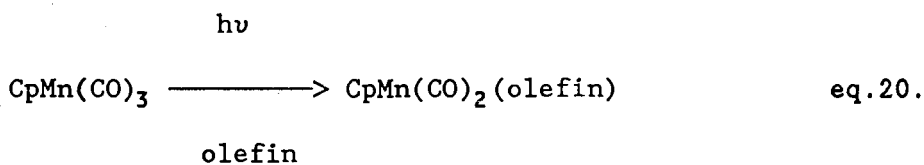
Scheme 5.



hydrocarbon C-H bonds.¹ Green³² noted that the β -hydrogen atoms of coordinated olefins may migrate to the metal giving η^3 -allylic hydrides in the case of tungsten (see eq.19).



In view of this, we expected that allylic C-H bond activation might be observed in some cases in the attempted synthesis of olefin complexes of rhenium. However, there are very few olefin complexes of Cp^*Re or CpRe , and $\text{Cp}^*\text{Re}(\text{CO})_2(\text{C}_2\text{H}_4)$ or $\text{CpRe}(\text{CO})_2(\text{C}_2\text{H}_4)$, for instance, are unknown. Known olefin complexes include $\text{CpRe}(\text{CO})_2(\eta^2\text{-cyclopentene})$,³³ and the mesityl oxide complex $\text{Cp}^*\text{Re}(\text{CO})_2(\eta^2\text{-Me}_2\text{C=CHCOMe})$.^{34a} The mesityl oxide complex was obtained from the reaction of $\text{Cp}^*\text{Re}(\text{CO})_2(\text{N}_2)$ with $[\text{Me}_3\text{O}][\text{BF}_4]$. $\text{CpMn}(\text{CO})_2(\text{olefin})$ complexes have been prepared using photochemical methods.³⁵



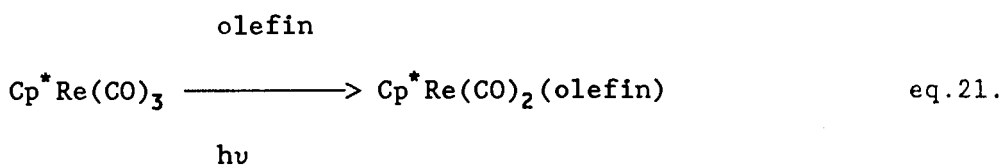
olefin = ethene, propene, 1-pentene,
cyclopentene, cyclooctene, etc.

In this chapter, the synthesis and characterization of several new pentamethylcyclopentadienyl olefin complexes of rhenium will be described, and their ^1H NMR and mass spectra will be discussed; the following chapter describes the observation of allylic C-H bond activation leading to η^3 -allyl(hydrido) complexes.

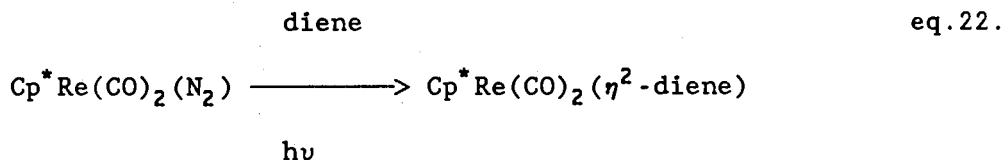
2.2. Synthesis

The pentamethylcyclopentadienylrhenium olefin complexes of the general formula $\text{Cp}^*\text{Re}(\text{CO})_2(\eta^2\text{-olefin})$ (olefin = ethene [1], propene [2], 2-pentene [3], 1-octene [4], *cis*-2-octene [5], cyclohexene [6], 4-methylcyclohexene [7], cyclooctene [8], allene [9], 1,3-cyclohexadiene [10], 1,4-cyclohexadiene [11]) and the trimethylphosphine(propene) complex $\text{Cp}^*\text{Re}(\text{CO})(\text{PMe}_3)(\eta^2\text{-propene})$ [12] were prepared by four different methods: (i) irradiation of the tricarbonyl complex $\text{Cp}^*\text{Re}(\text{CO})_3$ and the corresponding olefin in hexane yielded the η^2 -olefin rhenium complexes [1]-[4] and [6]-[8] (eq.21), and C-H activation products were also observed in most cases (see Chapter III); (ii) irradiation of the dinitrogen complex $\text{Cp}^*\text{Re}(\text{CO})_2(\text{N}_2)$ (or $\text{Cp}^*\text{Re}(\text{CO})(\text{PMe}_3)(\text{N}_2)$) and the appropriate diene (or propene) in hexane gave the η^2 -diene rhenium complexes [10] and [11] (eq.22) (or the trimethylphosphine(propene) complex [12], eq.23); (iii) irradiation of $\text{Cp}^*\text{Re}(\text{CO})_3$ in THF yielded the unstable

THF complex,^{34(b)} which further reacted with allene at room temperature without UV light to give the η^2 -allene complex [9] (eq.24); (iv) reduction of the η^3 -allylalkane cationic complex with NaBH_4 produced the related η^2 -olefin complexes [4] and [5] (eq.25, see Chapter IV).



olefin = ethene [1], propene [2], 2-pentene [3], 1-octene [4],
cyclohexene [6], 4-methylcyclohexene [7] and
cyclooctene [8]



diene = 1,3-cyclohexadiene [10] and 1,4-cyclohexadiene [11]

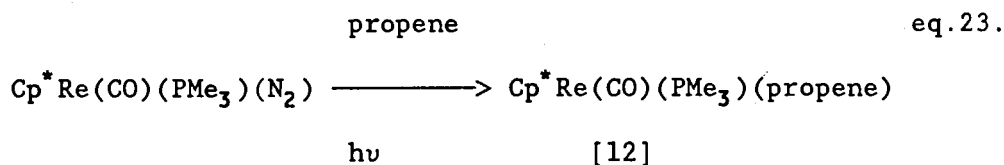
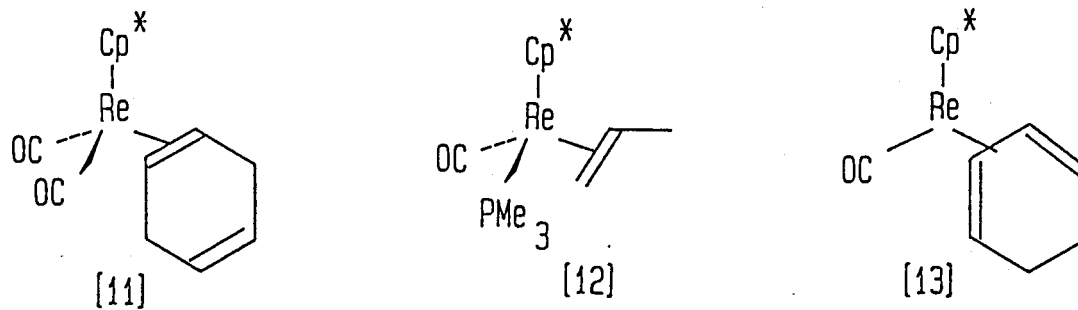
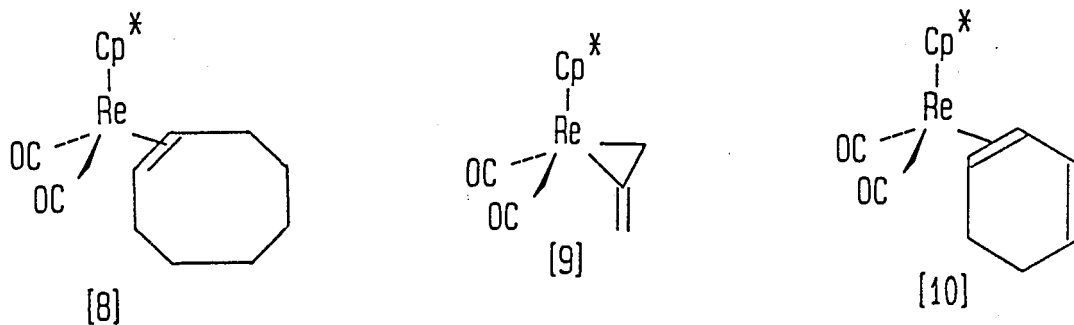
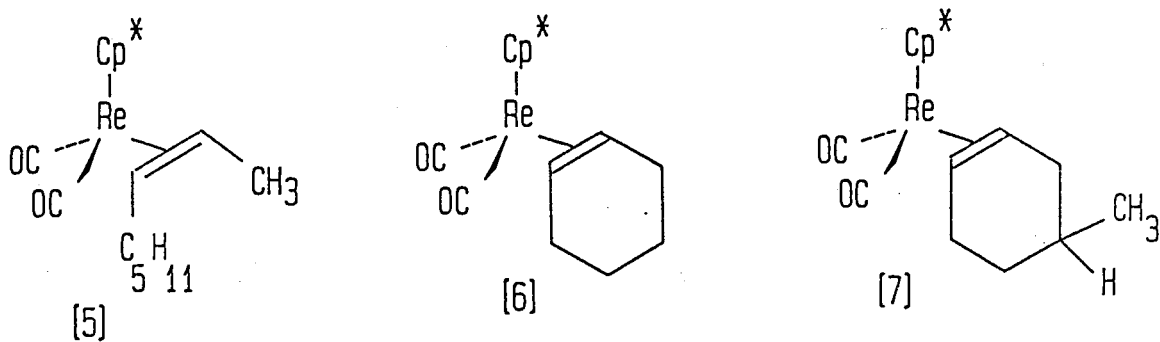
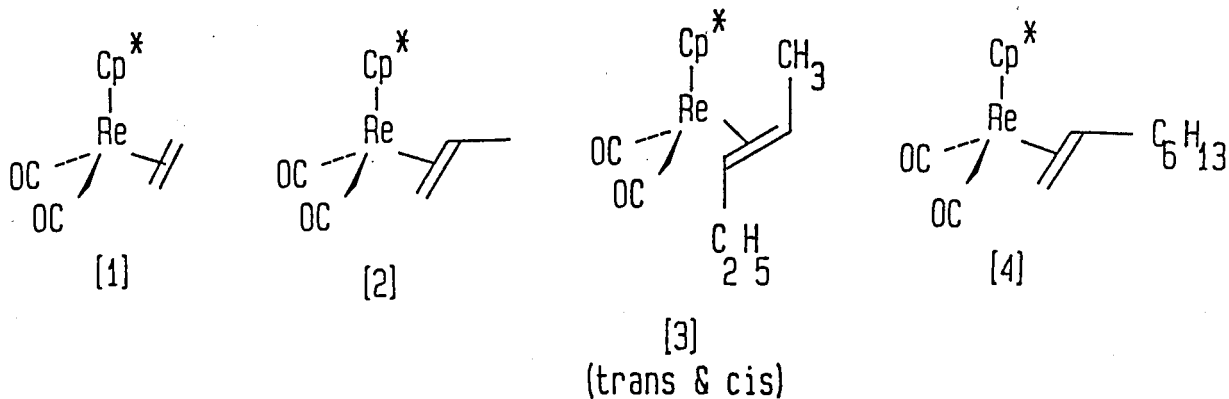
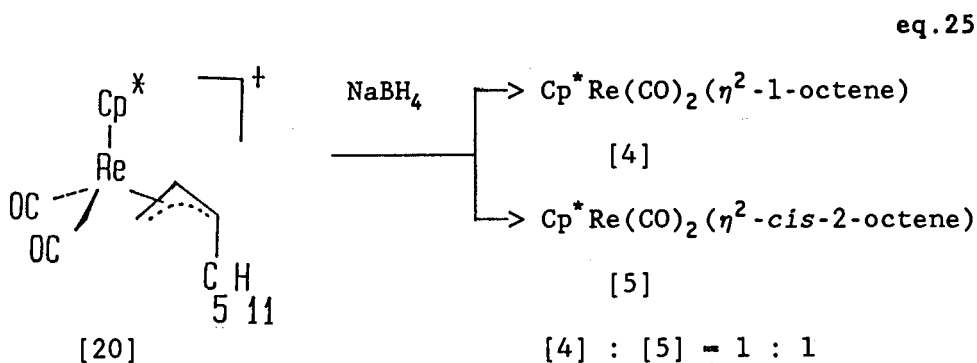
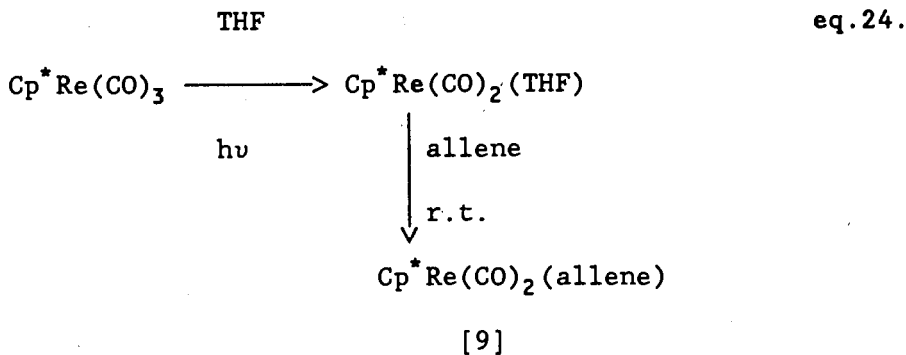


Table 3. Structures of New Olefin Complexes [1]-[13]





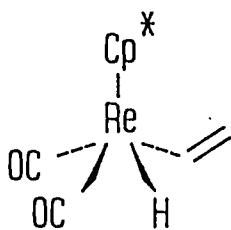
The η^2 -olefin complexes ([1]-[4], [6]-[8]) were made by the first method, but this is not suitable for making the diene and allene complexes, because of the instability of the dienes and allene under UV light for a prolonged time. Interestingly, the η^2 -diene complex [10] and the η^4 -1,3-cyclohexadiene complex [13] $\text{Cp}^* \text{Re}(\text{CO})(\eta^4\text{-1,3-cyclohexadiene})$ were both also isolated from the photochemical reaction of $\text{Cp}^* \text{Re}(\text{CO})_3$ with cyclohexene in hexane.

In general, the reactions were monitored by IR and were stopped when the IR band of the desired product reached maximum intensity. In all the cases, (except in the case of the complex

[12], which was chromatographed on silica gel (60G)), chromatography on an alumina column with hexane as an eluant resulted in separation of the pure olefin complex from the mixture with residual $\text{Cp}^*\text{Re}(\text{CO})_3$. The new η^2 -olefin rhenium complexes [1]-[12] were obtained as white microcrystalline solids, which were stable in a pure solid state. The η^4 -1,3-cyclohexadiene complex [13] was unstable and decomposed slowly to η^2 -1,3-cyclohexadiene [10] and tricarbonyl complexes at room temperature. Similarly, the instability of some η^4 -1,3-cyclohexadiene complexes has also been observed with complexes such as $\text{Cp}^*\text{Rh}(\eta^4\text{-1,3-hexadiene})$,^{36b} $\text{Cp}^*\text{Ir}(\eta^4\text{-1,3-hexadiene})$ ^{36b} and $\text{CpCo}(\eta^4\text{-1,3-cyclohexadiene})$.^{36a}

(1) $\text{Cp}^*\text{Re}(\text{CO})_2(\eta^2\text{-C}_2\text{H}_4)$ [1]. Irradiation of $\text{Cp}^*\text{Re}(\text{CO})_3$ with an ethene purge resulted in an IR spectrum containing $\nu(\text{CO})$ absorptions at 1964 and 1894 cm^{-1} for the ethene complex [1]. Following chromatography on an acidic alumina column with hexane as an eluant, the ethene complex [1] was isolated as a white solid. A comparison of reactions with $\text{Cp}^*\text{Re}(\text{CO})_3$ and $\text{Cp}^*\text{Re}(\text{CO})_2(\text{N}_2)$ showed that the conversion of the dinitrogen complex was much more efficient. Complete conversion to the ethene complex [1] (though also with a little of the tricarbonyl being produced) occurred after 20 min. photolysis of $\text{Cp}^*\text{Re}(\text{CO})_2(\text{N}_2)$ with ethene, whereas there was less than 50% conversion of $\text{Cp}^*\text{Re}(\text{CO})_3$ to the ethene complex in this time (and indeed it took more than 1 h for the IR absorptions of [1]

to become more intense than those of the tricarbonyl). No evidence for any further product was obtained. Bergman has reported the formation of a hydrido (vinyl) complex in the photochemical reaction of ethene with the related rhenium complex such as $\text{CpRe}(\text{PMe}_3)_3$.^{13a} We observed no evidence for the formation of a corresponding vinyl hydride complex (25) in our work.



(25)

(ii) $\text{Cp}^*\text{Re}(\text{CO})_2(\eta^2\text{-C}_3\text{H}_6)$ [2]. Irradiation of $\text{Cp}^*\text{Re}(\text{CO})_3$ at 0°C for 1h with a propene purge resulted in an IR spectrum containing absorptions at 1961 and 1890 cm^{-1} for the propene complex [2] and two absorptions at 1904 and 1912 cm^{-1} in addition to residual absorptions from the tricarbonyl. The 1904 and 1912 cm^{-1} absorptions intensified on further irradiation, relative to [2]. Following chromatography on a neutral alumina column with hexane as an eluant, the propene complex [2] was isolated as a white solid. Furthermore, two other products were isolated on the same column and shown by full characterization and X-ray structure to be the hydrido (η^3 -allyl) complexes [15] (*exo* and *endo* respectively, see Chapter III).

(iii) $\text{Cp}^*\text{Re}(\text{CO})_2(\eta^2\text{-}2\text{-C}_5\text{H}_{10})$ [3]. A solution of $\text{Cp}^*\text{Re}(\text{CO})_3$ in hexane and 2-pentene (a mixture of *cis* and *trans* isomers) was irradiated for 30 min. After this time the IR showed $\nu(\text{CO})$ absorptions at 1955 and 1884 cm^{-1} attributed to the product [3] (which were slightly less intense than the absorptions from unreacted tricarbonyl) and there was a significant amount of solid decomposition product. A weak band at 1891 cm^{-1} was also present, indicating the presence of one or more hydrido (allyl) complexes (see Chapter III). Complex [3] was shown by ^1H NMR to be a mixture of [3a]*cis* and [3b]*trans* isomers (ratio: *cis/trans* = 1/1.7).

(iv) $\text{Cp}^*\text{Re}(\text{CO})_2(\eta^2\text{-}1\text{-C}_8\text{H}_{16})$ [4]. By a similar method described in the above synthesis of the propene complex [2], not only the 1-octene complex [4], but also the hydrido(η^3 -allylpentane) complex [17b]*exo* were isolated. Only this one isomer of the hydrido(η^3 -allylpentane) complex [17] was obtained, and this was fully characterised (see Chapter III).

(v) $\text{Cp}^*\text{Re}(\text{CO})_2(\eta^2\text{-}i\text{-}2\text{-C}_8\text{H}_{16})$ [5]. This *cis*-2-octene compound was synthesized from nucleophilic attack of NaBH_4 with the corresponding allylalkane cation as described in Chapter IV.

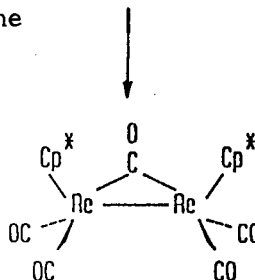
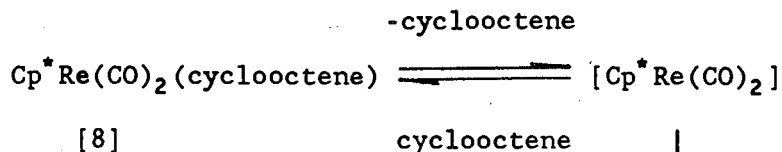
(vi) $\text{Cp}^*\text{Re}(\text{CO})_2(\eta^2\text{-C}_6\text{H}_{10})$ [6]. The solution of $\text{Cp}^*\text{Re}(\text{CO})_3$ in hexane and cyclohexene was irradiated at 0°C for 1h. The IR

spectrum at this time showed $\nu(\text{CO})$ absorptions at 1952, 1881 cm^{-1} attributed to the complex [6], and another band at 1891 cm^{-1} , which intensified on further irradiation relative to [6], indicating one or more new products. By chromatography four fractions were eluted and isolated. These are $\text{Cp}^*\text{Re}(\text{CO})_3$, complex [6] ($\nu(\text{CO})$ 1952, 1881 cm^{-1}), complex [10] (the η^2 -1,3-cyclohexadiene complex) ($\nu(\text{CO})$ 1960, 1891 cm^{-1}), and, as the final fraction, complex [13] (the η^4 -1,3-cyclohexadiene complex) ($\nu(\text{CO})$ 1891 cm^{-1}). The η^2 -1,3-cyclohexadiene complex [10] was directly synthesized from the reaction of $\text{Cp}^*\text{Re}(\text{CO})_2\text{N}_2$ with 1,3-cyclohexadiene for comparison. The η^4 -cyclohexadiene complex [13] was identified only on the basis of its IR, MS, and ^1H NMR spectra.

(vii) $\text{Cp}^*\text{Re}(\text{CO})_2(\eta^2\text{-C}_7\text{H}_{12})$ [7]. Irradiation of a solution of $\text{Cp}^*\text{Re}(\text{CO})_3$ with 4-methylcyclohexadiene in hexane for 90 min. resulted in an IR spectrum containing $\nu(\text{CO})$ bands at 1952 and 1881 cm^{-1} for the complex [7] that were slightly more intense than those of residual tricarbonyl. An absorption at 1890 cm^{-1} was also present, roughly equal in intensity to the absorptions of [7]. Following chromatography on a 25 cm column of neutral alumina, eluting with hexane, only the complex [7] and the tricarbonyl were recovered. Other products were apparently unstable and decomposed during the chromatography. Irradiation of [7] in hexane for 10 min.

resulted in an IR spectrum showing a new $\nu(\text{CO})$ band at 1890 cm^{-1} with intensity similar to the bands of [7]. However, the unknown complex corresponding to the new band (1890 cm^{-1}) was quite unstable. This probably arises from the further photochemical reaction of [7]. Unfortunately, we were not able to isolate the unknown complex.

(viii) $\text{Cp}^*\text{Re}(\text{CO})_2(\eta^2\text{-C}_8\text{H}_{14})$ [8]. The photolytic reaction of $\text{Cp}^*\text{Re}(\text{CO})_3$ with cyclooctene in hexane was inefficient. Even after 90 min., the IR showed $\nu(\text{CO})$ absorptions of the tricarbonyl still to be more intense than those of the cyclooctene complex [8] ($\nu(\text{CO})$ 1955, 1885). The yield was only about 14%. A possible reason may be that the bulky and flexible cyclooctene has difficulty approaching the rhenium atom closely, so that the cyclooctene complex [8] is not itself very stable and dissociates during further photolysis. Indeed, the known binuclear complex $(\text{Cp}^*\text{Re}(\text{CO})_2)_2\text{CO}^{37}$ was successfully isolated from the reaction residue. Furthermore, irradiation of the pure cyclooctene complex [8] in hexane only for 15 min., whether in a quartz or Pyrex tube, resulted in decomposition of [8] and formation of the binuclear compound $(\text{Cp}^*\text{Re}(\text{CO})_2)_2\text{CO}$ [14] (eq.26).

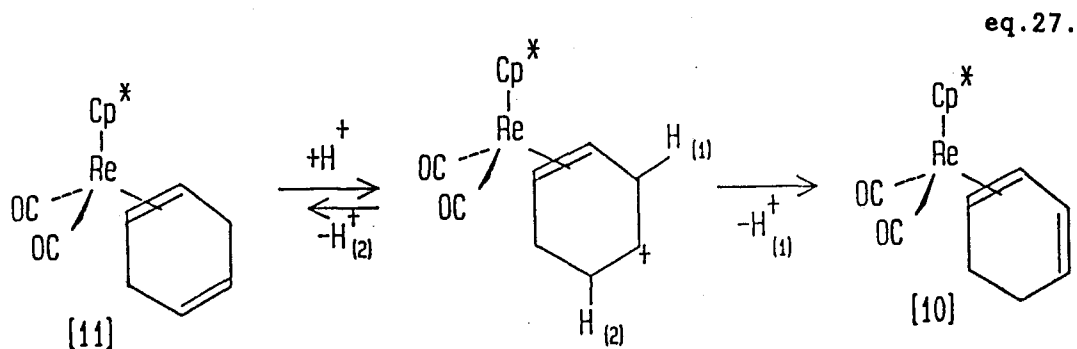


[14]

(ix) $\text{Cp}^* \text{Re}(\text{CO})_2(\eta^2\text{-C}_3\text{H}_4)$ [9]. The photolysis reaction of $\text{Cp}^* \text{Re}(\text{CO})_3$ in THF for 90 min. resulted in an IR spectrum containing two new absorptions at 1893 and 1823 cm^{-1} for the THF complex $\text{Cp}^* \text{Re}(\text{CO})_2(\text{THF})$. The solution of $\text{Cp}^* \text{Re}(\text{CO})_2(\text{THF})$ in THF was then stirred vigorously (no irradiation) and allene gas was bubbled through the solution for 1 h. The THF complex was completely converted to the allene complex [9] ($\nu(\text{CO})$ 1978, 1910 cm^{-1}), which was isolated by chromatography on a neutral alumina column with hexane as eluant. The allene complex [9] is stable in a pure state, but was observed to decompose slowly, and to convert predominantly to the propene complex [2] if it was not isolated promptly after reaction.

(x) $\text{Cp}^*\text{Re}(\text{CO})_2(\eta^2\text{-1,3-C}_6\text{H}_8)$ [10]. The photochemical reaction of $\text{Cp}^*\text{Re}(\text{CO})_2(\text{N}_2)$ with 1,3-cyclohexadiene was complete in only 15 min. at 0°C . The IR showed $\nu(\text{CO})$ absorptions at 1960 and 1891 cm^{-1} for the complex [10] and weak residual absorptions from the dinitrogen complex ($\nu(\text{NN})\ 2125\text{ cm}^{-1}$; $\nu(\text{CO})\ 1954$ and 1902 cm^{-1}). Chromatography on a neutral alumina column produced, firstly, small amounts of the dinitrogen and tricarbonyl complexes then the complex [10].

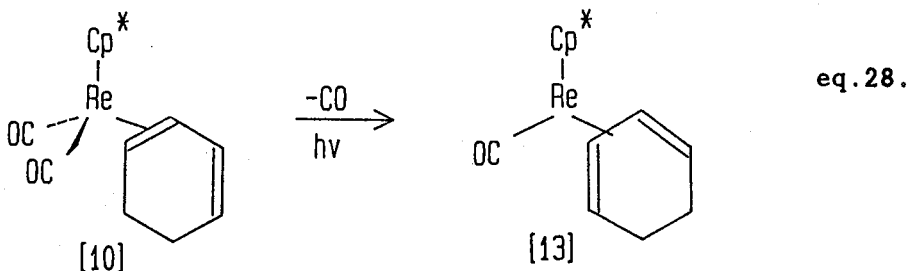
(xi) $\text{Cp}^*\text{Re}(\text{CO})_2(\eta^2\text{-1,4-C}_6\text{H}_8)$ [11]. The 1,4-cyclohexadiene complex [11] was synthesized by a method similar to that described in the above synthesis of complex [10]. However, it is crucial to use a neutral alumina column for chromatography, since the complex [11] was observed to be easily isomerized to complex [10] even on an acidic alumina column, or in acidic solution (eq.27).



(xii) $\text{Cp}^*\text{Re}(\text{CO})(\text{PMe}_3)(\eta^2\text{-C}_3\text{H}_6)$ [12]. Irradiation of solution of $\text{Cp}^*\text{Re}(\text{CO})(\text{PMe}_3)(\text{N}_2)$ in hexane with a propene purge for

20 min. at 0°C resulted in an IR spectrum having the most intense $\nu(\text{CO})$ absorption at 1845 cm^{-1} attributable to the complex [12]. Other weak $\nu(\text{CO})$ absorptions were at 1923 and 1860 cm^{-1} for $\text{Cp}^*\text{Re}(\text{CO})_2(\text{PMe}_3)$; 1912 and 1904 cm^{-1} for $\text{Cp}^*\text{Re}(\text{CO})(\text{H})(\text{allyl})$ (*endo*, *exo*) [15]; and at 1961 and 1890 cm^{-1} for $\text{Cp}^*\text{Re}(\text{CO})_2(\text{propene})$ [2]. Complex [12] was isolated by chromatography on a silica gel (60G) column with hexane as eluant. Furthermore, other by-products ($\text{Cp}^*\text{Re}(\text{CO})_2(\text{PMe}_3)$, [15](*endo* and *exo*), and [2]) were successfully isolated in small amounts. When isolation was attempted on a column of neutral alumina instead of silica gel (60G), the complex [12] decomposed completely.

(xiii) $\text{Cp}^*\text{Re}(\text{CO})(\eta^4\text{-1,3-C}_6\text{H}_8)$ [13]. The complex [13] was isolated in small amount as a by-product in the synthesis of the cyclohexene complex [6] (see complex [6] above). It is thought to result from the further photolysis of complex [10] as shown in eq.28. Recently, Kreiter^{36c} reported a similar result in a tungsten



system. Photolysis of the η^2 -diene dicarbonyl tungsten complex results in one CO loss and the formation of the η^4 -diene

monocarbonyl tungsten complex.

Irradiation of a solution of η^2 -1,3-cyclohexadiene complex [10] in hexane and 1,3-cyclohexadiene for 30 min. at 0°C resulted in an IR spectrum containing an absorption at 1891 cm^{-1} which is assigned to the complex [13], in addition to residual absorptions from the complex [10]. However, the $\nu(\text{CO})$ absorptions of complex [10] were still more intense than that of the complex [13] even after 90 min. irradiation. Additionally, it was observed that complex [13] is not very stable in solution even when stored under an atmosphere of N_2 in the freezer.

2.3. Characterization

These new complexes of rhenium [1]-[12] were fully characterized by elemental analysis and spectroscopy. They are air-stable as solids or when dissolved in non-polar organic solvents. The complex [13] was characterized by IR, MS and ^1H NMR, but there was insufficient sample for further analysis. The spectral properties of these new complexes [1]-[13] are shown in Table 4. The IR spectra show the expected one or two $\nu(\text{CO})$ absorptions. Some important points are: (i) alkyl substituents on the olefin act as electron-donor groups, since in any of complexes [2]-[8], which have one or two alkyl substituents, the two $\nu(\text{CO})$ absorptions are at lower wave number compared with the IR of [1], and comparing the IR

data among complexes [1], [2] and [3], or between [4] and [8], shows that $\nu(\text{CO})$ is lower the more alkyl substituents there are on ethene; (ii) the two $\nu(\text{CO})$ absorptions for a cyclic olefin are at lower wavenumbers than those of the comparable acyclic olefin; (iii) comparing the $\nu(\text{CO})$ absorptions of diene complexes [10], [11] with that of cyclohexene complex [6] shows the $\nu(\text{CO})$ bands are higher, suggesting that the diene is a stronger π -acceptor with respect to cyclohexene; (iv) the difference of the $\nu(\text{CO})$ absorptions between two diene complexes [10] and [11] shows that the conjugated diene 1,3-cyclohexadiene is a better π -acceptor than the non-conjugated 1,4-cyclohexadiene; (v) the $\nu(\text{CO})$ absorptions of allene complex [9] are the highest compared with the others, showing that the strongest $d\pi$ back-bond occurs between rhenium and allene.

^1H NMR data gave additional confirmatory evidence of the formulation of [1]-[13] as the new rhenium complexes described above. Some ^1H NMR spectra of these new complexes are shown in Figs.3-10. The ^1H NMR data for the olefin ligands (see Table 5) show that shielding by rhenium causes shifts upfield in the range of 0.60-2.52 ppm. The shielding constants for alkyl substituents can be estimated by comparing the olefinic proton chemical shifts for the acyclic ligands in complexes [1]-[5]. With reference to η^2 -ethene in complex [1], the shielding constants are: $C_\delta(\text{H}_{\text{gem}}) \approx 0.3$ ppm, $C_\delta(\text{H}_{\text{syn}}) = 0.3 - 0.8$ ppm and $C_\delta(\text{H}_{\text{anti}}) = -0.3 - 0.6$ ppm. The observed coupling constants are typical of η^2 -olefin complexes and

their values are as follows: $J_{gem} = 1.5 - 2.0$ Hz, $J_{cis} = 8.5 - 10.5$ Hz and $J_{trans} = 12.0 - 12.5$ Hz.

The electron impact (70 eV) mass spectra for these alkene complexes [1]-[13] are presented in Figs.17(a-m). In all cases the parent ion M^+ could be observed, though this is not the base peak. The fragmentation was observed to be dependent on the nature of the alkene and ancillary ligands, particularly where PMe_3 or dienes were present. This is discussed in Section 2.5.2.

2.4. Chemical Reactions

(i) The complex [7] cannot be converted to the dinitrogen complex $Cp^*Re(CO)_2(N_2)$ even at high pressure of N_2 (1900 Psi) for 48h at room temperature.

(ii) The photochemical intramolecular C-H activation of η^2 -linear or cyclo-olefin complexes ([2], [3], [4] and [6]) are described in more detail in Chapter III.

(iii) The η^2 -linear or cyclo-olefin complexes ([2], [4] and [6]) have been successfully converted to η^3 -allylalkane cationic complexes by reacting with $[Ph_3C][BF_4]$. This is discussed in Chapter IV.

(iv) The η^2 -diene complexes ([10] and [11]) can react with HBF_4 to produce the corresponding cationic complexes, see Chapter IV.

Table 4. Some Spectroscopic Parameters of the Olefin Complexes
 $\text{Cp}^*\text{Re}(\text{CO})_{1-2}\text{L}$ and $\text{Cp}^*\text{Re}(\text{CO})(\text{PMe}_3)(\text{propene})$

Cplx L	IR(hexane) $\nu(\text{CO}) \text{ cm}^{-1}$	$^1\text{H NMR}(\text{C}_6\text{D}_6)$ $\delta (\text{Cp}^*)^a \text{ ppm}$	MS(m/z) ^d M ⁺ ; base
[1] ethene	1964(s), 1894(s)	1.60	406; 348
[2] propene	1961(s), 1890(s)	1.61	420; 348
[3] 2-pentene	1955(s), 1884(s)	1.70 ^b ; 1.64 ^c	448; 348
[4] 1-octene	1960(s), 1888(s)	1.65	490; 378
[5] <i>cis</i> -2-octene	1955(s), 1883(s)	1.72	490; 348
[6] cyclohexene	1952(s), 1881(s)	1.62	460; 348
[7] 4-methyl- cyclohexene	1952(s), 1881(s)	1.62	474; 378
[8] cyclooctene	1955(s), 1885(s)	1.65	488; 378
[9] allene	1978(s), 1910(s)	1.61	418; 360
[10] η^2 -1,3- cyclohexadiene	1960(s), 1891(s)	1.60	458; 400
[11] η^2 -1,4- cyclohexadiene	1957(s), 1886(s)	1.61	458; 348
[12] $\text{Cp}^*\text{Re}(\text{CO})(\text{PMe}_3)$ (propene)	1846(s)	1.69	468 ^e ; 426
[13] η^4 -1,3- cyclohexadiene	1891(s)	1.51	430; 400

Abbreviation: s = strong. ^aCp* was a singlet peak in all cases.
^b η^2 -*trans*-2-pentene. ^c η^2 -*cis*-2-pentene. ^dfor ^{187}Re . ^efor ^{187}Re , ^{31}P .

Table 5. Proton Chemical Shifts and Coupling Constants
for Ligands of Compounds [1]-[13]^a

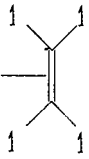
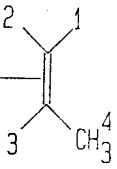
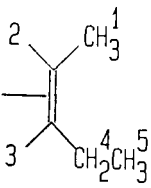
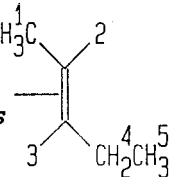
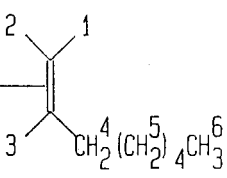
Ligand	Chem. Shifts δ (ppm) and Coupling Constants J (Hz)
[1] 	^b H(1) 1.68(s, 4).
[2] 	^b H(1) 2.16(dd, 1, $J_{1,2} = 1.7$, $J_{1,3} = 12.1$); H(2) 1.35(dd, 1, $J_{2,3} = 9.8$); H(3) 1.97(m, 1); H(4) 2.05(d, 3, $J_{3,4} = 5.7$).
[3] <i>cis</i> 	^{b, c} H(1) 1.83(d, 3, $J_{1,2} = 6.1$); H(2) 2.52(m, 1); H(3) 2.32(m, 1); H(4) 1.60(m, 2); H(5) 1.18(t, 3, $J_{4,5} = 7.3$).
[3] <i>trans</i> 	^{b, c} H(1) 2.06(d, 3, $J_{1,2} = 2$); H(2) 2.21(m, 1) or 2.14(m, 1); H(3) 2.14(m, 1) or 2.21(m, 1); H(4) 1.86(m, 2); H(5) 1.23(t, 3, $J_{4,5} = 7.3$).
[4] 	^b H(1) 2.47(m, 1); H(2) 2.19(d, 1, $J_{2,3} = 10.5$); H(3) 2.01(m, 1); H(4) 1.61(m, 2); H(5) 1.35-1.40(br m, 8); H(6) 0.95(br t, 3, $J_{5,6} = 6.9$).

Table 5 (continued).

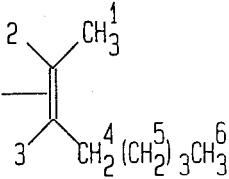
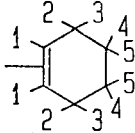
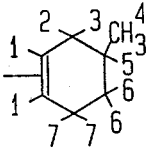
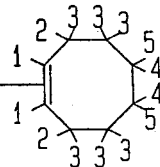
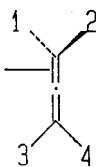
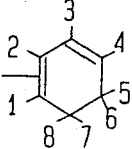
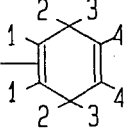
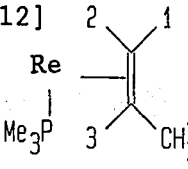
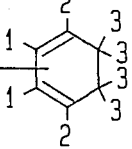
Ligand	δ (ppm) and J (Hz)
<p>[5]</p> 	$^d\text{H}(1)$ 1.87(d, 3, $J_{1,2} = 6.0$); $\text{H}(2)$ 2.52(m, 1, $J_{2,3} = 9.8$); $\text{H}(3)$ 2.40(m, 1); $\text{H}(4)$ 1.53-1.61(m, 2); $\text{H}(5)$ 1.37-1.45(m, 6); $\text{H}(6)$ 1.00(br t, 3, $J_{5,6} = 6$).
<p>[6]</p> 	$^d\text{H}(1)$ 2.42(dd, 2, $J_{1,2} = 2$, $J_{1,3} = 3$); $\text{H}(2)$ 2.85(m, 2); $\text{H}(3)$ 2.91(m, 2); $\text{H}(4)$ 1.57(m, 2); $\text{H}(5)$ 1.45(m, 2).
<p>[7]</p> 	$^b\text{H}(1)$ 2.50(m, 2); $\text{H}(2)$ 2.39(m, 1); $\text{H}(3)$ 2.64(m, 1); $\text{H}(4)$ 0.98(d, 2, $J_{4,5} = 6.6$); $\text{H}(5)$ 1.46-1.52(m, 1); $\text{H}(6)$ 1.10-1.32(m, 2); $\text{H}(7)$ 2.90(m, 2).
<p>[8]</p> 	$^b\text{H}(1)$ 1.98(d, 2, $J_{1,2} = 9.0$); $\text{H}(2)$ 2.70(d, 2, $J_{2,3} = 13.5$); $\text{H}(3)$ 1.70-1.78(m, 6); $\text{H}(4)$ 1.49-1.56(m, 2); $\text{H}(5)$ 1.37-1.44(m, 2).
<p>[9]</p> 	$^d, ^e\text{H}(1,2)$ 1.48(br s, 2); $\text{H}(3)$ 5.60(t, 1, $J_{1(2),3} = 2.7$); $\text{H}(4)$ 6.67(t, 1, $J_{1(2),4} = 2.7$).

Table 5 (continued).

Ligand	δ (ppm) and J (Hz)
<p>[10]</p> 	<p>^dH(1) 2.31(m, 1, $J_{1,2} = 9.0$); H(2) 2.40(m, 1, $J_{2,3} = 5.5$, $J_{2,4} = 1.0$); H(3) 6.52(m, 1, $J_{3,4} = 10$, $J_{3,5(6)} = 1.5$); H(4) 5.52(m, 1, $J_{4,5(6)} = 5.5$); H(5,6) 1.82(m, 2, $J_{5(6),7} = 5.0$, $J_{5(6),8} = 7.0$); H(7) 2.70(m, 1, $J_{7,8} = 14$); H(8) 2.87(m, 1).</p>
<p>[11]</p> 	<p>^bH(1) 2.34(br s, 2); H(2) 3.17(d, 2, $J_{2,3} = 17$); H(3) 3.44(d, 2, $J_{2,3} = 17$); H(4) 5.74(br s, 2).</p>
<p>[12]</p> 	<p>^bH(1) 1.78-1.85(br m, 1); H(2) 0.60(dt, 1, $J_{2,3} = 8.8$, $J_{PH} = 3.0$); H(3) 1.16-1.31(m, 1); H(4) 2.24(dd, 3, $J_{3,4} = 6$, $J_{1,4}$ or $J_{2,4} = 1.1$); PMe₃ 1.31(d, 9, $J_{PH} = 8.5$).</p>
<p>[13]</p> 	<p>^bH(1) 3.22(m, 2); H(2) 2.95(m, 2); H(3) 1.30-1.44(m, 4).</p>

Abbreviation: br = broad, d = doublet, dd = doublet of doublets, dt = doublet of triplets, m = multiplet, s = singlet and t = triplet.

^aAll samples were measured in C₆D₆ at 400MHz. ^bAs determined by ¹H NMR. ^cCompounds [3] *cis* and *trans* are present in a same sample (ratio: *cis/trans* = 1/1.7). ^dAs determined by decoupling experiments. ^eAs determined by NOE experiments.

Fig.3. ^1H NMR Spectrum

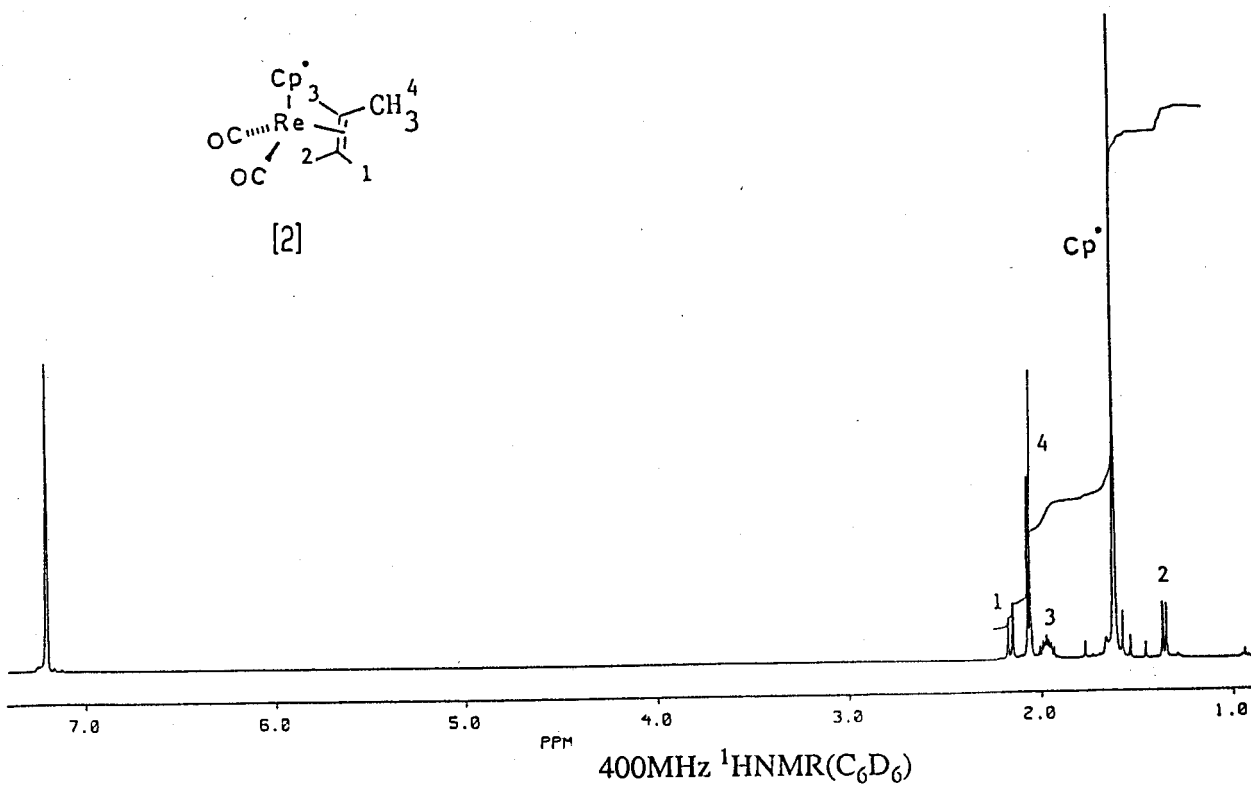


Fig.4. ^1H NMR Spectrum

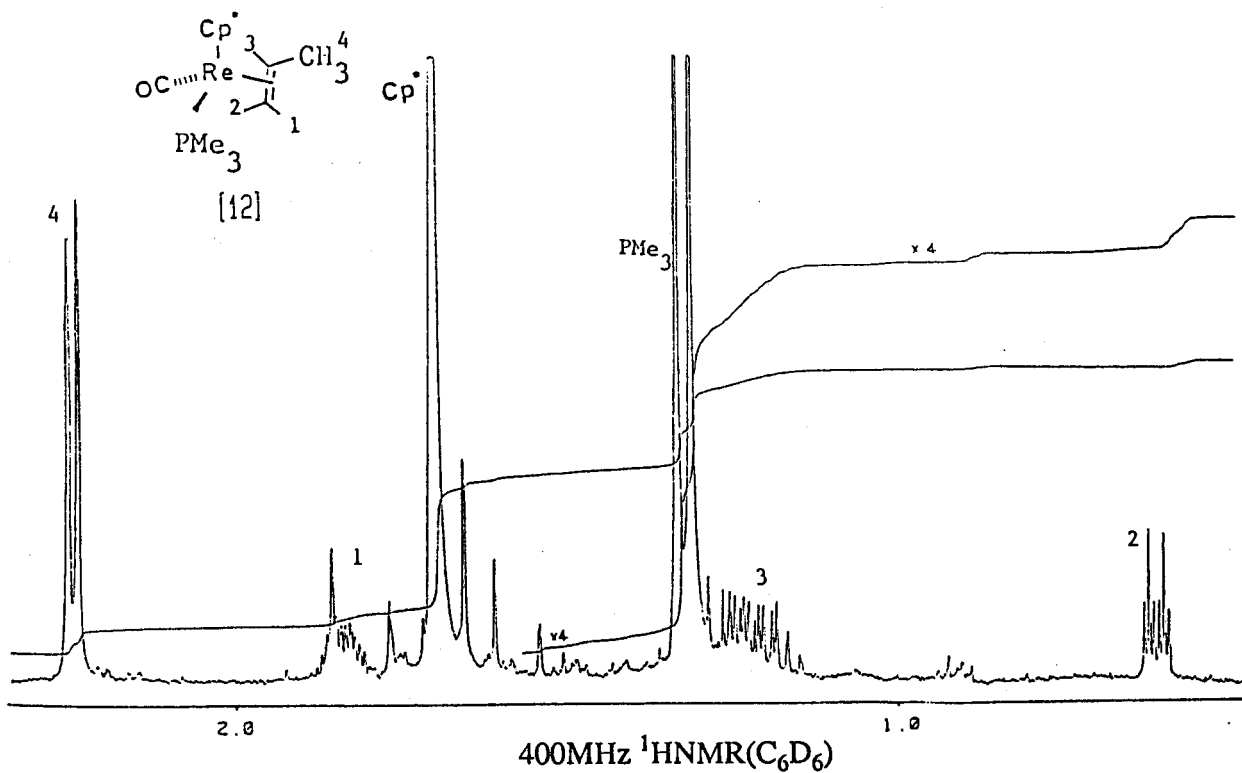


Fig. 5. ^1H NMR Spectrum

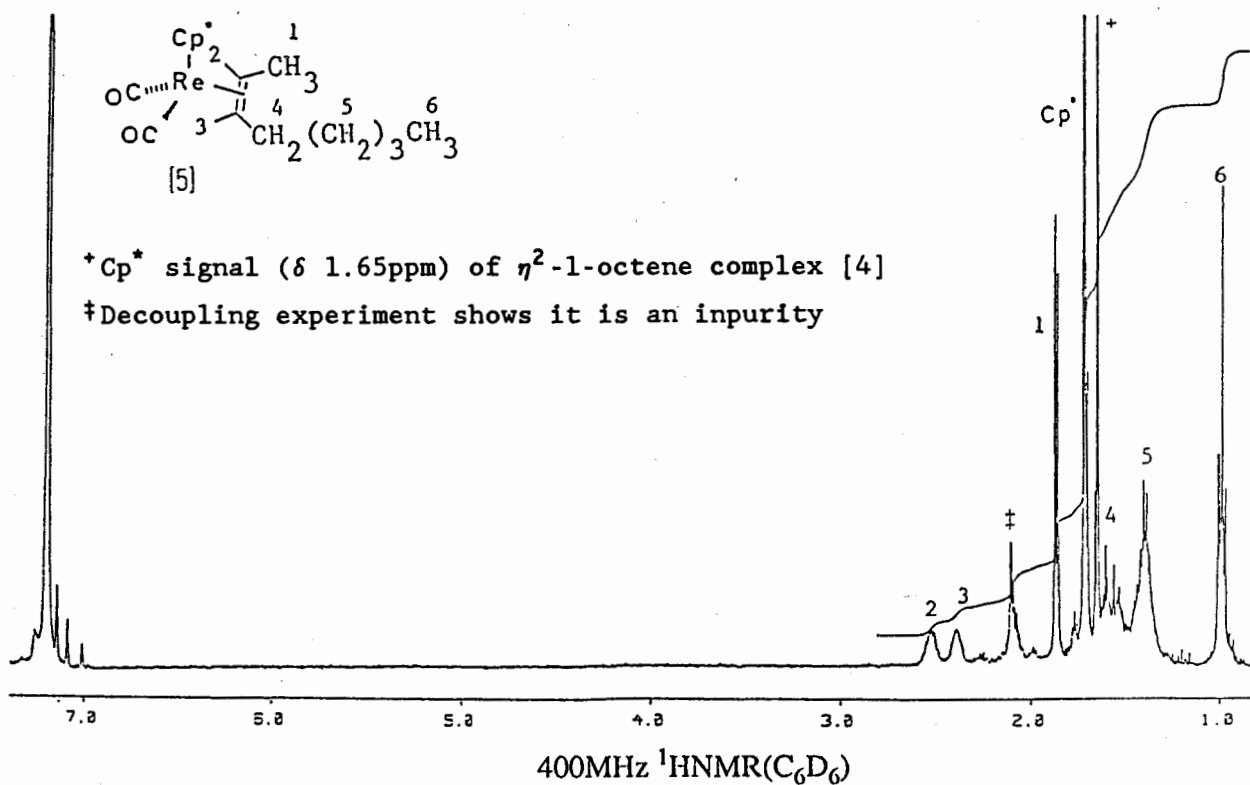


Fig. 6. ^1H NMR Spectrum

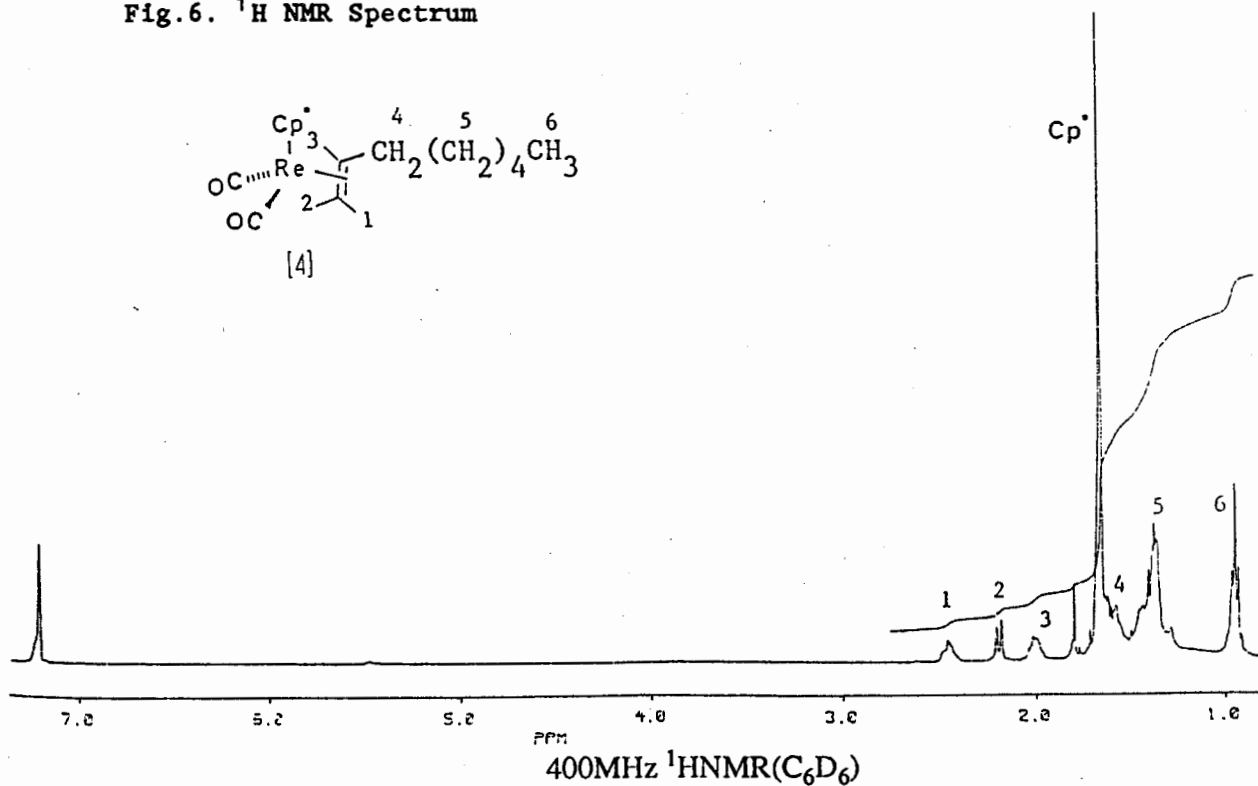


Fig.7. ^1H NMR Spectrum

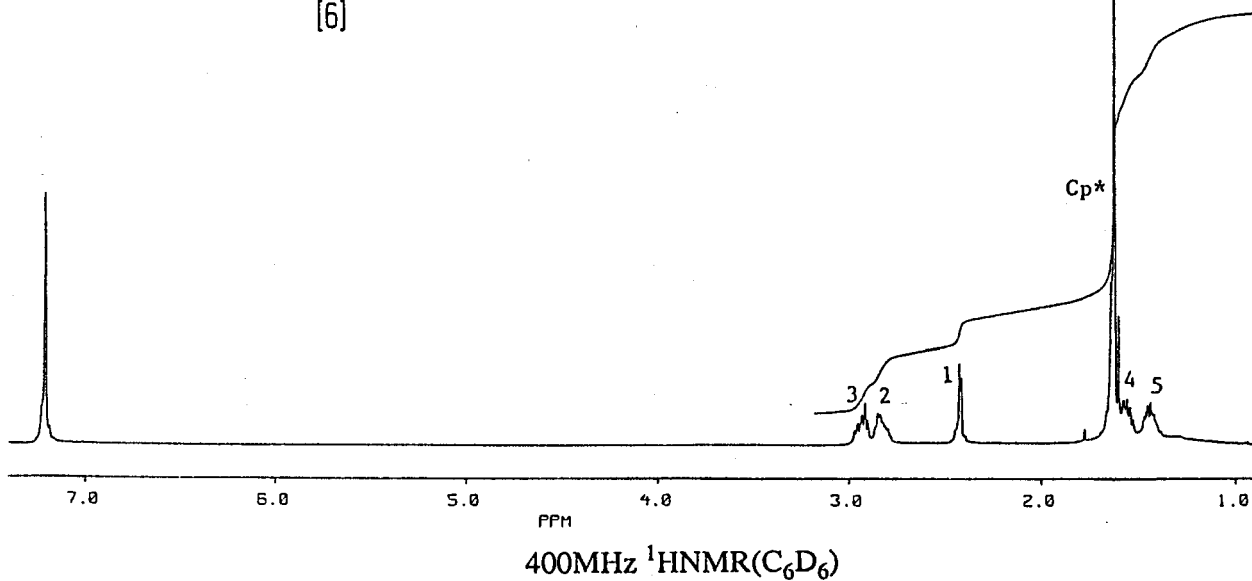
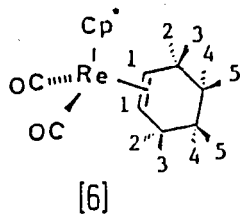


Fig.8. ^1H NMR Spectrum

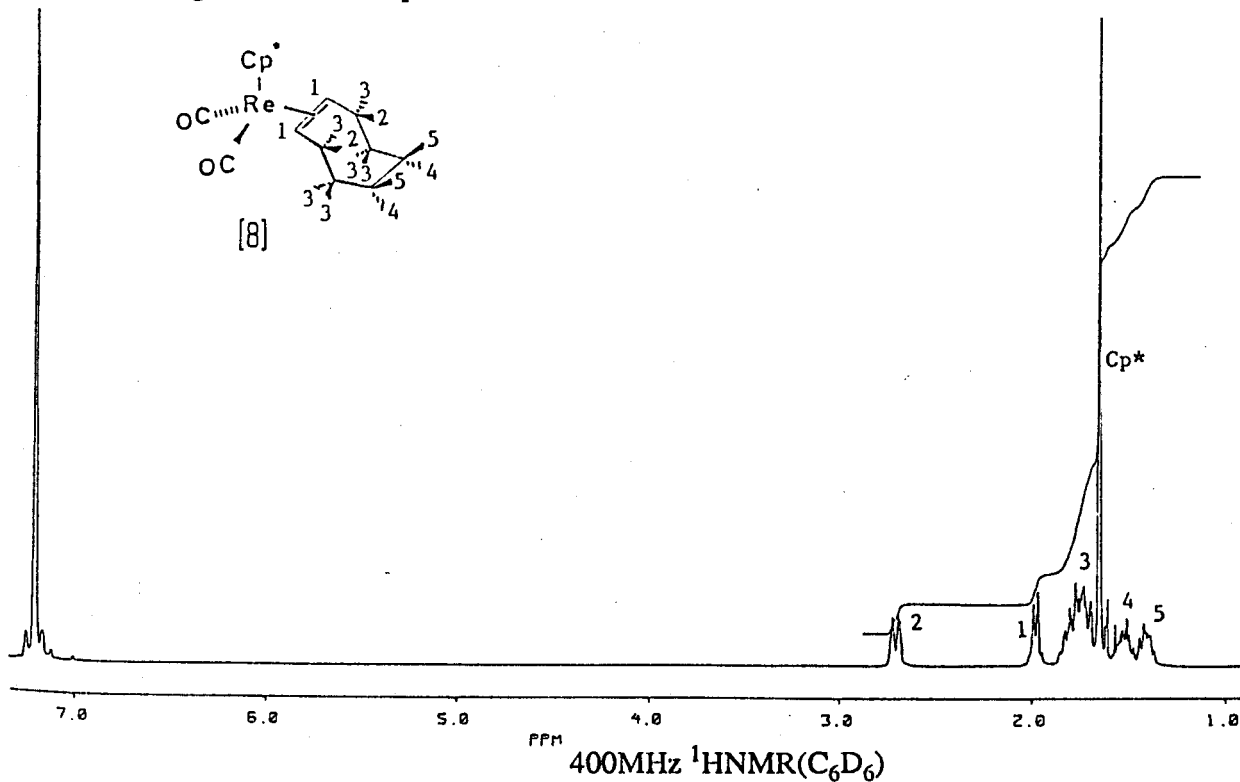
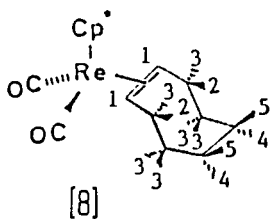
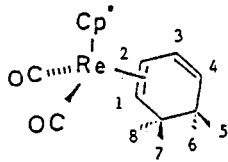


Fig.9. ^1H NMR Spectrum



[10]

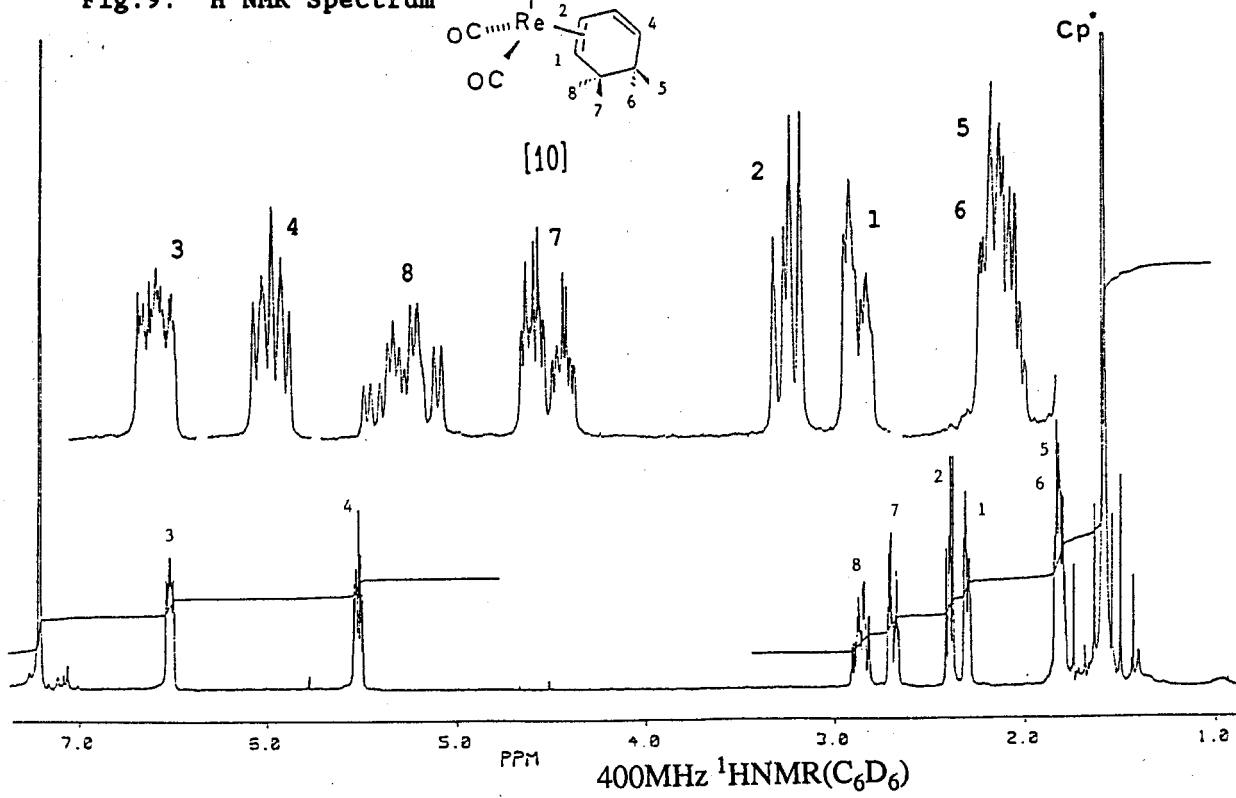
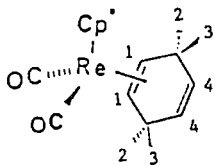


Fig.10. ^1H NMR Spectrum



[11]

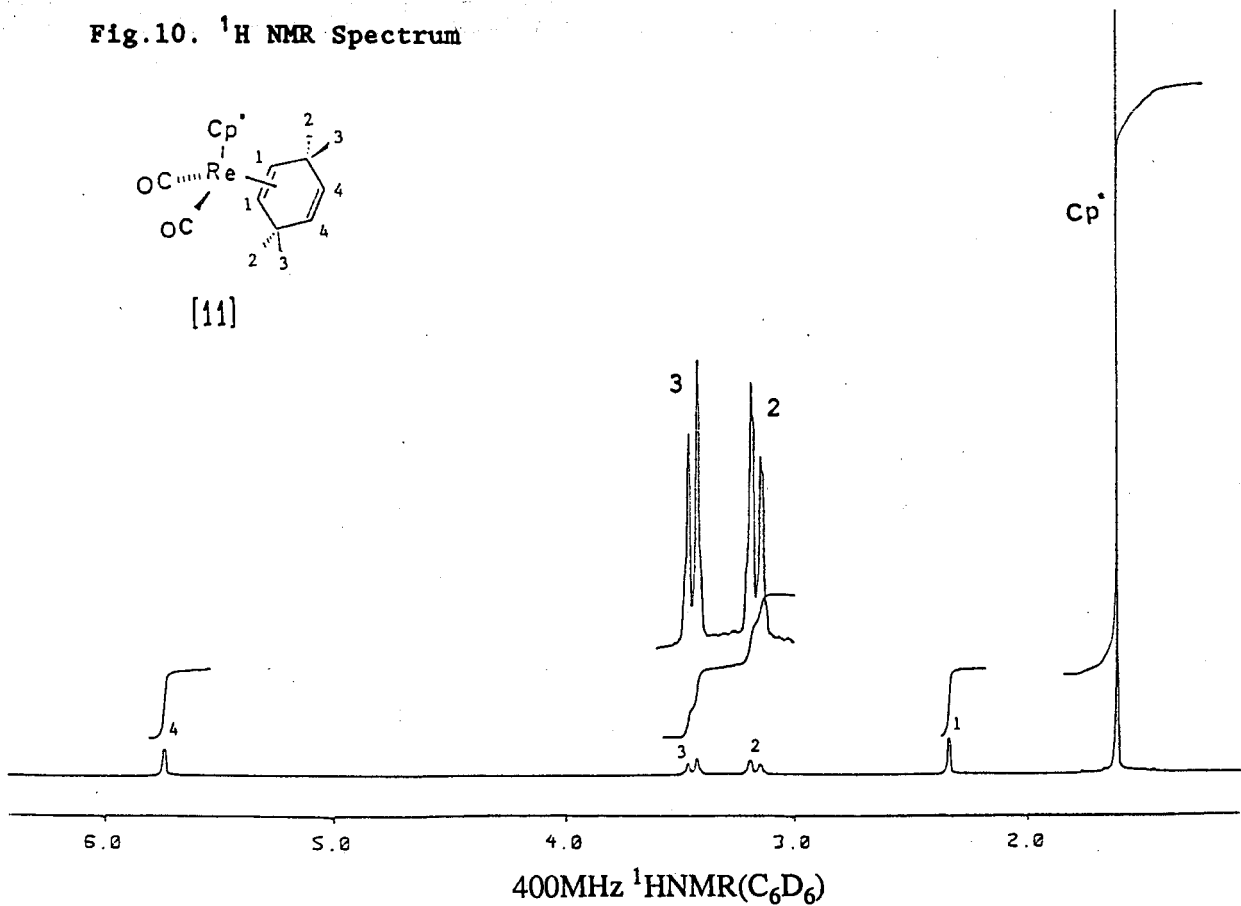
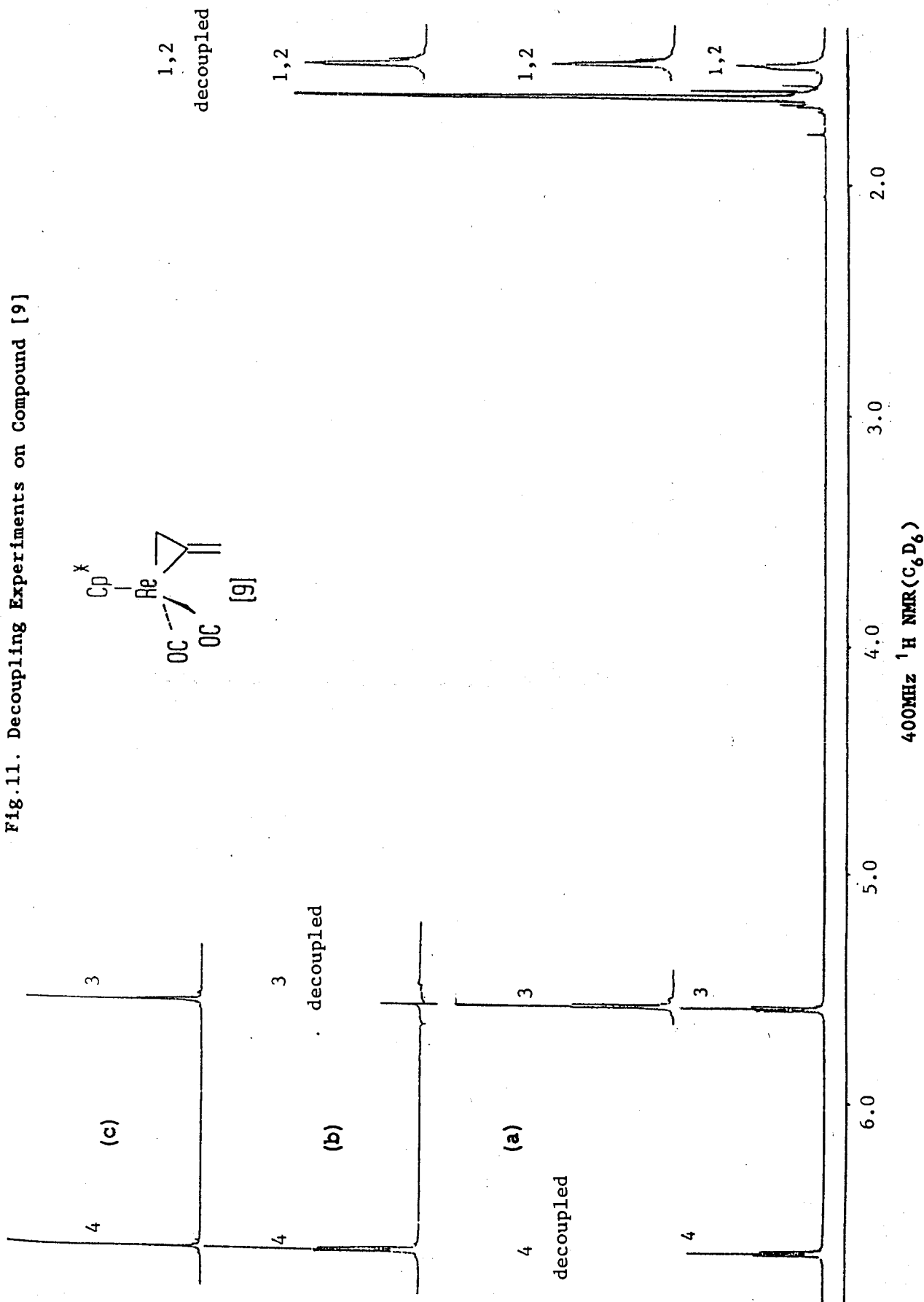


Fig.11. Decoupling Experiments on Compound [9]



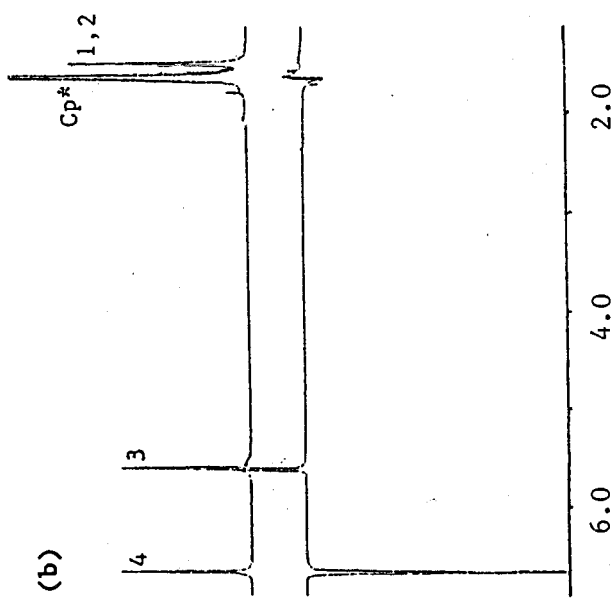
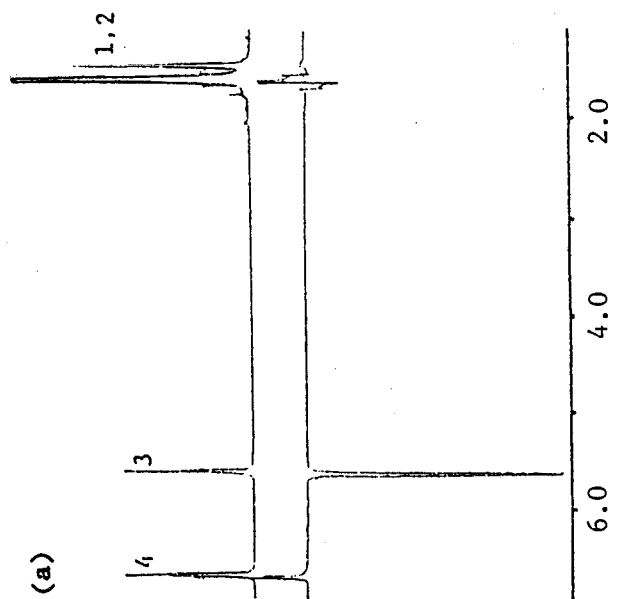
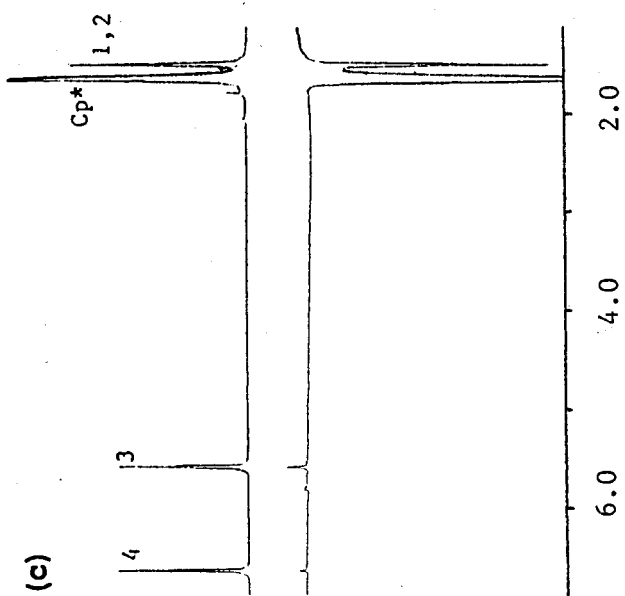
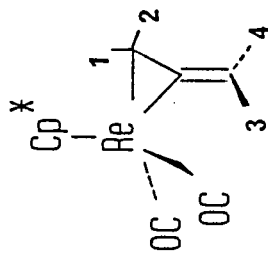


Fig. 12(a-c). NOE Experiments on Compound [9]

400MHz ^1H NMR(C_6D_6)



[9]

2.5. Discussion

2.5.1. ^1H NMR Spectroscopy

The room temperature 400 MHz ^1H NMR spectrum of the ethene complex [1] exhibits only a single resonance for the four ethene protons at δ 1.68 ppm indicating a rapid rotation of the ethene ligand at this temperature. The propene complex [2] exhibits individual resonances for protons H(1), H(2) and H(3), and the methyl protons H(4) as listed in Table 5. The multiplet at δ 1.97 with coupling to each olefinic proton and three methyl protons was reasonably assigned to H(3). The doublet of doublets at δ 2.16 with a larger coupling ($J_{1,3} = 12.1\text{Hz}$) was assigned to H(1) *trans* to H(3), and the doublet of doublets at δ 1.35 with a coupling ($J_{2,3} = 9.8$) was assigned to H(2) *cis* to H(3), because the *trans*-olefinic coupling constants are usually larger than *cis*-olefinic coupling constants, i.e., $J_{\text{cis}} = 6\text{-}12\text{ Hz}$, $J_{\text{trans}} = 12\text{-}18\text{ Hz}$.³⁸ It is not possible to determine whether the propene is static or rotating in this complex from the ^1H NMR spectrum.

The assignments for the complexes [5], [6], [9] and [10] were determined by decoupling or NOE experiments. In the case of the *cis*-2-octene complex [5], the triplet at δ 1.00 with a relative intensity three and a coupling ($J_{5,6} = 6$) was assigned the three

equivalent methyl protons H(6); this collapsed to a singlet when irradiating H(5). The multiplet at δ 1.37-1.45 with a relative intensity six was assigned to the methylene protons H(5). The broad multiplet at δ 1.53-1.61 with a relative intensity two was assigned to the methylene protons H(4). The doublet at δ 1.87 with a relative intensity three and a coupling ($J_{1,2} = 6$) was assigned to the methyl protons H(1), as it collapsed to a singlet while irradiating H(2). The multiplet at δ 2.52, with a relative intensity one, was assigned to H(2), and collapsed to a broad doublet with a coupling ($J_{2,3} = 9.8\text{Hz}$) upon irradiation at H(1). The multiplet at δ 2.40, with a relative intensity one, was assigned to H(3); it collapsed to a broad doublet with a coupling ($J_{2,3} = 9.8\text{Hz}$) while irradiating H(4). In the case of the cyclohexene complex [6], the two multiplets upfield at δ 1.57 and 1.45 with a relative intensity two each were assigned to protons H(4) and H(5) respectively, assuming H(5) which is closer to Cp^* to have the upper field chemical shift at δ 1.45; thus, H(4) occurred at δ 1.57. The two multiplets at δ 2.85 and 2.91, with a relative intensity two each, were assigned to protons H(2) and H(3) respectively, again assuming H(2) to be close to Cp^* and thus to be at δ 2.85. The doublet of doublets at δ 2.42, with a relative intensity two, was assigned to H(1), and give a AA'BB' complex pattern with a coupling $J_{1,2} = 2$ (or $J_{1,3} = 3$) when irradiating H(3) (or H(2)). In the case of the η^2 -1,3-cyclohexadiene

complex [10], the two multiplets downfield at δ 6.52 and 5.52 were assigned to protons H(3) and H(4) of the uncoordinated double bond. The inner proton H(3) was downfield (at δ 6.52) relative to the outer proton H(4) (at δ 5.52). Irradiating H(4) caused the resonance for H(3) to collapse to a broad doublet with a coupling ($J_{2,3} = 5.5\text{Hz}$). Irradiating H(3) caused the resonance for H(4) to result in a broad triplet (AMXX' splitting pattern) with couplings $J_{2,4} = 1$ and $J_{4,5(6)} = 5.5\text{ Hz}$. The multiplet at δ 2.40 was assigned to H(2), as it gave a doublet of doublets with couplings ($J_{1,2} = 9$, $J_{2,4} = 1\text{ Hz}$) when irradiating H(3). Irradiating H(2) caused the resonance for H(3) to collapse to a broad doublet of doublets with coupling $J_{3,4} = 10$ and $J_{3,5(6)} = 1.5\text{ Hz}$. The multiplet at δ 2.31 was assigned to H(1), as it gave a broad doublet with a coupling ($J_{1,2} = 9\text{ Hz}$) upon irradiation of H(7) or H(8). The two multiplets at δ 2.70 and 2.87 were assigned to H(7) and H(8). These gave two ABXX' complex splitting patterns with couplings ($J_{7,8} = 14$, $J_{5(6),7} = 5$, $J_{5(6),8} = 7\text{ Hz}$) respectively upon irradiation of H(1) and H(2) together. In the case of the allene complex [9], at 22°C the resonances for protons H(3) and H(4) each appear as triplets at δ 5.60 and 6.67 ppm, and the two protons H(1) and H(2) appear to give a broad resonance at δ 1.48 ppm, Fig.11. Irradiating H(4) or H(3) (Fig.11 (a) or (b)) simplified the resonance for H(1)/H(2) but had little effect on H(3) or H(4) respectively. Irradiating H(1)/H(2) (Fig.11 (c)) caused the resonances for H(3) and H(4) to collapse to

singlets. Hence $J_{3,4} = 0$ $J_{1(2),3} = 2.7$ and $J_{1(2),4} = 2.7$ Hz. Application of NOE procedures further distinguishes between H(3) and H(4) and shows that H(3), which is upfield relative to H(4), most closely approaches the Cp* group. The evidence is that irradiation of Cp* (and unavoidably also H(1) and H(2)) induces an obvious strong enhancement of H(3) but only a small enhancement of H(4) (Fig.12(c)).

The resonances for the remaining alkene complexes [3], [4], [7], [8] and [11]-[13] listed in Table 5 were all assigned by chemical shifts, coupling constants and the proton relative intensity. The ^1H NMR spectrum of 2-pentene complex [3] showed the presence of two isomers, *cis* and *trans* (ratio: *cis/trans* = 1/1.7). The protons of [3]*cis* were assigned by comparison with those of *cis*-2-octene complex [5]. It is not difficult to assign the methyl protons H(1), H(5) (at δ 2.06, 1.23 respectively) and the methylene protons H(4) (at δ 1.86) in the isomer [3]*trans* by the relative intensity and splitting patterns with couplings as listed in Table 5. However, it is not possible to distinguish between H(2) and H(3) from the ^1H NMR spectrum. In the case of 1-octene complex [4], the methyl protons H(6), methylene protons H(5) and vinylmethylene protons H(4) were first assigned by the relative intensity and splitting patterns with couplings as listed in Table 5. The doublet at δ 2.19, with a coupling ($J_{2,3} = 10.5$ Hz), was assigned to H(2). The remaining two multiplets were at δ 2.47 and

2.01 ppm. The larger chemical shift multiplet (δ 2.47) was assigned to H(1), and the lesser (δ 2.01) to H(3) by comparison with the propene complex [2] (for which H(1) was upfield relative to H(3)). The resonances for the complexes [7] and [8] were assigned by comparison with those of the complex [6] and on the basis of the relative intensity and splitting patterns with couplings as listed in Table 5. Similarly, it is possible to assign the protons of complex [12], as listed in Table 5, by comparison with those of the propene complex [2]. In the case of 1,4-cyclohexadiene complex [11], only four resonances were present in ^1H NMR indicating it was a symmetrical structure. The broad singlet at δ 5.74 was assigned to the two uncoordinated olefinic protons H(4). The broad singlet at δ 2.34 was assigned to the two coordinated olefinic protons H(1). The two doublets at δ 3.17 and 3.44 were assigned to H(2) and H(3) respectively, assuming H(2) to be close to Cp^* ring. The protons of η^4 -cyclohexadiene complex [13] were assigned by comparison with previous reported values for the similar compounds: $\text{CpIr}(\eta^4\text{-cyclohexadiene})$,³⁹ $\text{CpRh}(\eta^4\text{-cyclohexadiene})$,⁴⁰ $\text{CpCo}(\eta^4\text{-cyclohexadiene})$,^{36a} and $\text{Cp}^*\text{Ir}(\eta^4\text{-cyclohexadiene})$,^{36b} $\text{Cp}^*\text{Rh}(\eta^4\text{-cyclohexadiene})$.^{36b} In general, the chemical shifts of inner η^4 -diene protons are down field as compared with outer η^4 -diene protons. So the two multiplets at δ 3.22 and 2.95, with a relative intensity two each, were assigned to the inner protons H(1) and the outer protons H(2) respectively. The broad mutiplet at δ 1.30-1.44,

with a relative intensity four, was assigned to the remaining four protons H(3).

The η^2 -allene ligand is known to rotate in the complexes of iron and platinum.⁴¹ We therefore investigated whether rotation was occurring in the complex [9] by recording the variable temperature ¹H NMR. Such rotation would explain why H(1) and H(2) were appearing to be equivalent at 22°C and producing the broad signal. Fig.14 shows the ¹H NMR spectrum of [9] from 183K to 243K in the region 1.0-2.5 ppm only. The resonances for H(3) and H(4) were unaffected and are not shown. As the temperature is lowered from 273K, the broad resonance at δ 1.48 for H(1)/H(2) collapses into the baseline. Below 213K, two peaks either side of this grow in at δ 2.02 and 0.93 ppm. These begin to sharpen at 183K but at this temperature the limiting sharp spectrum has not yet been reached.

The rotational energy barrier ΔG^* for allene rotation around the Re-allene axis was determined by temperature-dependent ¹H NMR spectra of the allene complex [9] in toluene-*d*₈ (see Fig.14). At T = 183K, the lifetime of both (A) and (B) in Fig.13 is long relative to the timescale of the NMR experiment so that the spectrum shows two distinct peaks. This indicates that the allene rotation is very slow at this temperature. As the sample is warmed up, the two distinct peaks for H(1) and H(2) begin to broaden and merge (T = 193-213K), and at the coalescence temperature, T_c = 223K, they coalesce into a single broad peak with a flat top. On further

Fig.13. η^2 -Allene Rotation and 1,2-Shift in [9]

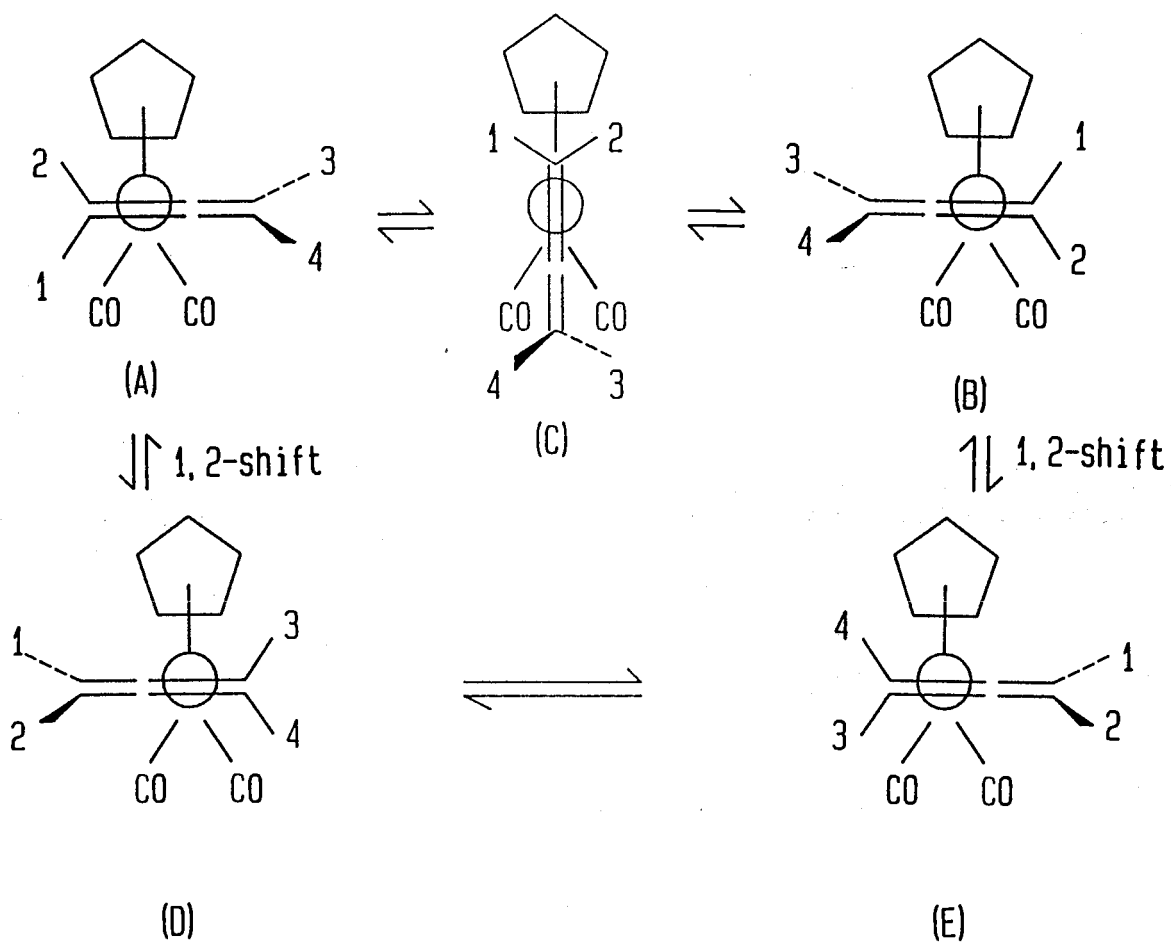
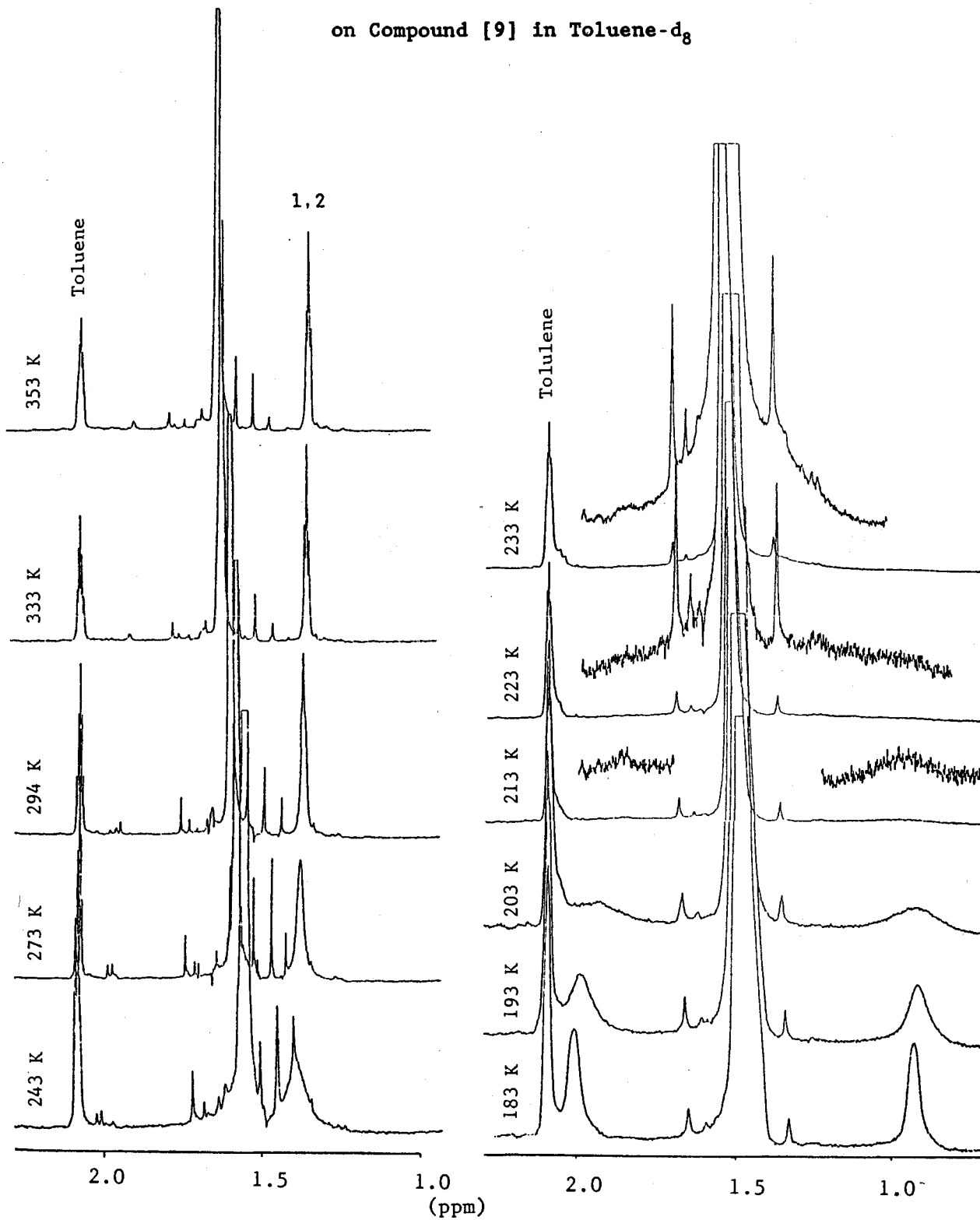


Fig.14. Variable-temperature ^1H NMR(400MHz) Experiments

on Compound [9] in Toluene- d_8



warming, the single peak sharpens ($T = 294\text{K}$), the allene rotation becoming fast at temperatures above 294K (21°C), where the lifetimes of both (A) and (B) are short relative to the timescale of the NMR experiment. There are several important equations that are applied at various temperatures.⁴² An approximation for obtaining rate constants at temperatures where slow allene rotation is taking place ($T = 193\text{-}213\text{K}$) involves using eq.29.

$$k = \pi\Delta\nu_s \quad \text{eq.29.}$$

where k is in s^{-1} , and $\Delta\nu_s$ is the peak broadening, and usually taken to be the difference between the observed peak width at half-height of the broadened peak and the peak width at half-height of the peak at the slow rotation limit (approximately $T = 183\text{K}$).

At the coalescence temperature ($T_c = 223\text{K}$), the rate constant for allene rotation can be obtained from eq.30.

$$k = \pi|\nu(1)-\nu(2)|/\sqrt{2} \quad \text{eq.30.}$$

where $\nu(1)-\nu(2)$ is the chemical shift difference between H(1) and H(2) at the slow rotation limit (in Hz; approximately $T = 183\text{K}$).

After coalescence, the rate constant can be calculated using the fast exchange between (A) and (B) approximation given by

equation 31.

$$k = \pi(v(1)-v(2))^2/2\Delta v_f \quad \text{eq.31.}$$

where Δv_f is the peak broadening, and is usually taken to be the difference between the observed peak width at half-height of the broadened peak and the peak width at half-height of the peak at the fast allene rotation limit ($T = 294\text{K}$).

The calculated values of rate constant k for allene rotation at different temperatures are listed in Table 6.

Table 6. Data for k and ΔG^* for Complex [9]

$T(^{\circ}\text{K})$	193	203	213	223	233	243	273
$k(\text{s}^{-1})$	18.8 ^a	87.2 ^a	195 ^a	955 ^b	^c 2.19×10^3	^c 10.1×10^3	^c 105×10^3
ΔG^{*d}	9.97	9.89	10.0	9.85	9.93	9.64	9.62

^aAs calculated by using eq.29. ^bAs calculated by using eq.30. ^cAs calculated by using eq.31. ^dAs calculated by using eq.33 in kcal/mol.

The Eyring equation (eq.32) gives the relationship of the rate constant k and free energy activation ΔG^* .

$$k = (kT/h)\exp(-\Delta G^*/RT) \quad \text{eq.32.}$$

thus,

$$\Delta G^* = -RT[\ln(k/T) + \ln(h/k)] \quad \text{eq.33.}$$

where

$$R = \text{Gas constant} = 1.98 \text{ cal/K.mol}$$

$$k = \text{Boltzmann's constant} = 1.3805 \times 10^{-16} \text{ erg/K}$$

$$h = \text{Planck's constant} = 6.63 \times 10^{-27} \text{ erg.sec}$$

The values of ΔG^* at different temperatures can be directly calculated by using the eq.33 and the data are listed in Table 6. Then, a straight line was drawn by fitting the free energy of activation ΔG^* at different temperatures to the eq.34 (see Fig.15). The straight line of ΔG^* vs. $(-T)$ can be expressed by the following eq.35 as well.

$$\Delta G^* = \Delta H^* - T\Delta S^* \quad \text{eq.34.}$$

$$\Delta G^* = 10.9 \times 10^3 - 4.7T \quad \text{eq.35.}$$

thus,

$$\Delta H^* = 10.9 \pm .3 \text{ kcal/mol}$$

$$\Delta S^* = 4.7 \pm 1.4 \text{ cal/K.mol}$$

Fig.15. A Plot of the ΔG^* Values vs. (-T)

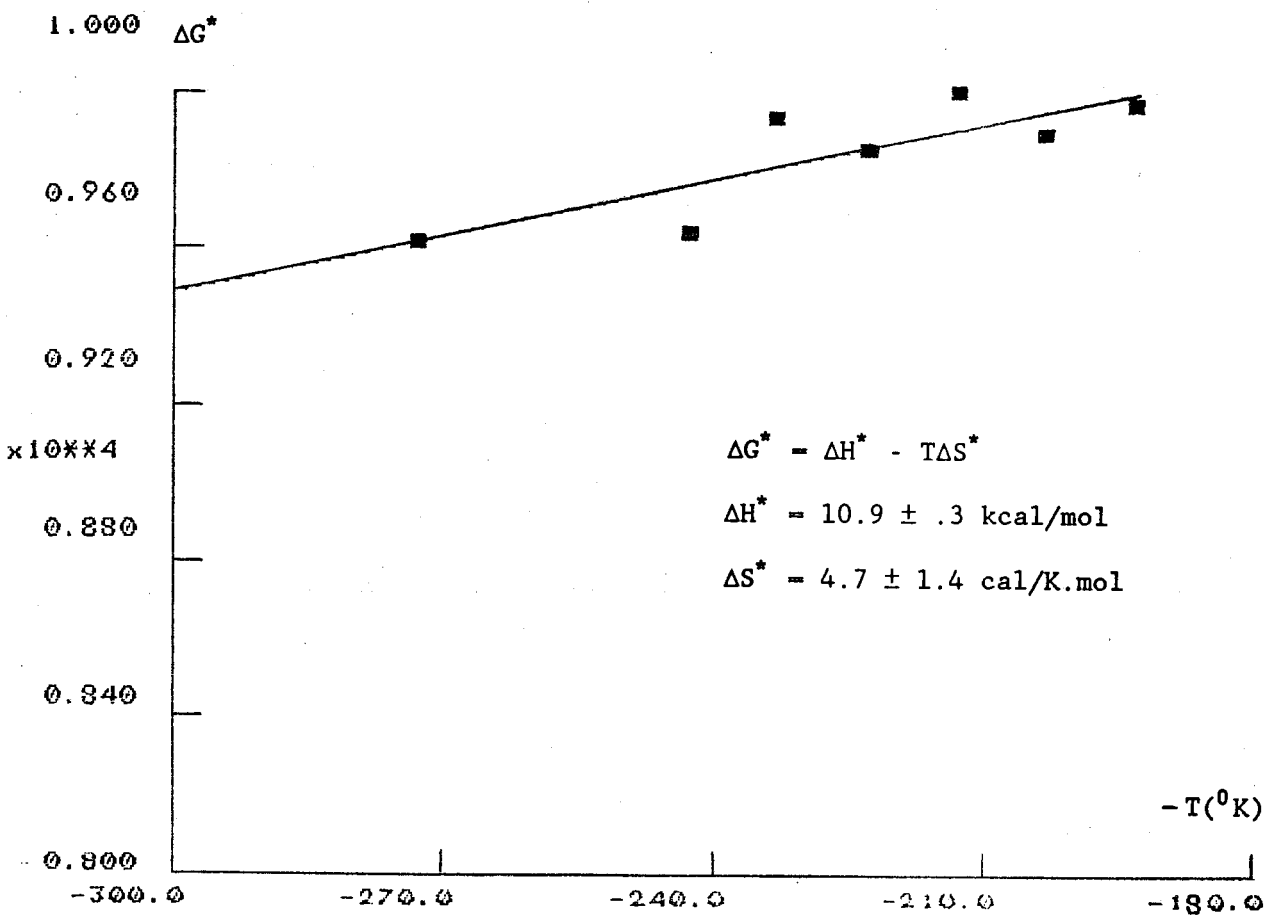
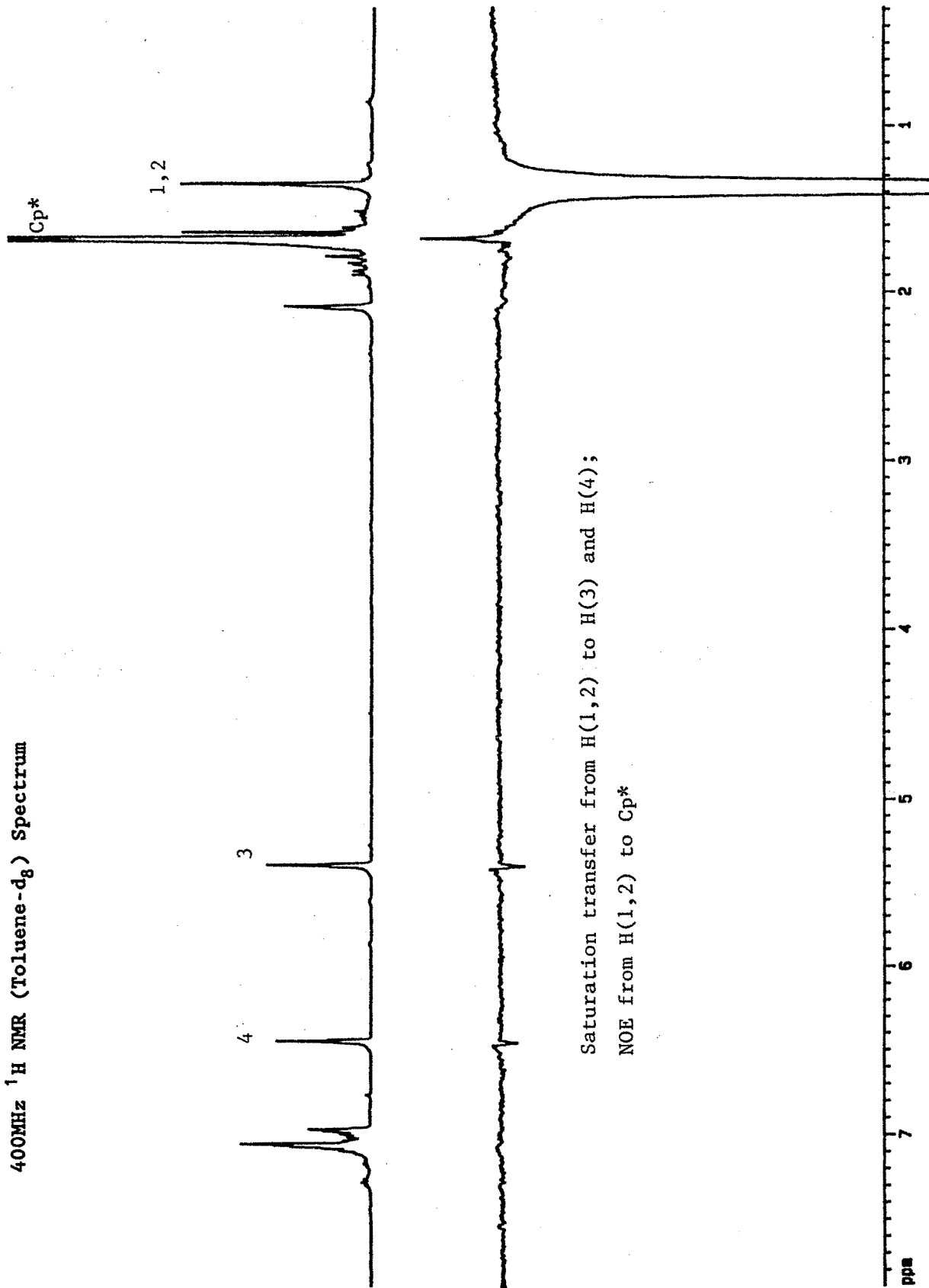


Fig. 16. Saturation Transfer Experiments on [9] at 100°C

400MHz ¹H NMR (Toluene-d₈) Spectrum



Saturation transfer from H(1,2) to H(3) and H(4);
NOE from H(1,2) to Cp*

The activation free energy (9.85 kcal/mol) determined from the NMR coalescence temperature is well within the range of allene rotational barriers (7-13 kcal/mol) observed for a number of neutral or cationic metal-allene complexes of platinum and iron.⁴¹ A comparison of allene rotational barriers between two isoelectronic analogs, the cationic iron complex^{41a} $[\text{CpFe}(\text{CO})_2(\eta^2\text{-allene})]^+$ (< 8 kcal/mol) and the complex [9] $\text{Cp}^*\text{Re}(\text{CO})_2(\eta^2\text{-allene})$, shows that a smaller allene rotational barrier is present in the cationic allene complex of iron. This could be explained by a smaller back-bonding interaction from iron to the π^* bond of allene, so that the electronic component of the rotational barrier is less important in the case of the cationic complex than in the case of the neutral complex [9]. In addition, the saturation transfer results at higher temperature (100°C) indicate a transfer of magnetization from protons H(1,2) to H(3) and H(4) with weak intensities, and also a NOE from H(1,2) to Cp^* (see Fig.16). It indicates that the 1,2-shift process (see Fig.13) is quite slow even at 100°C. Thus, we may conclude that the 1,2-shift barrier in [9] is larger than that in the iron cationic complexes (16-23 kcal.mol⁻¹).^{41a}

2.5.2. Mass Spectra.

The mass spectra of complexes [1]-[13] (Figs.17(a-w)) show interesting variations depending on the nature of the alkene and ancillary ligands.

(i) Linear Olefin Complexes. Firstly, we can compare the ethene complex [1] with propene complex [2] and the 3-methoxypropene complex [22] $\text{Cp}^*\text{Re}(\text{CO})_2(\text{C}_3\text{H}_5\text{OMe})$. The interpretation of the principal fragments for [1], [2] and [22] is given in Schemes 6, 7 and 8.

It is best to discuss the propene complex [2] since alkene loss can be distinguished from CO loss here, but not in the ethene complex [1]. Loss of propene from M^+ gives a moderate intensity peak at m/z 378 and this is followed by loss of 2H from the Cp^* to give a more intense m/z 376 peak. This fragment $[(\text{Cp}^*-2\text{H})\text{Re}(\text{CO})_2]^+$ then loses CO to give the base peak m/z 348. A second process indicated (by the similar intensities of 390 and 378) to be of comparable probability to the loss of propene from M^+ is loss of CO to give the fragment $[\text{Cp}^*\text{Re}(\text{CO})(\text{C}_3\text{H}_6)]^+$, m/z 392, accompanied by rapid loss of 2H to give m/z -390. We presume the 2H are also lost from Cp^* in this step, but we cannot rule out a contribution from the loss of 2H from propene. Subsequent loss of propene also results in the base peak 348, the species $[(\text{Cp}^*-2\text{H})\text{Re}(\text{CO})]^+$. The loss of 2H from Cp^* is well

Fig. 17(a-w). Mass Spectra for the Complexes Shown

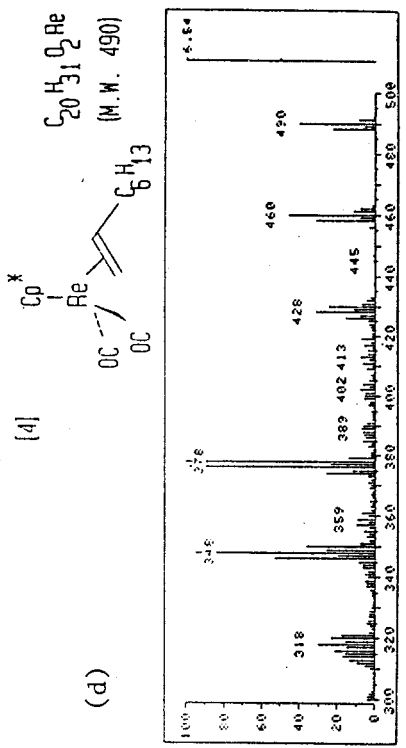
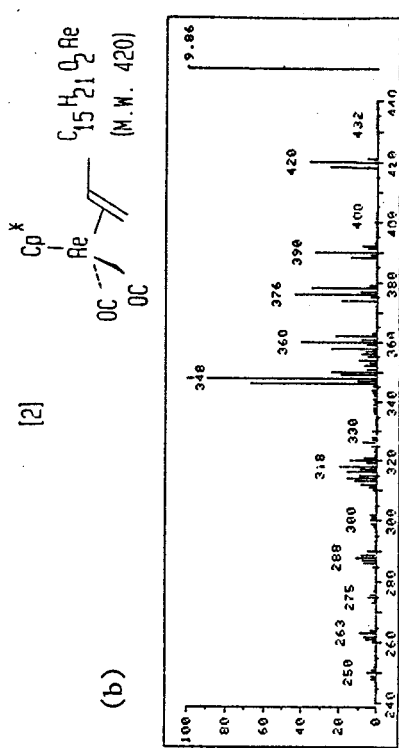
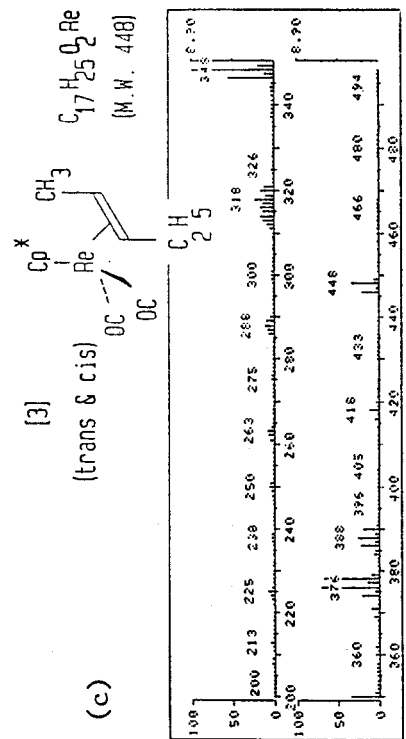
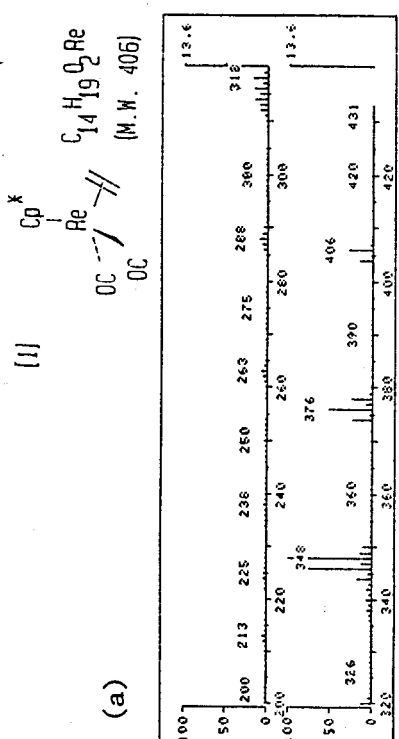


Fig. 17(a-w). Mass Spectra for the Complexes Shown

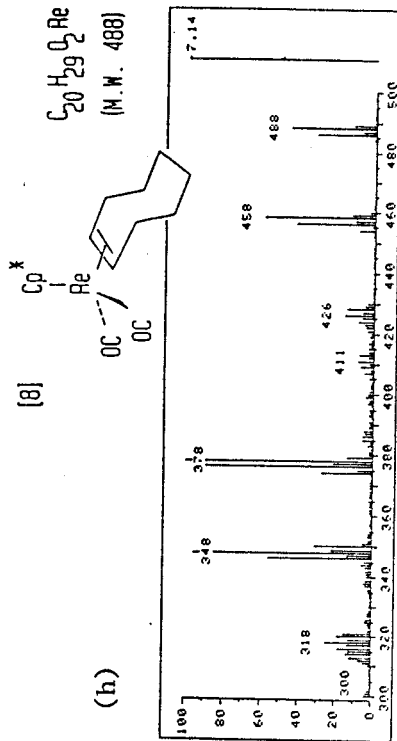
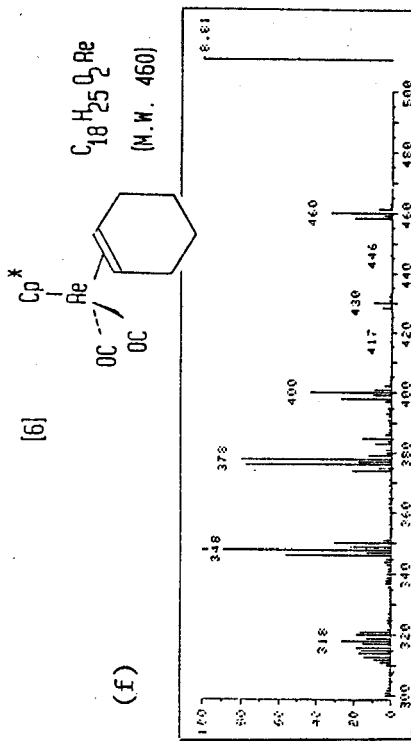
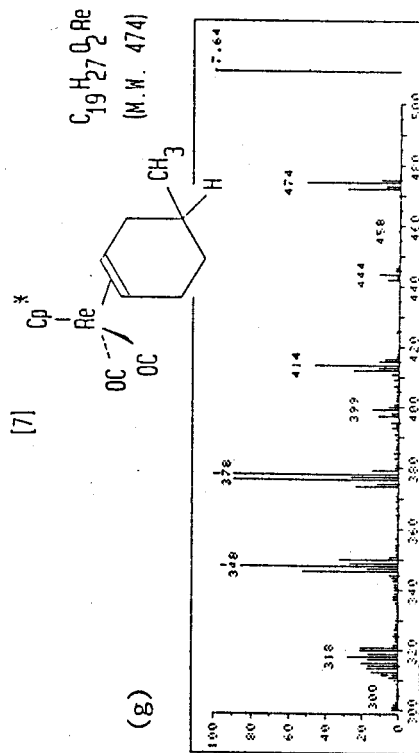
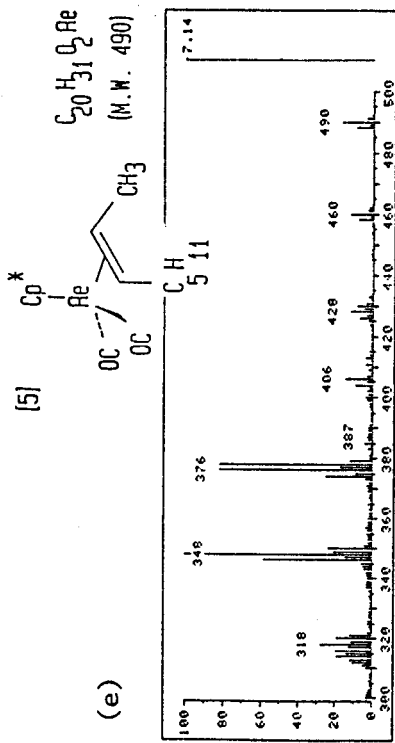


Fig. 17(a-w). Mass Spectra for the Complexes Shown

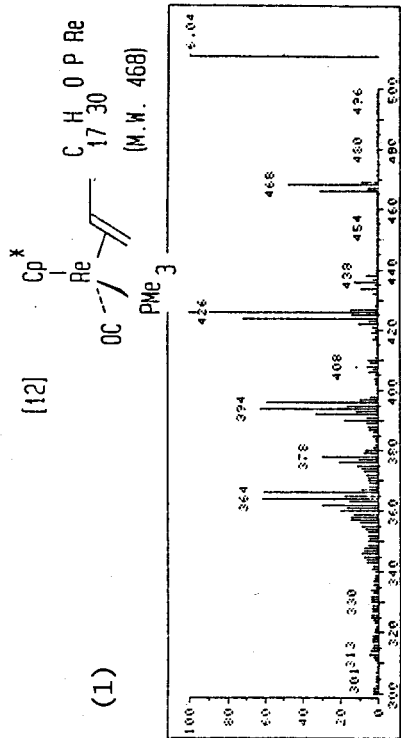
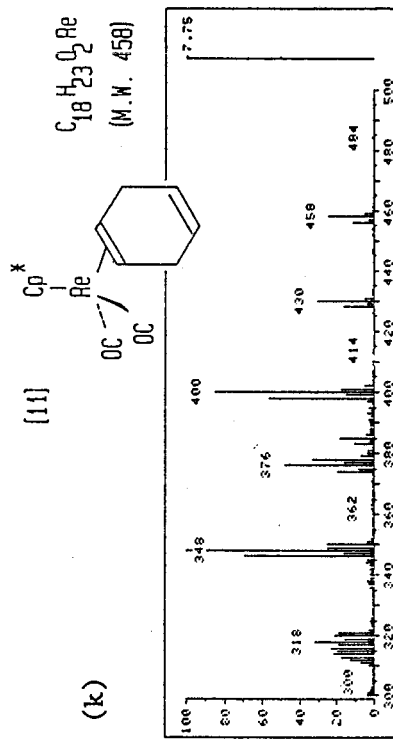
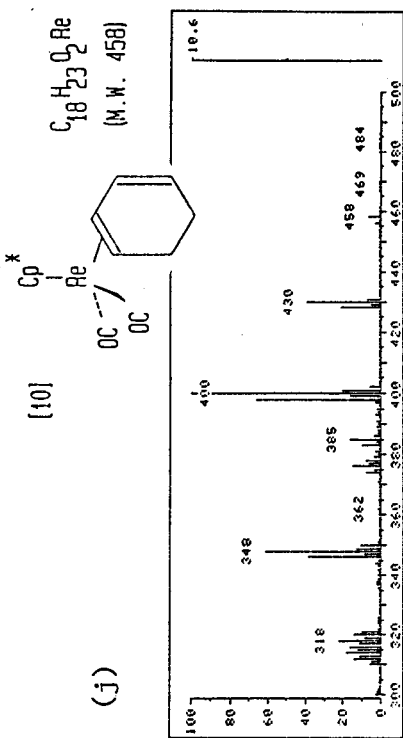
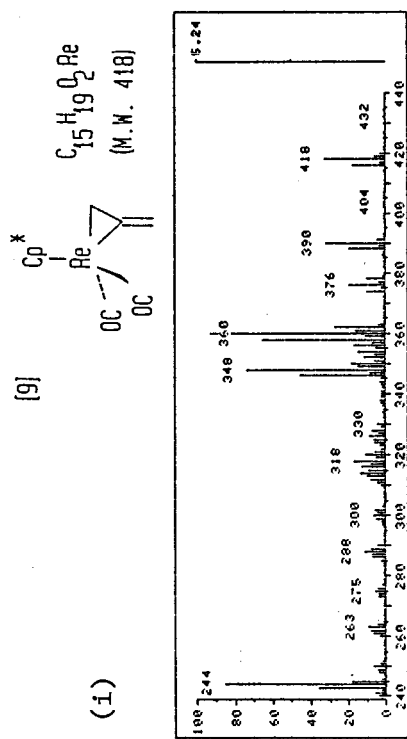


Fig.17(a-w). Mass Spectra for the Complexes Shown

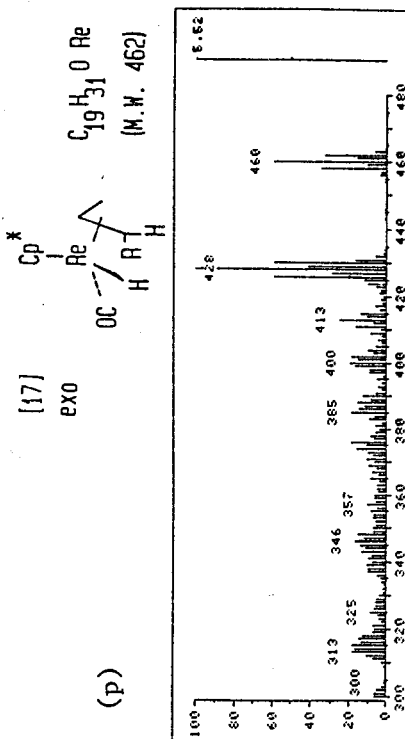
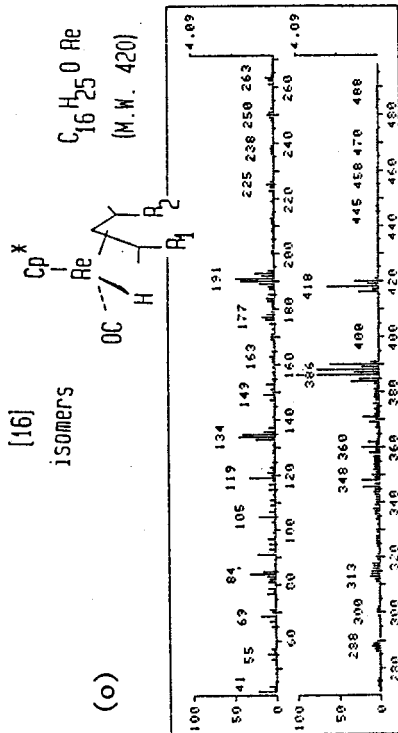
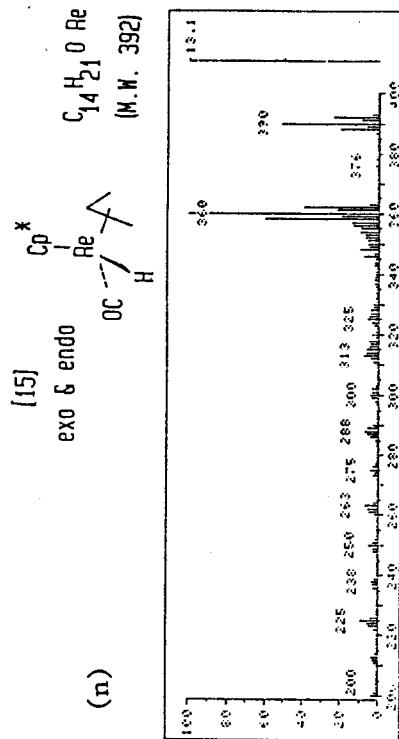
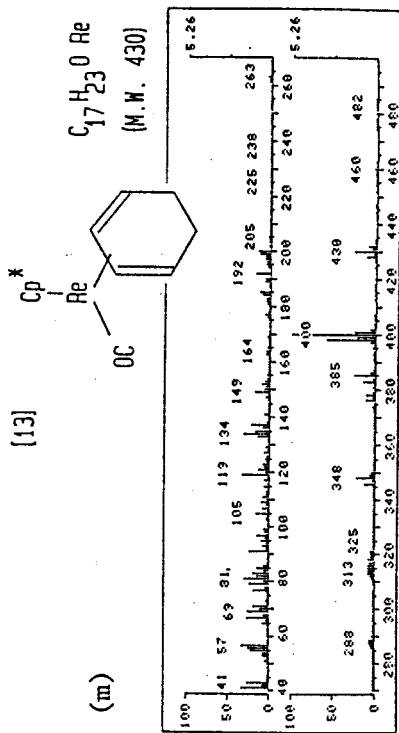


Fig. 17(a-w). Mass Spectra for the Complexes Shown

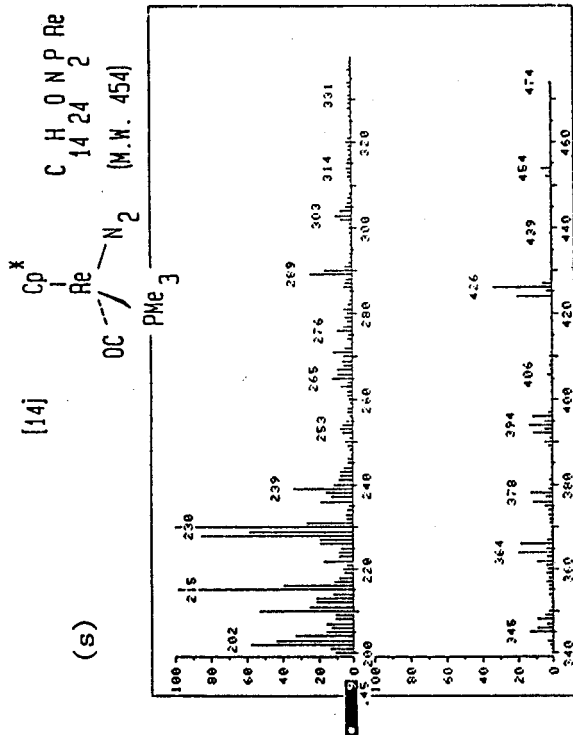
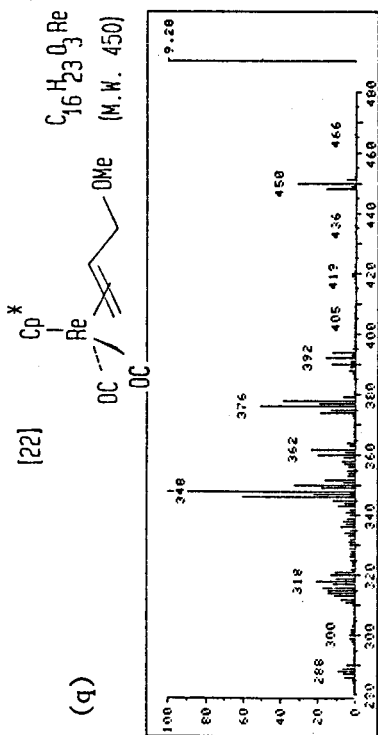
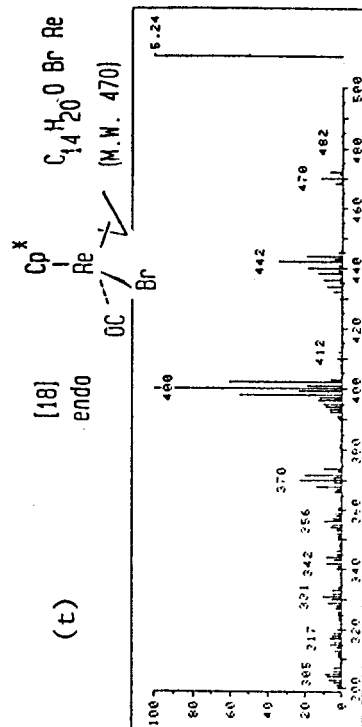
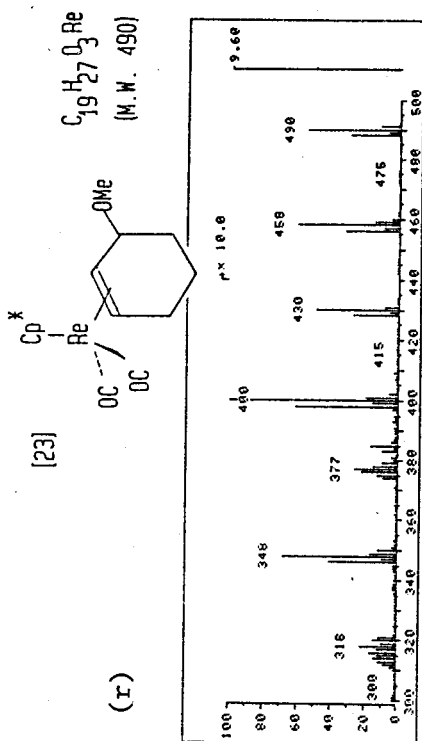
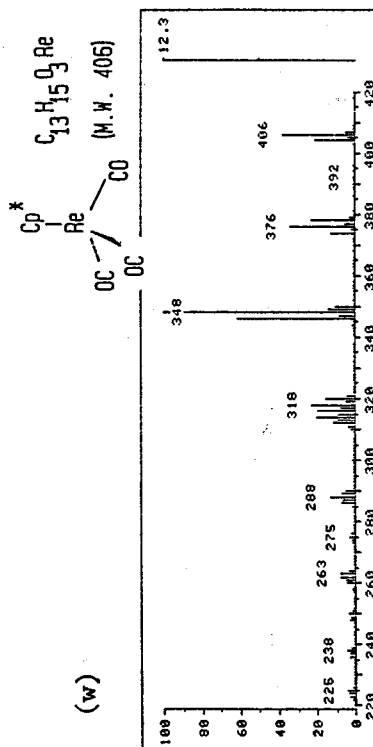
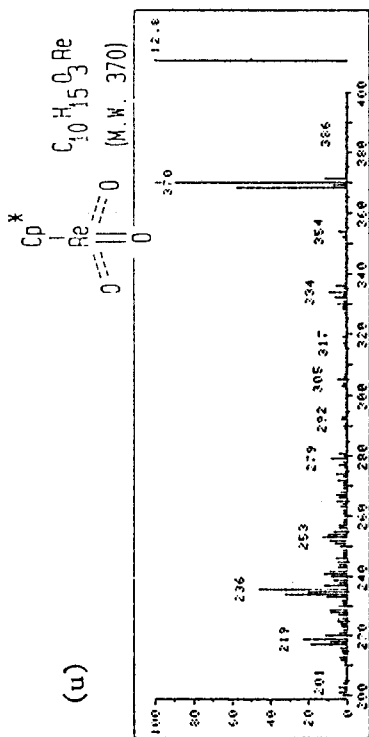
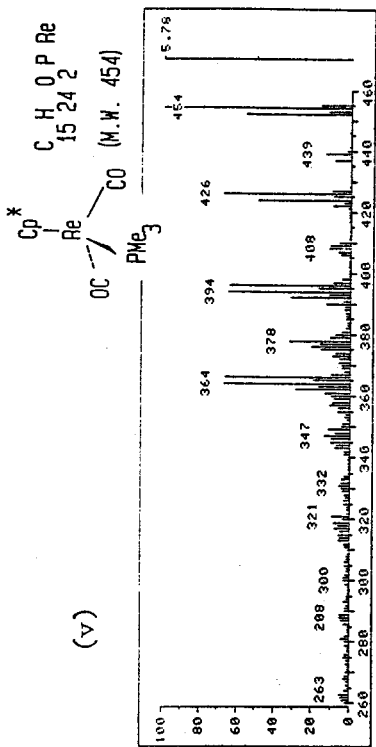
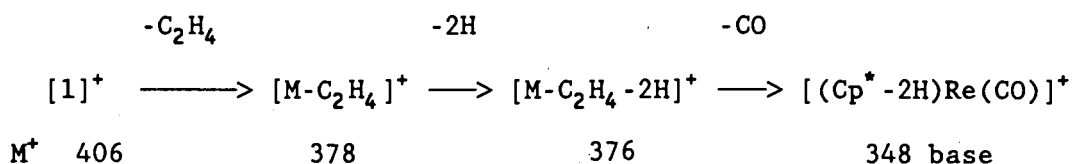


Fig.17(a-w). Mass Spectra for the Complexes Shown

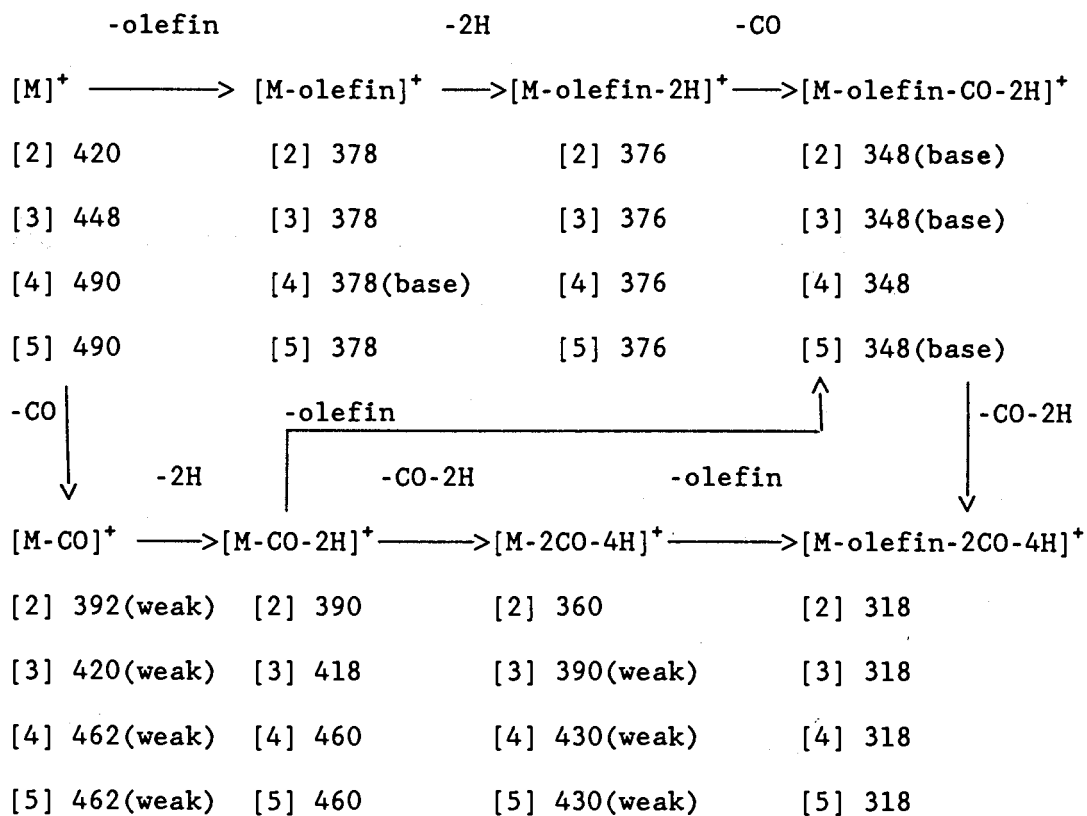


Scheme 6. Fragmentation of Cp*Re(CO)₂(C₂H₄) [1]

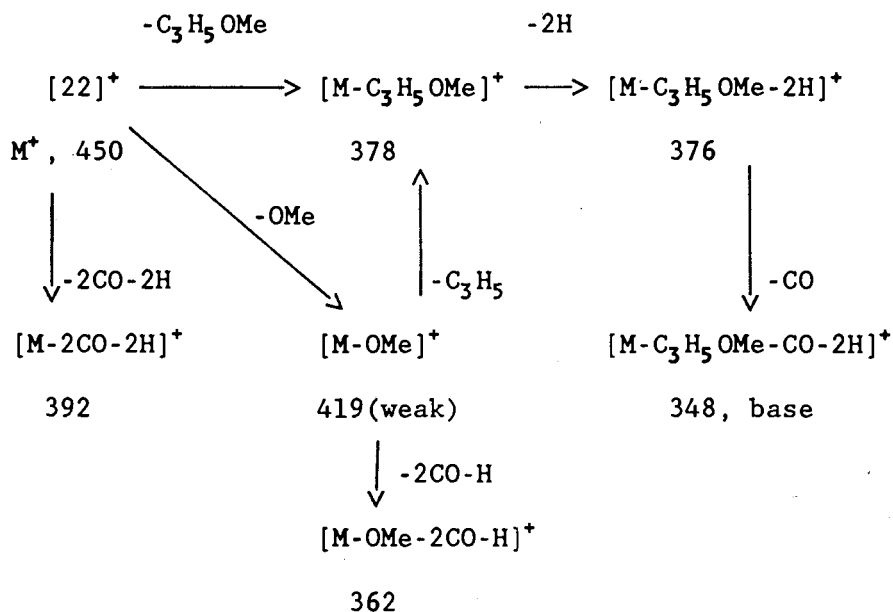


Scheme 7. Fragmentation of linear olefin complexes

[2], [3], [4] and [5]



Scheme 8. Fragmentation of $\text{Cp}^*\text{Re}(\text{CO})_2(\text{C}_3\text{H}_5\text{OMe})$ [22]



documented in Cp^* -rhenium complexes, and this species $m/z=348$ is, for example, observed as the base peak in the fragmentation of $\text{Cp}^*\text{Re}(\text{CO})_3$ ⁴⁷ (see Fig.17(w)). In summary, then, we observe evidence for parallel fragmentation processes; either first loss of CO or propene, accompanied by loss of 2H from Cp^* (more rapid when CO is lost first), then loss of propene or CO respectively. It is notable that loss of the second CO group can occur without release of the propene moiety, giving rise to moderate intensity peaks at $m/z362$ [$\text{Cp}^*\text{Re}(\text{C}_3\text{H}_6)-2\text{H}$]⁺ and $m/z360$ [$\text{Cp}^*\text{Re}(\text{C}_3\text{H}_6)-4\text{H}$]⁺. At the moment, we cannot say whether the propene is still present as such in these species or whether it has lost hydrogen to become an allyl group.

The fragmentation process of 3-methoxypropene complex [22] is similar to the propene complex [2] (see Schemes 7 and 8). The obvious difference between [22] and [2] is that the 3-methoxypropene complex [22] also probably loses OMe to give a very weak peak at m/z 419, which is followed by loss of 2CO accompanied by rapid loss of a single H atom, probably from Cp^* , to give a moderate intensity peak at m/z 362 $[(Cp^*-H)Re(C_3H_5)]^+$. This is the same as the observed peak m/z 362 $[Cp^*Re(C_3H_6)-2H]^+$ for propene [2]. Therefore, it is believed that in this fragment propene has lost one hydrogen to become an allyl group and the second hydrogen loss is from the Cp^* , i.e., $[(Cp^*-H)Re(C_3H_6-H)]^+$.

In view of the fact that the allyl complex cation $[Cp^*Re(CO)_2(C_3H_5)]^+$ has been synthesized in this work (see Chapter IV), it is notable that there is no evidence for loss of a single H atom from M^+ to produce this species in the mass spectrum of [2].

If we can assume that parallel fragmentation processes also operate in the case of the ethene complex [1], then the loss of C_2H_4 is the main contributor to m/z =378, while loss of $(CO+2H)$ and (C_2H_4+2H) both contribute to the more intense m/z 376 peak. This fragment loses CO to give the base peak m/z 348 which is $[(Cp^*-2H)Re(CO)]^+$. The same base peak also observed in the case of propene [2] and complexes [3] and [5]. It may also have a contribution from $[(Cp^*-2H)Re(C_2H_4)]^+$ which must be considered a possibility

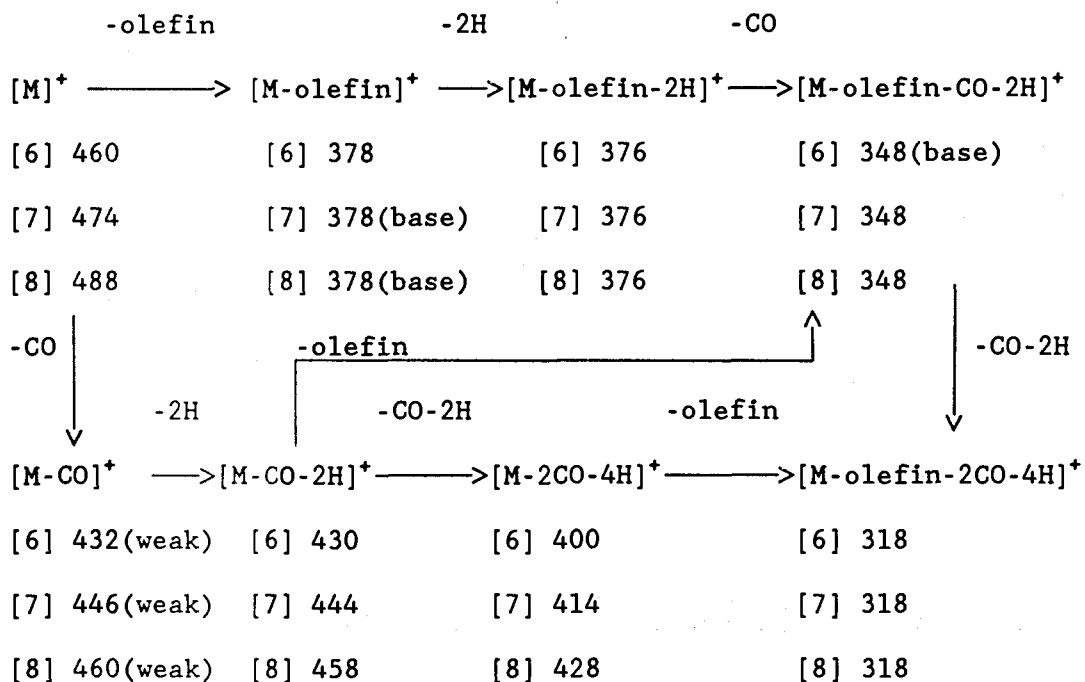
considering the fragments in which propene (or a derivative of propene) were retained in [2] (or [22]) above. Consistent with this is an excessively intense $m/z=346$ peak (too strong just to be the ^{185}Re satellite of $m/z=348$) and an observable peak at $m/z=344$ (likely a ^{185}Re satellite of $m/z=346$). This could be interpreted as the species $[\text{Cp}^*\text{Re}(\text{C}_2\text{H}_4)-4\text{H}]^+$ equivalent to that observed at $m/z=360$ for propene.

The fragmentation of linear olefin complexes [2]-[5] (see Figs.17(b-e)) show some interesting common characteristics: (a) the peak corresponding to the first CO loss $[\text{M-CO}]^+$ is generally quite weak, then a rapid loss of 2H probably from Cp^* , (or from linear olefin; or from both) gives a more intense peak $[\text{M-CO-2H}]^+$; (b) the loss of linear olefin may occur prior to CO, because the intensity of the peak at $m/z=378$ (or 376) corresponding to the fragment $[\text{M-olefin}]^+$ (or $[\text{M-olefin-2H}]^+$) is either the second base peak (in [2], [3] and [5]) or the base peak (in [4]). It implies that the bonding strength of olefin with rhenium is weaker than CO with rhenium, and that the bond strength varies for the different linear olefins.

If we assume the rate of loss of 2H from the fragment $[\text{Cp}^*\text{Re}(\text{CO})_2]$ is very similar in each case ([2], [3], [4] and [5]), then by comparing the relative intensity $[m/z378]/[m/z376]$ (= $[\text{M-olefin}]^+ / [\text{M-olefin-2H}]^+$), we can order the relative rates of olefin loss for different complexes.

Scheme 9. Fragmentation of cyclic olefin complexes

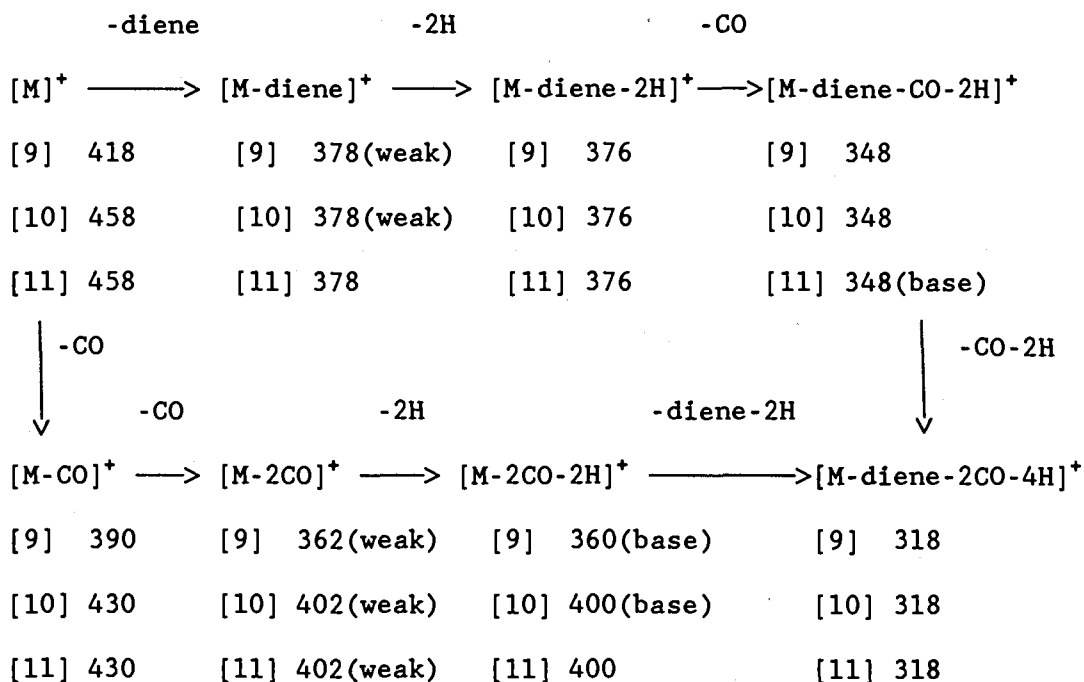
[6], [7] and [8]



(ii) Cyclic Olefin Complexes. The fragmentation of the cyclic olefin complexes [6], [7] and [8] (Scheme 9) is very similar to the linear olefin complexes [2]-[5]. Therefore, comparing the relative intensity $[m/z378]/[m/z376]$ again determines an order of cycloolefin loss from parent complexes.

Scheme 10. Fragmentation of diene complexes

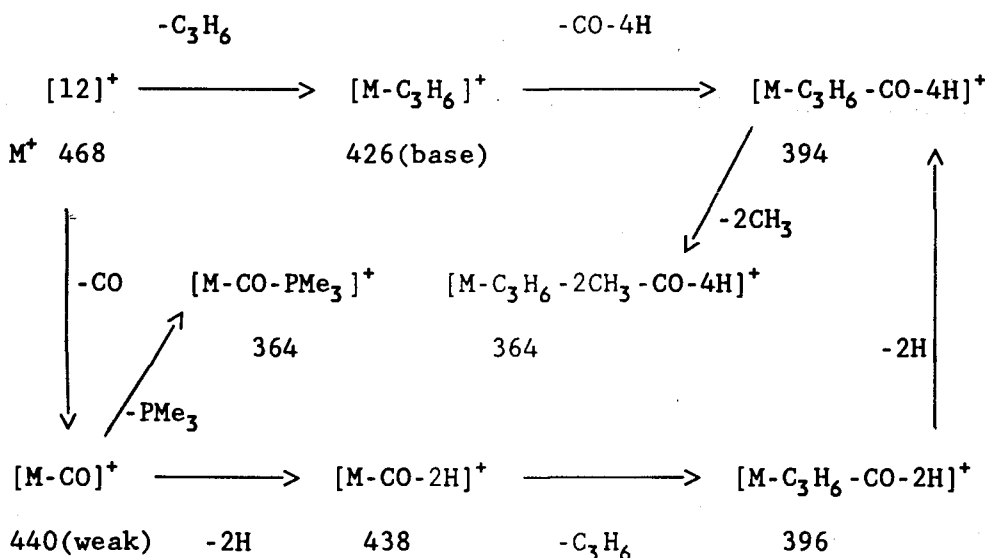
[9], [10] and [11]



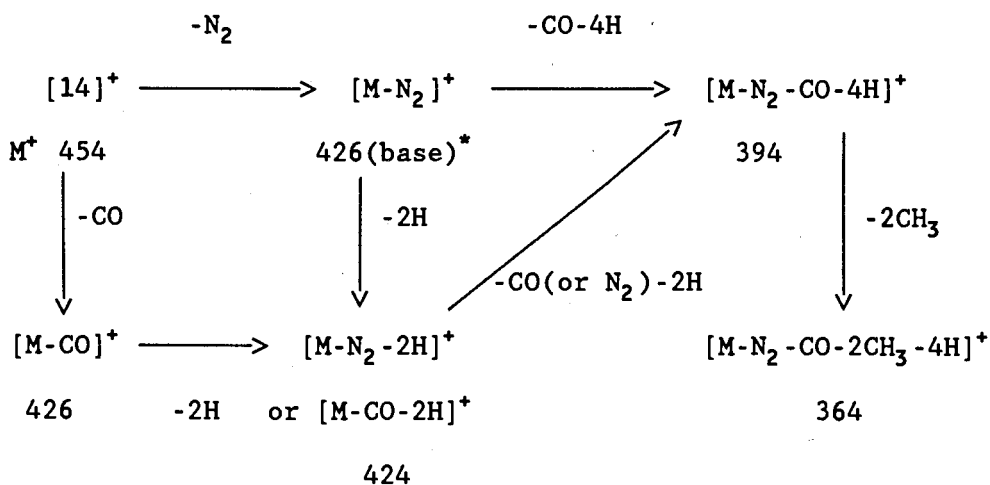
(iii) Diene Complexes. The fragmentation of diene complexes [9], [10] and [11] (Scheme 10) is somewhat different from that of linear or cyclic olefin complexes: (a) the isotopic abundance patterns of $[M\text{-CO}]^+$ are quite close to those expected by computer simulation (for example, see Figs.18(b-c)), which indicates that the first CO loss is not accompanied by 2H loss. But in the case of the η^4 -cyclohexadiene complex [13] (see Fig.17(m)), the loss of one CO is obviously accompanied by 2H loss; (b) the second CO loss is followed by a rapid 2H loss probably from Cp^* in [9], (or from

cyclic olefin; or from both in [10] and [11]); (c) In contrast to the linear or cyclo-olefins, loss of two CO's probably occurs in preference to loss of diene. The intensity of the peak corresponding to $[M-2CO-2H]^+$ is either the base peak (in [9] and [10]) or the second base peak (in [11]). However, the peaks of $[M-diene]^+$ are present in each case, although peak intensities vary with different dienes. In a similar manner to that discussed above (2.5.2.(1)), comparing the relative intensities $[m/z378]/[m/z376]$ can give the order of diene loss from the parent complexes.

Scheme 11. Fragmentation of $Cp^*Re(CO)(PMe_3)(C_3H_6)$ [12]

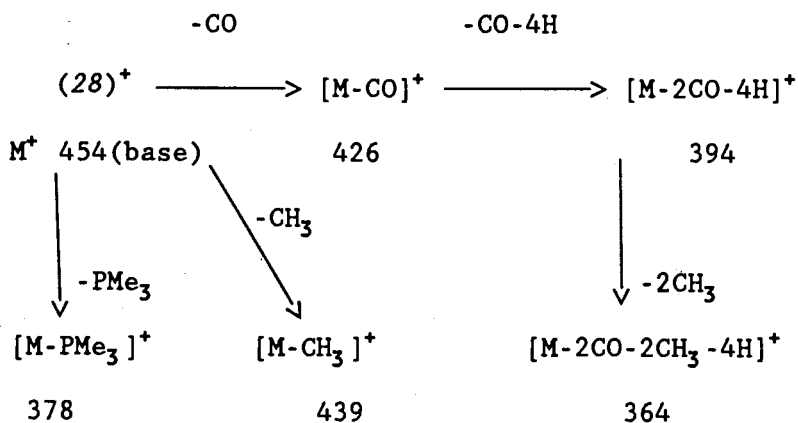


Scheme 12. Fragmentation of $\text{Cp}^*\text{Re}(\text{CO})(\text{PMe}_3)(\text{N}_2)$ (26)



(*m/e=426 is the most intense peak in the range from 300 to 500)

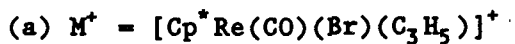
Scheme 13. Fragmentation of $\text{Cp}^*\text{Re}(\text{CO})_2\text{PMe}_3$ (28)



(iv) Others. We can compare the complex $\text{Cp}^*\text{Re}(\text{CO})(\text{PMe}_3)(\eta^2\text{-C}_3\text{H}_6)$ [12] with $\text{Cp}^*\text{Re}(\text{CO})(\text{PMe}_3)(\text{N}_2)$ (26) and $\text{Cp}^*\text{Re}(\text{CO})_2\text{PMe}_3$ (28). The interpretation of the principal fragments for [12], (26) and (28) is given in Schemes 11, 12 and 13.

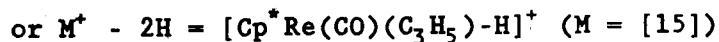
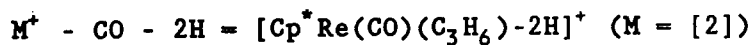
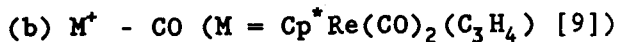
A comparison of fragmentation processes between (26) and (28) clearly shows that the molecular ion of (26) is quite unstable because of the presence of the weakly bound ligand N_2 . The molecular ion of (28) is more stable relative to other fragments; its M^+ peak is also the base peak. This reflects that CO is a strongly bound ligand, and also the phosphorus is not only a good σ -electron donor but also is a good π -electron acceptor through its empty d orbitals. The loss of the weakly bound N_2 ligand in (26) is expected to be very fast and to give the base peak at $m/z=426$ which is the fragment $[\text{Cp}^*\text{Re}(\text{CO})\text{PMe}_3]^+$. It is notable that this fragment $[\text{Cp}^*\text{Re}(\text{CO})\text{PMe}_3]^+$ is just the same base peak as in the case of complex [12]. Furthermore, the two fragmentation processes of [12] and (26) (see Schemes 11 and 12, Figs.17(1) and (s)) are very similar. It provides evidence that the propene is a more weakly bound ligand compared with CO and PMe_3 and is quickly released from molecular ion M^+ of [12] without accompanying loss of hydrogen atoms.

Fig.18(a-m) Computed Isotopic Abundance Patterns



C 14, H 20, O 1, BR 1, RE 1,

MASS	%	REL. INTEN.	
468	15.95	37.17
469	2.56	5.95	...
470	42.90	100.00
471	6.85	15.96
472	27.09	63.15
473	4.28	9.97
474	0.38	0.87	



C 14, H 19, O 1, RE 1,

MASS	%	REL. INTEN.	
388	31.56	58.43
389	5.05	9.34
390	54.01	100.00
391	8.60	15.92
392	0.75	1.39	.
393	0.05	0.09	

Fig.18(a-m) Computed Isotopic Abundance Patterns

(c) M^+ - CO (M = [10] or [11])

or M^+ - CO - 2H (M = [6])

C 17, H 23, O 1, RE 1,

MASS	%	REL. INTEN.
428	30.50	58.23
429	5.93	11.30
430	52.39	100.00
431	10.10	19.27
432	1.03	1.96
433	0.08	0.14
434	0.01	0.00

(d) M^+ - CO (or N_2) = $[Cp^*Re(CO)(PMe_3)]^+$

M = $Cp^*Re(CO)_2(PMe_3)$ or $Cp^*Re(CO)(N_2)(PMe_3)$

C 14, H 24, O 1, P 1, RE 1,

MASS	%	REL. INTEN.
424	31.54	58.42
425	5.07	9.39
426	53.97	100.00
427	8.63	15.99
428	0.76	1.40
429	0.05	0.09
430	0.01	0.00

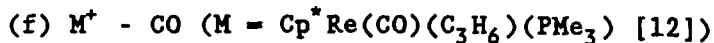
(e) M^+ - (CO+2H) or (N_2 +2H) = $[Cp^*Re(CO)(PMe_3)-2H]^+$

M = $Cp^*Re(CO)_2(PMe_3)$ or $Cp^*Re(CO)(N_2)(PMe_3)$

C 14, H 22, O 1, P 1, RE 1,

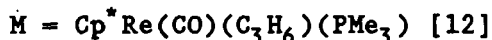
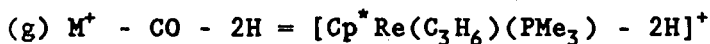
MASS	%	REL. INTEN.
422	31.55	58.42
423	5.06	9.37
424	53.99	100.00
425	8.62	15.96
426	0.76	1.39
427	0.05	0.09
428	0.01	0.00

Fig.18(a-m) Computed Isotopic Abundance Patterns



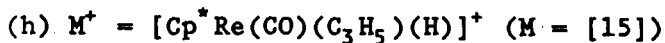
C 16, H 30, P 1, RE 1,

MASS	%	REL. INTEN.	
438	30.89	58.36
439	5.68	10.72
440	52.92	100.00
441	9.66	18.24
442	0.84	1.57
443	0.05	0.09
444	0.01	0.00



C 16, H 28, P 1, RE 1,

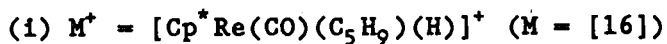
MASS	%	REL. INTEN.	
436	30.90	58.36
437	5.67	10.70
438	52.94	100.00
439	9.65	18.21
440	0.83	1.56
441	0.05	0.09
442	0.01	0.00



C 14, H 21, O 1, RE 1,

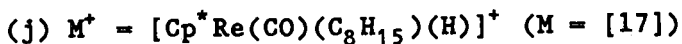
MASS	%	REL. INTEN.	
390	31.55	58.43
391	5.06	9.36
392	54.00	100.00
393	8.61	15.94
394	0.76	1.39
395	0.05	0.09
396	0.01	0.00

Fig.18(a-m) Computed Isotopic Abundance Patterns



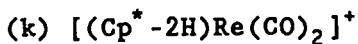
C 16, H 25, O 1, RE 1,

MASS	%	REL. INTEN.
418	30.84	58.30
419	5.65	10.68
420	52.89	100.00
421	9.63	18.20
422	0.94	1.77 .
423	0.07	0.12



C 19, H 31, O 1, RE 1,

MASS	%	REL. INTEN.
460	29.80	58.07
461	6.49	12.64
462	51.31	100.00
463	11.07	21.57
464	1.25	2.42 .
465	0.10	0.19



C 12, H 13, O 2, RE 1,

MASS	%	REL. INTEN.
374	32.22	58.47
375	4.42	8.01
376	55.10	100.00
377	7.53	13.65
378	0.70	1.26 .
379	0.05	0.09
380	0.01	0.00

Fig.18(a-m) Computed Isotopic Abundance Patterns

(1) $[\text{Cp}^*\text{Re}(\text{CO})_2]^+$

C 12, H 15, O 2, RE 1.

MASS	%	REL. INTEN.	
376	32.21	58.47
377	4.43	8.03
378	55.09	100.00
379	7.54	13.68
380	0.70	1.27	.
381	0.05	0.09	
382	0.01	0.00	

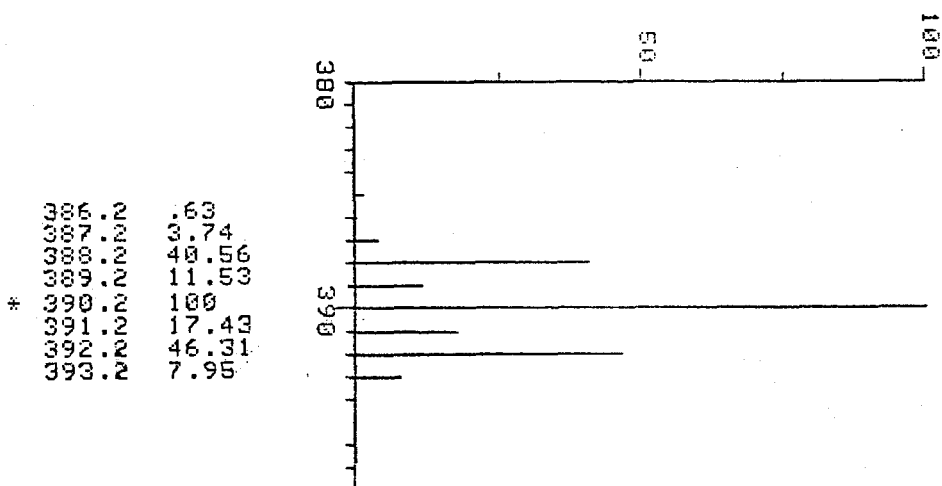
(m) $[(\text{Cp}^* - 2\text{H})\text{Re}(\text{CO})]^+$

C 11, H 13, O 1, RE 1,

MASS	%	REL. INTEN.	
346	32.66	58.59
347	4.10	7.35
348	55.74	100.00
349	6.98	12.51
350	0.52	0.92	

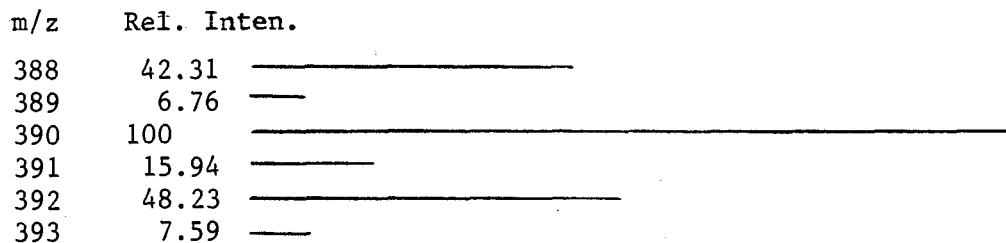
Fig.19. Isotopic Abundance Pattern of [15]

(a) Observed Isotopic Abundance Pattern of [15]



(b) Calculated Isotopic Pattern for the Superposition

of the Patterns for $m/z390 : m/z392 = 1 : 0.65$



(v) Summary

A single mass spectrum may tell us not only about the process of molecular fragmentation but also about the stability of fragments in the MS experiment.⁴³ For example, the fragment corresponding to the base peak should have a longer life, i.e., be more stable than other fragments. However, by comparing and analysing the mass spectra of the series of complexes $\text{Cp}^*\text{Re}(\text{CO})_2(\text{olefin})$, more interesting information may be discovered as follows.

(1) In the case of the $\text{Cp}^*\text{Re}(\text{CO})_2(\text{olefin})$ complexes, the mass spectra all have a M^+ peak of relatively low abundance. This implies that the molecular ion $[\text{Cp}^*\text{Re}(\text{CO})_2(\text{olefin})]^+$ is not stable. The charge lessens the Re-ligand back-bonding thereby weakening metal-ligand bonds, so the weakest bonded ligand may dissociate more readily. However, if the charge can be dispersed by the molecular system, (e.g., through contributing resonance structures or elements having lone pairs of electrons), the stability of M^+ can be increased, so that the abundance of M^+ peak will be expected to be greater. As an example, the base peak of Cp^*ReO_3 (27)^{34b} (Fig.17(u)) is indeed the M^+ peak, because the Cp^* ring and three coordinated oxygen atoms can effectively disperse the charge.⁴⁴ Similarly, in the EI(70 eV) mass spectra of complexes Cp^*_2Fe and Cp^*_2Ru , the base peaks are the M^+ peaks.⁴⁵ Obviously, the isotopic abundance patterns of M^+ will be of zero or low intensity in the cases of unstable

molecular ions. In other cases, where the observed isotopic abundance patterns of M^+ do not correspond to the computer-simulated isotopic abundance patterns, the loss of one or more hydrogen atoms is indicated. Such is the situation in the cases of allyl(hydrido) complexes [15]-[17] as shown in Figs.17(n-p) by comparison with the simulations in Figs.18(h-j). Further discussion of the mass spectra of complexes [15]-[17] will be given in Chapter III.

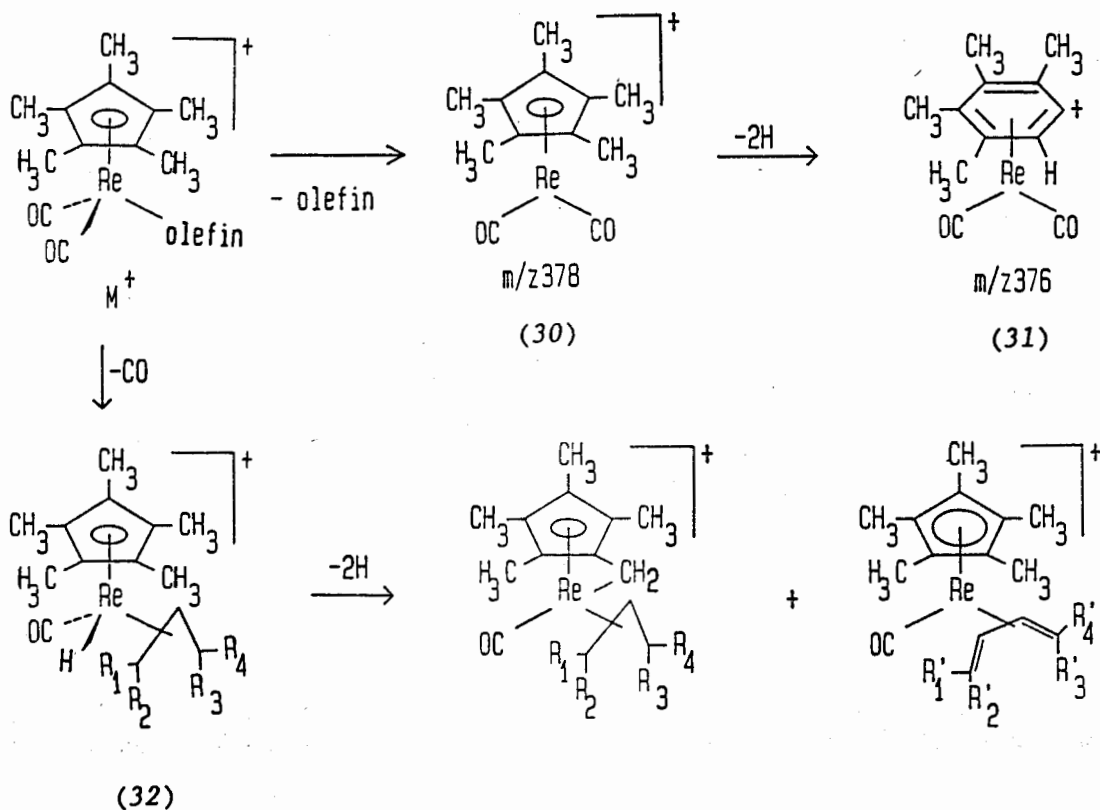
(2) The Cp^* is a strongly bonded ligand, with the result that Cp^*Re does not break apart during the entire molecular ion fragmentation (Schemes 6-13), although it may expand or C-H activate.

(3) The fragment ion $[Cp^*Re(CO)_2]^+$, ($m/z378$) shows an important dehydrogenation feature in mass spectra. We observed that the first CO loss followed by a rapid loss of 2H from M^+ ($M = Cp^*Re(CO)_3$ (29)) is typical of such a fragmentation. Additional evidence for this comes from the computer-simulated isotopic abundance patterns. If the observed relative abundances for an alleged fragment ion agree with the calculated isotopic abundance pattern of this fragment, then this is strong evidence for the presence of this fragment. If not, it indicates the possibility of the superposition of two or more fragments with different m/z values. In the case of $[Cp^*Re(CO)_3]^+$ fragmentation (Fig.17(w)), our observed data ($m/z376$ 35%; $m/z378$ 23%) do not agree with the

computer-simulated isotopic abundance pattern of $[M-CO]^+$ ($m/z376$ 58.5%; $m/z378$ 100%. Fig.18(1)). This indicates that our spectrum is the superposition of the isotopic abundance patterns of the two fragments $[M-CO]^+$ ($m/z378$) and $[M-CO-2H]^+$ ($m/z376$), with the fragment $[M-CO-2H]^+$ ($m/z376$) as the main contributor. That implies the first CO loss followed by 2H loss from Cp^* ring occurs at a very fast rate. However, the computer-simulated isotopic abundance pattern for $[M-2CO-2H]^+$ ($m/z350$ 0.9%; $m/z349$ 12.5%; $m/z348$ 100%. Fig.18(m)) is quite close to our observed data (see Fig.17(w), $m/z350$ 10%; $m/z349$ 14%; $m/z348$ 100%), which means that $[M-2CO-2H]^+$ is the dominant fragment shown at $m/z348$ in the mass spectra. So, this is why we believe the first CO loss followed by 2H loss is the dominant fragmentation of $Cp^*Re(CO)_3$ under our MS conditions.⁴⁶ Lyatifov⁴⁷ first noticed that $[Cp^*Re(CO)_3]^+$ showed the dehydrogenation feature which could be attributed to an active rhenium contribution.

(4) The Cp^* ring in the fragment $[Cp^*Re(CO)_2]^+$ ($m/z378$) could stabilize the extra charge by a ring expansion which produces a favourable resonance structure (see fragment ion (31), Scheme 14). This behaviour may be illustrated by reference to the mass spectrum of toluene in which $m/z91$ is the most abundant fragment ion.⁴⁸ It was suggested by isotopic labelling experiments that $m/z91$ was best represented as the relatively stable tropylium ion,⁴³ produced from the benzene by ring expansion.

Scheme 14.



So, m/z 376 (31) (m/z 376 - $[M\text{-olefin-}2H]^+$) always accompanies m/z 378 (30) $[M\text{-olefin}]^+$ (in addition to the ^{185}Re component of (30)) due to the very quick expansion of Cp^* ring (Scheme 14). Note, however, that the ratio of m/z 376 to m/z 378 is different in the case of each olefin complex. If we could assume the situation of $2H$ loss from Cp^* ring is very similar in each case, then comparing the relative intensity $[m/z378]/[m/z376]$ will yield the order of the different ligand loss from their parent complexes.

(5) From IR data in Table 4 and the discussion of the mass spectra (see 2.5.2.(i), (ii) and (iii)), it is clear that M^+ will first lose the weakly bonded ligand and the large ligand, for reasons of stereochemistry and π -back bond strength. The order is as follows:

cyclooctene, 4-methylcyclohexene, cyclohexene;

1-octene, *cis*-2-octene, 2-pentene, propene, ethene;

1,4-cyclohexadiene, allene, 1,3-cyclohexadiene.

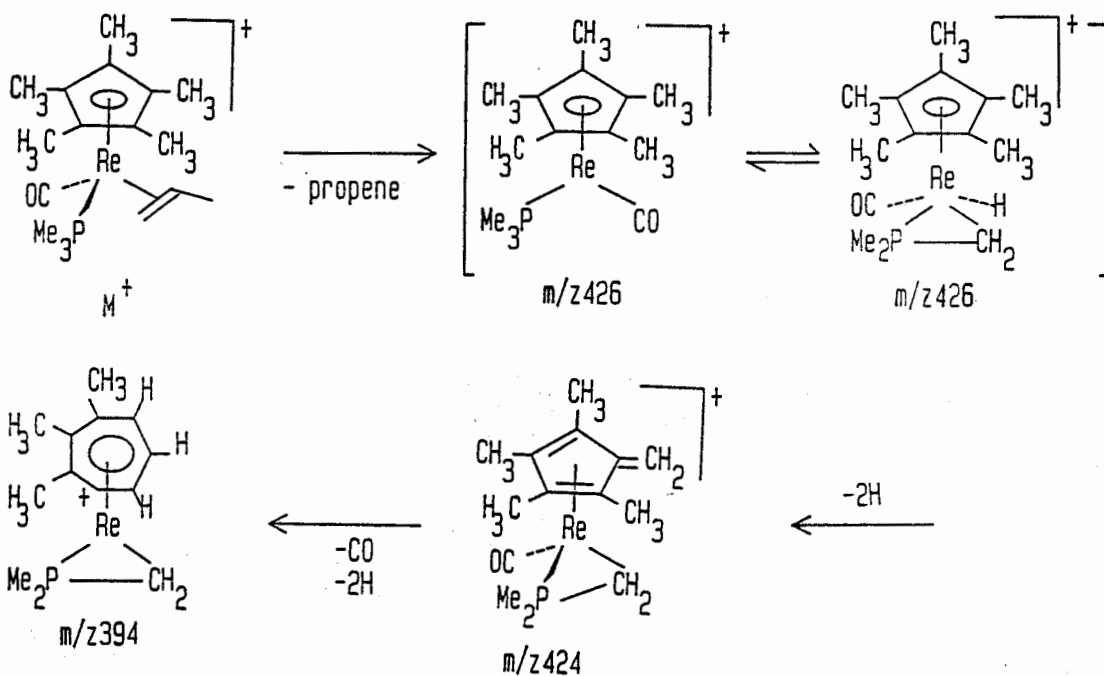
(6) The fragmentation of diene complexes [9], [10] and [11] shows that the η^2 -diene ligand is hardly released (see 2.5.2.(iii)). It means a stronger bond is present between rhenium and a diene, which is consistent with the results of IR(ν (CO)) absorptions (see Table 4), i.e., the diene has a stronger π -back bond with rhenium. Furthermore, an interesting MS difference of η^2 -dienes from the other olefins, [1]-[8], is that the η^2 -dienes have a preference for losing first CO alone, which is not favoured for the olefins, [1]-[8], which lose first CO followed by the Cp* ring expansion. The evidence is that the isotopic pattern of M-CO (M = [9], [10] and [11]) is similar to the computed isotopic abundance. However, the isotopic pattern of M-CO-2H (M = [1]-[8]) is similar to the computed abundance (see Figs. 18(b-c)). The possible reason for the

difference is that the η^2 -diene has a free double bond which could act as a ligand to rhenium following the first CO loss instead of the Cp* ring expansion losing 2H. For comparison, the η^4 -cyclohexadiene complex [13] (M^+ m/z430) preferred to lose CO followed by the Cp* ring expansion to lose 2H (the basic peak m/z400 - M^+ -30), because the ligand η^4 -cyclohexadiene has no free double bond to act as a ligand.

(7) In the Cp*Re(CO)(PMe₃)(η^2 -propene) [12] case, the preferential loss is of propene first accompanied by a small amount of 2H loss, probably from Cp* (or from a methyl group on the phosphine, or from both). However, we cannot rule out the possibility that the C-H bonds of a methyl group on the phosphine could be activated at this point (see Scheme 11). Additional evidence for this is that the computer-simulated isotopic abundance pattern of the fragment ion [Cp*Re(CO)(PMe₃)]⁺ (m/z424 58.42%; m/z426 100%, see Fig.18(d)) is different from its observed isotopic abundance pattern (m/z424 66%; m/z426 100%). The increased intensity of peak m/z424 indicates a small amount of 2H loss.

(8) Comparing the two situations of 2H loss in the fragments of [Cp*Re(CO)₂]⁺ and [Cp*Re(CO)(PMe₃)]⁺, both of the two fragments resulted from their parent molecular ions, Cp*Re(CO)₂(η^2 -C₃H₆) [2] and Cp*Re(CO)(PMe₃)(η^2 -C₃H₆) [12] respectively, losing the propene ligand, followed by a small amount of 2H loss. The amount of

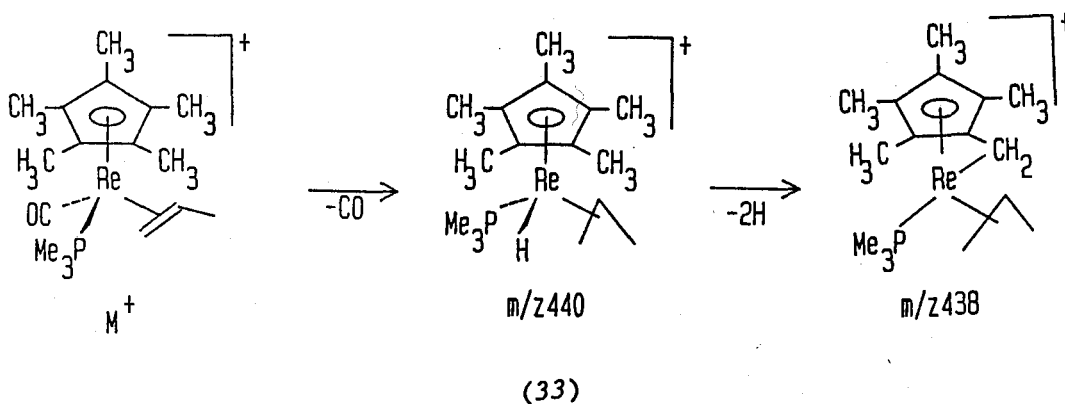
Scheme 15.



2H loss from $[\text{Cp}^*\text{Re}(\text{CO})_2]^+$ is larger relative to $[\text{Cp}^*\text{Re}(\text{CO})(\text{PMe}_3)]^+$ (Figs.17(b),(1); $[(\text{Cp}^* - 2\text{H})\text{Re}(\text{CO})_2]^+ / [\text{Cp}^*\text{Re}(\text{CO})_2]^+ = (m/z376)/(m/z378) > 1$; $[\text{Cp}^*\text{Re}(\text{CO})(\text{PMe}_3) - 2\text{H}]^+ / [\text{Cp}^*\text{Re}(\text{CO})(\text{PMe}_3)]^+ = (m/z424)/(m/z426) < 1$). The reason could be the well-known reversible C-H activation of a methyl group on the phosphine so that the mechanism of fragmentation of the complex [12] may be as shown in Scheme 15. However, it is worth further comparing the situations of 2H loss between two fragments of $[\text{Cp}^*\text{Re}(\text{CO})(\text{C}_3\text{H}_6)]^+$ $m/z392$

(resulting from $\text{Cp}^*\text{Re}(\text{CO})_2(\text{C}_3\text{H}_6)$ [2], Fig.17(b)) and $[\text{Cp}^*\text{Re}(\text{PMe}_3)(\text{C}_3\text{H}_6)]^+$ $m/z440$ (resulting from $\text{Cp}^*\text{Re}(\text{CO})(\text{PMe}_3)(\text{C}_3\text{H}_6)$ [12], Fig.17(1)). Both of the two fragments lose a large amount of 2H at a very fast rate, relative to the timescale of MS, resulting in the observed isotopic abundance patterns of $[\text{Cp}^*\text{Re}(\text{CO})(\text{C}_3\text{H}_6)-2\text{H}]^+$ $m/z390$ and $[\text{Cp}^*\text{Re}(\text{PMe}_3)(\text{C}_3\text{H}_6)-2\text{H}]^+$ $m/z438$, similar to the computed isotopic abundance patterns (Figs. 18(b), (g)). This feature could be attributed to a ready but largely irreversible allylic C-H activation in the Cp^*Re system (see Chapter III), so that the extremely short-lived fragments (32) and (33) very quickly lose 2H (Schemes 14, 16).

Scheme 16.



(9) Finally, it is very interesting that the 3-methoxy-cyclohexene complex [23] (M^+ m/z 490) is clearly converted to the cyclohexadiene complex [10] (M^+ m/z 458) by losing CH_3OH in its mass spectrum. Thereafter, the fragmentation is very similar to cyclohexene [10]. We have shown separately that the 3-methoxy-cyclohexene complex [23] can be converted to the cyclohexadiene complex [10] by heating, protonation or treatment with a base (see Chapter IV).

2.6. Conclusion

Several different methods have been used in the syntheses of the new olefin rhenium complexes [1]-[13]. Among these, the photochemical reactions of $Cp^*Re(CO)L_1L_2$ ($L_1 = CO, PMe_3$; $L_2 = CO, N_2$) with olefins yield the complexes [1]-[4], [6]-[8] and [10]-[13]; the thermal reaction of $Cp^*Re(CO)_2(THF)$ with allene offers the allene complex [9]; the reaction of the η^3 -allylpentane cationic complex [20] with sodium borohydride produces the η^2 -1-octene complex [4] and the η^2 -*cis*-2-octene complex [5]. In general, the dinitrogen ligand in $Cp^*Re(CO)_2(N_2)$ or $Cp^*Re(CO)(PMe_3)(N_2)$ is weakly bonded to rhenium and is quickly released under UV light to create a reactive vacant site on rhenium. These reagents therefore improve the yields of olefin complexes and simplify the purification of products; this is especially the case in the syntheses of the diene

complexes [10]-[11] avoiding isomerization. Since, under UV light, allene can readily isomerize and polymerize,⁴⁹ the allene complex [9] was prepared by the thermal reaction of $\text{Cp}^*\text{Re}(\text{CO})_2(\text{THF})$ with allene in a high yield (67.4%).

These complexes were fully characterized except for the unstable η^4 -cyclohexadiene complex [13], which was only identified by spectroscopic measurements. On the basis of IR and MS measurements, the bond strengths between olefin-Re were analyzed and ordered. The fragmentations of the olefin rhenium complexes were discussed in detail. Three different C-H activation mechanisms in MS were described: (a) Cp^* ring expansion; (b) allylic C-H activation; (c) C-H activation of PMe_3 . The Cp^* ring expansion involves the C-H activation of Cp^* ring by an active rhenium centre, and then 2H loss. By comparing the ratio of $[\text{M-olefin-2H}]^+$ to $[\text{M-olefin}]^+$ (i.e., $[(\text{Cp}^*-2\text{H})\text{Re}(\text{CO})_2]^+ / [\text{Cp}^*\text{Re}(\text{CO})_2]^+ = (m/z376)/(m/z378)$), we could determine that Cp^* ring expansion was occurring but was different in each case. However, in the case of $\text{Cp}^*\text{Re}(\text{CO})_2(\text{olefin})$ complexes, except the ethene complex [1], the observed isotopic abundance patterns of the fragments of $[\text{M-CO-2H}]^+$ (i.e., $[\text{Cp}^*\text{Re}(\text{CO})(\text{olefin})-2\text{H}]^+$) were similar to the computed isotopic abundance patterns in each case, indicating that the fragments $[\text{M-CO}]^+$ (i.e., $[\text{Cp}^*\text{Re}(\text{CO})(\text{olefin})]^+$) were very short-lived in MS. This can be attributed to the very ready but largely irreversible allylic C-H activation by

a Cp*Re system (see Chapter III). In the case of Cp*Re(CO)(PMe₃)L (L = CO, N₂, propene), however, the comparison between the observed isotopic abundance pattern and the computed isotopic pattern of the fragment [Cp*Re(CO)(PMe₃)]⁺ m/z 426 shows a small increase of the intensity m/z424 corresponding to [Cp*Re(CO)(PMe₃)-2H]⁺. Perhaps the C-H activation of the Cp* ring is prohibited by the preferential C-H activation of PMe₃ at this point, and also by the well-known quickly reversible C-H activation of a methyl group on the phosphine resulting in a low rate of 2H loss.

The barrier to rotation of the allene in the complex [9] has been investigated by temperature-dependent ¹H NMR experiments. The activation parameters for the η²-allene rotation in [9] have been determined to be ΔG* = 9.9 ± 0.2 kcal/mol, at the coalescence temperature (-50⁰C). Values of ΔH* = 10.9 ± 0.3 kcal/mol and ΔS* = 4.7 ± 1.4 cal/K.mol have been established by the fitting of the free energy activation, ΔG*, at different temperatures to the eq.35. Furthermore, the saturation transfer experiments show that a 1,2-shift occurs in the allene complex [9], but the 1,2-shift rate is quite small even at 100⁰C, indicating a large barrier for the process.

2.7. Experimental Section

All manipulations were carried out under dry N_2 in Schlenk apparatus connected to a switchable double manifold providing a purified nitrogen supply and a low vacuum. Solvents were purified by standard methods and were distilled under nitrogen and used immediately. Reaction yields are based on the rhenium reagent used, unless otherwise specified. Irradiations were carried out with a water-jacketed 200 W Hanovia Model 654A-0360 high pressure mercury vapour lamp. The radiation was otherwise unfiltered. The sample was either in a quartz (or, where specified, Pyrex) tube adjacent to the lamp or else was in a quartz immersion-type reactor and was continuously purged with nitrogen or appropriate gas. IR spectra were recorded on a Perkin-Elmer 983G instrument for solutions in CaF_2 cells. NMR were recorded in the NMR Services of S.F.U. by Mrs. M. Tracey on a Bruker WM-400 instrument operating at 400.13 MHz (1H). Mass spectra were obtained by Mr. G. Owen on a Hewlett-Packard Model 5985 instrument equipped with an electron impact (EI) source operating at 70 eV, or a Phrasor Scientific Inc. fast atom bombardment (FAB) accessory and xenon source. Masses are quoted for the ^{187}Re isotope. Microanalyses were performed by Mr. M.K. Yang of the S.F.U. microanalytical laboratory.

Gas or liquid olefin, decacarbonyldirhenium (Strem

Chemicals) and trimethylphosphine (Alfa) were used directly as purchased. Some starting materials were prepared by the published methods, e.g., $\text{Cp}^*\text{Re}(\text{CO})_3$ was synthesized by the method used by Gladysz⁵⁰; the dinitrogen complexes $\text{Cp}^*\text{Re}(\text{CO})_2(\text{N}_2)$ and $\text{Cp}^*\text{Re}(\text{CO})(\text{N}_2)(\text{PMe}_3)$ were synthesized according to an established route used in our laboratory.⁵¹

The experimentally observed data for IR and ¹H NMR of the complexes [1]-[13] are listed in Tables 4 and 5.

(1) $\text{Cp}^*\text{Re}(\text{CO})_2(\eta^2\text{-C}_2\text{H}_4)$ [1].

Method (1). A solution of $\text{Cp}^*\text{Re}(\text{CO})_3$ (100 mg, 0.246 mmol) in freshly distilled hexane (50 ml) was saturated with dry ethene gas for 15 min., then irradiated at 0°C for 20 min. under a continuous ethene purge. The resulting brown solution exhibited $\nu(\text{CO})$ bands due to the complex [1] and some residual tricarbonyl. It was filtered through Celite to remove solid decomposition products, reduced in volume, then chromatographed on an acidic alumina column by eluting with hexane. The residual $\text{Cp}^*\text{Re}(\text{CO})_3$ eluted first, then the complex [1], which was obtained as a white solid. Yield: 28 mg (0.086 mmol, 28.0%). Anal. Calcd. for [1]: C, 41.50; H, 4.69. Found: C, 41.92; H, 4.98. m.p. 126-127°C. MS (EI): m/z 406 [M]⁺, 378 [M-C₂H₄]⁺ and [M-CO]⁺, 376 [M-C₂H₄(or CO)-2H]⁺, 348 (base) [M-C₂H₄-CO-2H] or [M-2CO-2H]⁺.

Method (2). A solution of $\text{Cp}^*\text{Re}(\text{CO})_2(\text{N}_2)$ (70 mg, 0.172 mmol) was saturated with ethene as above and irradiated under ethene at 0°C for 20 min. Workup as above gave the complex [1] in yield 35mg (0.086 mmol, 50%).

(ii) $\text{Cp}^*\text{Re}(\text{CO})_2(\eta^2\text{-C}_3\text{H}_6)$ [2]. A solution of $\text{Cp}^*\text{Re}(\text{CO})_3$ (100 mg, 0.246 mmol) in hexane (50 ml) was irradiated at 0°C with a propene purge for 1h. After this time the IR spectrum showed strong $\nu(\text{CO})$ absorptions due to the propene complex [2], weaker bands at 2014 and 1923 cm^{-1} from residual tricarbonyl, and two bands at 1904 and 1912 cm^{-1} from the allyl(hydrido) complex [15] which intensified on further irradiation. The solution was filtered through Celite, reduced in volume, and chromatographed on a neutral alumina column. Elution with hexane removed the tricarbonyl, then the propene complex [2], and finally the allyl(hydrido) complex [15]. Yields after crystallization from hexane at -78°C were 41 mg of [2] (0.98 mmol, 40%) and ca. 5 mg of [15]. Anal. Calcd. for [2]: C, 42.94; H, 5.05. Found: C, 42.80; H, 4.84. m.p. $109\text{-}110^\circ\text{C}$. MS (EI): m/z 420 $[\text{M}]^+$, 390 $[\text{M-CO-2H}]^+$, 378 $[\text{M-C}_3\text{H}_6]^+$, 376 $[\text{M-C}_3\text{H}_6\text{-2H}]^+$, 362 $[\text{M-2CO-2H}]^+$, 360 $[\text{M-2CO-4H}]^+$, 348 (base) $[\text{M-CO-C}_3\text{H}_6\text{-2H}]^+$.

(iii) $\text{Cp}^*\text{Re}(\text{CO})_2(\eta^2\text{-2-C}_5\text{H}_{10})$ [3]. By a similar procedure to that used for [2], irradiation of the solution of $\text{Cp}^*\text{Re}(\text{CO})_3$ (100 mg, 0.246 mmol) and 3 ml of 2-pentene (a mixture of *cis* and *trans* isomers, ratio = $[\textit{cis}]/[\textit{trans}] \approx 1/3.5$ calculated by GC) in about 60 ml of hexane for 30 min. at 0°C yielded two products, which after chromatography on a neutral alumina column gave the complex [3] and ca. 8 mg of hydrido(allylalkane) complex [16] as white solids. Complex [3] was shown by ^1H NMR to be a mixture of [3]*cis* and [3]*trans* (ratio = $[\textit{cis}]/[\textit{trans}] = 1/1.7$) isomers. Yields: complex [3] 35 mg (0.078 mmol, 31.7%). Anal. Calcd. for [3]: C, 45.62; H, 5.63. Found: C, 45.58; H, 5.77. MS (EI): m/z 448 $[\text{M}]^+$, 418(weak) $[\text{M-CO-2H}]^+$, 390 $[\text{M-2CO-2H}]^+$, 388 $[\text{M-2CO-4H}]^+$, 378 $[\text{M-C}_5\text{H}_{10}]^+$, 376 $[\text{M-C}_5\text{H}_{10-2H}]^+$, 348(base) $[\text{M-CO-C}_5\text{H}_{10-2H}]^+$.

(iv) $\text{Cp}^*\text{Re}(\text{CO})_2(\eta^2\text{-1-C}_8\text{H}_{16})$ [4]. This complex [4] was synthesized following to the method used for [3]. Chromatography yielded the complex [4], 27 mg (0.055 mmol, 22.4%), and the hydride complex [17], 8 mg (0.017 mmol, 7.0%). Anal. Calcd. for [4]: C, 49.06; H, 6.38. Found: C, 49.08; H, 6.51. MS (EI): m/z 490 $[\text{M}]^+$, 460 $[\text{M-CO-2H}]^+$, 430 $[\text{M-2CO-4H}]^+$, 428 $[\text{M-2CO-6H}]^+$, 378(base) $[\text{M-C}_8\text{H}_{16}]^+$, 376 $[\text{M-C}_8\text{H}_{16-2H}]^+$, 348 $[\text{M-CO-C}_8\text{H}_{16-2H}]^+$.

(v) $\text{Cp}^*\text{Re}(\text{CO})_2(\eta^2\text{-cis-2-C}_8\text{H}_{16})$ [5]. This *cis*-2-octene compound was synthesized from nucleophilic attack of NaBH_4 upon the corresponding allylalkane cationic complex [20] as described in Chapter IV.

(vi) $\text{Cp}^*\text{Re}(\text{CO})_2(\eta^2\text{-C}_6\text{H}_{10})$ [6]. A solution of $\text{Cp}^*\text{Re}(\text{CO})_3$ (900 mg, 2.21 mmol) and about 5 ml of cyclohexene in 250 ml of hexane was irradiated at 0°C for 1 h. The resulting brown solution was filtered through a short Celite column to remove solid decomposition products, reduced in volume under vacuum, then chromatographed on a neutral alumina column (25x1 cm) with hexane as an eluant. The residual $\text{Cp}^*\text{Re}(\text{CO})_3$ was the first fraction, the complex [6] was the second fraction, the η^2 -1,3-cyclohexadiene complex [10] was the third fraction, the fourth and final fraction was the η^4 -1,3-cyclohexadiene complex [13]. Yields: complex [6] 117 mg (0.254 mmol, 11.4%); complex [10] 93 mg (0.203 mmol, 9.2%); complex [13] ca. 5 mg. Anal. Calcd. for [6]: C, 47.04; H, 5.48. Found: C, 46.90; H, 5.68. m.p. $153\text{-}154^\circ\text{C}$. MS (EI): m/z 460 $[\text{M}]^+$, 430 $[\text{M-CO-2H}]^+$, 400 $[\text{M-2CO-4H}]^+$, 378 $[\text{M-C}_6\text{H}_{10}]^+$, 376 $[\text{M-C}_6\text{H}_{10-2H}]^+$, 348(base) $[\text{M-CO-C}_6\text{H}_{10-2H}]^+$.

(vii) $\text{Cp}^*\text{Re}(\text{CO})_2(\eta^2\text{-C}_7\text{H}_{12})$ [7]. This complex [7] was prepared similarly to those previously described. Chromatography yielded the complex [7] 49 mg (0.103 mmol, 42.0%). Other products corresponding to a new $\nu(\text{CO})$ band at 1890 cm^{-1} were apparently unstable and decomposed during the chromatography. Anal. Calcd. for [7]: C, 48.18; H, 5.75. Found: C, 48.11; H, 5.90. MS (EI): m/z 474 $[\text{M}]^+$, 444 $[\text{M-CO-2H}]^+$, 414 $[\text{M-2CO-4H}]^+$, 399 $[\text{M-2CO-CH}_3\text{-4H}]^+$, 378(base) $[\text{M-C}_7\text{H}_{12}]^+$, 376 $[\text{M-C}_7\text{H}_{12}\text{-2H}]^+$, 348 $[\text{M-CO-C}_7\text{H}_{12}\text{-2H}]^+$.

(viii) $\text{Cp}^*\text{Re}(\text{CO})_2(\eta^2\text{-C}_8\text{H}_{14})$ [8]. This complex [8] was prepared following a similar procedure to that used for the preparation of [6]. Chromatography yielded the complex [8] 34 mg (0.070 mmol, 14.2%) and also the known binuclear complex $(\text{Cp}^*\text{Re}(\text{CO})_2)_2\text{CO}^8$, which was identified on the basis of the following spectroscopic properties. IR($\nu(\text{CO})$): 1971(w), 1930(s), 1901(s), 1877(w), 1714 in hexane; MS (EI): m/z 726 $[\text{M}]^+$; $^1\text{H NMR}(\text{C}_6\text{D}_6)$: δ 1.86 ppm (Cp^*). These data are consistent with those reported by Graham⁸. Anal. Calcd. for [8]: C, 49.26; H, 5.99. Found: C, 49.15; H, 6.00. m.p. 188-189⁰C. MS (EI): m/z 488 $[\text{M}]^+$, 458 $[\text{M-CO-2H}]^+$, 428 $[\text{M-2CO-4H}]^+$, 426 $[\text{M-2CO-6H}]^+$, 378(base) $[\text{M-C}_8\text{H}_{14}]^+$, 376 $[\text{M-C}_8\text{H}_{14}\text{-2H}]^+$, 348 $[\text{M-CO-C}_8\text{H}_{14}\text{-2H}]^+$.

(ix) $\text{Cp}^*\text{Re}(\text{CO})_2(\eta^2\text{-C}_3\text{H}_4)$ [9]. Solid $\text{Cp}^*\text{Re}(\text{CO})_3$ (90 mg, 0.222 mmol) was dissolved in about 100 ml of freshly distilled THF and irradiated at 0°C with a nitrogen purge for 90 min. After this time, the IR spectrum showed that two new absorptions at 1893 and 1823 cm^{-1} for the THF complex, $\text{Cp}^*\text{Re}(\text{CO})_2(\text{THF})$, were more intense than those of $\text{Cp}^*\text{Re}(\text{CO})_3$. The solution of $\text{Cp}^*\text{Re}(\text{CO})_2(\text{THF})$ in THF was then stirred vigorously (no irradiation) and allene gas was bubbled through the solution for 1 h. until the two $\nu(\text{CO})$ bands for $\text{Cp}^*\text{Re}(\text{CO})_2(\text{THF})$ disappeared. The solution was filtered through a short column (1.5x2 cm) of Silica G60 and dried under vacuum. The residual brown solid was dissolved in hexane and chromatographed on a neutral alumina column (30x1 cm) with hexane as an eluant. Following chromatography, the unreacted starting material $\text{Cp}^*\text{Re}(\text{CO})_3$ (18 mg, 0.044 mmol) was recovered, and the complex [9] was isolated. Yield 50 mg (0.120 mmol, 67.4%). Anal. Calcd. for [9]: C, 43.15; H, 4.59. Found: C, 43.01; H, 4.80. m.p. $115\text{-}117^\circ\text{C}$. MS (EI): m/z 418 $[\text{M}]^+$, 390 $[\text{M-CO}]^+$, 378(weak) $[\text{M-C}_3\text{H}_4]^+$, 376 $[\text{M-C}_3\text{H}_4\text{-2H}]^+$, 360(base) $[\text{M-2CO-2H}]^+$, 348 $[\text{M-CO-C}_3\text{H}_4\text{-2H}]^+$.

(x) $\text{Cp}^*\text{Re}(\text{CO})_2(\eta^2\text{-1,3-C}_6\text{H}_8)$ [10].

Method (1). This complex [10] was isolated as a product in yield 9.2% from the photochemical reaction of $\text{Cp}^*\text{Re}(\text{CO})_3$ with

cyclohexene (see the above preparation of complex [6]), or was directly formed in the photolysis of the cyclohexene complex [6].

Method (2). A solution of $\text{Cp}^*\text{Re}(\text{CO})_2(\text{N}_2)$ (175 mg, 0.431 mmol) and 1 ml of 1,3-cyclohexadiene in 200 ml hexane was irradiated at 0°C for 15 min., reduced in volume and chromatographed on a neutral alumina column. Elution with hexane removed the tricarbonyl complex $\text{Cp}^*\text{Re}(\text{CO})_3$ and a small amount of unreacted $\text{Cp}^*\text{Re}(\text{CO})_2(\text{N}_2)$, then the pure complex [10]. Yield 101 mg (0.220 mmol, 51.0%). Anal. Calcd. for [10]: C, 47.25; H, 5.07. Found: C, 47.40; H, 5.07. m.p. $155\text{-}157^\circ\text{C}$. MS (EI): m/z 458 $[\text{M}]^+$, 430 $[\text{M-CO}]^+$, 400(base) $[\text{M-2CO-2H}]^+$, 378(weak) $[\text{M-C}_6\text{H}_8]^+$, 376 $[\text{M-C}_6\text{H}_8\text{-2H}]^+$, 348 $[\text{M-CO-C}_6\text{H}_8\text{-2H}]^+$.

(xi) $\text{Cp}^*\text{Re}(\text{CO})_2(\eta^2\text{-1,4-C}_6\text{H}_8)$ [11]. This complex [11] was synthesized by the direct photochemical reaction of $\text{Cp}^*\text{Re}(\text{CO})_2(\text{N}_2)$ and 1,4-cyclohexadiene in a similar procedure described in the above synthesis method (2) of complex [10]. Yield: 130 mg (0.284 mmol, 53.7%). Anal. Calcd. for [11]: C, 47.25; H, 5.07. Found: C, 47.50; H, 5.05. m.p. $138\text{-}139^\circ\text{C}$. MS (EI): m/z 458 $[\text{M}]^+$, 430 $[\text{M-CO}]^+$, 400 $[\text{M-2CO-2H}]^+$, 378(weak) $[\text{M-C}_6\text{H}_8]^+$, 376 $[\text{M-C}_6\text{H}_8\text{-2H}]^+$, 348(base) $[\text{M-CO-C}_6\text{H}_8\text{-2H}]^+$.

(x11) $\text{Cp}^*\text{Re}(\text{CO})(\text{PMe}_3)(\eta^2\text{-C}_3\text{H}_6)$ [12]. The dinitrogen complex $\text{Cp}^*\text{Re}(\text{CO})(\text{PMe}_3)(\text{N}_2)^{51}$ (100 mg, 0.22 mmol) in hexane (50 ml) at 0°C was purged with propene gas and irradiated for 20 min. The IR spectrum showed disappearance of the starting material and a strong $\nu(\text{CO})$ band at 1845 cm^{-1} from the complex [12]. The solution was filtered through Celite, reduced in volume, and chromatographed on silica gel 60G. Elution with hexane removed firstly $\text{Cp}^*\text{Re}(\text{CO})_2(\text{PMe}_3)$, secondly the propene complex [2], thirdly the hydrido(allyl) complex [15](*exo* and *endo*) and finally the complex [12]. Yield: 37 mg (0.08 mmol, 36.0%). Anal. Calcd. for [12]: C, 43.67; H, 6.48. Found: C, 43.58; H, 6.46. m.p. $93\text{-}94^\circ\text{C}$. MS (EI): m/z 468 $[\text{M}]^+$, 438(weak) $[\text{M-CO-2H}]^+$, 426(base) $[\text{M-C}_3\text{H}_6]^+$, 394 $[\text{M-CO-C}_3\text{H}_6\text{-4H}]^+$, 392 $[\text{M-PMe}_3]^+$, 364 $[\text{M-PMe}_3\text{-CO}]^+$.

(x111) $\text{Cp}^*\text{Re}(\text{CO})(\eta^4\text{-1,3-C}_6\text{H}_8)$ [13]. This complex [13] was isolated in small amount as a by-product in the above synthesis of the cyclohexene complex [6]. It was observed that complex [13] is not very stable in solution even when stored under an atmosphere of N_2 in the freezer. MS (EI): m/z 430 $[\text{M}]^+$, 400(base) $[\text{M-CO-2H}]^+$, 350(weak) $[\text{M-C}_6\text{H}_8]^+$, 348 $[\text{M-C}_6\text{H}_8\text{-2H}]^+$.

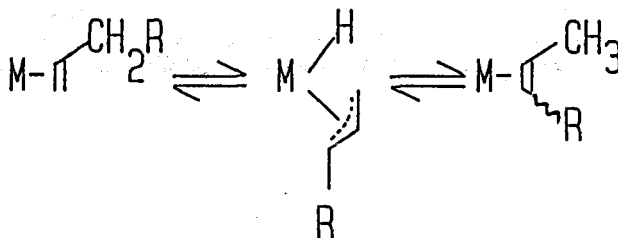
CHAPTER III

Photochemical Allylic C-H Activation in a Cp*Re System

3.1. Introduction

In studies of alkene isomerization catalyzed by a transition metal, it was proposed that the reversible formation of an η^3 -allyl(hydrido) intermediate (Scheme 17) occurs by oxidative addition of an allylic C-H bond to the metal.⁵²⁻⁵⁴

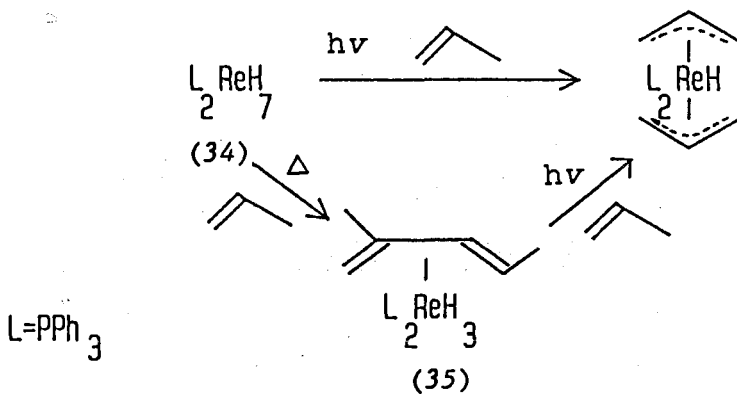
Scheme 17.



However, there is no case in which the crucial step of allylic C-H activation has been observed starting from the well-defined alkene complex. So far, only a small number of well-characterized η^3 -allyl(hydrido) complexes have been synthesized,⁵³⁻⁶¹ while there are some examples which are only stable at low temperature or which have only been observed spectroscopically in

solution.^{61,62} To our knowledge, only one previous study⁵⁶ mentions the photochemical formation of an η^3 -allyl(hydrido) complex. Baudry and co-workers⁵⁶ showed that $(\text{PPh}_3)_2\text{ReH}_7$ reacted thermally with propene to give the trihydridodiene complex $(\text{PPh}_3)_2(\eta\text{-CH}_2\text{-CMeCH-CHMe})\text{ReH}_3$. In the presence of propene, the photolysis of the two complexes (34) and (35), gave the bis-allyl hydride compound $(\text{PPh}_3)_2(\eta^3\text{-C}_3\text{H}_5)_2\text{ReH}$ (Scheme 18).

Scheme 18.



In this chapter, we describe the first example of photochemical allylic C-H bond activation in a Cp^*Re system. Irradiation of $\text{Cp}^*\text{Re}(\text{CO})_3$ or $\text{Cp}^*\text{Re}(\text{CO})_2(\text{N}_2)$ with propene forms the propene complex $\text{Cp}^*\text{Re}(\text{CO})_2(\eta^2\text{-C}_3\text{H}_6)$ [2] as described in Chapter II. This undergoes allylic C-H activation on further irradiation to give the η^3 -allyl(hydrido) complex $\text{Cp}^*\text{Re}(\text{CO})(\text{H})(\eta^3\text{-allyl})$ [15] (Table 7). This was verified by independently irradiating a solution of pure

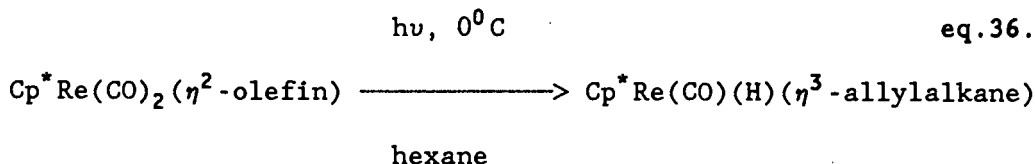
[2] in hexane under a purge of propene. Furthermore, we have been successful in isolating two stereoisomers, [15a]exo and [15b]endo, differing in the orientation of the η^3 -allyl group, and the structures of both have been determined by X-ray crystallography. This type of reaction has been investigated for a range of acyclic and cyclic alkenes. The results are not necessarily similar. For example, the cyclohexene complex [6] gave no observable cyclohexenyl hydride but instead the product of an apparent double C-H activation, the diene complex $\text{Cp}^*\text{Re}(\text{CO})_2(\eta^2\text{-1,3-C}_6\text{H}_8)$ [10]. However, the acyclic alkenes studied all gave allylalkane(hydrido) complexes [15]-[17]. The hydride complexes, [15a]exo and [15b]endo, were also converted to the complex [18]endo $\text{Cp}^*\text{Re}(\text{CO})(\text{Br})(\eta^3\text{-allyl})$. In the following sections of this chapter, the synthesis and characterization of the new hydride complexes, η^2 -diene complexes (which were derived from C-H bond activation), and bromide complex [18]endo will be discussed. At the same time, some mechanistic aspects related to the formation of the above compounds will be considered.

Part of the work described in this chapter has already been published.^{63,64}

3.2. Synthesis

Photolysis of a solution of the η^2 -olefin rhenium complexes

([2], [3] and [4]) in hexane resulted in intramolecular allylic C-H activation and the formation of new allyl(hydrido) rhenium complexes. The photochemical reaction is shown in eq.36.

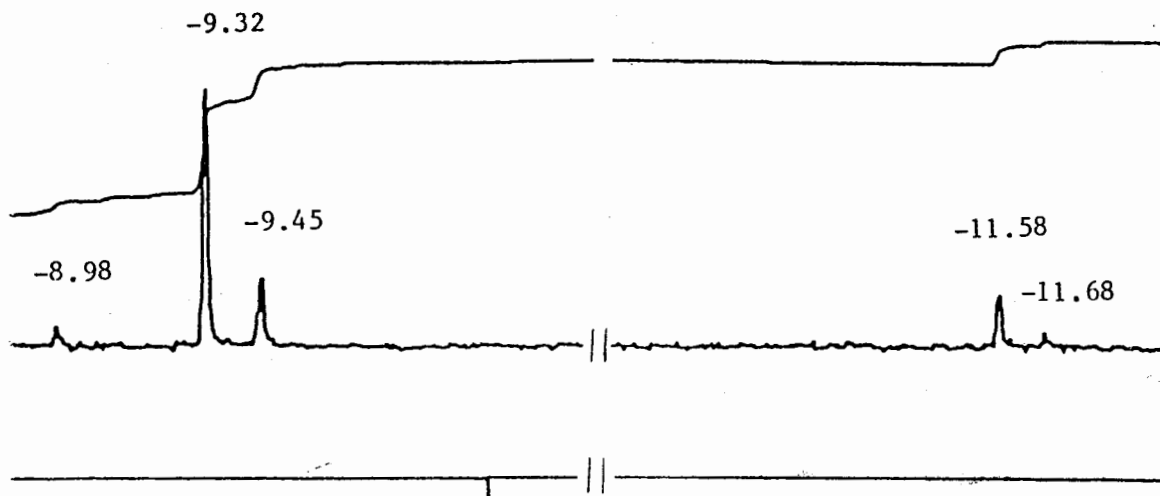


olefin = propene [2], 2-pentene [3] and 1-octene [4]

The major results for the different alkene complexes, [2]-[4] and [6], may be summarized as follows. In the case of the propene complex [2], two isomers of the allyl(hydrido) rhenium complexes ([15a]*exo* and [15b]*endo*) were observed, by IR, in the above reaction (eq.36). These two isomers were successfully isolated by chromatography as they only interconvert slowly in solution at room temperature.

In the case of 2-pentene [3], five isomers of the allyl(hydrido) rhenium complex [16] were detected by ^1H NMR (Fig.20), even though the IR showed only one $\nu(\text{CO})$ absorption at 1891 cm^{-1} . These are assigned as [16c,d,e,f,k]. However, in the photochemical reaction of 1-octene [4], only one isomer of the allyl(hydrido) rhenium complex, [17b]*exo*, was observed and isolated as the only product.

Fig. 20. 400MHz ^1H NMR (C_6D_6) Spectrum in Metal-Hydride
Region for Isomers [16c,d,e,f,k]



Irradiation of the solution of η^2 -cyclohexene complex [6] in hexane resulted in apparent double C-H activation to form the η^2 -1,3-cyclohexadiene compound [10], and further photolysis gave a second product, the η^4 -1,3-cyclohexadiene complex [13] which was presumed to be formed by CO loss from compound [10] (see eq.37). No evidence was found for the formation of a hydrido(cyclohexenyl) complex, analogous to [15]-[17].

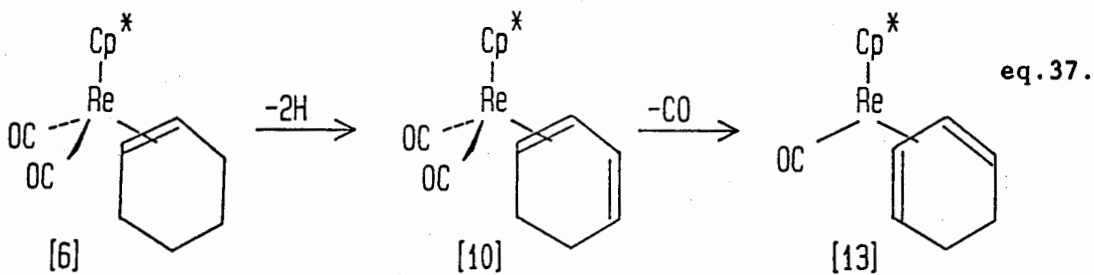


Table 7. Structures of Monocarbonyl η^3 -Allyl Complexes [15]-[18]

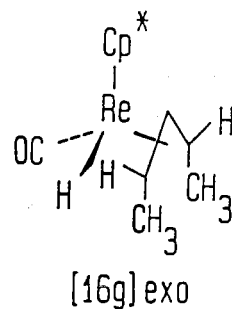
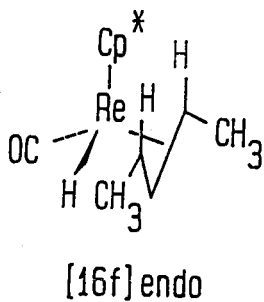
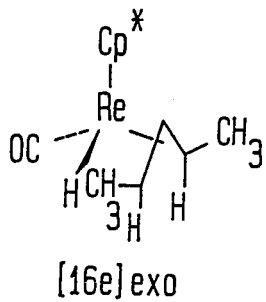
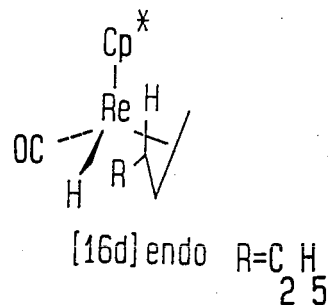
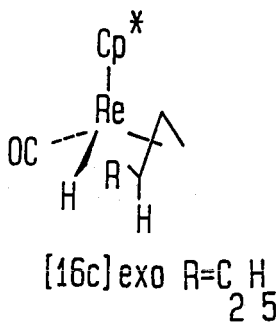
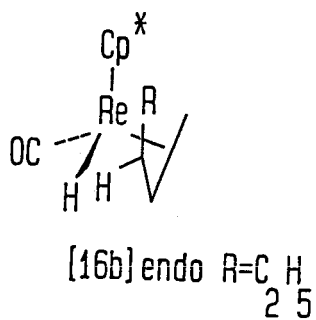
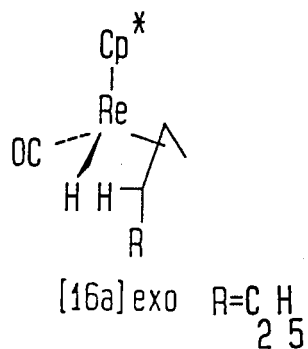
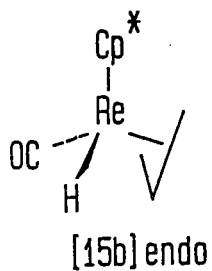
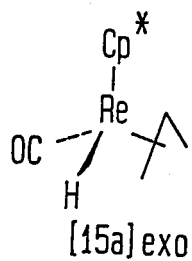
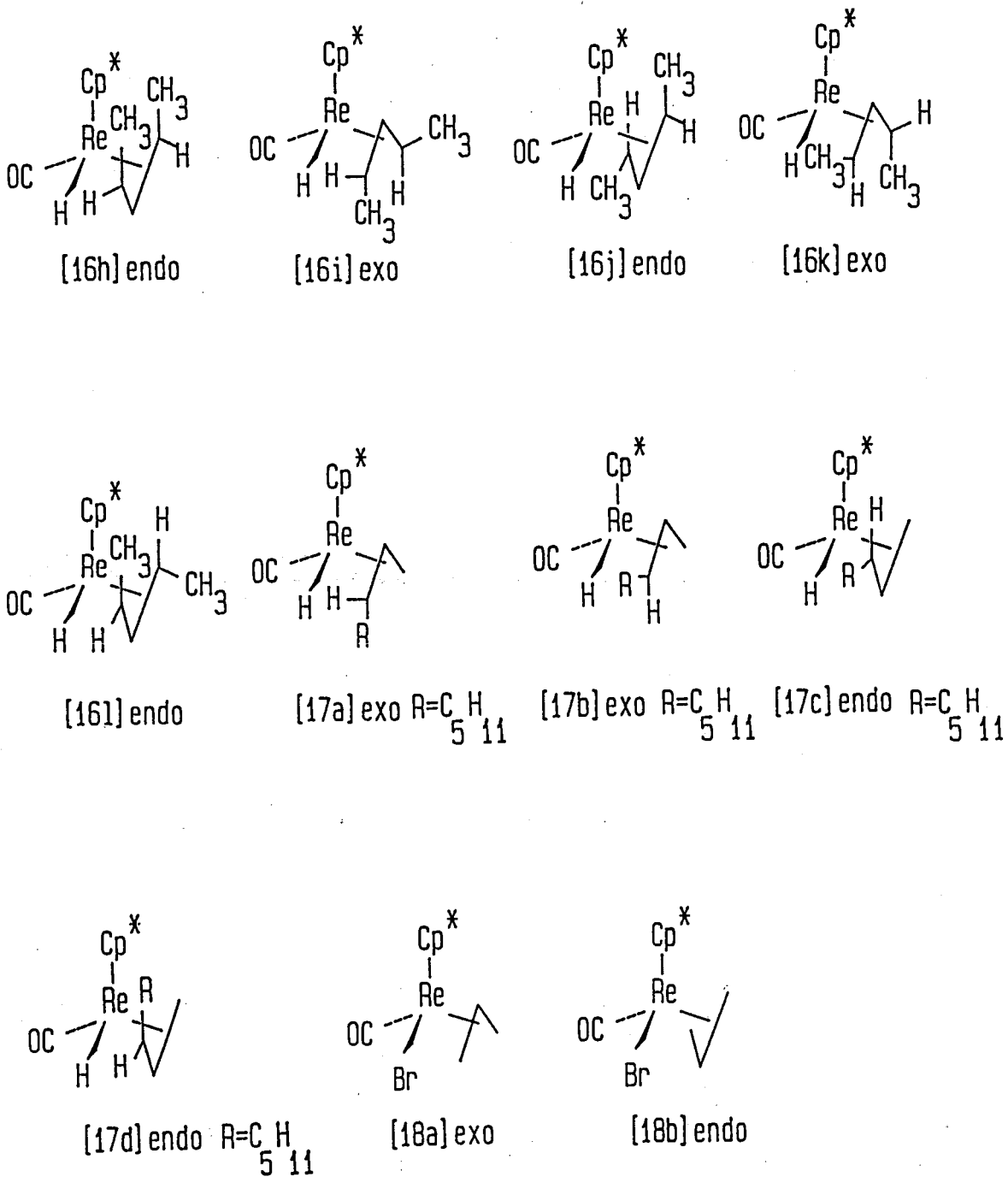


Table 7 (continued).



For most synthetic purposes, the intramolecular allylic C-H activation complexes were made directly by the photolysis of $\text{Cp}^*\text{Re}(\text{CO})_3$ with the corresponding olefin in hexane rather than by first isolating the alkene complex. In all the cases, the isolation of C-H activation products was carried out on a neutral alumina column with hexane as eluant.

(i) $\text{Cp}^*\text{Re}(\text{CO})(\text{H})(\eta^3\text{-C}_3\text{H}_5)$ [15]. Irradiation of $\text{Cp}^*\text{Re}(\text{CO})_3$ in a quartz tube at 0°C for 1 h with a propene purge resulted in an IR spectrum having strong absorptions at 1961 and 1890 cm^{-1} for the propene complex [2], and weaker ones at 1904 and 1912 cm^{-1} for [15a]exo and [15b]endo respectively, plus residual absorptions from $\text{Cp}^*\text{Re}(\text{CO})_3$. Further irradiation intensified the absorptions from [15](exo, endo) relative to [2]. Following chromatography on neutral alumina and crystallization at -78°C , compounds [2], [15a]exo and [15b]endo were separated and fully characterized.

(ii) $\text{Cp}^*\text{Re}(\text{CO})(\text{H})(\eta^3\text{-C}_5\text{H}_9)$ [16]. In a similar procedure to that used in the synthesis of [15](exo, endo), the photochemical reaction of $\text{Cp}^*\text{Re}(\text{CO})_3$ and 2-pentene (a mixture of cis and trans isomers, ratio = [cis]/[trans] \approx 1/3.5 calculated by GC) in hexane gave a mixture of isomers of the η^3 -allylalkane rhenium hydrides [16c,d,e,f,k]. The photolysis reaction was carried out initially for

30min. at 0°C. The IR spectrum at this time showed $\nu(\text{CO})$ absorptions at 1955 and 1884 cm^{-1} attributable to the η^2 -2-pentene complex [3], and a weak band at 1891 cm^{-1} indicating the presence of one or more mono-carbonylhydride complexes [16]. The 1891 cm^{-1} absorption intensified relative to [3] on further irradiation for 60 min. Following chromatography on a neutral alumina column with hexane as eluant, the mixture of isomers [16c,d,e,f,k] was separated from 2-pentene complex [3] and the residual $\text{Cp}^*\text{Re}(\text{CO})_3$ and was isolated as a white solid. The mixture of isomers [16] could not be separated further, but was characterized by IR($\nu(\text{CO})$), MS and elemental analysis. The ^1H NMR clearly showed the presence of five isomers assigned to be [16c,d,e,f,k] (Fig.20). The hydride chemical shifts of -8.98, -9.32 and -9.45 ppm, indicated the presence of *exo* isomers, assigned to [16k], [16c] and [16e]. The two chemical shifts of -11.58 and -11.68 ppm, indicated the presence of *endo* isomers, assigned to [16d] and [16f] (see section 3.5.3.).

(iii) $\text{Cp}^*\text{Re}(\text{CO})(\text{H})(\eta^3\text{-C}_8\text{H}_{15})$ [17]. The complex [17] was synthesized by a similar method to that used for [15]. Irradiation of $\text{Cp}^*\text{Re}(\text{CO})_3$ and 1-octene in hexane for 30 min. resulted in an IR spectrum having absorptions at 1960 and 1888 cm^{-1} for the 1-octene complex [4], and another absorption (with about one half intensity of the former) at 1899 cm^{-1} for hydride complex [17b]*exo*, plus

residual absorptions from $\text{Cp}^*\text{Re}(\text{CO})_3$. Chromatography on an alumina column with hexane as the eluant gave two pure complexes [4] and [17b]exo. [17b]exo was fully characterized by IR($\nu(\text{CO})$), MS, element analysis and ^1H NMR, which verified it to be a monocarbonyl hydride. Furthermore, the ^1H NMR showed only one hydride resonance at -8.94 ppm indicating it to be the exo isomer, [17b]exo (see section 3.5.3.).

(iv) $\text{Cp}^*\text{Re}(\text{CO})_2(\eta^2\text{-C}_6\text{H}_8)$ [10]. In an analogous manner to that used for [16], irradiation of $\text{Cp}^*\text{Re}(\text{CO})_3$ and cyclohexene in hexane yielded three products, (complexes of cyclohexene [6], η^2 -1,3-cyclohexadiene [10] and η^4 -1,3-cyclohexadiene [13]), which were separated by chromatography on an alumina column with hexane as an eluant. The complex [10] was also formed separately by the photochemical reaction of the cyclohexene complex [6] and cyclohexene in hexane solvent under a purge of nitrogen gas. Under these conditions product formation is accompanied by decomposition of the cyclohexene complex [6] to give $\text{Cp}^*\text{Re}(\text{CO})_3$, so that the yield of [10] was low. The η^2 -1,3-cyclohexadiene complex [10] was separately synthesized by the direct photochemical reaction of $\text{Cp}^*\text{Re}(\text{CO})_2(\text{N}_2)$ and 1,3-cyclohexadiene (see Chapter II) in order to confirm its formation as a product in the above reaction, as this apparently involves the photochemical double C-H activation of

coordinated cyclohexene in $\text{Cp}^*\text{Re}(\text{CO})_2(\eta^2\text{-cyclohexene})$ [6]. These results for complex [10] were included in Chapter II.

(v) $\text{Cp}^*\text{Re}(\text{CO})(\text{Br})(\eta^3\text{-C}_3\text{H}_5)$ [18]. This compound was directly derived from the hydrido(allyl) complex [15](*exo*, *endo*). A solution of the isomers of [15a]*exo* and [15b]*endo* in CHBr_3 solvent was stirred overnight at room temperature. The IR spectrum showed the $\nu(\text{CO})$ absorption at the position 1944 cm^{-1} in CHBr_3 . Workup of the mixture by passing it through a neutral alumina column with hexane as an eluent eluted first a mixture of $\text{Cp}^*\text{Re}(\text{CO})_2\text{Br}_2$ and propene complex [2], then the pure complex [18], which was isolated as a yellowish solid and characterized.

3.3. Characterization

The hydride complexes [15]-[17] were isolated as white solids. They are soluble in non-polar organic solvents such as hexane and benzene. [15] dissolves in CHBr_3 with bromination to produce the bromide complex $\text{Cp}^*\text{Re}(\text{CO})_2(\eta^3\text{-allyl})(\text{Br})$ [18]. These hydride complexes must be kept under nitrogen at low temperature (-78°) to prevent decomposition and *exo-endo* isomerization. The compounds were characterized by elemental analysis, $\text{IR}(\nu(\text{CO}))$, mass spectroscopy, $^1\text{H NMR}$ and, in the case of *exo* and *endo* isomers of

[15], also by X-ray structure determination. Spectroscopic data are collected in Tables 8-10.

(1) $\text{Cp}^*\text{Re}(\text{CO})(\text{H})(\eta^3\text{-C}_3\text{H}_5)$ [15]. The *exo* and *endo* isomers of [15] each gave satisfactory elemental analyses and exhibited similar EI mass spectra, consisting of the parent peak at m/z 392 with similar fragmentation patterns (see Section 3.5.4.). In the IR spectra, the expected single $\nu(\text{CO})$ absorption in hexane occurred at 1904 cm^{-1} (*exo*) and 1912 cm^{-1} (*endo*). The ^1H NMR spectrum provided the best evidence for the presence of the hydride, Cp^* and η^3 -allyl groups and for the isomeric purity of each isomer. The hydride resonances occurred at δ -9.23 (*exo*) and -11.65 ppm (*endo*) (C_6D_6 solutions). The five allylic protons are all inequivalent in both isomers and their chemical shift assignments were carried out by NOE experiments, by decoupling, and by computer simulation, as discussed in Section 3.5.3. The X-ray structures of [15a]*exo* and [15b]*endo* were determined by Dr. R.J. Batchelor and Dr. R.H. Jones in Professor F.W.B. Einstein's laboratory at S.F.U.

Crystals of [15a]*exo* and [15b]*endo* are composed of equal amounts of the R- and S- enantiomers of these chiral complexes. The X-ray structures of one enantiomer of each are depicted in Fig.23(a) ([15a]*exo*) and Fig.23(b) ([15b]*endo*).⁶³ In both cases the hydride position was located. The η^3 -allyl group is symmetrically bonded to

Fig.21. ^1H NMR Spectrum

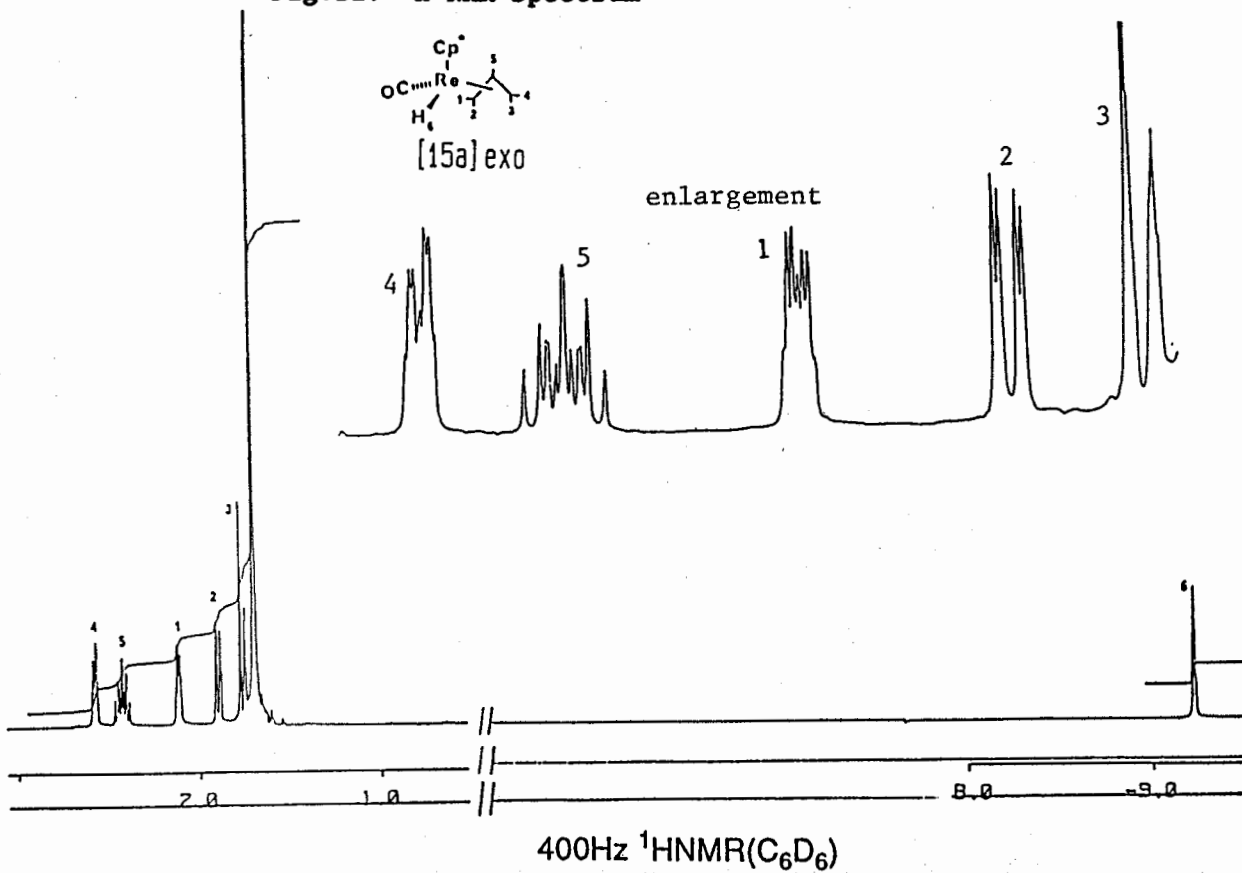
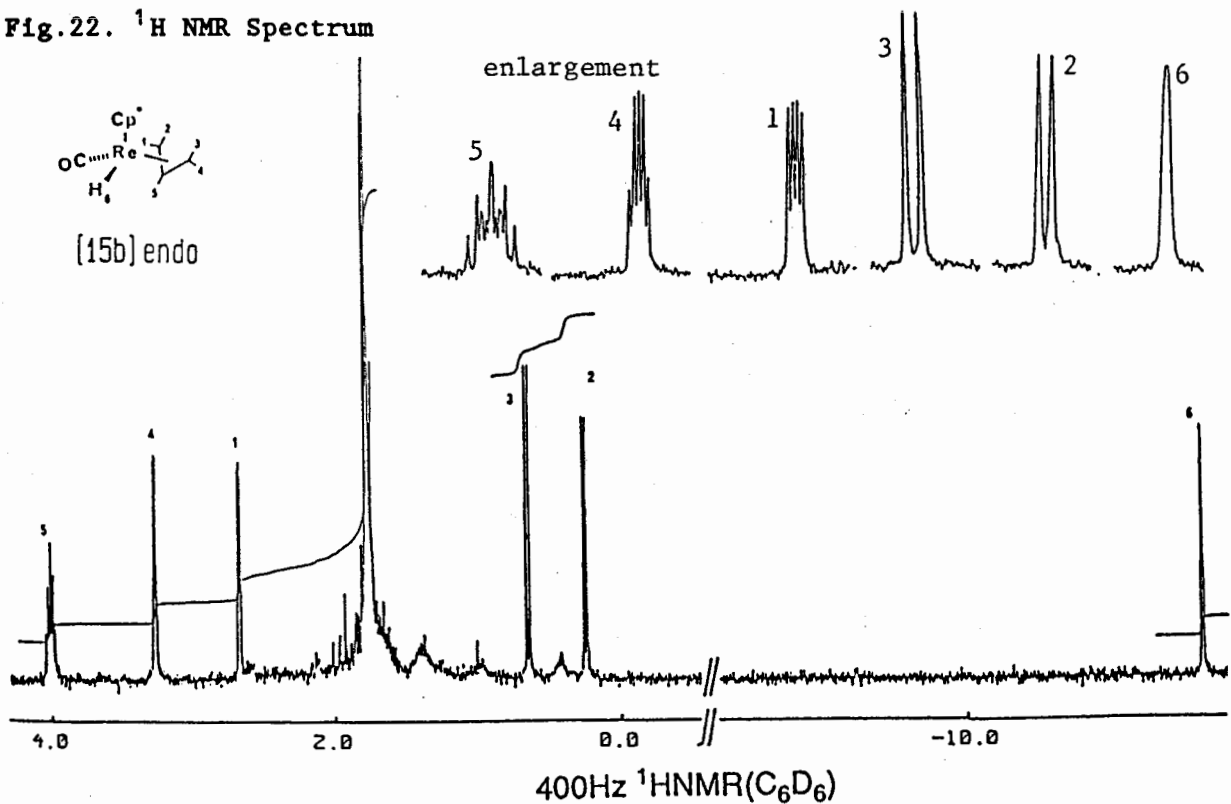
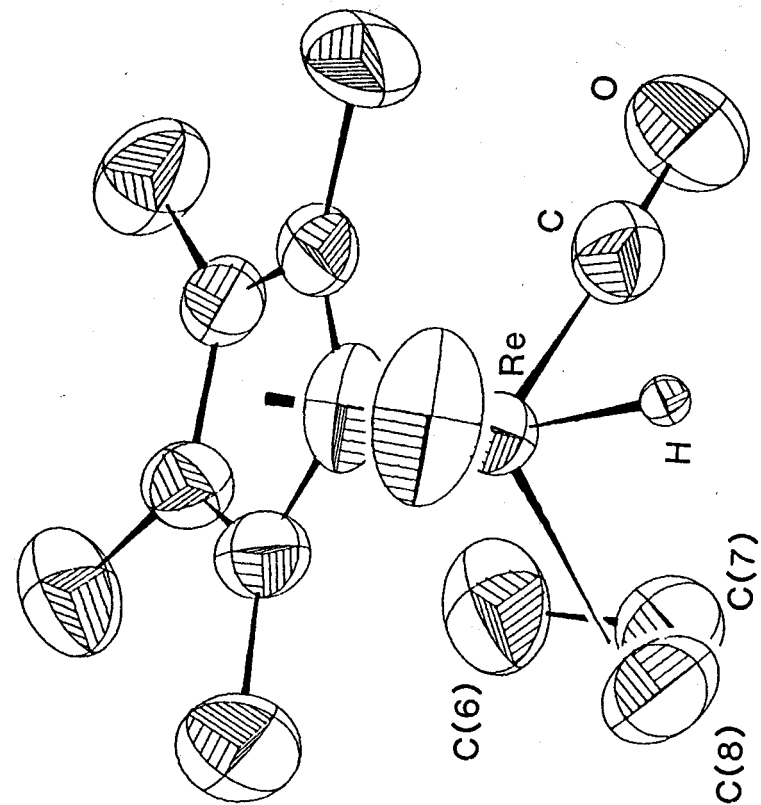
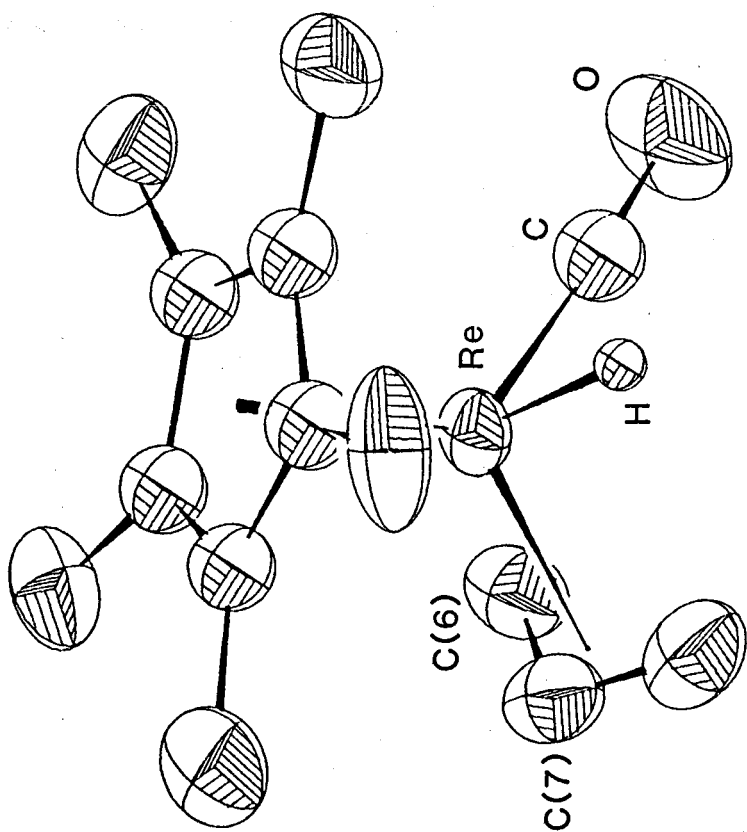


Fig.22. ^1H NMR Spectrum





[15b]endo



[15a]exo

Fig. 23. Perspective View of Isomers of $\text{Cp}^*\text{Re}(\text{CO})(\text{H})(\eta^3\text{-C}_3\text{H}_5)$ [15]

Fig.24. Computer Simulation of ^1H NMR Spectrum

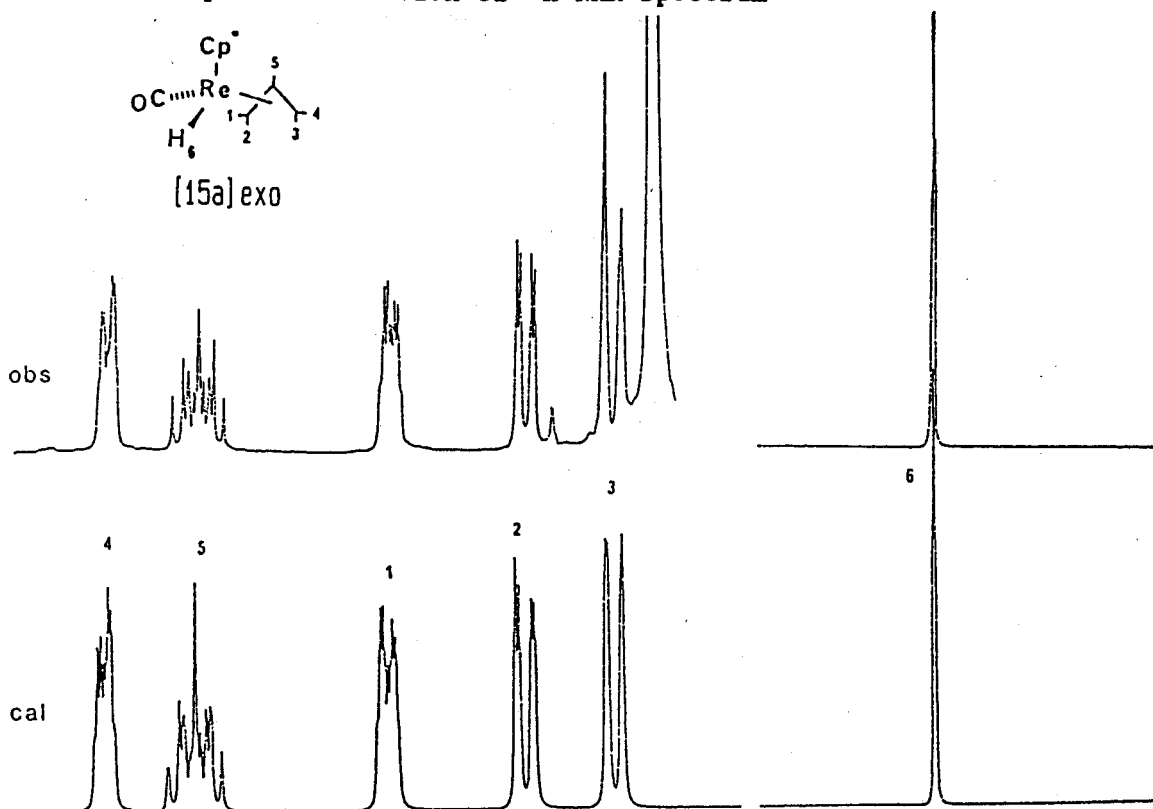


Fig.25. Computer Simulation of ^1H NMR Spectrum

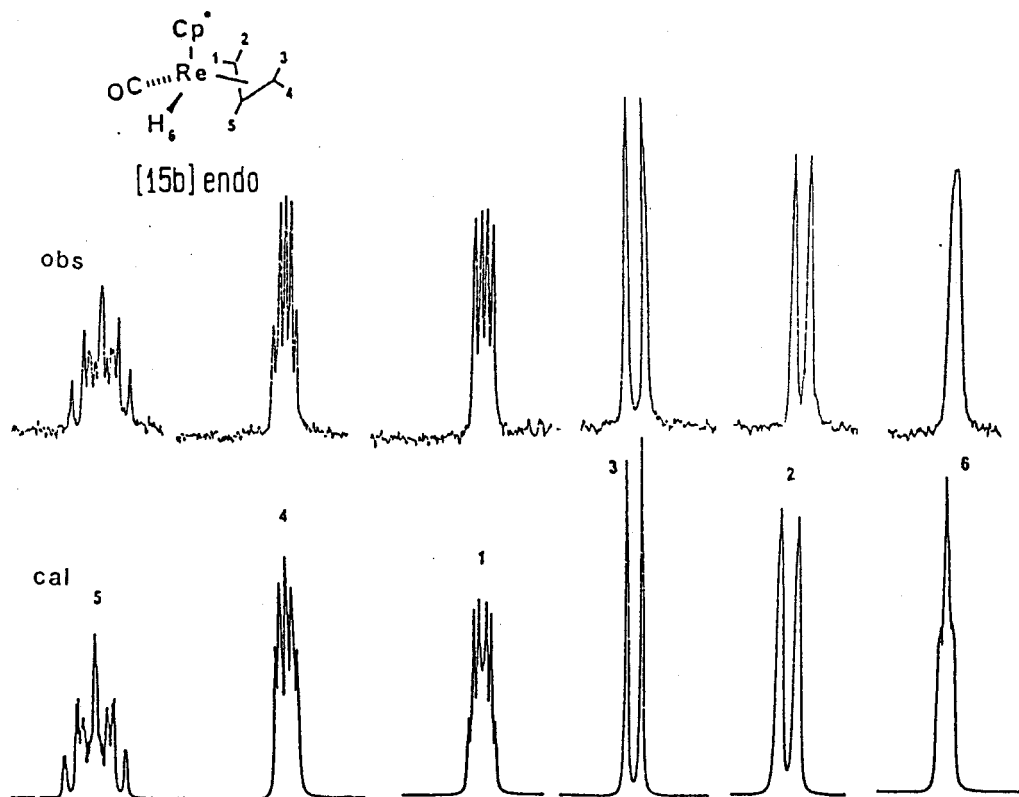


Fig.26. Computer Simulation of ^1H NMR Spectrum

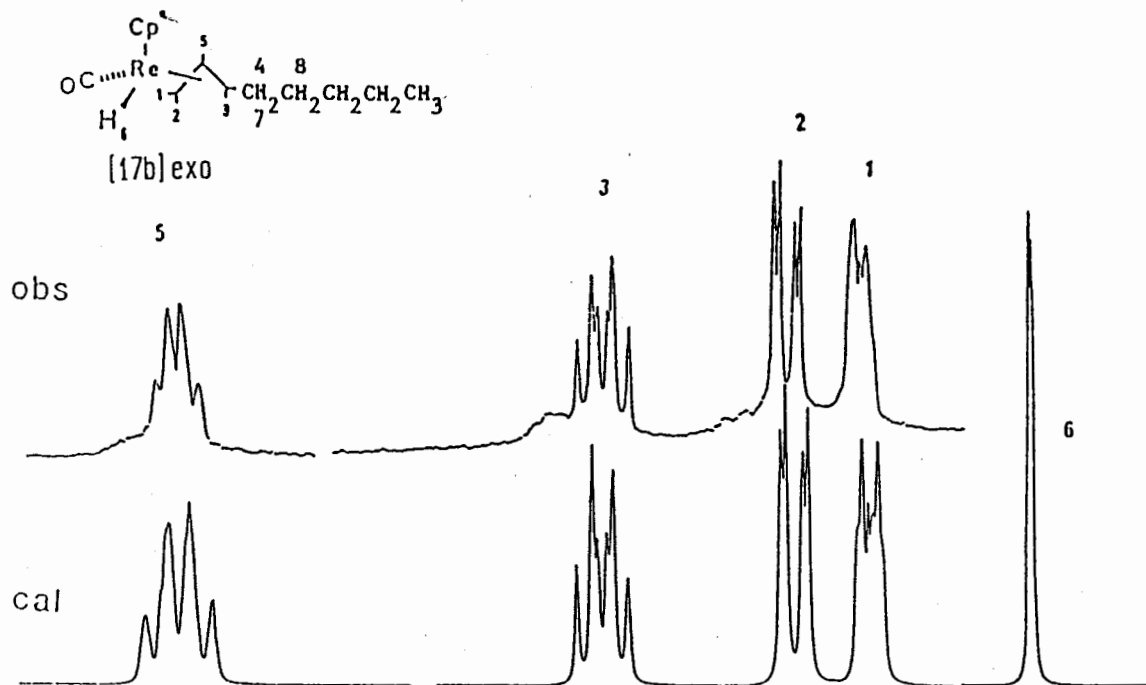
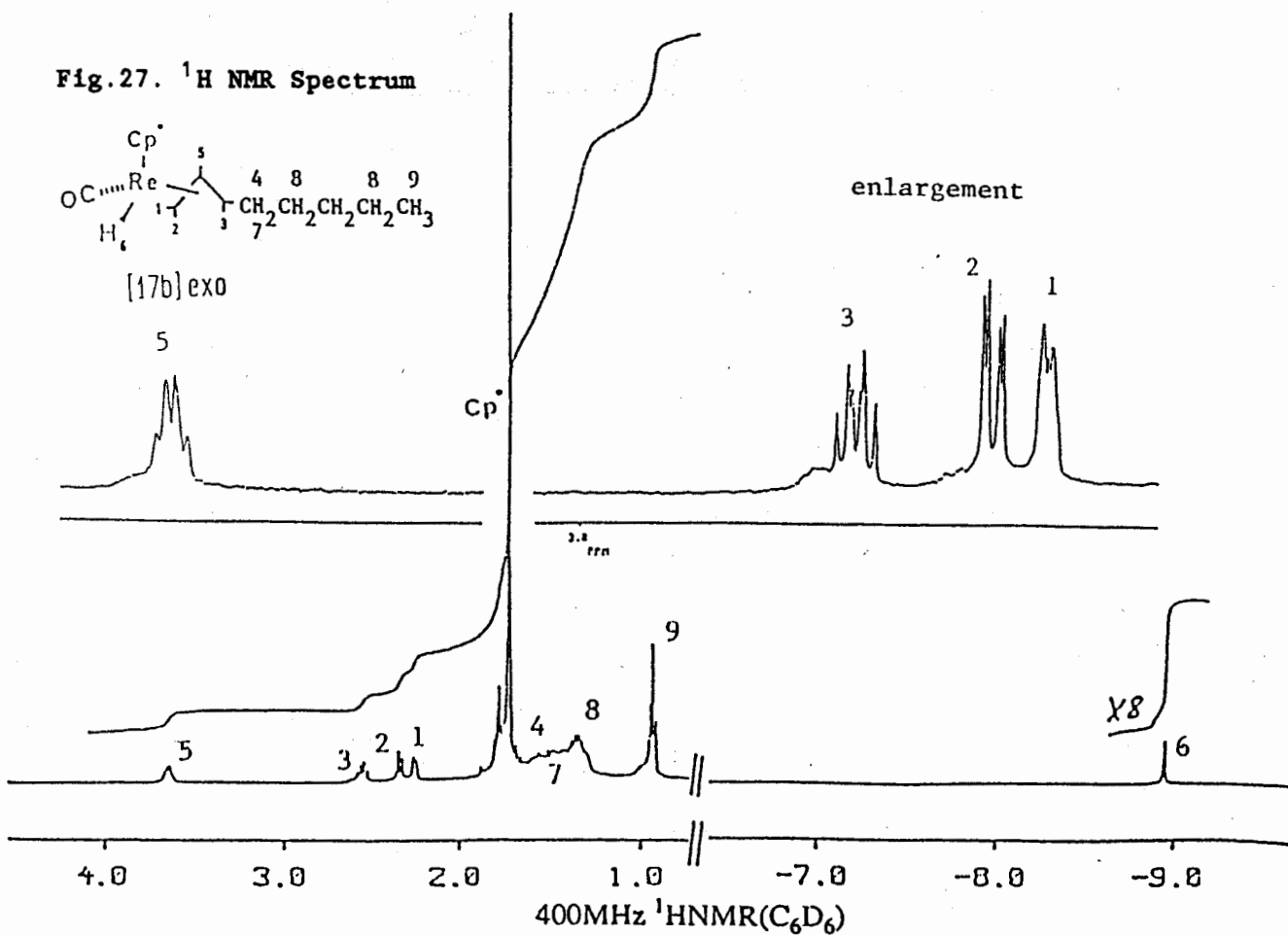


Fig.27. ^1H NMR Spectrum



Re in [15a]exo with distances Re-C(6) = 2.260(9) Å and Re-C(8) = 2.257(10) Å to the terminal carbons and Re-C(7) = 2.179(9) Å to the central carbon atom; however in [15b]endo, the allyl group is somewhat asymmetrically bonded, with distances Re-C(6) = 2.191(9) Å and Re-C(8) = 2.242(9) Å to the terminal carbons and Re-C(7) = 2.215(9) Å to the central carbon atom. Correspondingly, the C-C bond lengths of the allyl group in [15a]exo are equal within error (C(6)-C(7) = 1.374(16) Å; C(7)-C(8) = 1.363(17) Å), but they differ in [15b]endo (C(6)-C(7) = 1.446(13) Å; C(7)-C(8) = 1.386(13) Å). The carbon atom C(6) that is pseudotrans to the hydride ligand is the one having shorter Re-C and longer C-C bond length in [15]endo.

The allyl group of [15b]endo appears to be more strongly bonded to Re than that of [15a]exo as shown by the D values⁶³ (the distances from Re to the centre of mass of the three carbon atoms) in [15a]exo (D = 1.984 Å) and in [15b]endo (D = 1.957 Å). The more strongly bonded allyl group in [15b]endo relative to [15a]exo appears to be compensated for by a more weakly bound carbonyl in the former, as shown by the Re-C and C-O distances in [15a]exo (Re-C = 1.842(10) Å; C-O = 1.184(12) Å) and in [15b]endo (Re-C = 1.889(9) Å; C-O = 1.140(11) Å). Consistent with this, the IR(ν (CO)) of [15b]endo (1912 cm⁻¹) is higher than that of [15a]exo (1904 cm⁻¹).

(ii) $\text{Cp}^*\text{Re}(\text{CO})(\text{H})(\eta^3\text{-C}_5\text{H}_9)$ [16]. This product was not separated into isomers, though it is believed to be a mixture of five distinct isomers by ^1H NMR. It gave satisfactory elemental analysis and the expected M^+ peak at m/z 420 in the mass spectrum. The IR spectrum in hexane gave only one broad $\nu(\text{CO})$ absorption at 1891 cm^{-1} ; the absorptions for specific isomers are either all coincident or could not be distinguished at the resolution of this spectrum ($\pm 5\text{ cm}^{-1}$). The evidence for five isomers is that the ^1H NMR spectrum in C_6D_6 shows the presence of five individual resonances in the hydride region (Fig.20), three occur near δ -9 and are assigned to *exo* isomers by comparison with [15a]*exo* and two near δ -11 and are assigned to *endo* isomers by comparison with [15b]*endo*. The tentative basis for assigning the isomers involved is discussed in section 3.5.3.

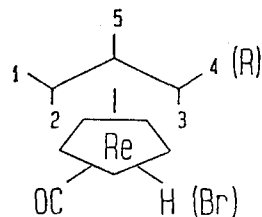
(iii) $\text{Cp}^*\text{Re}(\text{CO})(\text{H})(\eta^3\text{-C}_8\text{H}_{15})$ [17]. This was isolated as a single complex that gave the expected elemental analysis and M^+ parent at m/z 462 in the mass spectrum. The IR exhibits a single $\nu(\text{CO})$ absorption at 1899 cm^{-1} (hexane). In the ^1H NMR the hydride resonance occurs at δ -8.94 (C_6D_6) and on this basis it is assigned as the *exo* isomer [17b]. The resonances of the $\eta^3\text{-C}_8\text{H}_{15}$ group were completely assigned by decoupling experiments and by a computer simulation as described in section 3.5.3.

Table 8. Some Spectroscopic Parameters
of the Complexes [15]-[18]

Complex	IR(hexane) $\nu(\text{CO}) \text{ cm}^{-1}$	$^1\text{H NMR}(\text{C}_6\text{D}_6)$		MS(m/z) ^h	
		$\delta(\text{Cp}^*)^a$	$\delta(\text{Re-H})^b$	M ⁺	base
[15a]exo	1904(s)	1.69	-9.23	392	360
[15b]endo	1912(s)	1.77	-11.65	392	360
[16c,d,e,f,k] ^c	1891(s)	1.75 ^d	-8.98 ^e -9.32 ^e -9.45 ^e -11.58 ^f -11.68 ^f	420	386
[17b]exo	1899(s)	1.71	-8.94	462	428
[18b]endo	1962(s)	1.87 ^g		470 ⁱ	400

Abbreviation: s = strong. ^aCp* was a singlet peak in all cases. ^bHydrido was a singlet broad peak in all cases. ^c [16c,d,e,f,k] was a mixture and not separated. ^dThis Cp* is assignable to [16c]exo. ^e Hydrido chemical shifts of exo isomers, the ratio is -8.98/-9.32/-9.45 = 1/6.5/2.2 = [16k]exo/[16c]exo/[16e]exo. ^fHydrido chemical shifts of endo isomers, the ratio is -11.58/-11.68 = 2.5/1 = [16d]endo/[16f]endo. ^g[18b]endo was measured at 400MHz in CDCl₃ and others were in C₆D₆. ^hfor ¹⁸⁷Re. ⁱfor ¹⁸⁷Re and ⁷⁹Br.

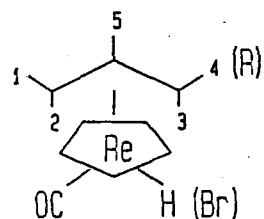
Table 9. Experimentally Observed Chemical Shifts for the Complexes [15]-[18]



Complex	Chemical Shift ^a δ (ppm)						
	Cp*	1-	2-	3-	4-	5-	6-
[15a]exo	1.69	2.11	1.89	1.76	2.57	2.42	-9.23
[15b]endo	1.77	2.67	0.25	0.65	3.26	4.01	-11.65
[17b]exo	1.71	2.25	2.34	2.56		3.65	-8.94
[18b]endo	1.87	2.98	1.05	1.80	3.15	4.59	

^aAll measurements were performed at 400MHz in C₆D₆ except [18b]endo in CDCl₃.

Table 10. Coupling Constants from Experimental
¹H NMR Spectra of Complexes [15]-[18]

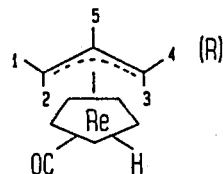


Complex	Coupling Constant ^a (in Hz)										
	J _{1,2}	J _{3,4}	J _{1,5}	J _{4,5}	J _{2,5}	J _{3,5}	J _{1,6}	J _{2,6}	J _{3,6}	J _{4,6}	J _{5,6}
[15a]exo ^b	2.3	2.3	6.7	7.2	9.5	10.2	2.5	0.0	0.0	2.0	0.5
[15b]endo ^b	1.5	1.0	5.5	5.5	8.4	9.3	2.5	0.0	0.0	2.8	1.0
[17b]exo ^{b,c}	2.7	7.2 ^d	6.8	1.5 ^d	10.0	9.8					
[18b]endo ^{b,c}	1.5	1.5	6.9	6.9	7.1	9.4					

^aAll coupling constants have errors smaller than ± 0.2 Hz and are given as absolute values. ^bAs determined by decoupling experiment.

^cThe error of these coupling constants is less than ± 0.5 Hz due to complicated spectra and second order coupling effects. ^dThe coupling constants are between the 4-methenyl and 3- or 5- proton.

Table 11. The calculated Coupling Constants for Complexes [15](*exo,endo*) and [17b]*exo*^a



Coupling Constants ^b J (Hz)	Complex			Coupling Constants ^b J (Hz)	Complex		
	[15a]	[15b]	[17b]		[15a]	[15b]	[17b]
J(1,2)	1.7	1.9	2.6	J(3,4)	2.5	0.4	7.2 ^c
J(1,3)	0.5	0.5	0.6	J(3,5)	10.5	8.8	9.7
J(1,4)	2.1	2.1	0.0	J(3,6)	0.3	0.6	0.0
J(1,5)	7.1	5.6	7.0	J(3,7)			6.5 ^c
J(1,6)	2.5	2.9	2.6	J(4,5)	7.1	5.8	1.5
J(1,7)			0.0	J(4,6)	2.0	3.2	0.3
J(2,3)	0.6	0.5	0.5	J(4,7)			10.0 ^c
J(2,4)	0.6	0.5	0.0	J(5,6)	0.9	1.0	1.0
J(2,5)	10.0	8.3	10.0	J(5,7)			1.5 ^c
J(2,6)	0.2	0.6	0.5	J(6,7)			0.0
J(2,7)			0.0				

^aThe calculated coupling constants are given by running the Panic programme in a Bruker WM-400 instrument on the basis of the data shown in Tables 9, 10 and in the literature.⁶⁶ ^bAll coupling constants are absolute magnitudes in Hz. ^c4- and 7- are two inequivalent protons of 4-methenyl group in complex [17b]*exo*.

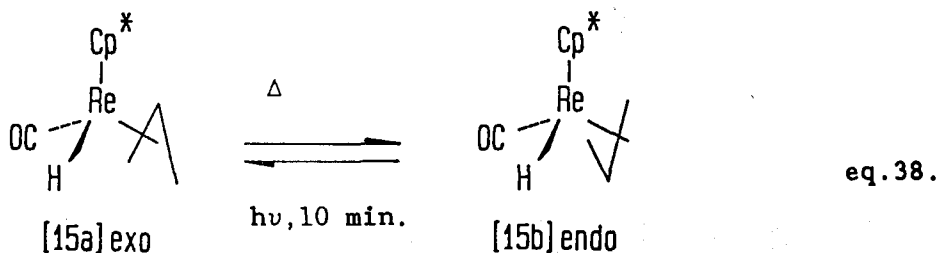
(iv) $\text{Cp}^*\text{Re}(\text{CO})(\text{Br})(\eta^3\text{-C}_3\text{H}_5)$ [18]. Although this was synthesized by bromination of a mixture of [15](*exo*, *endo*) using CHBr_3 , the spectroscopic properties show that only a single isomer of [18] results. This gave the correct elemental analysis, and M^+ at m/z 470 (^{187}Re , ^{79}Br). The IR spectrum exhibits the expected single $\nu(\text{CO})$ band at 1962 cm^{-1} (hexane). The ^1H NMR spectrum was assigned by NOE and decoupling procedures which showed that the allyl group is *endo* to the Cp^* ring (see section 3.5.3.).

(v) Computer-Simulation of ^1H NMR. The coupling constants for complexes [15a]*exo*, [15b]*endo*, [17b]*exo* and [18b]*endo* listed in Table 10 were those estimated experimentally from the decoupling experiments. The calculated coupling constants for complexes [15a]*exo*, [15b]*endo* and [17b]*exo* in Table 11 were obtained by using the Panic programme in a Bruker WM-400 instrument using the observed estimated chemical shifts and coupling constants shown in Tables 9-10 as input to best fit the observed ^1H NMR spectra (see Figs.24-26).

Table 10 gives the magnitude of the observed coupling constants from the decoupling experiments. These data show: (1) the *geminal* constants ($J(1,2)$ and $J(3,4)$) are 0.8-1.2 Hz greater in magnitude in the *exo* configuration than in the *endo* configuration; (2) the *trans* vicinal constants ($J(2,5)$ and $J(3,5)$) are 1.3-2.9 Hz

greater in the *exo* configuration than in the *endo* configuration.

(vi) **Exo-endo Isomerization of [15]** Studies on the conformation interconversion between [15a]*exo* and [15b]*endo* have displayed that it is an irreversible conformational conversion from [15a]*exo* to [15b]*endo* under thermal conditions. However, there is a photochemical conformational conversion from [15b]*endo* to [15a]*exo*.



[15a]*exo* can slowly convert to [15b]*endo* even at -12°C . The conversion rate of [15a]*exo* to [15b]*endo* has been measured by using ^1H NMR spectroscopy. The following experimental results indicated that [15b]*endo* could not convert to [15a]*exo* under thermal conditions: A pure sample of [15a]*exo* was kept at 31°C in the dark for one week, and the ^1H NMR spectrum showed that [15b]*endo* was present in a ratio of [15a]*exo* to [15b]*endo* ≈ 0.34 . Then, this mixture of two isomers was kept at 5°C in a dark for forty days and checked by ^1H NMR again to show the ratio of [15a]*exo* to [15b]*endo* ≈ 0.32 , indicating a small change of the ratio within the error range

of ^1H NMR experiments. Subsequently, this sample was kept at 25°C for another two weeks and checked by ^1H NMR showing a similar ratio of [15a]exo to [15b]endo ≈ 0.32 . Furthermore, during saturation transfer experiments at 74°C , no evidence for conversion from [15b]endo to [15a]exo was detected when each proton of [15b]endo was saturated separately. However, [15b]endo can readily convert to the isomer [15a]exo under UV light. The evidence comes from the IR and ^1H NMR spectroscopic data. A pure sample of [15b]endo in hexane solution has only one IR band ($\nu(\text{CO})$) at 1912 cm^{-1} . Irradiation of this solution gave an IR($\nu(\text{CO})$) spectrum that exhibited two strong absorptions at 1912 and 1904 cm^{-1} with an intensity ratio of 1912 to $1904 \approx 0.5$, indicating that [15a]exo ($\nu(\text{CO}): 1904\text{ cm}^{-1}$) was present as the major isomer. Other very weak bands from $\text{Cp}^*\text{Re}(\text{CO})_3$ (2013 , 1922 cm^{-1}) and [2] (1961 , 1890 cm^{-1}) indicated a very small amount of decomposition. Similarly, the ^1H NMR spectrum showed two hydride signals at $\delta -9.2$ (exo), -11.7 (endo) with an integral ratio of *exo/endo* $\approx 2.5:1$, indicating that [15b]endo can convert to [15a]exo under UV light.

Kinetic parameters for the *exo-endo* interconversion of [15a]exo to [15b]endo have been evaluated using ^1H NMR spectroscopy. Four samples of a mixture of [15a]exo and [15b]endo in NMR tubes wrapped with aluminium foil were kept at temperatures of 25 , 30 , 35

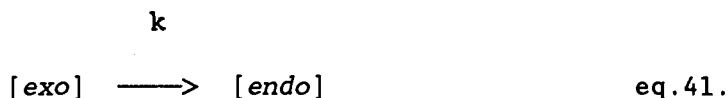
and 40°C respectively, and monitored by 100MHz ¹H NMR. The intensities of the two hydride resonances were carefully measured to determine the rate constant k using the rate eq.39.

$$\ln Y = kt \quad \text{eq.39.}$$

$$\text{where } Y = (1 + r)^{-1} (1 + ([endo]_t/[exo]_t))$$

$$r = [endo]_0/[exo]_0 \quad \text{eq.40.}$$

The rate eq.39 is deduced as follows.



initial $t = t_0$

concentration $[exo]_0$ $[endo]_0$

when $t = t_0 + \Delta t$

concentration $[exo]_t$ $[endo]_t$

$$\text{Given } [exo]_0 + [endo]_0 = [exo]_t + [endo]_t = \text{const.} \quad \text{eq.42.}$$

The rate of disappearance of [15a]exo can be written as

$$R = -(1/a)(d[exo]/dt) = k[exo] \quad \text{eq.43.}$$

where a is the reactant coefficient.

Assuming that the $\text{exo} \rightarrow \text{endo}$ interconversion is a first-order unimolecular reaction, in which the rate of reaction depends only on one reactant, i.e., only one [15a]exo molecule disappears to produce one [15b]exo molecule. Thus, the reactant coefficient $a = 1$ and eq.43 becomes

$$-(d[\text{exo}]/dt) = k[\text{exo}] \quad \text{eq.44.}$$

Integration of eq.44 leads to

$$-\int_{[\text{exo}]_0}^{[\text{exo}]_t} (d[\text{exo}]/[\text{exo}]) = k \int_{t_0}^t dt \quad \text{eq.45.}$$

This gives

$$-(\ln[\text{exo}]_t - \ln[\text{exo}]_0) = k(t - t_0) = k\Delta t \quad \text{eq.46.}$$

and hence, the standard expression for the first-order $\text{exo} \rightarrow \text{endo}$ interconversion is given

$$\ln([\text{exo}]_0/[\text{exo}]_t) = k\Delta t \quad \text{eq.47.}$$

By definition of the half-life, at $\Delta t = t_{1/2}$, $[\text{exo}]_t = [\text{exo}]_0/2$; therefore, eq.47 can be rewritten as

$$\ln 2 = kt_{1/2} \quad \text{eq. 48.}$$

the half-life is then

$$t_{1/2} = (\ln 2)/k \quad \text{eq. 49.}$$

Assuming that the initial concentration ratio of $[endo]_0$ to $[exo]_0$ is r , eq. 42 becomes

$$[exo]_0 + r[exo]_0 = [exo]_t + [endo]_t \quad \text{eq. 50.}$$

and

$$(1 + r)[exo]_0 = [exo]_t + [endo]_t$$

$$(1 + r)([exo]_0/[exo]_t) = \{1 + ([endo]_t/[exo]_t)\}$$

so that

$$[exo]_0/[exo]_t = \{1 + ([endo]_t/[exo]_t)\}(1 + r)^{-1} \quad \text{eq. 51.}$$

Assuming

$$Y = [exo]_0/[exo]_t = \{1 + ([endo]_t/[exo]_t)\}(1 + r)^{-1}$$

thus, eq. 47 becomes $\ln Y = k\Delta t \quad \text{eq. 39.}$

Eq. 39 is practically more convenient than the standard expression (eq. 47). Eq. 39 does not require the measurement of the

absolute concentrations of $[exo]_0$ and $[exo]_t$, and only needs the ratios of $[endo]_0$ to $[exo]_0$ and $[endo]_t$ to $[exo]_t$. Thus, the calculation of the results will not involve the errors from the measurements of the concentrations of $[exo]_0$ and $[exo]_t$.

The data for the [15a]exo to [15b]endo conversion rates are listed in Table 12. Each conversion rate constant, k , was obtained by a least-squares fit of $\ln Y$ vs. Δt at four different temperatures (25, 30, 35, 40°C) respectively. The Arrhenius activation energy can be evaluated from the following, eq.52 or eq.53.

$$k = A \exp(-E_a/RT) \quad \text{eq.52.}$$

Where R is the gas constant and A is a constant known as the frequency factor.

$$R = 8.314 \text{ JK}^{-1}\text{mol}^{-1} = 1.98 \text{ cal.K}^{-1}\text{mol}^{-1}$$

or $\ln k = -(E_a/RT) + \text{const.} \quad \text{eq.53.}$

Then, a straight line was drawn by a least-squares fit of $\ln k$ vs. $-(1/T)$ at four different temperatures, (see Fig.28). The straight line of $\ln k$ vs. $-(1/T)$ can be expressed by the following eq.54 as well.

$$\ln k = 14.6 \times 10^3 (-1/T) + 39.6 \quad \text{eq.54.}$$

Table 12. Kinetic data for *exo* \rightarrow *endo* conversion of [15]

T = 298K $r^a = 0.626$ $k^b = (9.21 \pm 0.68) \times 10^{-5}$ $\tau_{1/2} = 125 \text{ h}^e$

Δt (min.)	$[\textit{endo}]_t / [\textit{exo}]_t^c$	Y^d	$\ln Y$
0	0.626	1.000	0
180	0.662	1.022	0.0217
360	0.684	1.036	0.0354
540	0.711	1.052	0.0507

T = 303K $r^a = 0.484$ $k^b = (19.33 \pm 0.55) \times 10^{-5}$ $\tau_{1/2} = 59.8 \text{ h}^e$

Δt (min.)	$[\textit{endo}]_t / [\textit{exo}]_t^c$	Y^d	$\ln Y$
0	0.484	1.000	0
90	0.506	1.014	0.0139
180	0.537	1.035	0.0344
270	0.562	1.052	0.0507
360	0.590	1.071	0.0686

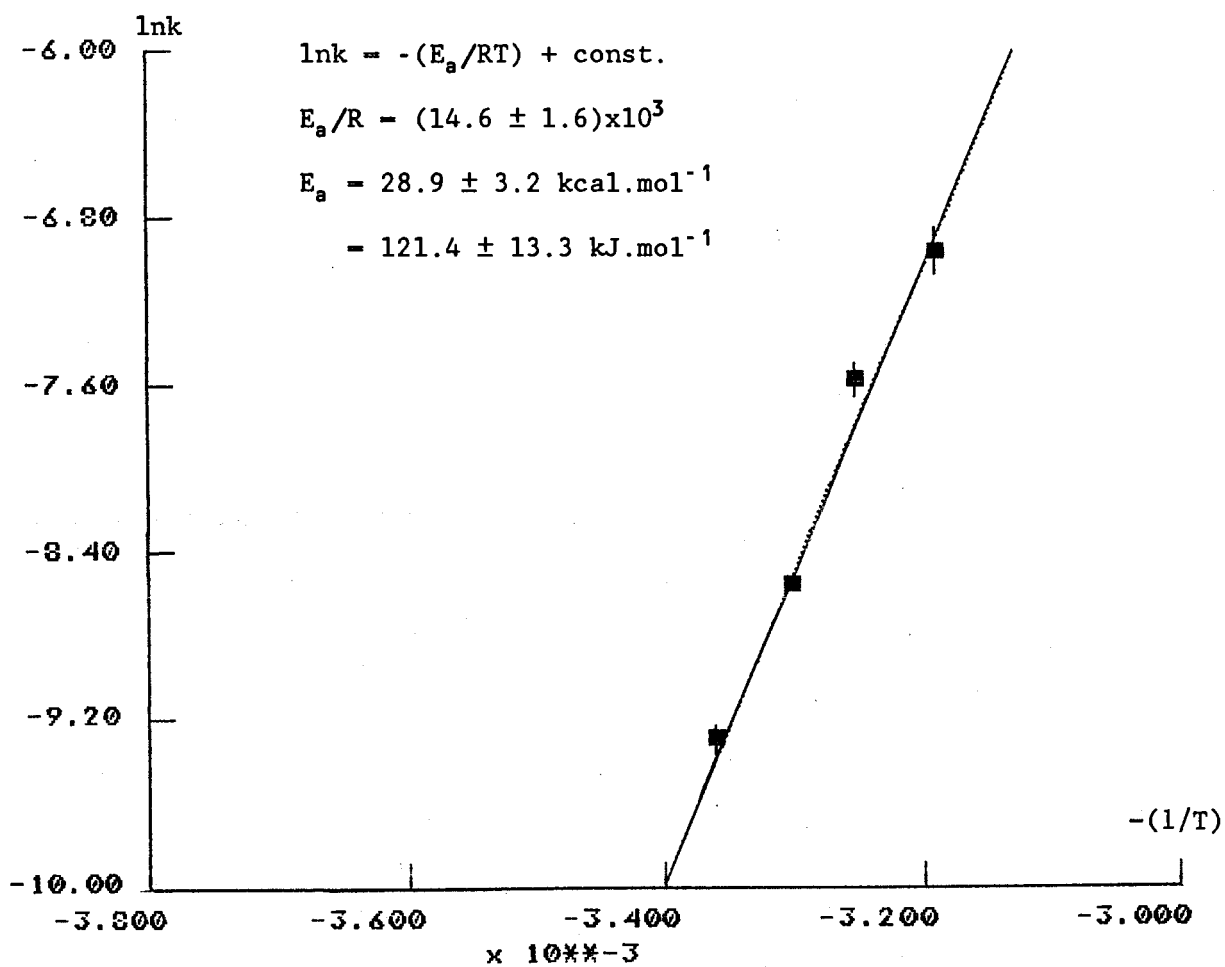
Table 12. (continued)

T = 308K r ^a = 1.007 k ^b = (51.45 ± 4.00)x10 ⁻⁵ t _{1/2} = 22.5 h ^e			
Δt (min.)	[endo] _t /[exo] _t ^c	Y ^d	lnY
0	1.007	1.000	0
60	1.058	1.025	0.0247
90	1.105	1.049	0.0478
140	1.154	1.073	0.0705

T = 313K r ^a = 0.543 k ^b = (94.95 ± 10.41)x10 ⁻⁵ t _{1/2} = 12.2 h ^e			
Δt (min.)	[endo] _t /[exo] _t ^c	Y ^d	lnY
0	0.543	1.000	0
60	0.620	1.050	0.0488
90	0.700	1.102	0.0971
140	0.754	1.137	0.1284

^aAs calculated by eq.40. ^bAs obtained by a least-squares fit of lnY vs. Δt in min⁻¹, see eq.39. ^cAs determined by integration of 100MHz ¹H NMR in toluene-d₈. ^dSee eq.39. ^eAs calculated by eq.49.

Fig.28. $\ln k$ vs. $-(1/T)$



From the slope of this plot

$$E_a/R = (14.6 \pm 1.6) \times 10^3$$

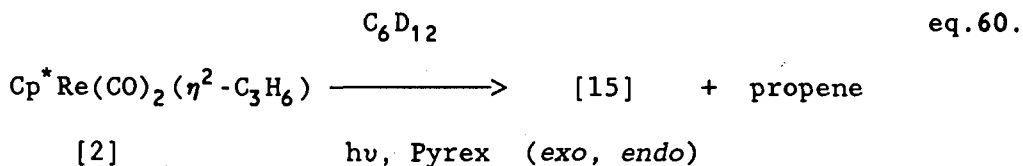
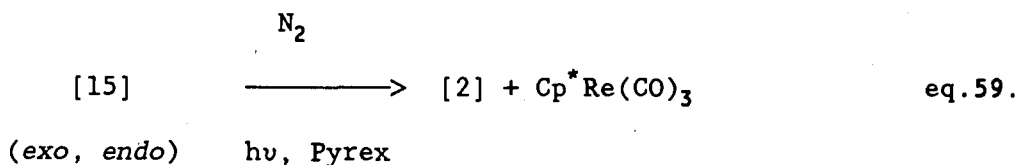
so that $E_a = 28.9 \pm 3.2 \text{ kcal.mol}^{-1} = 121.4 \pm 13.3 \text{ kJ.mol}^{-1}$

This value of the Arrhenius activation energy is larger than those (12-17 kcal.mol⁻¹) found for the fast fluxion allylic complexes of molybdenum or tungsten,^{65b} and is very close to the energy barrier (28.9-31.4 kcal.mol⁻¹) in the irreversible *endo*→*exo* conversion of allyl ruthenium complexes reported by Gibson.⁶⁶ⁱ

3.4. Chemical Reactions

In the synthetic method (eq.55), irradiation of a hexane solution of Cp^{*}Re(CO)₃ under a propene purge resulted in the propene complex [2] being formed first, accompanied by a small amount of the two isomers of [15](*exo*, *endo*). If irradiation was prolonged, the two isomers of [15](*exo*, *endo*) became the major products (see eq.55). No evidence for the complex Cp^{*}Re(CO)₂(H)(σ-C₃H₅) (36), which would be the expected product of intermolecular allylic C-H activation, was observed during the experiment. The results suggest that [15](*exo*, *endo*) are formed via the intramolecular allylic C-H activation of the propene complex [2] upon loss of CO.

formation of the tricarbonyl was suppressed and the product was a mixture of [15](*exo*, *endo*) with unreacted [2], see eq.57. We interpret the formation of the tricarbonyl in eq.56 to be due to the loss of CO from [2] and reaction of this CO with further [2]. In agreement with this, complex [2] was found to react with CO at 0°C when irradiated (but not otherwise) in a Pyrex tube to give the tricarbonyl (see eq.58). When a mixture of [2] and [15](*exo*, *endo*) was irradiated at 0°C under 1 atm CO, the IR bands of complex [15](*exo*, *endo*) rapidly disappeared followed, more slowly, by the disappearance of those of [2], suggesting that the propene complex [2] was initially reformed by addition of CO to [15](*exo*, *endo*). In addition, irradiation of a hexane solution of [15](*exo*, *endo*) in a Pyrex tube under a nitrogen purge for 15 min. gave products [2] and Cp*Re(CO)₃ (eq.59).



CO to give [15]. Irradiation of [2] in a Pyrex tube in the presence of PMe_3 (eq.61) gave a mixture of residual [2] and a small amount of [15] (*exo, endo*), but mainly $\text{Cp}^*\text{Re}(\text{CO})_2(\text{PMe}_3)$ (37) (Fig.29), and no formation of $\text{Cp}^*\text{Re}(\text{CO})(\text{PMe}_3)(\eta^2\text{-C}_3\text{H}_6)$ [12] ($\nu(\text{CO})$: 1845 cm^{-1} , see Table 4). The formation of (37) is consistent with the capture of 16e- intermediate $[\text{Cp}^*\text{Re}(\text{CO})_2]$ by PMe_3 . The formation of [12] would have been expected if a corresponding 16 e- intermediate $[\text{Cp}^*\text{Re}(\text{CO})(\eta^2\text{-C}_3\text{H}_6)]$ were formed by CO loss from [2] prior to C-H activation. An alternative explanation could be that compound [12] is itself unstable under the photolysis conditions, or that the rate of C-H activation is much greater than that of PMe_3 capture. To test the former, [12] was synthesized according to eq.63, then irradiated, in hexane, in a quartz tube (eq.64). [12] was still the major component after 40 min. This shows that the compound [12] is stable under the photolysis conditions. Consequently, loss of CO from [2] prior to C-H activation of the propene ligand remains a possible mechanism (see Section 3.5.6 for discussion of possible mechanisms).

(iii) Irradiation of $\text{Cp}^*\text{Re}(\text{CO})_2(\text{PMe}_3)$ (37) in hexane at 0°C with a propene purge (eq.62) was carried out to determine whether CO and PMe_3 are both able to dissociate from (37) leading to different propene products, and to attempt the synthesis of the hydrido(allyl) complex $\text{Cp}^*\text{Re}(\text{PMe}_3)(\text{H})(\eta^3\text{-C}_3\text{H}_5)$. It resulted in an IR spectrum

(Fig.30) having a strong absorption at 1845 cm^{-1} for $\text{Cp}^*\text{Re}(\text{CO})(\text{PMe}_3)(\eta^2\text{-C}_3\text{H}_6)$ [12] (see Table 4), weaker bands for [15] (*exo*, *endo*) ($1904, 1912\text{ cm}^{-1}$) and [2] ($1961, 1890\text{ cm}^{-1}$), and a very weak band for $\text{Cp}^*\text{Re}(\text{CO})(\text{H})(\text{CH}_2\text{PMe}_2)$ (38)⁹ at 1878 cm^{-1} . The ^1H NMR spectrum of the products in C_6D_6 confirmed the interpretation, with hydride resonances at δ -9.23 (major, [15a]*exo*), -11.66 (minor, [15b]*endo*), -9.92 (weak, (38)⁹). These results are understandable, if (37) loses either CO or PMe_3 when irradiated. Loss of CO yields the unsaturated fragment $[\text{Cp}^*\text{Re}(\text{CO})(\text{PMe}_3)]$ which is known⁹ to undergo intramolecular cyclometallation of the PMe_3 group to give (38) (which is observed in small yield here) but would preferentially capture propene to give a good yield of [12]. Loss of PMe_3 from (37) gives the same fragment $[\text{Cp}^*\text{Re}(\text{CO})_2]$ formed in photolysis of the tricarbonyl and thus the expected products [2] and [15]. Note that no evidence was found for the formation of $\text{Cp}^*\text{Re}(\text{PMe}_3)(\text{H})(\eta^3\text{-C}_3\text{H}_5)$ (40), indicating that the product $\text{Cp}^*\text{Re}(\text{CO})(\text{PMe}_3)(\eta^2\text{-C}_3\text{H}_6)$ [12] does not lose CO on further irradiation and undergo the allylic C-H activation reaction. It is possible that instead it loses PMe_3 , which would provide a second route to [15].

(iv) The photolabile N_2 ligand in $\text{Cp}^*\text{Re}(\text{CO})(\text{N}_2)(\text{PMe}_3)$ (39) provides a method for synthesizing [12] in good yield. Irradiation

Fig. 29. IR spectrum ($\nu(\text{CO})$, hexane) (eq. 61).

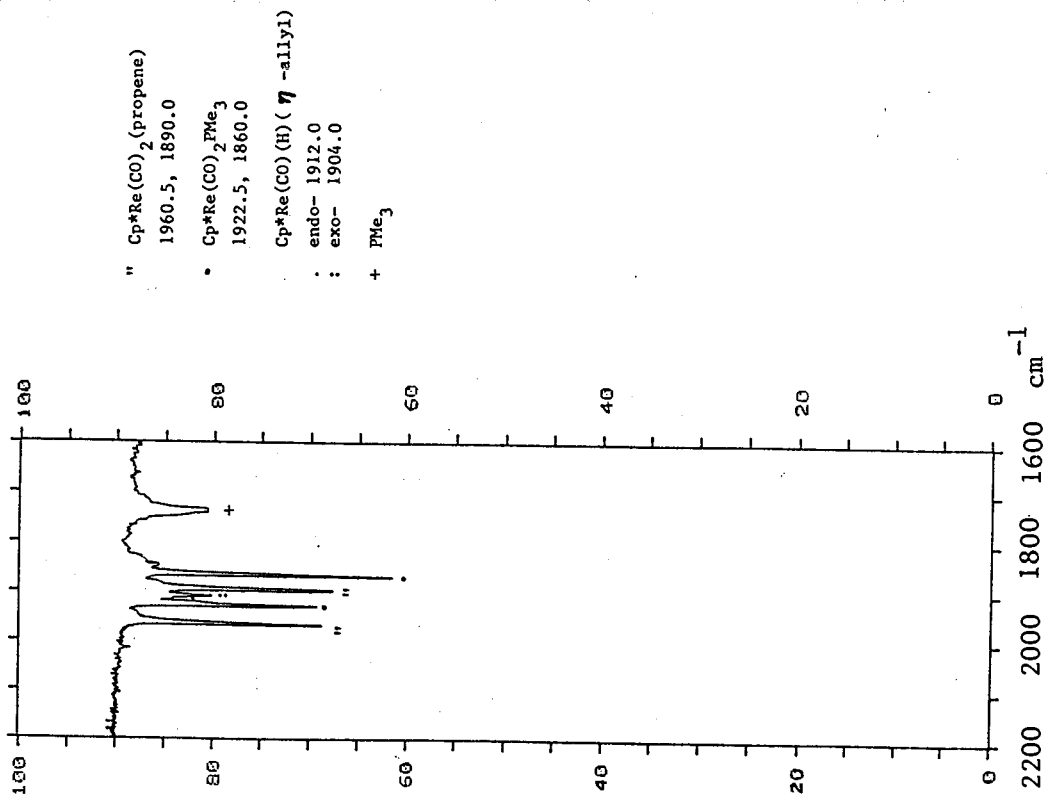


Fig. 30. IR spectrum ($\nu(\text{CO})$, hexane) (eq. 62).

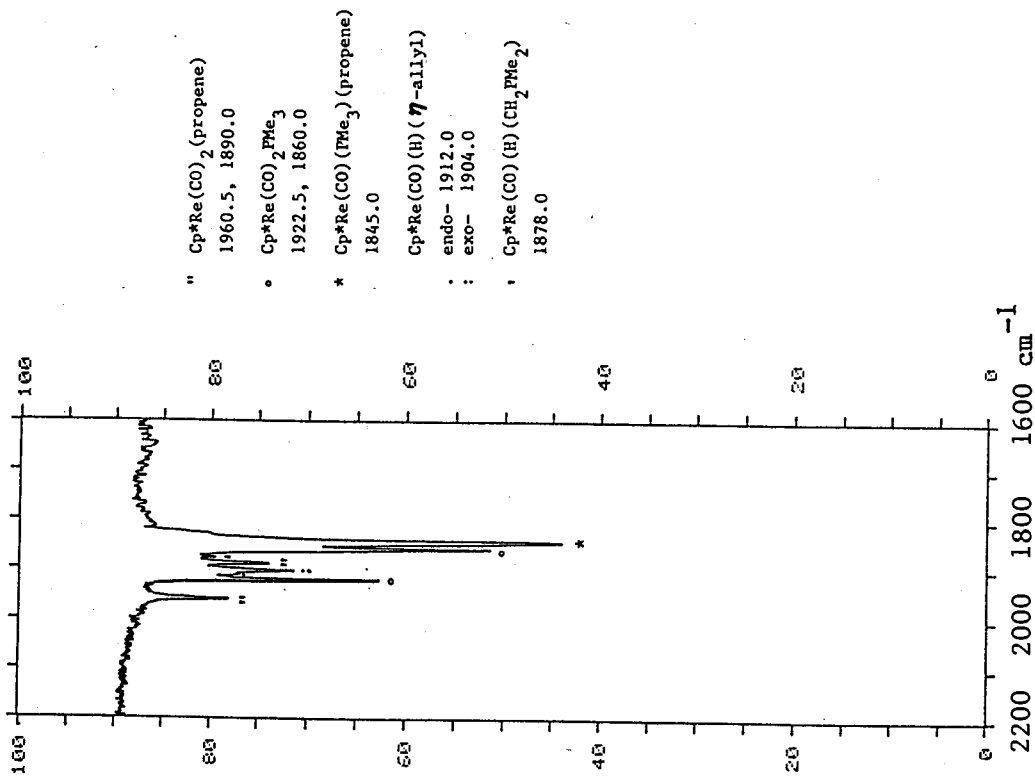


Fig.31. IR spectrum ($\nu(\text{CO})$, hexane) (eq.64).

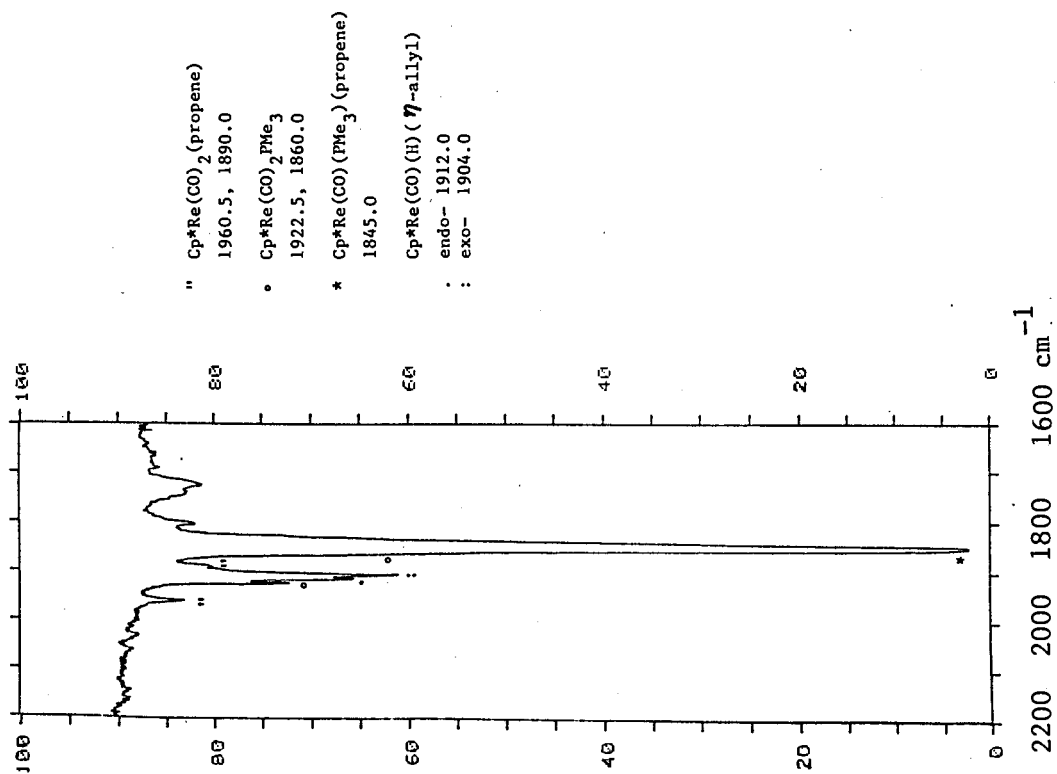
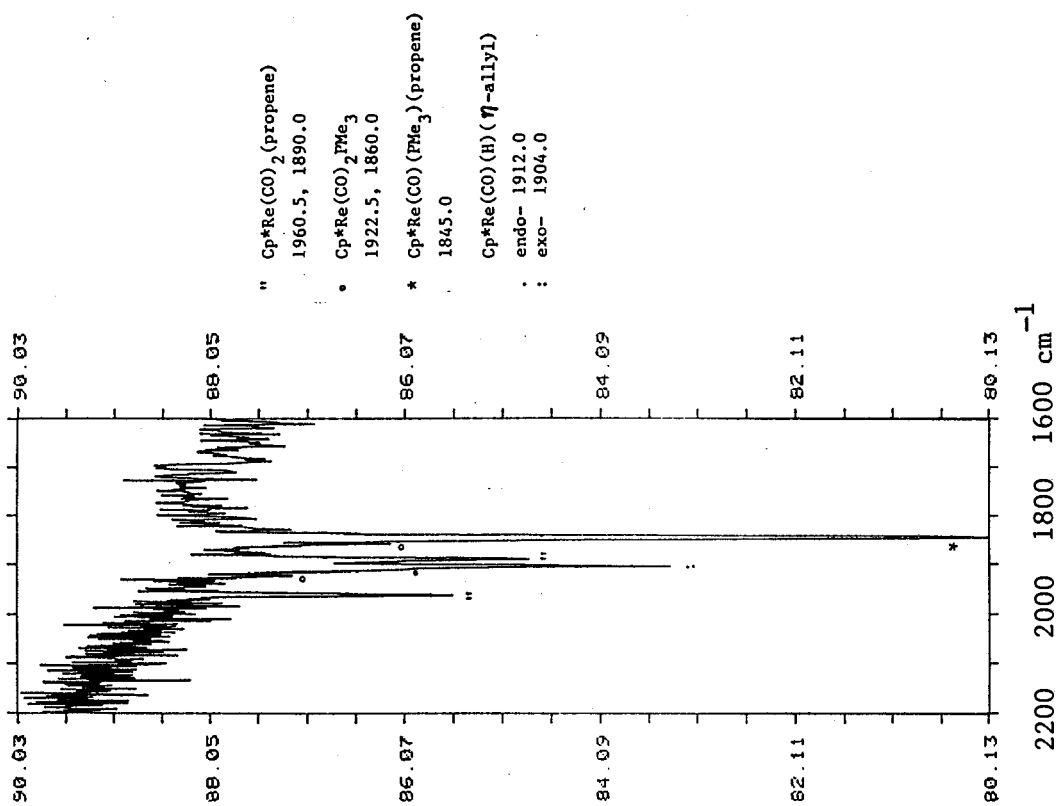
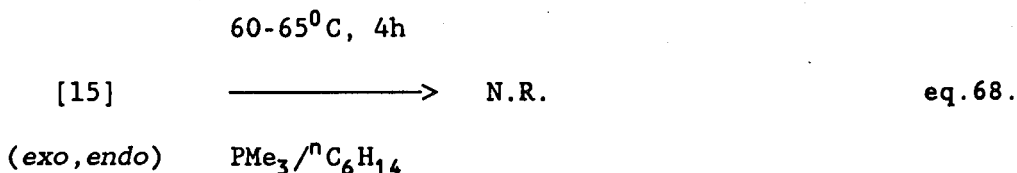
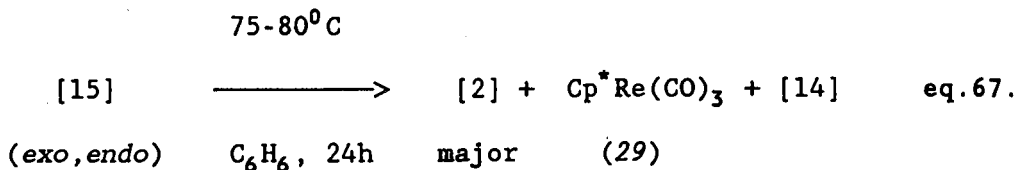


Fig.32. IR spectrum ($\nu(\text{CO})$, hexane) (eq.63).





(vi) The bromination of [15](*exo, endo*) with the solvent bromoform (CHBr_3) produced only one isomer [18b]*endo* in 63.6% yield (see Section 3.7.(v)). The bromide [18b]*endo* was reduced by lithium triethylborohydride (LiEt_3BH) to yield a mixture of two isomers of [15](*exo,endo*). On the basis of ^1H NMR and IR spectroscopic data (see Section 3.7.(xiv)), the ratio of [15a]*exo* to [15b]*endo* is \approx 0.26 (eq.65).

(vii) Irradiation of [15](*exo,endo*) in cyclohexane- d_{12} in a NMR tube produced free propene and [2] as the major product. The IR and MS data clearly showed the presence of other complexes ($\text{Cp}^*\text{Re}(\text{CO})_2)_2\text{CO}$ [14] and $\text{Cp}^*\text{Re}(\text{CO})_3$) (Section 3.7.(xii)).

(viii) A benzene solution of [15](*exo, endo*) was heated under nitrogen at $75-80^{\circ}\text{C}$ for 24h (eq.67). The products [2], $\text{Cp}^*\text{Re}(\text{CO})_3$ and ($\text{Cp}^*\text{Re}(\text{CO})_2)_2\text{CO}$ [14] were identified by the ^1H NMR and IR spectroscopic data (see Section 3.7.(xiii)). No reaction of

[15] with benzene was observed.

(ix) A hexane solution of [15] (*exo,endo*) with PMe_3 in a sealed tube was heated at $60-65^\circ\text{C}$ for 4h. No reaction of [15] with PMe_3 or hexane was observed.

3.5. Discussion

3.5.1. X-ray Structures of [15a]*exo* and [15b]*endo*

Two previous X-ray structures of (η^3 -allyl)hydrido compounds have been published,^{53,56} but only for $\text{IrHCl}(\eta^3\text{-CH}_2\text{CHCHPh})(\text{PPh}_3)_2$ has the hydride been located and full structural details published.⁵³ The allyl ligand is asymmetrically bonded in this complex, but this may be partly a consequence of the phenyl group. The existence of two isomers of the allyl(hydrido) complex $[\text{Ir}(\text{H})(\text{C}_3\text{H}_5)(\text{PMe}_3)_3]^+$, postulated to involve different rotational orientation of the allyl group, was not confirmed.⁵⁸

Exo and *endo* isomeric forms for the allyl ligand in cyclopentadienyl complexes with piano-stool structures like [15] have been amply studied, notably by Faller and co-workers.⁶⁵ While X-ray structures have been determined for either *exo* or *endo* forms of several such compounds,⁶⁶ there are two examples where the

structures of the both *exo* and *endo* isomers of the same complex have been determined. They are the complex $\text{CpRu}(\text{CO})(\eta^3\text{-C}_3\text{H}_4\text{Me})$ ^{66h} and the cationic complex $[\text{CpMo}(\text{NO})(\text{CO})(\text{phenylallyl})]^+$.^{66k} Both of these compounds provide the opportunity for a detailed comparison of the ligand in its two orientations without complications from differing ligands. Although the ligand is slightly asymmetrically bound in the *endo* isomer of [15], there is no doubt that it is still a true η^3 -allyl group rather than a σ - π allyl as found, for example, for the very asymmetrically bound group in *endo*- $\text{CpMo}(\text{NO})(\text{I})(\eta^3\text{-C}_3\text{H}_5)$ and its tungsten analogue.^{66f,g}

3.5.2. IR Spectroscopy

The IR spectra of [15]-[18] show the single $\nu(\text{CO})$ absorption expected for a monocarbonyl(η^3 -allyl) rhenium complex. IR($\nu(\text{CO})$) data show: (i) the carbonyl is somewhat more strongly bound to rhenium in [16] or [17] relative to that in [15] as shown by the lower IR($\nu(\text{CO})$) in [16] and [17] (1891, 1899 cm^{-1} respectively) compared with [15] (1904, 1912 cm^{-1} respectively for *exo* and *endo*) perhaps reflecting the presence of the bulky, electron-donor alkyl group; (ii) the $\nu(\text{CO})$ absorption of [15b]*endo* is at higher wave-number compared with that of [15a]*exo*. This implies that the *endo* η^3 -allyl group is more strongly bound to rhenium than is the *exo* η^3 -allyl group; (iii) the electron-acceptor

Fig.33(a-c). NOE Experiments on [15a]exo
400MHz ^1H NMR (C_6D_6) at r.t.

Fig.33(a).

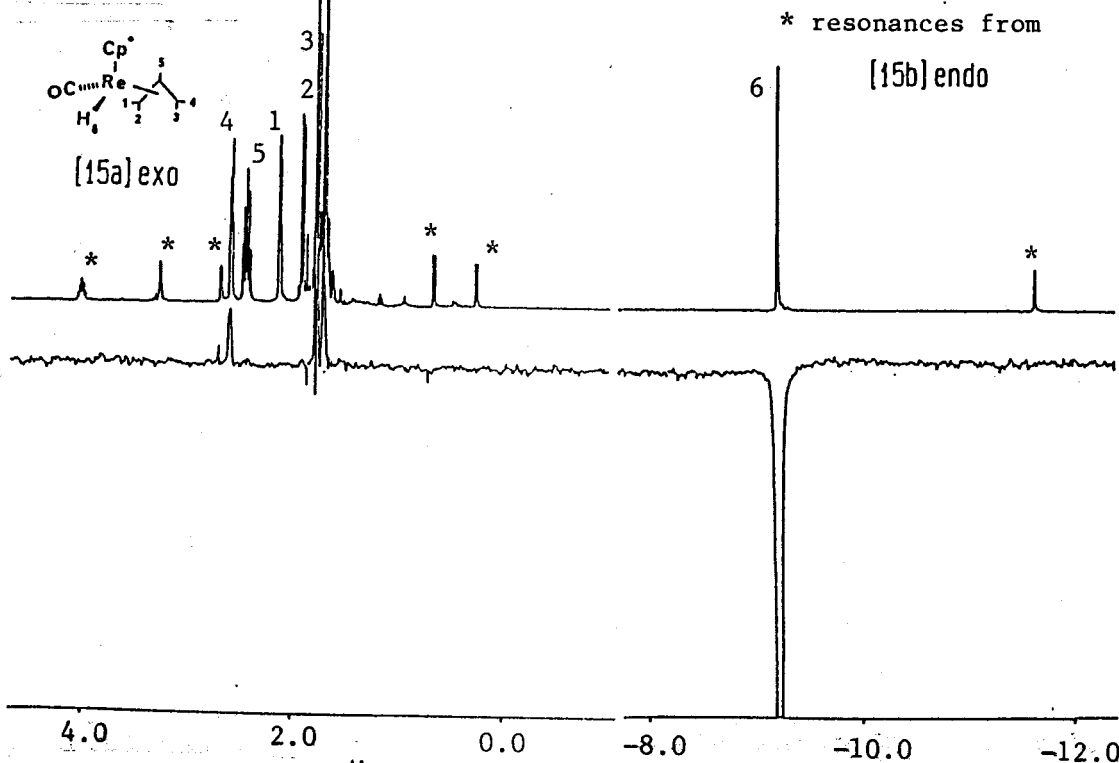


Fig.33(b).

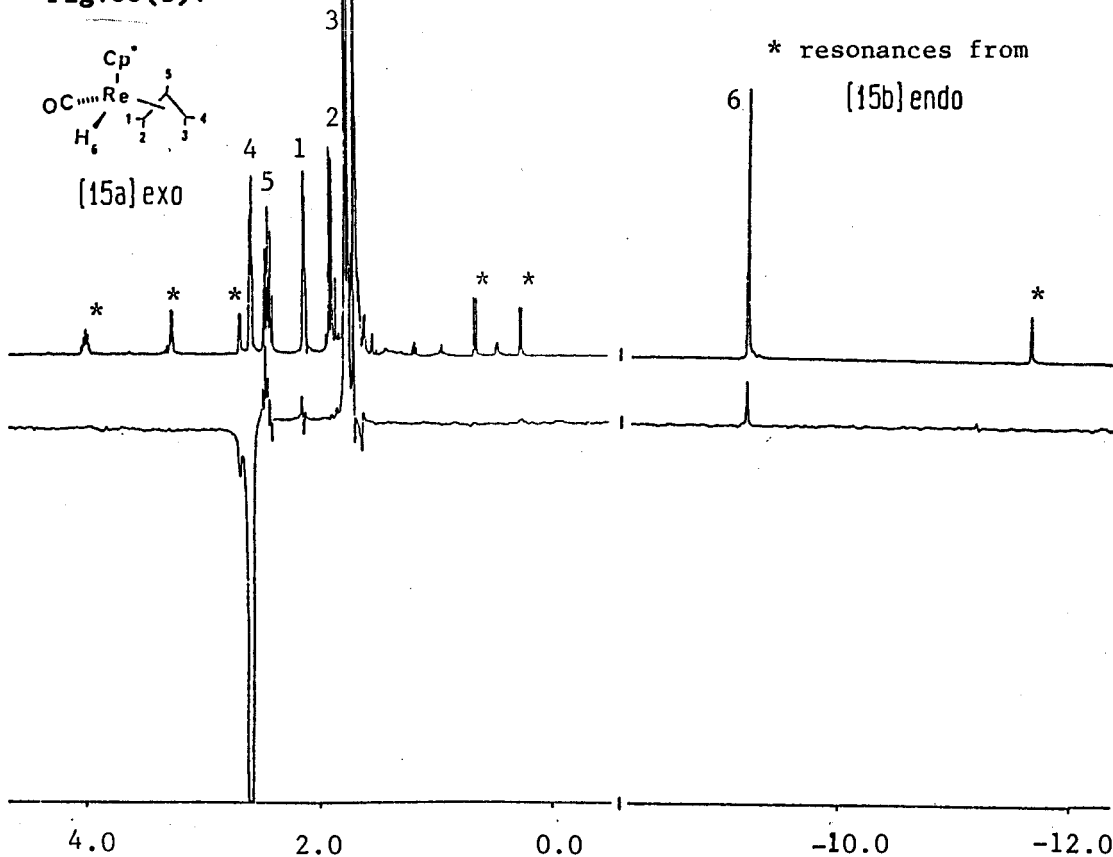


Fig. 33(c).

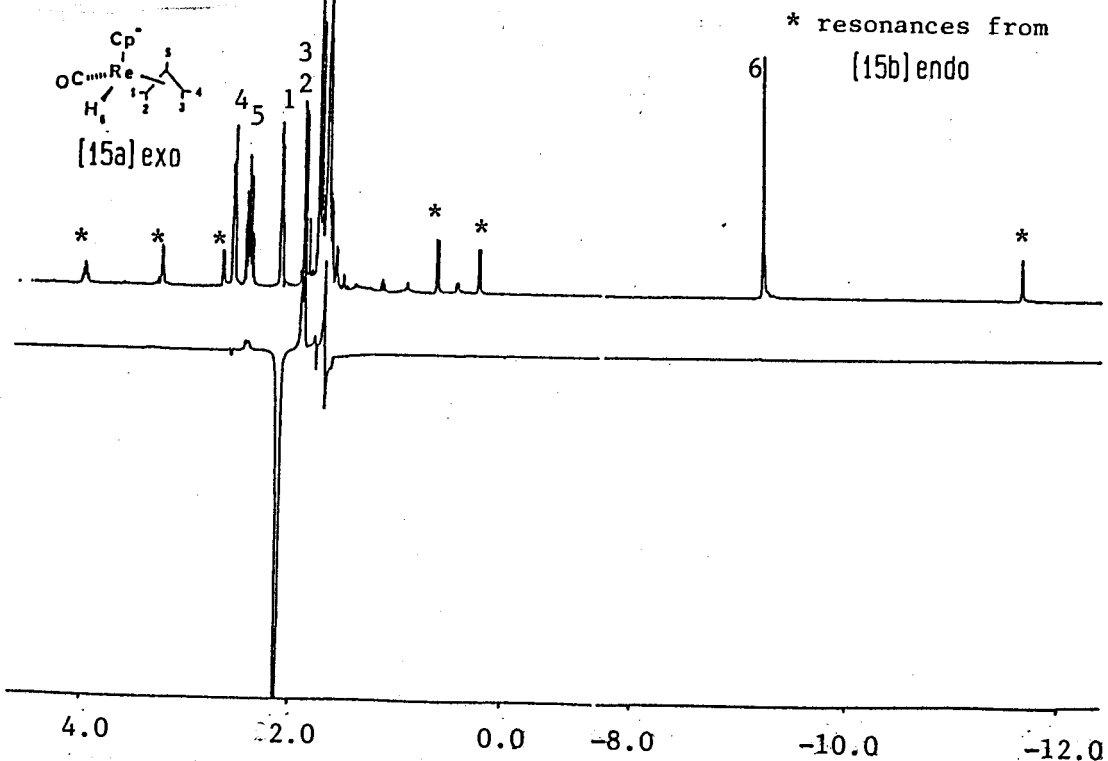


Fig. 34(a-c). NOE Experiments on [15b]endo

Fig. 34(a). 400MHz ^1H NMR(C_6D_6) at r.t.

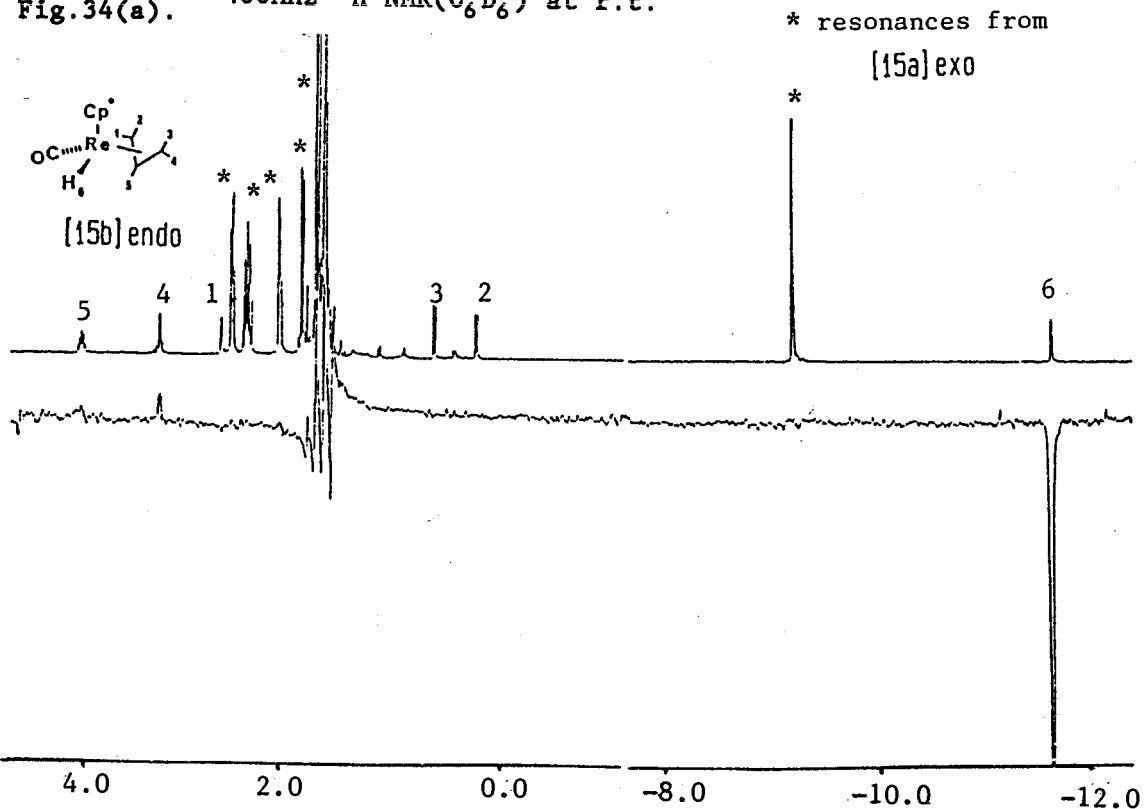


Fig. 34(b).

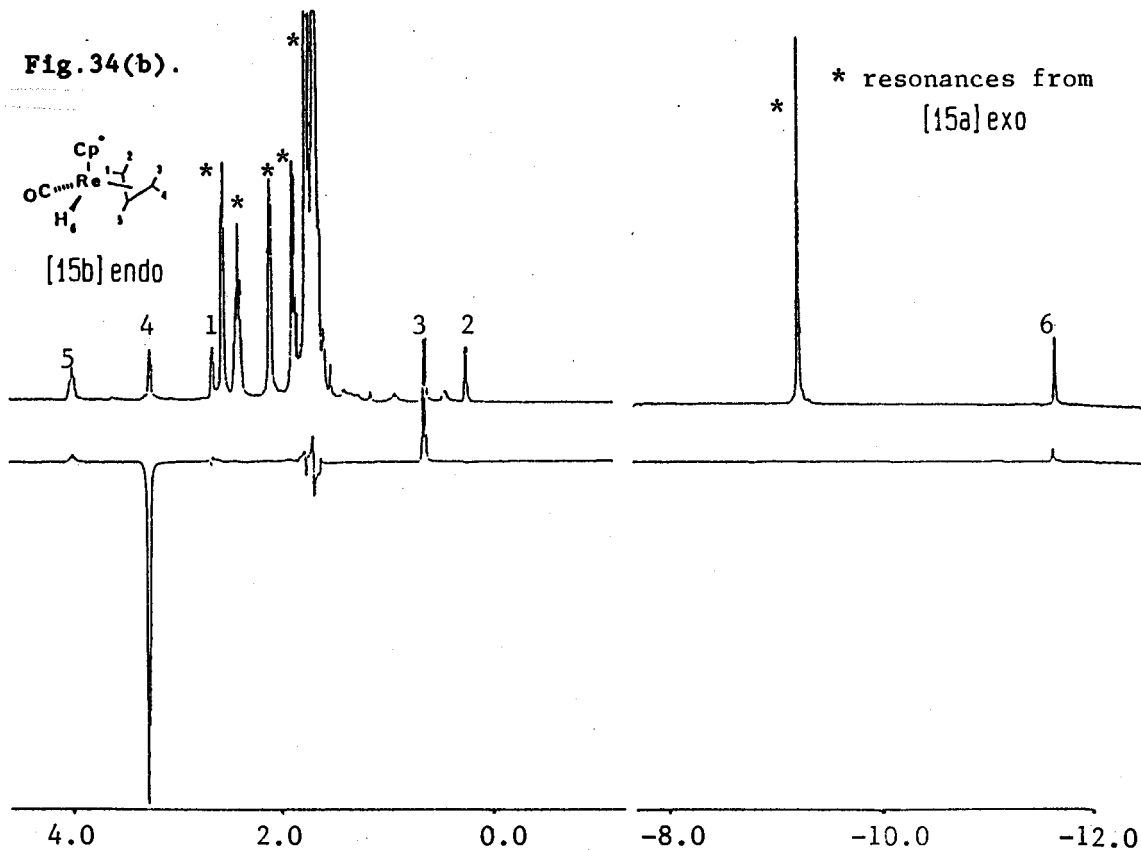
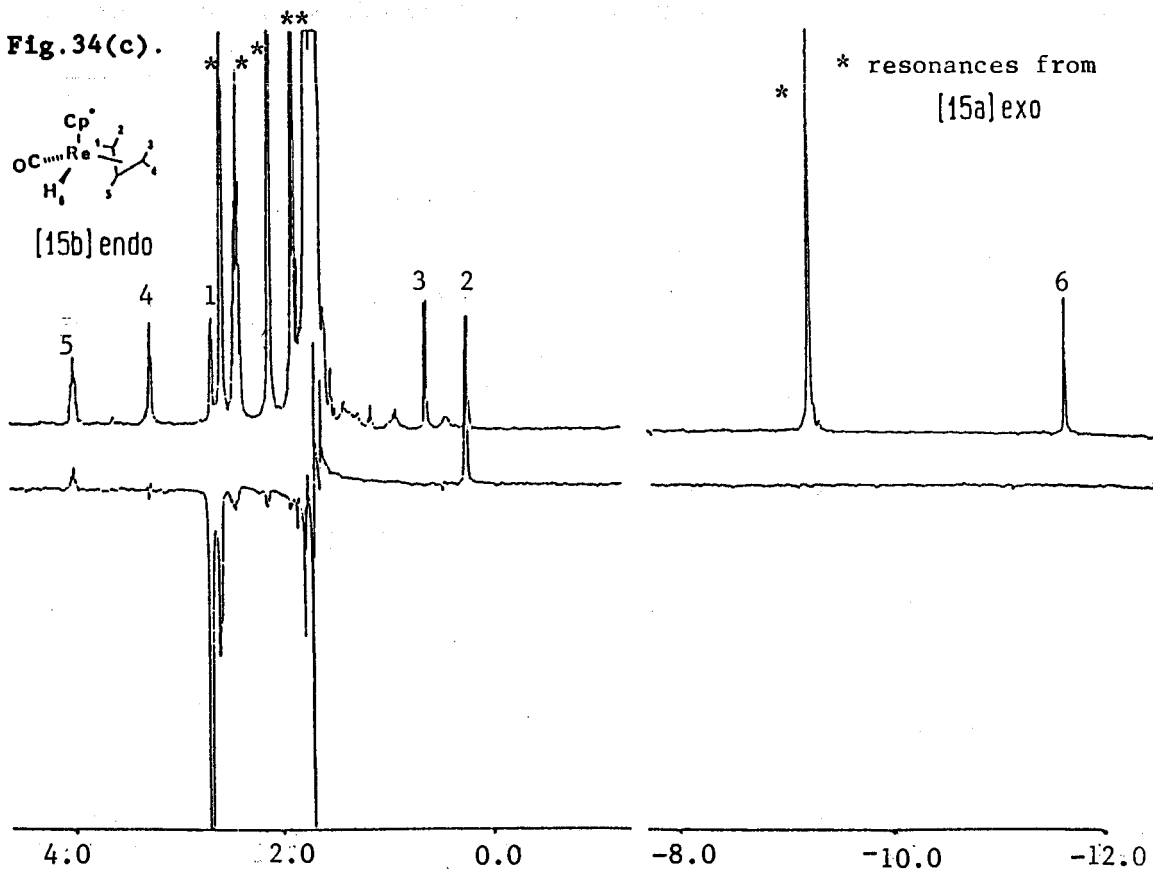


Fig. 34(c).

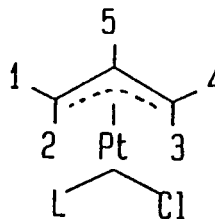


bromide group in [18] decreases the d- π^* backbond between the carbonyl and rhenium, resulting in $\nu(\text{CO})$ increasing to 1962 cm^{-1} compared with the hydrides [15]-[17].

3.5.3. ^1H NMR Spectroscopy

A comparison of ^1H NMR data of [15]-[18] (see Tables 8-10) shows some interesting correlations: (i) the *anti* protons (H(2) and H(3)) of unsubstituted allyl are generally at higher field than the *syn* protons (H(1) and H(4)); (ii) the *anti* protons of allyl in [15b]*endo* are at higher field compared with those in [15a]*exo*, and the central proton of allyl in [15a]*exo* is at higher field relative to that of [15b]*endo*, indicating that the Cp^* ring shielding effect causes an upfield shift for protons which approach nearest the ring; (iii) the alkyl substituent of allyl in [17b]*exo* (4-R group) makes the chemical shifts of the other four protons 1-, 2-, 3- and 5- move downfield by 0.14, 0.45, 0.80 and 1.23 ppm respectively relative to those of [15a]*exo*; (iv) the bromide group in [18b]*endo* induces the chemical shifts of allylic protons 1-, 2-, 3- and 5- to move down field by 0.31, 0.80, 1.15 and 0.58 ppm respectively but 4- to move upfield by 0.11 ppm relative to those of [15b]*endo*; (v) the hydride of [15a]*exo* is at higher field compared with that in [15b]*endo*; (vi) coupling constants provide additional evidence for a typical η^3 -allyl ligand and their values in [15] vary as follows: $J_{\text{anti}} = 9.5 -$

Table 13. NMR Data for Complexes^a
 $\text{Pt}(\eta^3\text{-C}_3\text{H}_5)\text{Cl(L)}^{67\text{b}}$



L	Parameters ^b	H(1)	H(2)	H(3)	H(4)	H(5)
PMe ₃	δ	3.28	2.14	2.88	4.25	4.73
	J	J _{1,5} =6.5	J _{2,5} =11.2	J _{3,5} =13.5	J _{4,5} =6.0	
		J _{1,4} =2.2	J _{1,2} =1.7			
PCy ₃	δ	3.13	2.00	2.83	4.23	4.70
	J	J _{1,5} =6.4	J _{2,5} =10.9	J _{3,5} =13.3	J _{4,5} =6.6	
PMe ₂ Ph	δ	3.15	2.13	2.93	4.31	4.78
	J	J _{1,5} =6.5	J _{2,5} =11.3	J _{3,5} =13.2	J _{4,5} =7.4	
		J _{1,4} =2.3	J _{1,2} =2.6			
PMePh ₂	δ	2.98	2.13	2.97	4.35	4.84
	J	c	J _{2,5} =10.2	J _{3,5} =12.8	J _{4,5} =6.0	
P(4-FC ₆ H ₄) ₃	δ	2.84	2.28	3.10	4.44	4.98
	J	J _{1,5} =6.5	J _{2,5} =11.2	J _{3,5} =13.3	J _{4,5} =7.3	
		J _{1,4} =2.1	J _{1,2} =2.4	J _{3,4} =1.2	J _{2,4} =0.7	

^aIn CDCl₃ at room temperature. ^bChemical shifts δ (ppm) referenced to tetramethylsilane (TMS); coupling constants J in Hz. ^cObscured by H(3).

10.5 (exo) and 7.1 -9.7 (endo) Hz; $J_{\text{syn}} = 6.7 - 7.2$ (exo) and 5.5 - 6.9 (endo) Hz; $J_{\text{gem}} = 2.3 - 2.7$ (exo) and ≈ 1.5 (endo) Hz. These ^1H NMR correlations for exo and endo η^3 -allyl isomers were well-studied by Faller^{65b,c} and others.⁶⁷ Their results are similar to those described above. For example, Clark^{67b} reported the proton chemical shifts and coupling constants of allyl ligands in $\text{PtCl}(\eta^3\text{-allyl})(\text{PR}_3)$ complexes (see Table 13). All five protons of allyl are inequivalent, and the coupling constants are also very similar to those measured in this study (see Tables 10, 11).

(i) $\text{Cp}^*\text{Re}(\text{CO})(\text{H})(\eta^3\text{-C}_3\text{H}_5)$ [15]. The ^1H NMR spectra of the two isomers (see Figs. 21, 22) have been completely assigned by NOE and decoupling procedures. NOE difference spectroscopy is particularly useful in determining the identity of each stereoisomer. In this procedure, one spectrum is accumulated while simultaneous saturating irradiation is applied at the resonance position of a proton of interest. This spectrum is subtracted from a second spectrum for which the irradiation frequency is moved to a region free of any transitions. The resultant spectrum shows a large negative resonance corresponding to the first irradiation frequency, plus any resonances which are enhanced by the NOE. It should be emphasized that NOE occurs through space rather than through chemical bonds. The results of NOE enhancements provide evidence for protons that are within a short distance of the proton of

interest.⁶⁸

In the case of [15a]*exo*, as expected, the ¹H NMR spectrum showed clearly the presence of the hydrido H(6) at δ -9.23 (s, 1H) and Cp* at δ 1.69 (s, 15H). The multiplet at δ 2.42 with coupling (J = 6.7, 7.2, 9.5 and 10.2 Hz, see Table 10) to each one of other four allylic protons was assigned to central proton H(5). Then, application of NOE unambiguously provided the assignment of the chemical shift of each allylic proton, as follows.

First, irradiation at the hydride H(6) (Fig.33(a)) gave an NOE enhancement to protons H(3), H(4) and Cp*, indicating that H(3) and H(4) must be located *cis* to the hydride ligand. Next, irradiation of H(4) (Fig.33(b)) gave NOE enhancements as expected to H(3) and H(6), and to H(5), thereby identifying H(4) to be in the *syn* position. Irradiation at position H(1) (Fig.33(c)) gave NOE enhancements to protons H(2) and H(5), indicating H(1) to be the other *syn* proton. Irradiation at the remaining positions H(2), H(3) and H(5) gave appropriate NOE enhancements in agreement with these assignments, and located the positions of protons H(2), H(3) and H(5) unambiguously.

The chemical shift of each proton of [15b]*endo* was assigned by a similar manner. Irradiation at the hydride H(6) (Fig.34(a)) gave an NOE enhancement to protons H(4) and Cp*, indicating that H(4) must be located *cis* to the hydride ligand. Next, irradiation of H(4) (Fig.34(b)) gave NOE enhancements as expected to H(3), H(5) and

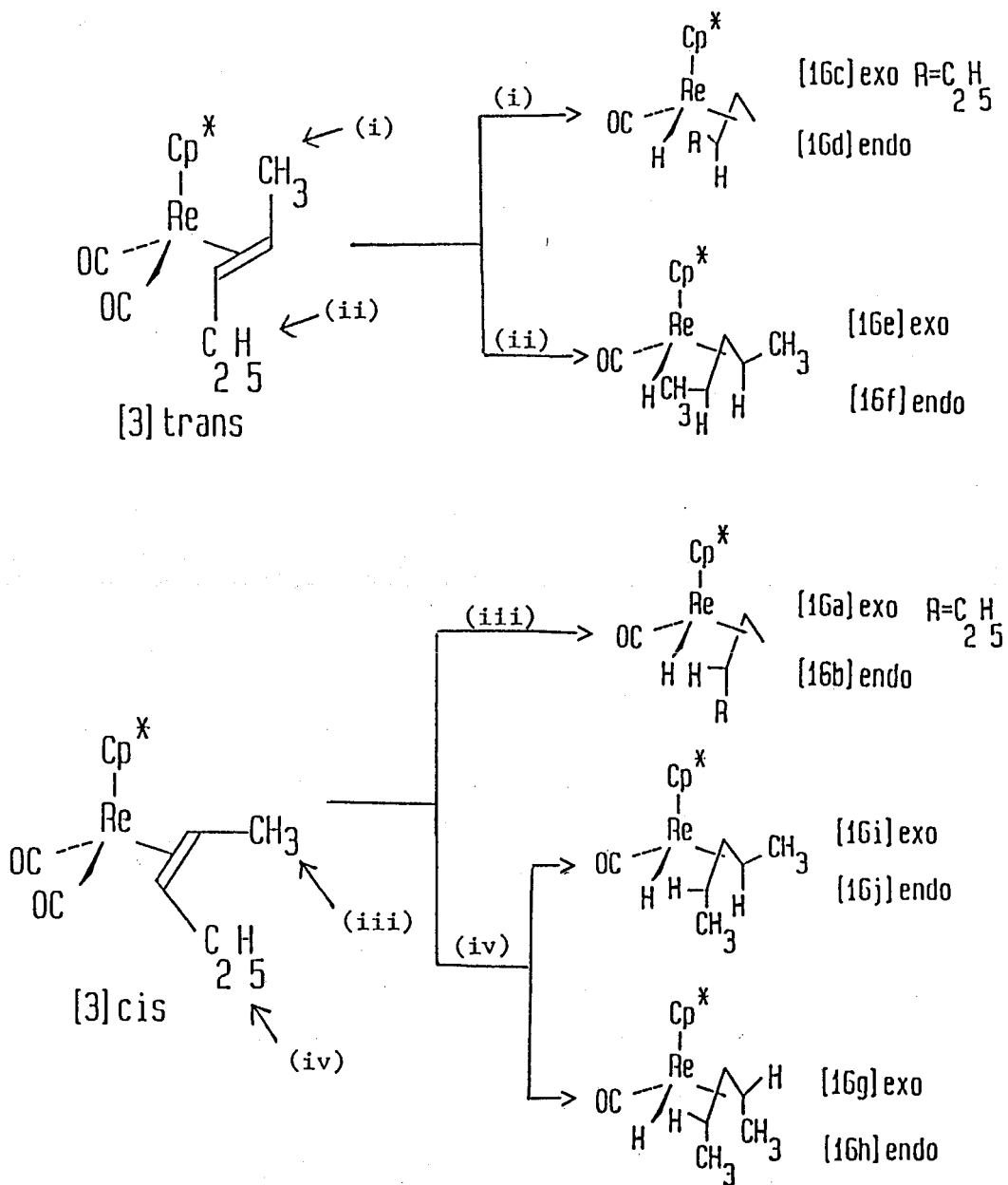
H(6), thereby identifying H(4) to be in the *syn* position. Irradiation at position H(1) (Fig.34(c)) gave NOE enhancements to protons H(2) and H(5), indicating H(1) to be the other *syn* proton. Irradiation at the remaining positions H(2), H(3) and H(5) gave appropriate NOE enhancements in agreement with these assignments, and located the positions of protons H(2), H(3) and H(5) unambiguously.

It is important to note the absence of any observable magnetization transfer to the *endo* isomer when resonances of the *exo* isomer in the mixture of the two are irradiated (see for example irradiation of the hydride H(6) in Fig.33(a)). This would be indicated by a corresponding negative peak (in this case at the position of H(6) *endo*); none is observed. Thus, although *exo*→*endo* interconversion has been observed for [15] on the synthetic time scale, it is too slow to be observed on the NMR timescale.

The experimentally observed chemical shifts for the complexes [15a]*exo* and [15b]*endo* are listed in Tables 8, 9.

(ii) $\text{Cp}^*\text{Re}(\text{CO})(\text{H})(\eta^3\text{-C}_5\text{H}_9)$ [16]. Homologous isomers of [16] were produced in the photolysis of the η^2 -2-pentene complex [3] (*cis* and *trans*) or of $\text{Cp}^*\text{Re}(\text{CO})_3$ with 2-pentene (*cis* and *trans*). It is believed that the allylic C-H bonds of η^2 -2-pentene ligand in complex [3] (*cis* and *trans*) are activated to give the five hydride isomers as shown in Scheme 19. The ^1H NMR spectrum shows that five

Scheme 19.



hydride resonances are present (see Fig.20), which could represent three *exo* isomers corresponding to the chemical shifts at δ -8.98, -9.32 and -9.45 ppm, and two *endo* isomers corresponding to the chemical shifts at δ -11.58 and -11.68 ppm by comparison with the assignments of ^1H NMR spectra of complexes [15a]*exo*, [15b]*endo* and [17b]*exo*. The mixture of isomers in [3] contains more of the *trans* form ([3]*trans*/[3]*cis* = 1.7/1). The allylic C-H activation is expected to be more facile on the methyl compared to the methylene, because the methyl group (involving three C-H bonds) has a greater probability of C-H activation than the methylene group involving two C-H bonds. The methyl group is also better able to approach the rhenium centre during the allylic C-H activation compared with the methylene group. Therefore, it is proposed that the major isomer observed, corresponding to the hydride at δ -9.32, is [16c]*exo* given by route (i) in Scheme 19. The significant peak at δ -11.58 can be assigned to the complex [16d]*endo*, which is the *syn-anti* isomer of [16c]*exo*. The medium intensity peak at δ -9.45 can be assigned to the complex [16e]*exo* given by route (ii), which is the *syn-anti* isomer of [16f]*endo* corresponding to the hydride resonance at δ -11.68. The weaker intensity of the peak at δ -8.98 could indicate the presence of a small amount of [16a]*exo*, but the *syn-anti* isomer [16b]*endo* would be too small to be detected or may not be formed in this case. Possible assignment of these resonances to the other two pairs of isomers given by route (iv), ([16i]*exo* and [16j]*endo*;

[16g]exo and [16h]endo), was rejected for the following reasons: (1) the route (iv) requires the allylic C-H activation to occur on the methylene group, which is considered less able to approach the rhenium centre compared with the methyl group in route (iii); (2) if the alkyl substituent of η^3 -allyl is in the *anti* orientation, this will disadvantage the transition state for allylic C-H activation because of steric hindrance (see Fig.36). This is in accord with previous publications by Faller^{65b} and Clarke⁶⁹, which showed that the *syn* isomer was expected to predominate in η^3 -allyl transition-metal complexes substituted at a terminal carbon atom of allyl. Faller^{65b} further indicated that the *syn* orientation was the thermodynamically more stable one in the molybdenum complexes $\text{CpMo}(\text{CO})_2(\eta^3\text{-1-methylallyl})$ and $(\text{Indenyl})\text{Mo}(\text{CO})_2(\eta^3\text{-1-methylallyl})$.

Fig.35. Advantageous
transition state

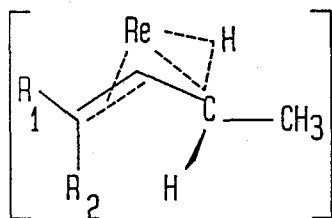
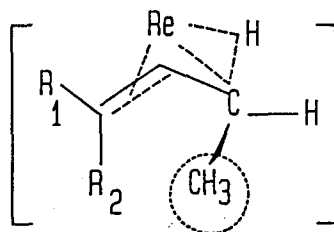


Fig.36. Disadvantageous
transition state



(iii) $\text{Cp}^*\text{Re}(\text{CO})(\text{H})(\eta^3\text{-C}_8\text{H}_{15})$ [17]. The ^1H NMR spectrum of complex [17] was successfully assigned by decoupling experiments and by computer simulation (Fig.26). The ^1H NMR spectrum of complex [17] showed clearly the presence of the hydride H(6) at δ -8.94 (s, 1H) in the region expected for an *exo* isomer and Cp^* at δ 1.71 (s, 15H). The multiplet at δ 4.59 with coupling ($J = 6.8, 10.0$ and 9.8 Hz) to each one of other three allylic protons was assigned to the central proton H(5) of the allyl group. The doublet of doublets at δ 2.34 (dd, 1H) with a larger coupling ($J = 10.0$ Hz) to the central proton H(5) was assigned to the *anti* proton H(2). The broad multiplet at δ 2.25 (br m, 1H) with a smaller coupling ($J = 6.8$ Hz) to central proton H(5) was assigned to the *syn* proton H(1). The doublet at δ 2.56 (d, 1H) with larger coupling ($J = 7.2$ Hz) to 4-methene protons H(4) was assigned to H(3). The larger coupling between the proton H(3) and the central proton H(5) ($J = 9.8$ Hz) indicates that H(3) is in the *anti* orientation, i.e., the 4-alkyl substituent is oriented *syn* to the central proton H(5). The reason only one *syn* configuration of [17] was formed could be explained by the transition state of this orientation in Fig.35 involving less steric interaction.

The above assignment was further confirmed by computer-simulation of the ^1H NMR spectrum (see Fig.26). The final calculated coupling constants differ little from the approximate values derived

experimentally from the decoupling experiments. The conformation of [17] is considered to be [17b]exo on the basis of the following: (1) in general, the δ values for the allyl protons and the proton coupling constants of [17] are closer to the corresponding ones of [15a]exo compared with [15b]endo (see Tables 8-10); (2) the hydride chemical shift is closer to that of [15a]exo relative to [15b]endo; (3) since, complex [15b]endo was converted to [15a]exo isomer under UV light, and [15a]exo was a major product in the photochemical synthesis of [15] $\text{Cp}^*\text{Re}(\text{CO})(\text{H})(\eta^3\text{-C}_3\text{H}_5)$, these indicate that the *exo* η^3 -allyl isomer is generally expected to be the major product in photochemical allylic C-H activation.

(iv) $\text{Cp}^*\text{Re}(\text{CO})(\text{Br})(\eta^3\text{-C}_3\text{H}_5)$ [18]. Application of NOE and decoupling procedures allowed unambiguous assignment of the chemical shift of each proton of the η^3 -allyl group, and showed the allyl group to be *endo* to the Cp^* ring (see Tables 8, 9 and Figs.38(a-e)).

From the NOE experiments as shown in Figs.38(a-e), the following observations were obtained:

(1) Irradiation of H(5) induced great enhancements of H(1) and H(4), Fig.38(a).

(2) Irradiation of Cp^* (which necessitated also irradiating H(3)) induced great enhancements of H(2) and H(4) and a small enhancement of H(5), Fig.38(b).

Fig. 38(a).

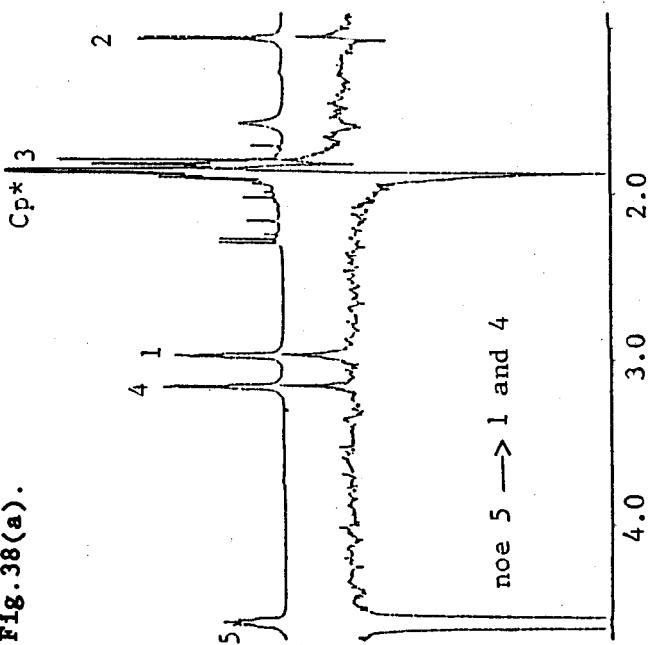
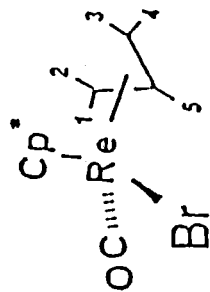


Fig. 38(a-e). NOE Experiments on Complex [18]

400MHz ¹H NMR(CDCl₃) at r.t.

Fig. 37. ¹H NMR Spectrum



[18]

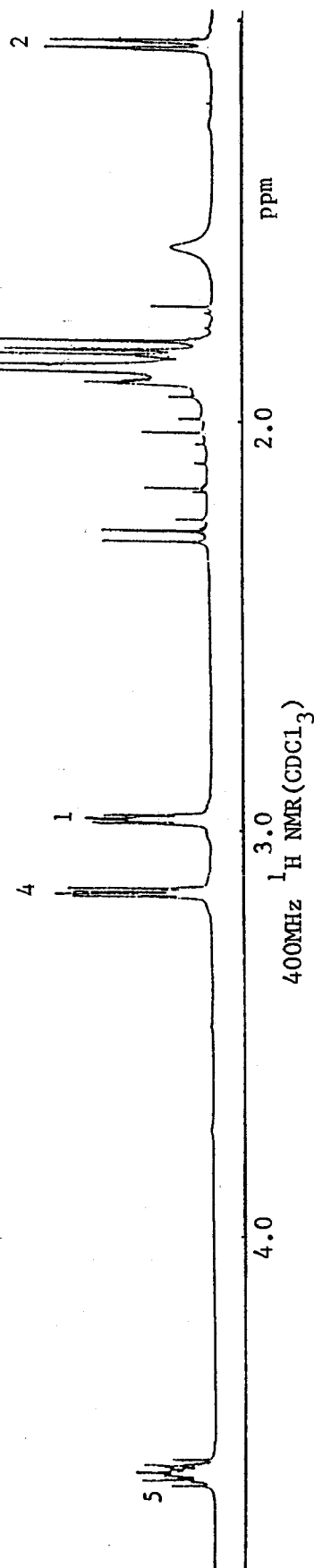


Fig. 38(b).

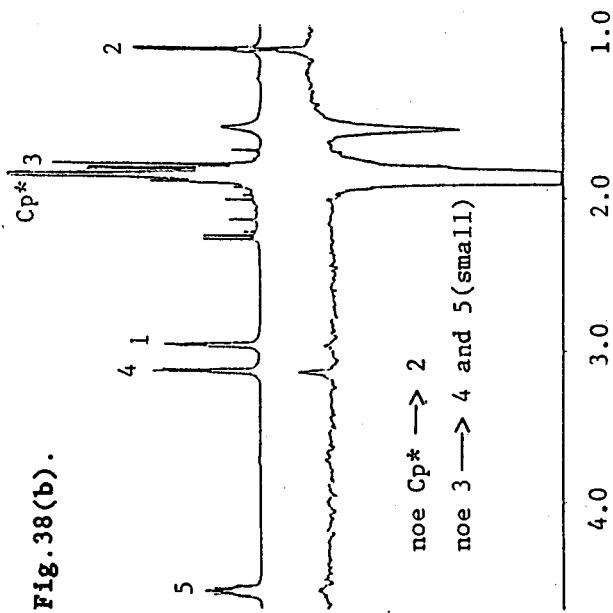


Fig. 38(d).

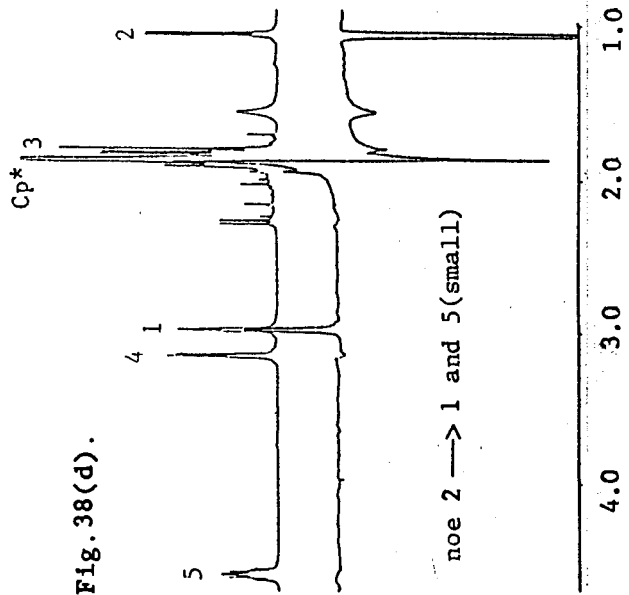


Fig. 38(c).

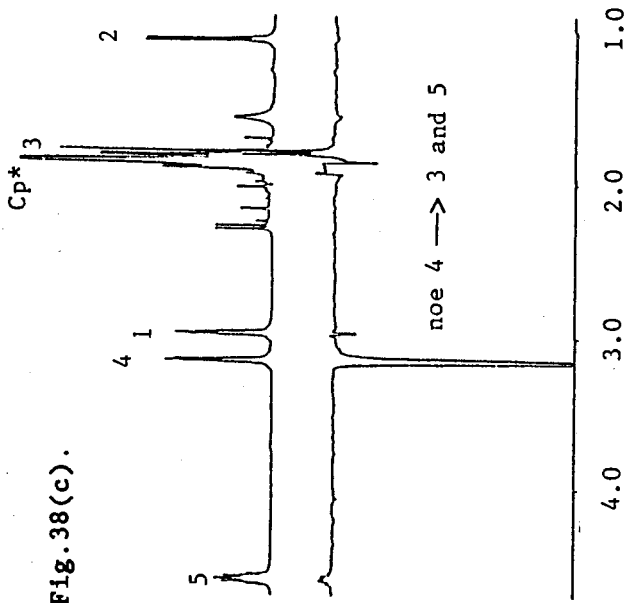
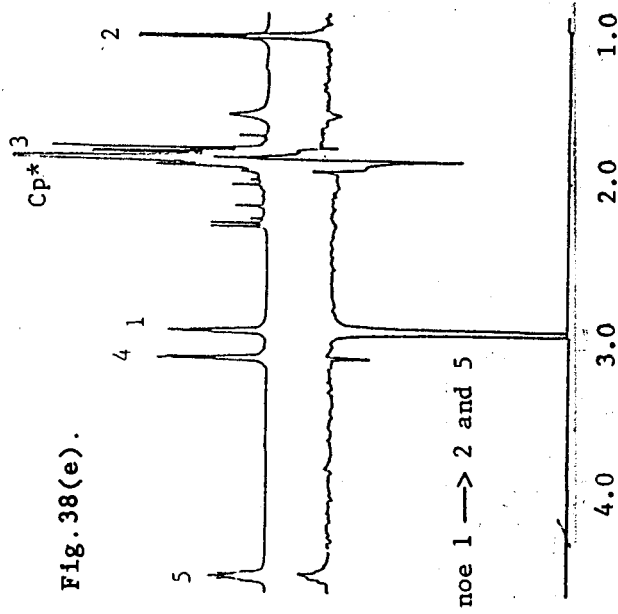


Fig. 38(e).



(3) Irradiation of H(4) enhanced H(3) and H(5), Fig.38(c).

(4) Irradiation of H(2) enhanced H(1) and Cp^{*}, Fig.38(d).

(5) Irradiation of H(1) enhanced H(2) and H(5), Fig.38(e).

Combination of (1), (2) and (4) indicates that the η^3 -allyl must be endo to Cp^{*}. Combination of (1), (3) and (5) indicates that H(1) and H(4) must be *syn* to H(5). Combination of (2) and (4) indicates that H(2) and H(3) must be *anti* to H(5). ¹H NMR data are listed in Tables 8-10.

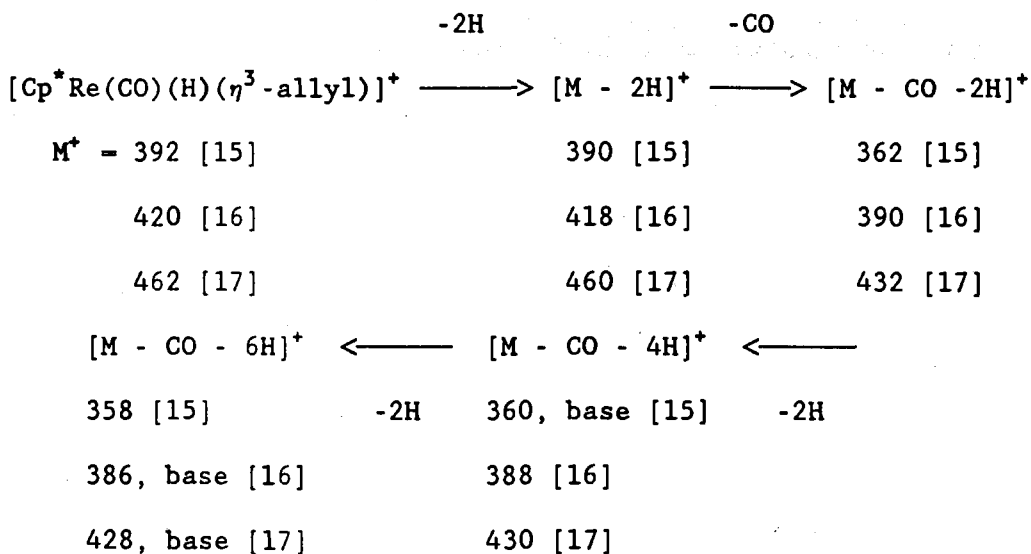
3.5.4. Mass Spectroscopy

The EI mass spectra of the hydrido(allyl) complexes [15]-[17] and the bromo(allyl) complex [18] are shown in Figs.17(n-p,t) (p.70), and the fragmentation pathways of [15]-[17] are shown in a similar procedure in Scheme 20. The most notable feature of the hydride complexes [15]-[17] is that the observed isotopic patterns for M⁺ do not correspond to the calculated patterns. Here the hydride complexes differ from the alkene complexes of Chapter II, and from the bromo complex [18] all of which exhibit patterns for M⁺ close to the computed ones. The anomalies therefore appear to be related to the presence of the hydride ligand in [15]-[17]. Taking the hydrido(allyl) complex [15] as an illustration, it can be seen (Fig.19, p.87) that the observed M⁺ pattern can be fitted by the

superposition of the patterns for M^+ and M^+-2H in a ratio of approximately 0.65 to 1. The patterns for complexes [16] and [17] can be similarly ascribed to superposition of M^+ and M^+-2H . The facile loss of 2H from the parent is not observed for the bromide [18] and therefore one of the hydrogens lost is presumed to be the hydride ligand. The other is most likely to arise from a Cp^+ ring methyl group^{45,47} and we suggest the following Scheme 21.

We presume that loss of the 2H occurs through a rhenium dihydride intermediate, and possible structures involving an expansion (41) or a ring-slip of the Cp^+ ligand (42) are shown in Fig.39.

Scheme 20.



Scheme 21.

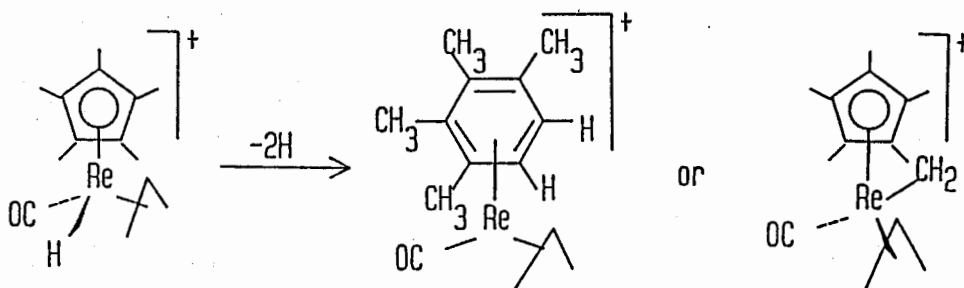
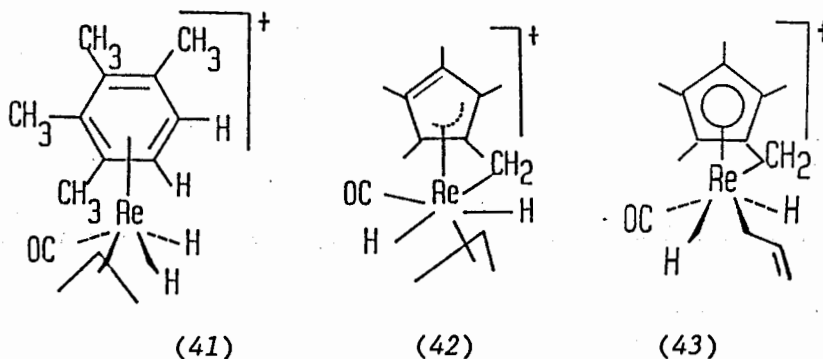


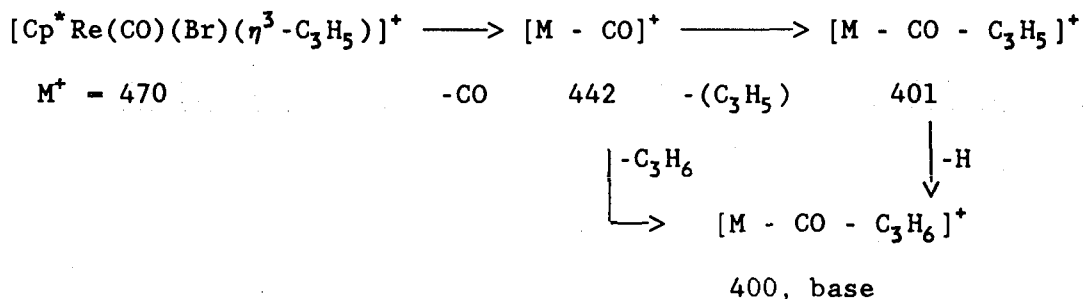
Fig. 39. Dihydride Intermediates



Most noticeable is the absence of fragmentation by loss of the allyl group or the alkene in any of these complexes, whereas it was noted that loss of alkene occurs readily in the mass spectra of the alkene complexes in Chapter II. Therefore, we believe that hydrogen migration to the allyl group to form the alkene complex does not occur in the fragmentation of M^+ . For this reason σ -allyl intermediates, (where the Cp* ring is still η^5), such as (43) are not considered plausible, since these should readily reductively eliminate the alkene.

Another noticeable feature is that loss of CO is accompanied by a further loss of 2H or 4H to give ions $[M-CO-4H]^+$ and $[M-CO-6H]^+$. For the allyl complex [15] $[M-CO-6H]^+$ is of low contribution, but this seems to make increasingly strong contributions for the pentenyl and octenyl complexes [16] and [17]. This suggests that one source is loss of H atoms from the alkyl chain to form a dienyl ligand, and that this becomes increasingly facile with increasing chain length.

Scheme 22.



As a comparison, the mass spectrum of complex [18] $Cp^*Re(CO)(Br)(\eta^3\text{-allyl})$ shows that the M^+ pattern is similar to the computer-simulated isotopic abundance pattern (Fig.18(a), p.82). Because the ligand Br in [18] has lone pairs of electrons to delocalize the charge, so the stability of M^+ can be increased (see Chapter II Section 2.5.2). Fragmentation pathways as shown in Scheme 22 suggest that Br is more strongly bonded to the rhenium centre

than are CO and $\eta^3\text{-C}_3\text{H}_5$, since the base peak $m/z400$ indicates that the ligand Br is still bonded to rhenium atom and the CO and $\eta^3\text{-C}_3\text{H}_5$ ligands are already lost.

3.5.5. Exo-endo Interconversion of η^3 -Allyl

The *exo-endo* interconversion of the two isomers [15a]*exo* and [15b]*endo* has been studied by using IR and ^1H NMR spectroscopies. The isomers [15a]*exo* and [15b]*endo* are readily distinguished by their characteristic $\nu(\text{CO})$ absorptions in IR spectroscopy and the hydrido chemical shifts in the ^1H NMR spectrum. Conformational conversion from [15a]*exo* to [15b]*endo* does indeed occur at room temperature but it is very slow. That is why the two isomers [15a]*exo* and [15b]*endo* can be successfully separated even at room temperature. As expected, the rate of conversion of [15a]*exo* to [15b]*endo* increased with temperature. When kept at 38.5°C for two weeks in the dark, a mixture of [15a]*exo* and [15b]*endo* in toluene- d_8 was detected by ^1H NMR and IR to decompose slightly to give very small amounts of complexes $\text{Cp}^*\text{Re}(\text{CO})_2(\eta^2\text{-C}_3\text{H}_6)$ [2], $\text{Cp}^*\text{Re}(\text{CO})_3$ and free propene. Nevertheless, a mixture of [15a]*exo* and [15b]*endo* is reasonably stable for short times (ca 0.5h) at temperatures up to 74°C , as no evidence of decomposition at this temperature was detected by 400MHz ^1H NMR. Furthermore, we found

that the conversion of [15a]exo to [15b]endo was irreversible on the basis of the following experiments. When a pure sample of [15a]exo was kept at 31⁰C in the dark for one week, ¹H NMR showed that [15b]endo was now present in a ratio of [15a]exo to [15b]endo \approx 0.34. Then, this sample of the two isomers was kept in the dark, at 5⁰C, for forty days, and finally kept at 25⁰C for another two weeks. The ¹H NMR spectra showed a small change of the [15a]exo to [15b]endo ratios (\approx 0.32, 5⁰C; \approx 0.32, 25⁰C) within the error range of ¹H NMR experiments. So, no evidence for conversion from [15b]endo to [15a]exo was detected as the temperature was lowered. Consistently, the saturation transfer experiments at 74⁰C did not detect evidence for conversion from [15b]endo to [15a]exo while each proton of [15b]endo was saturated separately. Therefore, the thermal conversion of [15a]exo to [15b]endo is an irreversible process.

However, irradiation of a pure sample of [15b]endo ($\nu(\text{CO})$: 1912 cm^{-1}) in hexane solution resulted in an IR($\nu(\text{CO})$) spectrum showing two strong absorptions at 1912 and 1904 cm^{-1} with an intensity ratio of 1912 to 1904 \approx 0.5, indicating that [15a]exo ($\nu(\text{CO})$: 1904 cm^{-1}) was now present as the major isomer; other very weak bands from $\text{Cp}^*\text{Re}(\text{CO})_3$ (2013, 1922 cm^{-1}) and [2] (1961, 1890 cm^{-1}), indicated a very small amount of decomposition. Similarly, the ¹H NMR spectrum now showed two hydride chemical shifts at δ -9.2 (exo), -11.7 (endo) ppm with an integral ratio of exo/endo \approx 2.5:1.

Therefore, [15b]endo can readily convert to the isomer [15a]exo under UV light.

To date, three different situations of η^3 -allyl in organometallic complexes have been described: (a) the first is the well-known, fast fluxional behaviour;^{65b,67} (b) the second is the very slow *exo-endo* isomerization;^{66i,j} and (c) the third is static η^3 -allyl bonding to transition-metal atoms.^{65c,70} The energy barriers for allyl rearrangement clearly tend to increase in the order (a)<(b)<(c). The fluxional allylic complexes with "piano-stool" structures are usually observed to have a small energy difference between *exo-endo* isomers, as, for example,^{65b,67} the values of ΔH for molybdenum or tungsten allylic complexes are 0.3-2.1 kcal.mol⁻¹, the values of ΔS are 0.2-7 cal.K⁻¹.mol⁻¹, and the values for the activation energy are 12-17 kcal.mol⁻¹. In several examples,^{65c,70} it was reported that a static η^3 -allyl was present rather than a dynamic allyl, such that the ¹H NMR spectra of complexes *trans*-Pt(η^3 -allyl)(Ar)(PPh₃)₂ (allyl = C₃H₅, 2-MeC₃H₄; Ar = 2,3,5,6-C₆HCl₄) were temperature independent in the range of 23-160⁰C, indicating the maintenance of the rigid π -allyl structure even at high temperature.⁷⁰ While the two isomers of *exo* and *endo*-CpRu(CO)(η^3 -2-MeC₃H₄)⁶⁶ⁱ do not interconvert in solution at room

temperature, it was observed that thermal *endo*→*exo* isomerization occurred at 130-140°C, leading to a ratio of [*endo*]/[*exo*] < 0.02.

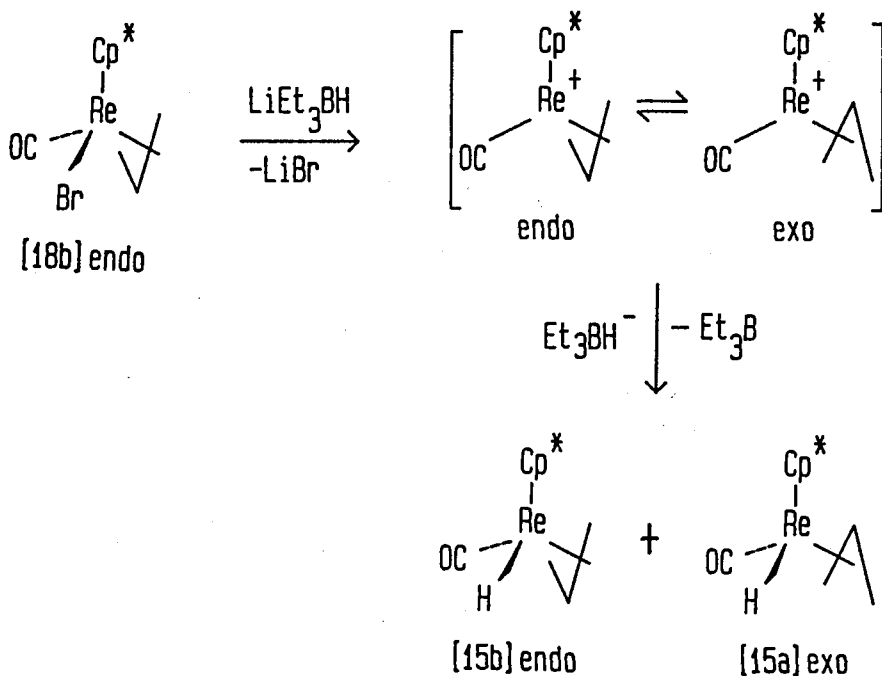
In the case of the slow interconversion from [15a]*exo* to [15b]*endo*, we have estimated the Arrhenius activation energy. The value is $E_a = 28.9 \pm 3.2 \text{ kcal.mol}^{-1}$ obtained by using the procedures described in the section 3.3.(vi). This is obviously larger, as expected, than those values (12-17 kcal.mol⁻¹) found for fast fluxional allylic complexes of molybdenum or tungsten,^{65b} and is very close to the energy barrier (28.9-31.4 kcal.mol⁻¹) in the irreversible *endo*→*exo* conversion of allyl in ruthenium complexes reported by Gibson.⁶⁶ⁱ Although this value of the Arrhenius energy is not very accurate, (because of the uncertainty in the integration of ¹H NMR peaks which varied in the range of 10-15%), the larger value of the Arrhenius activation energy is consistent with the observed slow conformational interconversion from [15a]*exo* to [15b]*endo*. We have already pointed out that a stronger bond exists between the *endo* η^3 -allyl and Re relative to the case of the *exo* η^3 -allyl conformation, based on the comparison of the IR and X-ray structures data for [15a]*exo* and [15b]*endo*, and this may be the reason for the greater thermodynamic stability of the *endo* isomer.

Nevertheless, when the two isomers of [15] (*exo*, *endo*) are brominated, only one isomer [18b]*endo* is observed, which does not convert to [18a]*exo* even on prolonged standing in solution at temperatures up to 60°C. But the complex [18b]*endo* can be readily

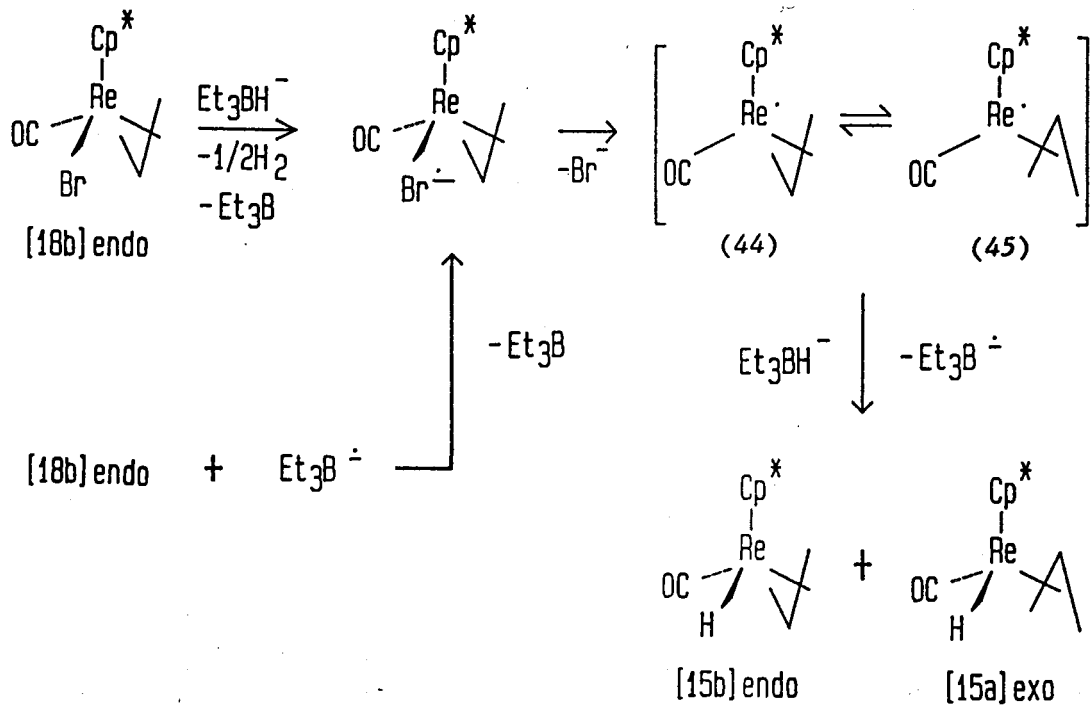
reduced to a mixture of two isomers of [15a](*exo*, *endo*) in a ratio of *exo/endo* \approx 1/3.5 by LiEt_3BH at room temperature in the dark. This may imply that the reduction of the complex [18b]*endo* by lithium triethylborohydride (LiEt_3BH) takes place by an $\text{S}_{\text{N}}1$ (Scheme 23) or a single electron transfer (Scheme 24) mechanism. For example, in Scheme 24, the η^3 -allyl in the unsaturated intermediates (44) and (45) would be expected to rotate as was observed for the fluxional behaviour of the cationic complex $[\text{Cp}^*\text{Re}(\text{CO})_2(\eta^3\text{-allyl})]^+$ [19] shown in Chapter IV, and thus would probably result in a mixture of [15a]*exo* and [15b]*endo* following H^- attack.

Complex [17b]*exo* does not show evidence for conversion to the [17a]*endo* isomer at room temperature.

Scheme 23.

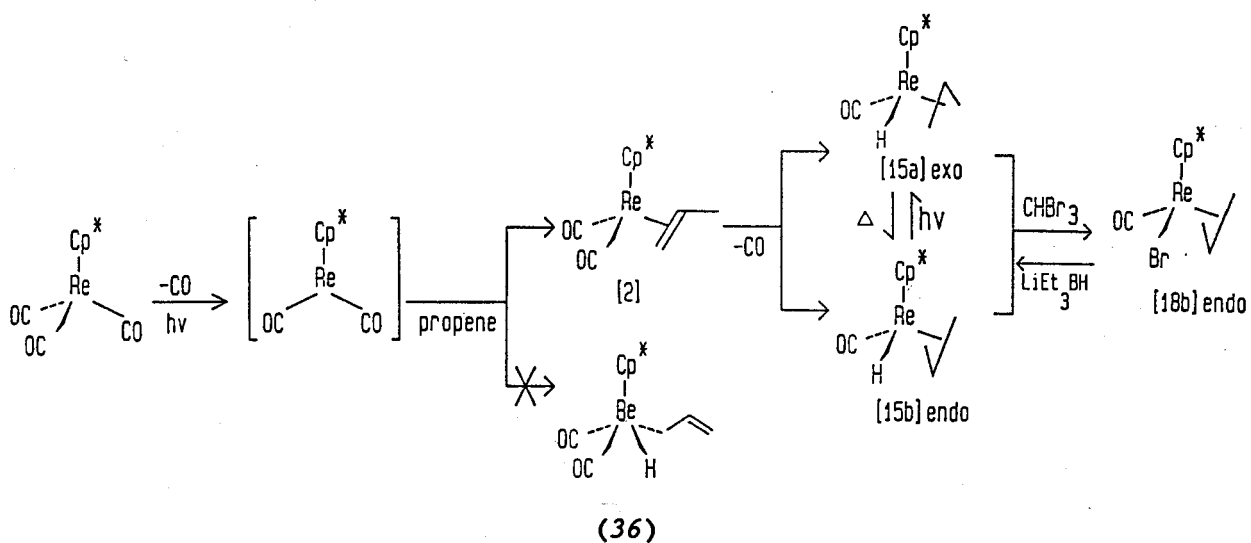


Scheme 24.



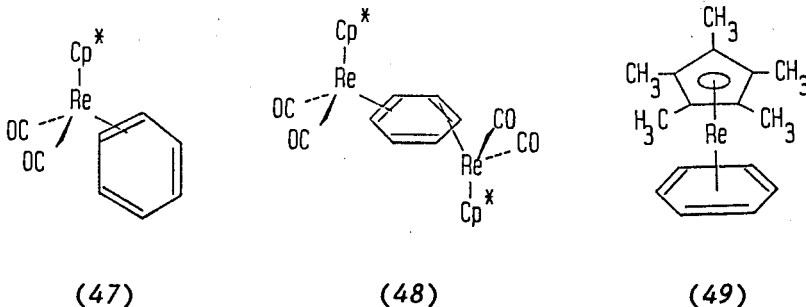
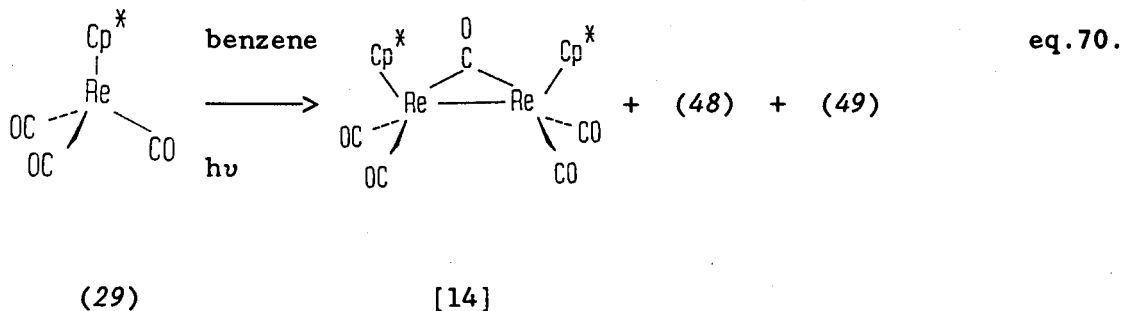
3.5.6. Chemical Reactions

Scheme 25



and the dimerization of $[\text{Cp}^*\text{Re}(\text{CO})_2]$. Similar results in the $\text{CpRe}(\text{CO})_3$ system were also obtained by Graham.⁷¹ However, no product of C-H activation was observed even though the reactive intermediate $[\text{Cp}^*\text{Re}(\text{CO})_2]$ was reasonably postulated to explain the formation of the products in these reactions.

Pasman⁷² reported a very interesting photochemical reaction (eq.70), in which the irradiation of $\text{Cp}^*\text{Re}(\text{CO})_3$ in benzene gave three isolable rhenium complexes [14], (48) and (49). Pasman believed that the intermediacy of the η^2 -benzene complex (47) (observed to be formed directly after photolysis) could account for the formation of all products. The η^2 -benzene complex (47) could react with the unconverted tricarbonyl to give the known dimer [14],



while the dimerization of (47) with loss of one molecule of benzene would give (48). Prolonged irradiation of (47) resulted in loss of two more moles of CO to form (49). This reaction (eq.70) shows the reactive intermediate $[\text{Cp}^*\text{Re}(\text{CO})_2]$ only coordinates the double bond of benzene, but cannot activate a C-H bond of benzene. However, when a CO group is replaced by PMe_3 , the activation of a C-H bond of benzene then occurs, as has been observed by Bergman¹³ for the complexes $\text{Cp}^*\text{Re}(\text{CO})_{2-n}(\text{PMe}_3)_{1+n}$ ($n = 0, 1$ or 2). In the present case, we also do not observe intermolecular C-H activation of propene by $\text{Cp}^*\text{Re}(\text{CO})_3$. However, we do observe intramolecular C-H activation of propene, once it is in the coordinated form $\text{Cp}^*\text{Re}(\text{CO})_2(\eta^2\text{-C}_3\text{H}_6)$ [2]. This contrasts with Pasman's result where no C-H activation of the η^2 -benzene complex occurs.

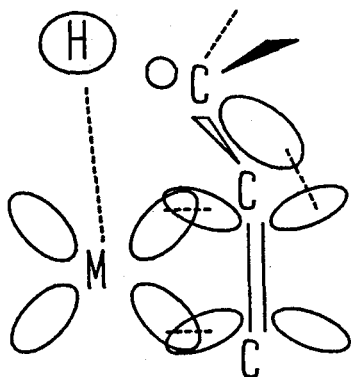


Fig.40. Intramolecular allylic C-H activation through $d-\pi^*-\sigma^*$ interaction

We believe that it is possible for the intramolecular allylic C-H activation to occur because it is assisted by a $d-\pi^*-\sigma^*$

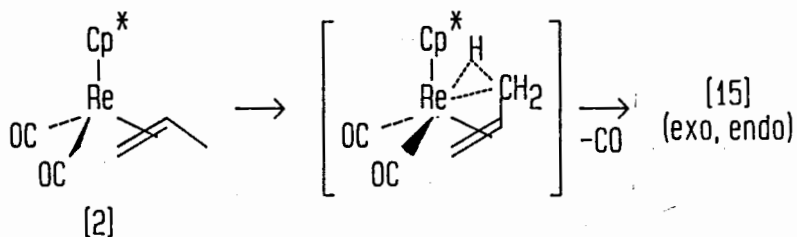
interaction such as is shown in Fig.40, i.e., the π^* -orbital of the alkene will transfer electron density from the $d\pi$ back-bond with the metal to the σ^* -orbital of an allylic C-H bond which is partially overlapped with the allyl π^* -orbital. But it would be difficult for the corresponding intermolecular C-H activation to be assisted by this olefinic $d-\pi^*-\sigma^*$ interaction, because the σ^* -orbital of the C-H bond in an external hydrocarbon molecule would be difficult to overlap with the π^* -orbital of a rotating η^2 -alkene ligand (see Chapter II). Furthermore, the stereochemistry is advantageous for the intramolecular allylic C-H activation, since the allylic C-H bonds of η^2 -propene are already very close to the rhenium atom.

On the basis of the experimental results described earlier and shown in eqs.55-60, three different mechanisms may be considered for the intramolecular allylic C-H activation in a Cp^*Re system. These are (1) concerted, (2) sequential and (3) ring slip mechanisms as shown in Fig.41.

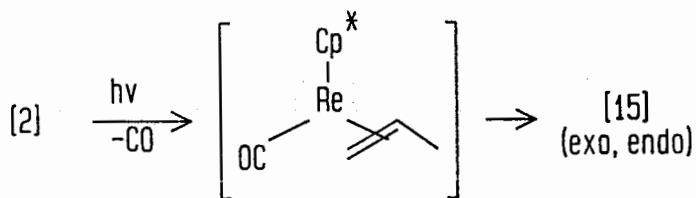
If the process by which [2] is converted to [15] (*exo*, *endo*) involves dissociation of one CO as a first step (i.e., the sequential mechanism) to give a discrete intermediate [$\text{Cp}^*\text{Re}(\text{CO})(\eta^2\text{-C}_3\text{H}_6)$], it might reasonably be expected that this intermediate would be intercepted by PMe_3 to give the complex [12]. This complex [12] was synthesized by an alternative route (see Chapter II) and has $\nu(\text{CO})$ at 1845 cm^{-1} . However, no apparent absorption at this position

Fig.41. Intramolecular Allylic C-H Activation Mechanisms

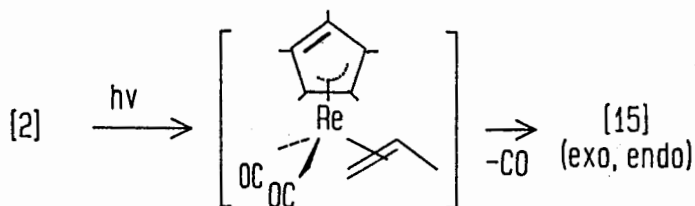
Mechanism I. Concerted state



Mechanism II. Sequence



Mechanism III. η^3 -pentamethylcyclopentadienyl intermediate



was observed when [2] was irradiated in the presence of PMe_3 (eq.61). Additionally, [15] (*exo*, *endo*) was shown to be stable even at 60-65°C in the presence of PMe_3 (eq.68). This result does not necessarily rule out prior dissociation of a CO group from [2]. It is possible that the rate of reaction of the intermediate with PMe_3 is much slower than the intramolecular allylic C-H activation to give [15]. In the concerted mechanism, it is envisaged that the allylic C-H activation occurs with corresponding loss of a CO group in the same process. This would also account for the inability to form [12] in the presence of PMe_3 . In the same manner, we also cannot discount the third possibility in which a $\eta^3\text{-Cp}^*$ 16e- intermediate would be present. It would be very difficult to distinguish between a "concerted state" and a $\eta^3\text{-Cp}^*$ 16 e- intermediate in experiments. On the available evidence, no firm conclusion about the mechanism is possible.

The photolysis of the PMe_3 derivative $\text{Cp}^*\text{Re}(\text{CO})_2(\text{PMe}_3)$ (37) with propene allows the influence of the PMe_3 ligand to be evaluated (eq.62, p.143). In previous photolyses of (37) with hydrocarbons, Bergman has observed the retention of the phosphine group in the products, indicating that CO is preferentially lost.¹³ In the reaction of (37) with propene loss of PMe_3 would give the same 16 e- intermediate $[\text{Cp}^*\text{Re}(\text{CO})_2]$ as does the tricarbonyl and therefore the same expected products. But loss of CO would give the different 16 e- intermediate $[\text{Cp}^*\text{Re}(\text{CO})(\text{PMe}_3)]$. This could then coordinate

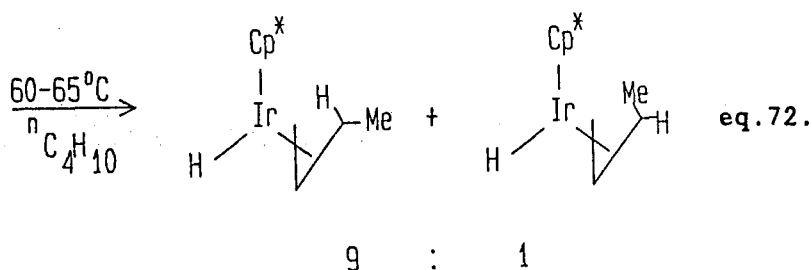
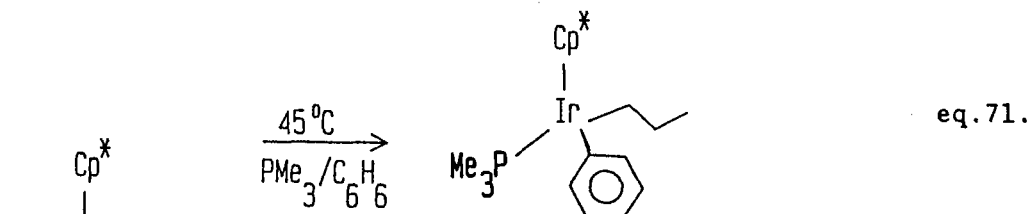
propene to give $\text{Cp}^*\text{Re}(\text{CO})(\text{PMe}_3)(\text{propene})$ [12]. In fact, [12] is a major product in eq.62. If [12] were to undergo CO loss on further photolysis in the manner of the propene complex [2], then a new hydrido(allyl) complex $\text{Cp}^*\text{Re}(\text{PMe}_3)(\text{H})(\eta^3\text{-C}_3\text{H}_5)$ would be produced. There was no evidence for this compound. Alternatively, loss of PMe_3 from [12] during photolysis would produce the hydrido(allyl) complex [15], and this is observed also in the products. A small amount of the cyclometallated product $\text{Cp}^*\text{Re}(\text{CO})(\text{H})(\text{CH}_2\text{PMe}_2)$ (38)^{9,13} was also formed by internal C-H activation of the PMe_3 ligand in the intermediate $[\text{Cp}^*\text{Re}(\text{CO})(\text{PMe}_3)]$ as has been observed before.^{9,13}

Photochemical loss of the N_2 ligand from $\text{Cp}^*\text{Re}(\text{CO})(\text{N}_2)\text{PMe}_3$ (39) is known to be very rapid.⁹ Irradiation of this complex in the presence of propene (eq.63, p.143) produced mainly the complex $\text{Cp}^*\text{Re}(\text{CO})(\text{PMe}_3)(\eta^2\text{-C}_3\text{H}_6)$ [12] plus some of (37), [15] and [2]. These other products most probably arise from further photodecomposition of [12] itself. Thus, when a pure sample of [12] was irradiated in hexane under N_2 , these products were observed to be formed (eq.64 and Fig.32).

The results of eqs. 38 and 65-68 show that the chemical behaviour of the rhenium allyl hydride [15](*exo*, *endo*) is significantly different to that of the iridium allyl hydride²⁹ $\text{Cp}^*\text{Ir}(\text{H})(\eta^3\text{-C}_3\text{H}_5)$. Bergman reported that $\text{Cp}^*\text{Ir}(\text{H})(\eta^3\text{-allyl})$ is highly air sensitive and it was obtained by the reduction of $\text{Cp}^*\text{Ir}(\text{Cl})(\eta^3\text{-allyl})$ with LiEt_3BH .²⁹ Its proposed structure has a

static η^3 -allyl, as supported by the spectroscopic data.

Bergman successfully reacted $\text{Cp}^* \text{Ir}(\text{H})(\eta^3\text{-allyl})$ with arenes and alkanes, and discovered the sequential intermolecular C-H oxidative addition and hydride to alkene migratory insertion reactions.²⁹ Two examples are shown as eqs.71, 72.



By contrast, [15](*exo, endo*) did not react with benzene (eq.67), nor with hexane in the presence of PMe_3 under thermal conditions (eq.68). Thermolysis of [15](*exo, endo*) yielded the propene complex [2], $\text{Cp}^* \text{Re}(\text{CO})_3$ and the binuclear complex $(\text{Cp}^* \text{Re}(\text{CO})_2)_2(\text{CO})$ [14] (eq.67). Similarly, these same products and free propene were yielded by photolysis of [15](*exo, endo*) (eq.66).

The experimental results of eqs.66-67 show that the rhenium

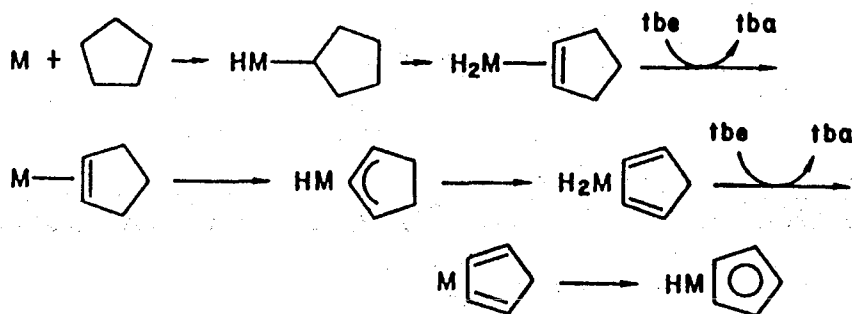
atom is a good CO-trap for traces of CO that are released in these reactions as a result of a small amount of decomposition. This characteristic CO-trap of the rhenium atom is also shown in the X-ray structure of the heterobimetallic complex [26] $\text{Cp}(\text{CO})\text{Re}(\mu_2\text{-CO})_2\text{Ir}(\text{CO})\text{Cp}^*$, which was made by the reaction of $\text{CpRe}(\text{CO})_2\text{L}$ (L = THF or N_2) with $\text{Cp}^*\text{Ir}(\text{CO})_2$ (see Chapter V). The carbonyl groups $\mu_2\text{-CO}$ are primarily bound to the Re atom and semibridging to the Ir atom. Also, the fragmentation behaviour of this complex [26] in MS exhibits the strong appearance of the fragment $\text{Cp}^*\text{Ir}(\text{CO})$ m/z 356, and $(\text{Cp}^* - 2\text{H})\text{Ir}(\text{CO})$ m/z 354 indicating that fragmentation of the molecular ion is similar to CO abstraction reactions by way of the loss of $\text{CpRe}(\text{CO})_3$ (see Chapter V).

As a consequence of this CO uptake, [15](*exo,endo*) converts upon irradiation to the stable complexes [2], $\text{Cp}^*\text{Re}(\text{CO})_3$ and the binuclear complex $(\text{Cp}^*\text{Re}(\text{CO})_2)_2(\text{CO})$ [14] (eq.66, p.148).

Finally, it is worth considering the photochemical dehydrogenation of $\text{Cp}^*\text{Re}(\text{CO})_2(\eta^2\text{-C}_6\text{H}_{10})$ [6] to yield $\text{Cp}^*\text{Re}(\text{CO})_2(\eta^2\text{-1,3-C}_6\text{H}_8)$ (eq.37). We have not studied this reaction in detail yet. A few published examples have already demonstrated that transition-metal complexes^{5,30,73} are effective in dehydrogenation of hydrocarbons. Crabtree⁵ reported the dehydrogenation of cycloalkanes by $[\text{Ir}(\text{H})_2(\text{Me}_2\text{CO})_2\text{L}_2][\text{BF}_4]$ (L = PPh_3) and *tert*-butylethylene (tbe). Based on the studies of dehydrogenation of cyclopentane, Crabtree^{5,30} proposed that the initial step is oxidative addition of

a cyclopentane C-H bond to the metal atom to form the unstable intermediate alkyl hydride. Thus, the subsequent β -elimination would give the corresponding olefin dihydride, which could be dehydrogenated by the *t*-butylethylene. This cycle of dehydrogenation could continue until a stable product has been formed. This mechanism, shown in Scheme 26, was supported by the similar behaviour of the proposed intermediates synthesized independently.³⁰

Scheme 26.



tbe: *t*-BuCH=CH₂; tba: *t*-BuEt

Similarly, the photochemical dehydrogenation of [6] to yield the η^2 - and η^4 -1,3-cyclohexadiene complexes ([10] and [13], eq.37, p.112) could be explained by the above hydrido(allyl) mechanism. The last CO loss in [13] would give the known complex Cp*Re(η^6 -C₆H₆)⁷². This proposition needs to be proved by further investigation.

3.6. Conclusions

The photochemical C-H activation of coordinated alkenes in Cp*Re systems has been investigated for a range of linear and cyclic alkenes. Two types of photochemical C-H activation of alkenes in Cp*Re systems have been discovered: (1) the intramolecular allylic C-H activation of linear alkenes yields the rhenium allyl hydride complexes; (2) the photochemical double C-H activation of coordinated cyclohexene results in the formation of Cp*Re(CO)₂(η^2 -1,3-cyclohexadiene) [10]. The photochemical C-H activation of the 1-octene complex yielded only one isomer [17b]*exo*, the *exo* conformation of the η^3 -allyl group determined by ¹H NMR decoupling experiments (Section 3.5.3) which also established that the 4-alkyl substituent of the allyl group is located in the *syn* position. The fragmentations of the hydride complexes [15]-[17] in MS exhibit a notable feature, that the observed isotopic patterns for M⁺ do not correspond to the calculated patterns. This has been attributed to the unstable Re-H bond.

Furthermore, two conformational isomers of [15](*exo*, *endo*) have been successfully separated. The structures of [15a](*exo*) and [15b](*endo*) were determined by the X-ray crystal analysis (see Section 3.3), indicating that the η^3 -allyl group is symmetrically bonded to Re in [15a]*exo*, and is somewhat asymmetrically bonded in [15b]*endo*. Correspondingly, the C-C bond lengths of the allyl group

in [15a]exo are equal within error, but they differ in [15b]endo.

The conformational interconversion between the two isomers of [15](exo, endo) has been examined. An irreversible conversion from [15a]exo to [15b]endo occurs under thermal conditions; however, irradiation favours the conversion from [15b]endo to [15a]exo. An estimate of the Arrhenius activation energy gives a value $E_a = 28.9 \pm 3.2 \text{ kcal.mol}^{-1}$, which is larger than values (12-17 kcal.mol^{-1}) found for the fast fluxion allylic complexes of molybdenum or tungsten,^{65b} and is very close to the energy barrier (28.9-31.4 kcal.mol^{-1}) in the irreversible endo \rightarrow exo conversion of allyl in ruthenium complexes.⁶⁶ⁱ Finally, it has been established that the rhenium allyl hydride [15] does not show the same reactivity as does the related iridium allyl hydride complex $\text{Cp}^* \text{Ir(H)}(\eta^3\text{-C}_3\text{H}_5)$.

3.7. Experimental Section

General synthetic procedures, purification of solvents and spectroscopic measurements, were as described in Chapter II. Bromoform was dried with anhydrous calcium chloride and then passed through a column of neutral alumina to remove traces of water. The eluate was collected under nitrogen and used directly. Lithium triethylborohydride ($\text{LiB(C}_2\text{H}_5)_3\text{H}$, 1 M in THF) was available commercially (Aldrich) and used directly. Electron-impact mass spectral data (m/z) are reported based on ^{187}Re and ^{79}Br . The

experimentally observed data for the IR and ^1H NMR spectra of the complexes [15]-[18] are listed in Tables 8-10.

(1) $\text{Cp}^*\text{Re}(\text{CO})(\text{H})(\eta^3\text{-C}_3\text{H}_5)$ [15]. A solution of $\text{Cp}^*\text{Re}(\text{CO})_3$ (800 mg, 1.97 mmol) in about 100 ml of freshly distilled hexane was irradiated in a quartz tube at 0°C for 1 h with a propene purge. This resulted in an IR spectrum having strong absorptions at 1961 and 1890 cm^{-1} for the propene complex [2], and weaker ones at 1904 and 1912 cm^{-1} for [15a]exo and [15b]endo respectively, plus residual absorptions from $\text{Cp}^*\text{Re}(\text{CO})_3$. Further irradiation for another 30 min. intensified the absorptions from [15a]exo and [15b]endo relative to [2]. After removal of the solvent under vacuum at room temperature, the residual brown solid was redissolved in hexane and transferred to a neutral alumina column (about $25 \times 1\text{ cm}$) and eluted with hexane. By chromatography, four fractions were eluted and isolated. These are $\text{Cp}^*\text{Re}(\text{CO})_3$, complex [2], complex [15b]endo, and, as the final fraction, complex [15a]exo. The isomers [15a]exo and [15b]endo were separately recrystallized from freshly distilled hexane and ether (ratio = hexane/ether = 1/2) at -78°C as white microcrystals. Yield: [15a]exo 105 mg (0.268 mmol, 13.6%), [15b]endo 49 mg (0.125 mmol, 6.3%), complex [2] 310 mg (0.738 mmol, 37.5%). MS (EI) for two isomers of [15]: m/z 392 $[\text{M}]^+$, 390 $[\text{M}-2\text{H}]^+$, 362 $[\text{M}-\text{CO}-2\text{H}]^+$, 360 (base) $[\text{M}-\text{CO}-4\text{H}]^+$, 358 $[\text{M}-\text{CO}-6\text{H}]^+$. Anal. Calcd. for [15]: C, 42.95; H, 5.41. Found: C, 43.48; H, 5.26 for [15a]exo. C, 43.55; H, 5.27

for [15b]endo.

(ii) $\text{Cp}^*\text{Re}(\text{CO})(\text{H})(\eta^3\text{-C}_5\text{H}_9)$ [16]. A procedure similar to that described for the preparation of [15] was used for the synthesis of the complex [16]. The photochemical reaction of $\text{Cp}^*\text{Re}(\text{CO})_3$ (200 mg, 0.493 mmol) and 4 ml of 2-pentene (a mixture of *cis* and *trans* isomers, ratio = $[\textit{cis}]/[\textit{trans}] \approx 1/3.5$ calculated by GC) in hexane was carried out for 60 min. at 0°C, and gave a mixture of isomers of η^3 -allylalkane rhenium hydrides [16c,d,e,f,k]. Following chromatography on a neutral alumina column with hexane as eluant, the mixture of isomers [16c,d,e,f,k] was separated from the 2-pentene complex [3] and the residual $\text{Cp}^*\text{Re}(\text{CO})_3$ and was isolated as a white solid. Yields: complex [16] 45 mg (0.107 mmol, 21.7%), complex [3] 58.9 mg (0.132 mmol, 26.7%). The mixture of isomers [16] could not be separated further and decomposed in a few days. Anal. Calcd. for [16]: C, 45.80; H, 6.01. Found: C, 46.18; H, 5.80. MS (EI) for isomers of [16]: m/z 420 $[\text{M}]^+$, 418 $[\text{M}-2\text{H}]^+$, 390 $[\text{M}-\text{CO}-2\text{H}]^+$, 388 $[\text{M}-\text{CO}-4\text{H}]^+$, 386(base) $[\text{M}-\text{CO}-6\text{H}]^+$.

(iii) $\text{Cp}^*\text{Re}(\text{CO})(\text{H})(\eta^3\text{-C}_8\text{H}_{15})$ [17]. The complex [17] was synthesized analogously to [15] and [16] as a white solid in yield 7.0%. Anal. Calcd. for [17]: C, 49.43; H, 6.77. Found: C, 49.54; H, 6.91. MS (EI): m/z 462 $[\text{M}]^+$, 460 $[\text{M}-2\text{H}]^+$, 432 $[\text{M}-\text{CO}-2\text{H}]^+$, 430 $[\text{M}-\text{CO}-4\text{H}]^+$, 428(base) $[\text{M}-\text{CO}-6\text{H}]^+$.

(iv) $\text{Cp}^*\text{Re}(\text{CO})_2(\eta^2\text{-C}_6\text{H}_8)$ [10]

Method (1). This complex [10] was isolated as a product in yield 9.2% from the photochemical reaction of $\text{Cp}^*\text{Re}(\text{CO})_3$ with cyclohexene (see Chapter II), or was directly formed in the photolysis of the cyclohexene complex [6].

Method (2). The complex [10] was also synthesized by the direct photochemical reaction of $\text{Cp}^*\text{Re}(\text{CO})_2(\text{N}_2)$ and 1,3-cyclohexadiene, details of which were included in Chapter II.

(v) $\text{Cp}^*\text{Re}(\text{CO})(\text{Br})(\eta^3\text{-C}_3\text{H}_5)$ [18]. A solid sample of [15] (42 mg, 0.107 mmol, a mixture of *exo* and *endo*, ratio = *exo/endo* \approx 3/1) was dissolved in about 10 ml of freshly dried bromoform. The solution was stirred at room temperature over night. The solution was transferred to a neutral alumina column (10x1 cm) with hexane as an eluant. Following chromatography, the complex [18] was isolated in yield 63.6%. Anal. Calcd. for [18]: C, 35.74; H, 4.29. Found: C, 35.96; H, 4.10. MS (EI): 470 $[\text{M}]^+$, 442 $[\text{M-CO}]^+$, 400(base) $[\text{M-CO-C}_3\text{H}_5\text{-H}]^+$.

(vi) Thermal Conformational Conversion *exo* \rightarrow *endo* of [15]

Pure samples of each of [15a]*exo* (7 mg, 0.018 mmol) and 0.7 ml of C_6D_6 were added to two separate NMR tubes under N_2 . The two sample tubes were flame sealed and wrapped with aluminum foil. Then, one sample tube was kept in a cooling bath at different temperatures for

a period of time, starting from low to high temperature, and checked by ^1H NMR at 400MHz. The ratio of *exo* to *endo* was measured by integration of hydride peaks and listed in Table 14 (No.1). Another sample tube was first kept at 31°C for one week, then at 5°C for forty days, and finally at 25°C for another two weeks. The ^1H NMR measurements give the ratio of *exo* to *endo* by integration of hydride peaks as are listed in Table 14 (No.2), p.194.

(vii) Kinetics of the Conversion *exo*→*endo* of [15] Four NMR samples each of a mixture of [15a]*exo* and [15b]*endo* (7 mg, 0.018 mmol) were prepared in C_6D_6 (0.7 ml) under nitrogen. Then, the four NMR sample tubes were wrapped with aluminum foil, and kept at different temperatures 25, 30, 35 and 40°C respectively. The ratios of $[\textit{endo}]_t$ to $[\textit{exo}]_t$ were monitored by 100MHz ^1H NMR. The intensities of the two hydride resonances were carefully measured to determine the rate constants k at different temperatures by using the rate eq.39. The data for the rate constants k are listed in Table 12.

(viii) Photolysis of [2] (a) Irradiation of a hexane (10 ml) solution of [2] (10 mg, 0.024 mmol) under a nitrogen purge at 0°C for 30min. in a Pyrex tube resulted in an IR($\nu(\text{CO})$, hexane) spectrum having strong absorptions at 2014, 1922 cm^{-1} for

$\text{Cp}^*\text{Re}(\text{CO})_3$, and other absorptions at 1904 and 1912 cm^{-1} for [15a]exo and [15b]endo respectively, plus residual absorptions at 1961, 1890 cm^{-1} from [2], indicating that the major product was $\text{Cp}^*\text{Re}(\text{CO})_3$. (b) In a quartz tube, and using a purge of propene, the IR ($\nu(\text{CO})$, hexane) spectrum showed only two new bands at 1904, 1912 cm^{-1} for [15a]exo and [15b]endo respectively, indicating that the formation of the tricarbonyl was suppressed. (c) A mixture of [2] and [15](exo, endo) (12 mg) in a hexane (10 ml) was irradiated at 0°C under 1 atm CO, and monitored by IR. The IR($\nu(\text{CO})$) spectra showed that the bands of complex [15](exo, endo) rapidly disappeared first in 10 min., followed, more slowly, by those of [2] in 20 min., suggesting that the propene complex [2] was initially reformed by addition of CO to [15](exo, endo). (d) A 10 ml hexane solution of [2] (10 mg, 0.024 mmol) was irradiated for 30 min. under a CO purge at 0°C to give an IR spectrum showing the bands at 2013, 1922 cm^{-1} for $\text{Cp}^*\text{Re}(\text{CO})_3$. (e) Irradiation of a 10 ml hexane solution of [2] (10 mg, 0.024 mmol) in a Pyrex tube at 0°C in the presence of added PMe_3 gave an IR($\nu(\text{CO})$) spectrum showing the bands at 1923, 1860 cm^{-1} from $\text{Cp}^*\text{Re}(\text{CO})_2(\text{PMe}_3)$, and weaker ones at 1904 and 1912 cm^{-1} for [15a]exo and [15b]endo respectively, plus residual absorptions at 1961, 1890 cm^{-1} from the unreacted [2]. (f) Photolysis of [2] (5 mg, 0.012 mmol) in cyclohexane- d_{12} (0.7 ml) in a NMR tube for 30 min. gave a ^1H NMR spectrum showing δ 5.75 (m, 1H), 4.95 (d, 1H; $J = 16.5$

Hz), 4.87 (d, 1H; J = 8.7 Hz), attributable to the three vinyl protons of propene, and δ 1.65 (d, 3H; J = 7.0 Hz), attributable to the three protons of methyl of propene, and δ -9.2, -11.7, attributable to the hydrides of [15a]exo and [15b]endo respectively.

Table 14. Data for the Ratio of Exo to Endo^a

No.1 <i>exo/endo</i>	35.7	32.3	15.4	6.94	1.36	.328	.274
t ⁰ C	-12	-2.5	3	7	17.5	27.5	32
days	21	21	14	14	14	14	7
No.2 <i>exo/endo</i>	.34	.32	.32				
t ⁰ C	31	5	25				
days	7	40	14				

^aAs determined by integration of hydride peaks at 400MHz ¹H NMR.

(ix) Photolysis of $\text{Cp}^*\text{Re}(\text{CO})_2(\text{PMe}_3)$ (37) Irradiation of (37) (30 mg, 0.066 mmol) in hexane (30 ml) at 0°C with a propene purge for 30 min. resulted in an IR($\nu(\text{CO})$) spectrum (Fig.30) having a strong absorption at 1845 cm^{-1} for $\text{Cp}^*\text{Re}(\text{CO})(\text{PMe}_3)(\eta^2\text{-C}_3\text{H}_6)$ [12], weaker bands for [15](*exo*, *endo*) ($1904, 1912\text{ cm}^{-1}$) and [2] ($1961, 1890\text{ cm}^{-1}$) and a weakest band for $\text{Cp}^*\text{Re}(\text{CO})(\text{H})(\text{CH}_2\text{PMe}_2)$ (38) (1878 cm^{-1}). The hexane solution was filtered through a short Celite column and dried under vacuum. The residual solid was dissolved in C_6D_6 (0.7 ml) and then checked by ^1H NMR. The ^1H NMR spectrum shows the hydrides at δ -9.23 (for [15a]*exo*), -11.66 (for [15b]*endo*), and -9.92 (for $\text{Cp}^*\text{Re}(\text{CO})(\text{H})(\text{CH}_2\text{PMe}_2)$ (38)).

(x) Photolysis of $\text{Cp}^*\text{Re}(\text{CO})(\text{N}_2)(\text{PMe}_3)^{51}$ (39) Irradiation of (39) (100 mg, 0.22 mmol) with a propene purge at 0°C yielded the major product $\text{Cp}^*\text{Re}(\text{CO})(\text{PMe}_3)(\eta^2\text{-C}_3\text{H}_6)$ [12] (yield: 37 mg, 0.08 mmol, 36.4%) and small amounts of by-products involving [15](*exo*, *endo*), [2] and $\text{Cp}^*\text{Re}(\text{CO})_2(\text{PMe}_3)$ (37) (see Chapter II Section 2.7(xii) for details).

(xi) Photolysis of [12] Irradiation of the hexane (25 ml) solution of [12] $\text{Cp}^*\text{Re}(\text{CO})(\text{PMe}_3)(\eta^2\text{-C}_3\text{H}_6)$ (15 mg, 0.032 mmol) was continued for 40 min. at 0°C . A small quantity of brown solid was produced. The IR($\nu(\text{CO})$) spectrum of the solution showed a strong

absorption from the starting material [12] (1845 cm^{-1}), weaker bands for [15](*exo*, *endo*) (1904 , 1912 cm^{-1} respectively) and [2] (1961 , 1890 cm^{-1}) and two weakest bands for $\text{Cp}^*\text{Re}(\text{CO})_2(\text{PMe}_3)$ (37) (1923 , 1860 cm^{-1}) (see Fig.32). After chromatography on an alumina column ($7 \times 1\text{ cm}$) with hexane as an eluant, a mixture of [2] and [15](*exo*, *endo*) was isolated from the unconverted [12].

(xii) Irradiation of [15] (a) A pure sample of [15b]*endo* (5 mg, 0.013 mmol) in hexane (3 ml) solution, irradiated in a Pyrex tube at 0°C or room temperature for 5 min., gave an IR($\nu(\text{CO})$) spectrum showing two strong absorptions at 1904 and 1912 cm^{-1} from [15a]*exo* and [15b]*endo* respectively, (the intensity ratio of 1904 to 1912 was about 2:1), and other very weak bands from $\text{Cp}^*\text{Re}(\text{CO})_3$ (2013 , 1922 cm^{-1}) and [2] (1961 , 1890 cm^{-1}) which indicated a very small amount of decomposition. Removal of hexane, and dissolution of the solid residue in C_6D_6 gave a ^1H NMR spectrum showing two hydride chemical shifts at δ -9.2 (*exo*) and -11.7 (*endo*) ppm with an integral ratio of *exo/endo* \approx 2.5:1. Further irradiation for 15 min. led to an increase in the decomposition products $\text{Cp}^*\text{Re}(\text{CO})_3$ and $\text{Cp}^*\text{Re}(\text{CO})_2(\eta^2\text{-C}_3\text{H}_6)$ [2]. (b) Irradiation of [15](*exo*, *endo*) (7 mg, 0.018 mmol) in cyclohexane- d_{12} (0.7 ml) in a NMR tube for 30 min. gave a ^1H NMR spectrum which revealed the production of free propene [δ : 5.75(m, 1H), 4.95(d, 1H), 4.87(d, 1H), 1.65(d, 3H)] and the

formation of [2] [δ : 2.16(dd, 1H), 1.97(m, 1H), 1.35(dd, 1H), 2.05(d, 3H)], as the major product, accompanied by a significant amount of the starting material [15](*exo*, *endo*). The IR(ν (CO), in hexane) spectrum clearly showed five bands at 1971(w), 1930(s), 1901(s), 1877(w), 1714(m) cm^{-1} attributable to the known binuclear complex $(\text{Cp}^*\text{Re}(\text{CO})_2)_2\text{CO}$ [14], and other bands at 2013, 1922 cm^{-1} (from $\text{Cp}^*\text{Re}(\text{CO})_3$), 1961, 1890 cm^{-1} (from [2]). The binuclear complex $(\text{Cp}^*\text{Re}(\text{CO})_2)_2\text{CO}$ [14] was further confirmed by the MS (EI) in the range of m/z 400 to m/z 750 showing its molecular ion peak at m/z 726 with the isotopic abundance pattern similar to the computed isotopic abundance pattern. These data for the binuclear complex [14] are consistent with those reported by Graham.³⁷

(xiii) Thermolysis of [15] (a) A benzene (10 ml) solution of [15](*exo*, *endo*) (10 mg, 0.026 mmol) was heated under nitrogen in an oil bath at 75-80⁰C for 24h. The IR(ν (CO)) showed absorptions at 1961, 1890 cm^{-1} from [2]; 2013, 1922 cm^{-1} from $\text{Cp}^*\text{Re}(\text{CO})_3$ and five bands at 1971(w), 1930(s), 1901(s), 1877(w), 1714(m) cm^{-1} assignable to the known binuclear complex $(\text{Cp}^*\text{Re}(\text{CO})_2)_2\text{CO}$ [14]. Furthermore, the ¹H NMR spectrum showed the chemical shifts at δ -9.2, -11.7 ppm assignable to the hydrides of [15a]*exo* and [15b]*endo* respectively, with an integral ratio [15a]*exo* to [15b]*endo* \approx 0.28. (b) A hexane solution of [15](*exo*, *endo*) (12 mg, 0.031 mmol) with 3 drops of PMe_3

in a sealed tube was heated in an oil bath at 60-65⁰C for 4h. The IR spectrum did not show any change.

(xiv) Reduction of $\text{Cp}^*\text{Re}(\text{CO})(\text{Br})(\eta^3\text{-C}_3\text{H}_5)$ [18] A solution of [18b]*endo* (10 mg, 0.021 mmol) in about 10 ml of freshly distilled ether was stirred at room temperature in the dark. Five drops of lithium triethylborohydride (LiEt_3BH , 1 M in THF) were added dropwise to the ether solution. Then, the reaction solution was stirred for 2 h. The solvent was removed under vacuum to give a white solid residue, which was washed with hexane (10x3 ml). The hexane washings were collected and filtered through a short Celite column (1x1 cm). Removal of hexane gave a white solid which was identified by IR($\nu(\text{CO})$): 1912 cm^{-1} from [15b]*endo*, 1904 cm^{-1} from [15a]*exo*; and ^1H NMR (C_6D_6): δ -11.7, -9.2 ppm attributable to the hydrides of [15b]*endo* and [15a]*exo* respectively, with a integral ratio of [15a]*exo* to [15b]*endo* \approx 0.26.

Chapter IV

Syntheses, Characterizations and Reactions of η^3 -Allyl Cationic Complexes of Rhenium

4.1. Introduction

The synthesis, characterization and reactions of allyl cationic complexes have been investigated in several transition-metal systems.^{66k,74} In some cases, remarkable regioselectivity was observed in nucleophilic attack on these η^3 -allyl cationic complexes of molybdenum⁷⁵ and tungsten.³³ As a result of further studies, it is believed that in the case of the complexes $[\text{CpMo}(\text{CO})(\text{NO})(\eta^3\text{-allyl})]^+$ and $[\text{CpM}(\text{CO})_2(\eta^3\text{-allyl})]^+$ (where M = Mn, Re) complexes, the mechanism for *exo-endo* isomerization involves pseudorotation of the η^3 -allyl group about the allyl-metal bond axis.^{66k,67a} However, in the case of neutral iron^{66c} and ruthenium⁶⁶ⁱ complexes $\text{CpM}(\text{CO})(\eta^3\text{-allyl})$ (where M = Fe, Ru), the *exo-endo* isomerization behaviour was suggested to involve an $\eta^3\text{-}\eta^1\text{-}\eta^3$ allyl transformation. We have described the formation of the hydrido(allyl) complex [15](*exo,endo*) $\text{Cp}^*\text{Re}(\text{CO})(\text{H})(\eta^3\text{-C}_3\text{H}_5)$ by photolysis of the propene complex $\text{Cp}^*\text{Re}(\text{CO})_2(\eta^2\text{-C}_3\text{H}_6)$ [2] (see Chapter III). Here, the two isomers of [15](*exo,endo*) display an interesting *exo-endo* interconversion. We

were interested to study the *exo-endo* interconversion further in Cp*Re cationic systems as well as the chemical behaviour of η^3 -allyl rhenium cationic complexes.

In this chapter, the synthesis and characterization of several new η^3 -allyl cationic complexes of rhenium [19]-[21] will be described. The fast *exo-endo* isomerization of η^3 -allyl cationic complex [19] has been determined by NOE experiments. Nucleophilic addition to these cationic complexes [19]-[21] yielded some derivatives [5], [23] and [24]. The characterization and chemical behaviour of these derivatives will be illustrated.

4.2. Synthesis

The rhenium η^3 -allyl cationic complexes [19]-[21] have been synthesized according to equation 73, using the rhenium η^2 -alkene complexes described in Chapter II as starting materials. Treatment of the rhenium η^2 -alkene complexes ([2], [4] and [6]) with $[\text{Ph}_3\text{C}][\text{BF}_4]$ in nitromethane produced the η^3 -allyl cationic complexes [19]-[21] respectively in moderate yield. This synthetic route is different from the conventional route, which presumably involves the dehydration of the allylic alcohol complex, as was utilized in the synthesis of the Cp analogue of the complex [19] (eq.74).^{67a,76,77} Derivatives of these cationic allyl complexes, i.e., the η^2 -3-methoxypropene complex [22] and η^2 -3-methoxycyclohexene complex [23]

Table 15. Structures of Complexes [19]-[23]

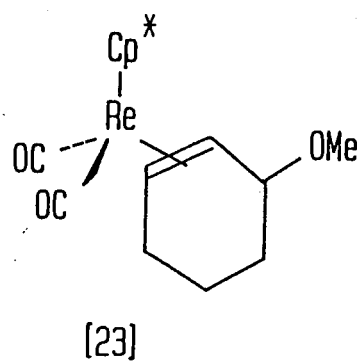
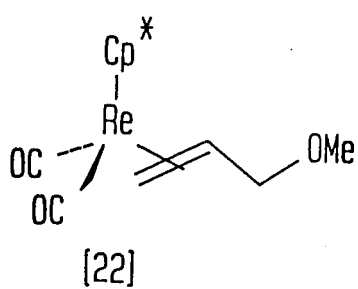
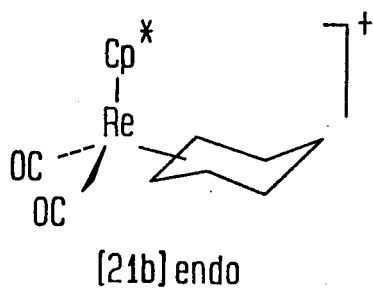
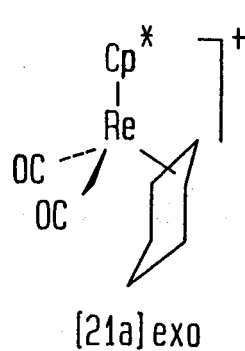
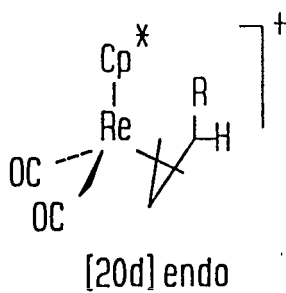
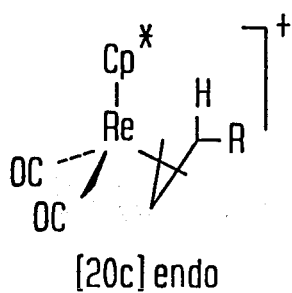
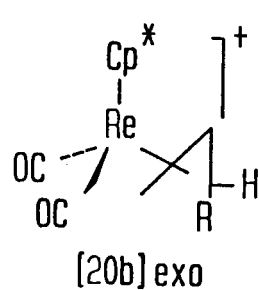
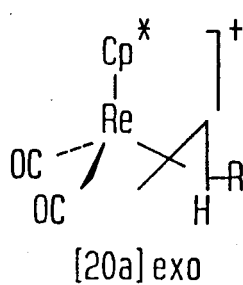
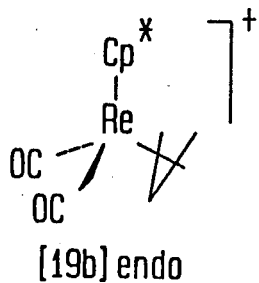
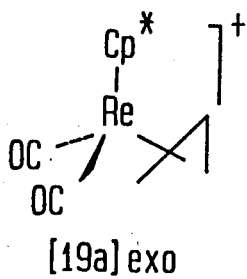


Table 16. Some Spectroscopic Parameters
of the Complexes [19]-[23]

Complex	IR $\nu(\text{CO}) \text{ cm}^{-1}$	$^1\text{H NMR}$ $\delta(\text{Cp}^*)^{\text{d}}$ ppm	MS(m/z) ^g M ⁺ ; base
[19a] <i>exo</i>	2038(s), 1977(s) ^a	2.16 ^e	419 ^h
[19b] <i>endo</i>	2051(s), 1997(s) ^a	2.17 ^e	419 ^h
[20b] <i>exo</i>	2045(s), 1990(s) ^b	2.13 ^e	489 ^h
[21a] <i>exo</i>	2024(s), 1963(s) ^b	2.12 ^e	459 ^h
[22]	1964(s), 1893(s) ^c	1.52 ^f	450 ; 348
[23]	1954(s), 1883(s) ^c	1.61 ^f	490 ; 400

Abbreviation: s = strong. ^ain CH₃NO₂; in CH₂Cl₂, there are only two broad absorptions at 2053, 1999 cm⁻¹ for [19](*exo*, *endo*). ^bin CH₂Cl₂. ^cin hexane. ^dCp* was a singlet peak in all cases. ^ein CD₂Cl₂. ^fin C₆D₆. ^gfor ¹⁸⁷Re. ^hcation (FAB, thioglycerol).

Table 17. Hydrogen-1 Chemical Shifts and Coupling Constants
for Ligands of Compounds [19]-[23]^a

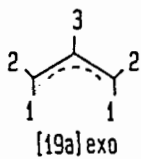
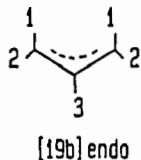
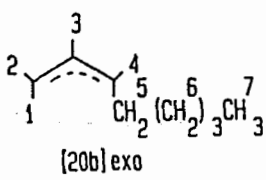
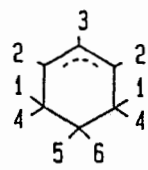
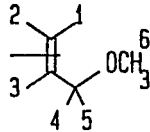
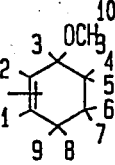
Ligand	Chem. Shifts δ (ppm) and Coupling Constants J (Hz)
 <p>[19a] exo</p>	^{a, c, d, e} H(1) 2.53(d, 2, $J_{1,3} = 10.9$); H(2) 3.29(d, 2, $J_{2,3} = 7.0$); H(3) 3.83(m, 1).
 <p>[19b] endo</p>	^{a, c, d, e} H(1) 1.77(d, 2, $J_{1,3} = 10.1$); H(2) 3.83(d, 2, $J_{2,3} = 6.7$); H(3) 4.76(m, 1).
 <p>[20b] exo</p>	^a H(1,5) 1.95-2.05(br m, 3); H(2) 3.72(d, 1, $J_{2,3} = 6.7$); H(3) 4.62(m, 1); H(4) 2.37(m, 1); H(6) 1.25-1.43(br m, 6); H(7) 0.92(t, 3, $J_{6,7} = 6.9$).
 <p>[21a] exo</p>	^{a, d} H(1) 2.47(m, 2, $J_{1,4} = 16.0$, $J_{1,5} = 12.0$, $J_{1,6} = 5.5$); H(2) 4.20(br s, 2); H(3) 3.89(br t, 1, $J_{2,3} = 6.0$); H(4) 2.00(m, 2); H(6) 1.44(m, 1). H(5) 0.42(m, 1, $J_{5,6} = 14.5$);

Table 17. (continued)

Ligand	Chem. Shifts δ (ppm) and Coupling Constants J (Hz)
[22]	^{b, d} H(1) 2.08(dd, 1, $J_{1,2} = 2.7$, $J_{1,3} = 10.5$, $J_{1,5} = 0.7$); H(2) 1.36(br d, 1, $J_{2,3} = 8.2$, $J_{2,5} = 1.2$); H(3) 2.05(m, 1); H(4) 2.97(t, 1, $J_{3,4} = 10.5$, $J_{4,5} = 10.5$); H(5) 4.30(dd, 1, $J_{3,5} = 3.7$); H(6) 3.25(s, 3).
	
[23]	^{b, d} H(1) 2.39(m, 1, $J_{1,8(9)} = 3.5$); H(2) 2.46(d, 1, $J_{1,2} = 9.3$); H(3) 4.56(t, 1, $J_{3,4} = 7.4$, $J_{3,5} = 6.3$); H(4,7) 1.39-1.49(br m, 2); H(5) 2.01(m, 1, $J_{4,5} = 12.6$, $J_{5,6} = 7.5$, $J_{5,7} = 2.5$); H(6) 1.27(m, 1, $J_{4,6} = 2.5$, $J_{6,7} = 12.8$); H(8,9) 2.81(m, 2); H(10) 3.42(s, 3).
	

Abbreviation: br = broad, d = doublet, dd = doublet of doublets, m = multiplet, s = singlet, and t = triplet. ^aThe samples were measured in CD_2Cl_2 at 400MHz. ^bThe samples were measured in C_6D_6 at 400MHz. ^cTwo isomers of *exo* and *endo* are present in a same sample (ratio: *exo/endo* = 1/6.4). ^dAs determined by decoupling experiments. ^eAs determined by NOE experiments.

4.3. Characterization

The η^3 -allyl cationic complexes ([19]-[21]) and the derivatives ([22], [23]) are air-stable, both in solution and as solids. They have been fully characterized by elemental analysis, IR, ^1H NMR and in two cases (for [19] and [21]), by X-ray structure determination. The complex [20] was identified only by spectroscopy, but too little sample was available to analyse further. The spectral data for these new complexes [19]-[23] are shown in Tables 16, 17.

The IR($\nu(\text{CO})$) data for the cationic complexes [19]-[21] show that alkyl substituents on the allyl act as electron-donor groups, so that the two $\nu(\text{CO})$ absorptions for [21] are at lower wave number compared with the IR of [19]. This IR change due to alkyl substituents on the allyl is similar to that in the case of the neutral η^3 -allyl complexes [15]-[17], see Chapter III. Also, the $\nu(\text{CO})$ absorptions of [19] are at lower wave number compared with its Cp analogue $[\text{CpRe}(\text{CO})_2(\eta^3\text{-allyl})][\text{BF}_4]$ (IR in CH_3NO_2 : 2047, 1982 cm^{-1} for *exo*; 2060, 2004 cm^{-1} for *endo*)^{67a} showing that the Cp^* is a better electron-donor than Cp.

The ^1H NMR spectra of these new cationic complexes show the presence of η^3 -allyl group, and some ^1H NMR spectra are shown in Figs. 44-46. The room temperature ^1H NMR spectrum of [19] in CD_2Cl_2 at 400 MHz clearly shows separate methyl and allyl resonances for

Fig.42. View of the cationic complex in $[\text{Cp}^*\text{Re}(\text{CO})_2(\eta^3\text{-C}_3\text{H}_5)]^+[\text{BF}_4]^-$ [19] with atom numbering. Note the disorder of the allyl group (superposition of *endo* and *exo* isomers in ratio *endo* : *exo* 4:6).

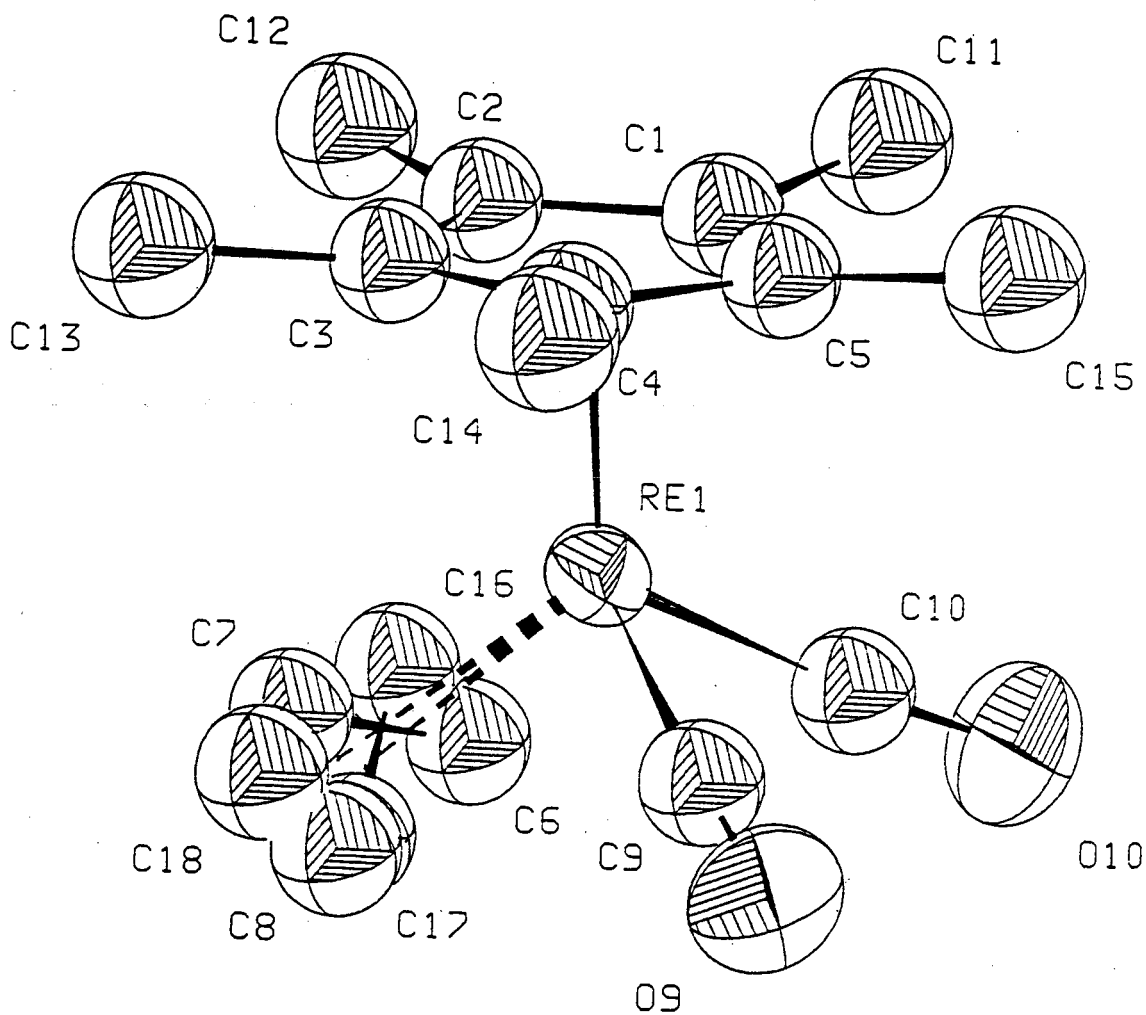
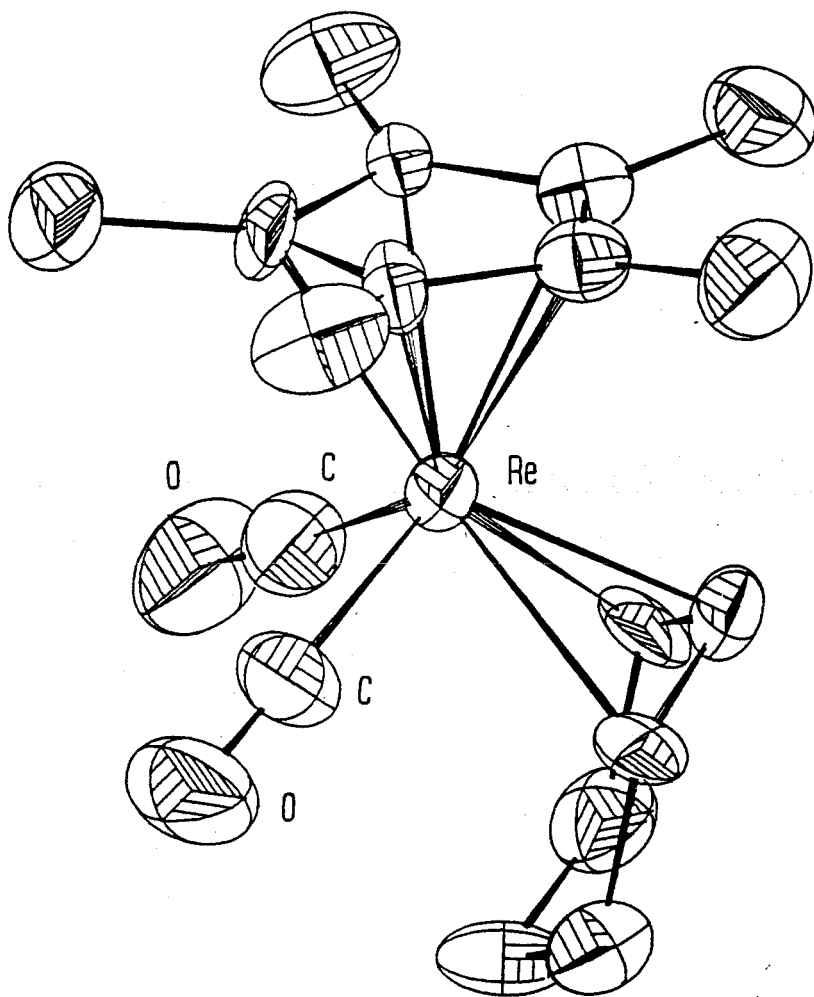
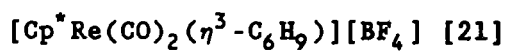


Fig.43. Perspective view of the complex



two isomers in an approximate ratio of 6.4:1 (Fig.44). These correspond to the *endo* and *exo* isomers respectively. The resonances that are identified with each isomer were determined by application of the nuclear Overhauser effect (see Section 4.5.1). Magnetization transfer results show that *exo-endo* interconversion occurs with no scrambling of *syn* and *anti* protons, consistent with a pseudorotation mechanism but not a $\eta^3-\eta^1-\eta^3$ mechanism. The two isomers cannot be further separated due to the very fast isomerization even at low temperature (-60°C).

The crystal structures of the complexes [19] and [21] were determined by X-ray crystallography, kindly carried out by Dr. R.J. Batchelor and Dr. R.H. Jones in Professor F.W.B. Einstein's laboratory at S.F.U.

The structure of the cation of [19] is illustrated in Fig.42. The most evident feature is the disorder of the allyl group, showing that the crystals are composed of both *exo* and *endo* isomers. The final occupancies of the two sites give the approximate distribution of the isomers to be 6:4 - *exo:endo*. In most of the other cases where *exo* and *endo* isomers have been evident in solution, only one of the isomers crystallizes and the equilibrium readjusts the concentrations of the two isomers as crystallization proceeds. For example, $\text{CpMo}(\text{CO})_2(\eta^3\text{-C}_3\text{H}_5)^{66f}$ and $\text{Cp}^*\text{W}(\text{CO})_2(\eta^3\text{-C}_3\text{H}_5)^{78}$ have both been structurally analyzed as the *exo* isomers.

Only in very rare cases is it possible to isolate, crystallize and determine the structure of both the *exo* and *endo* isomers of an allyl complex. Where the interconversion is either sufficiently slow or non-existent, isomers may be separated by chromatography or fractional crystallization.^{63,66(i,k)} This has been achieved with $\text{Cp}^*\text{Re}(\text{CO})(\text{H})(\eta^3\text{-C}_3\text{H}_5)$ [15], the η^3 -2-methylallyl ruthenium complex $\text{CpRu}(\text{CO})(\eta^3\text{-C}_4\text{H}_7)^{66\text{h}}$ and the cationic complex $[\text{CpMo}(\text{CO})(\text{NO})(\eta^3\text{-CH}(\text{Ph})\text{CHCH}_2)]^+$.^{66k} Despite numerous other structure determinations of *exo* and *endo* allyl isomers (many of these are cited in references 66) we know of no previous case where both isomers have occurred in a disordered structure. Unfortunately, the presence of the disorder means that the allyl carbon positions are not determined with sufficient accuracy to permit a detailed discussion of the metrical details.

The configuration of the complex [21], involving a cyclic symmetrical *exo* η^3 -allyl structure, was also confirmed by an X-ray structure determination, and is illustrated in Fig.43.

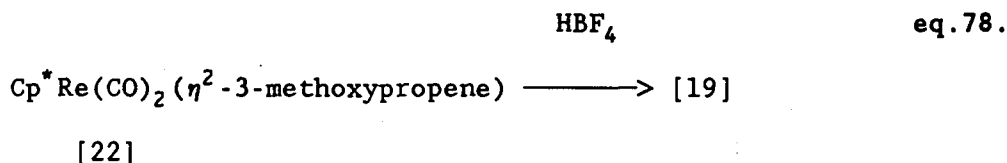
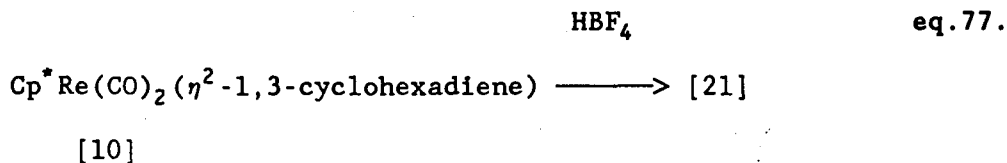
The cationic complexes [19]-[21] were further characterized by the positive ion fast atom bombardment spectra which indicated the molecular mass of the cation in each case.

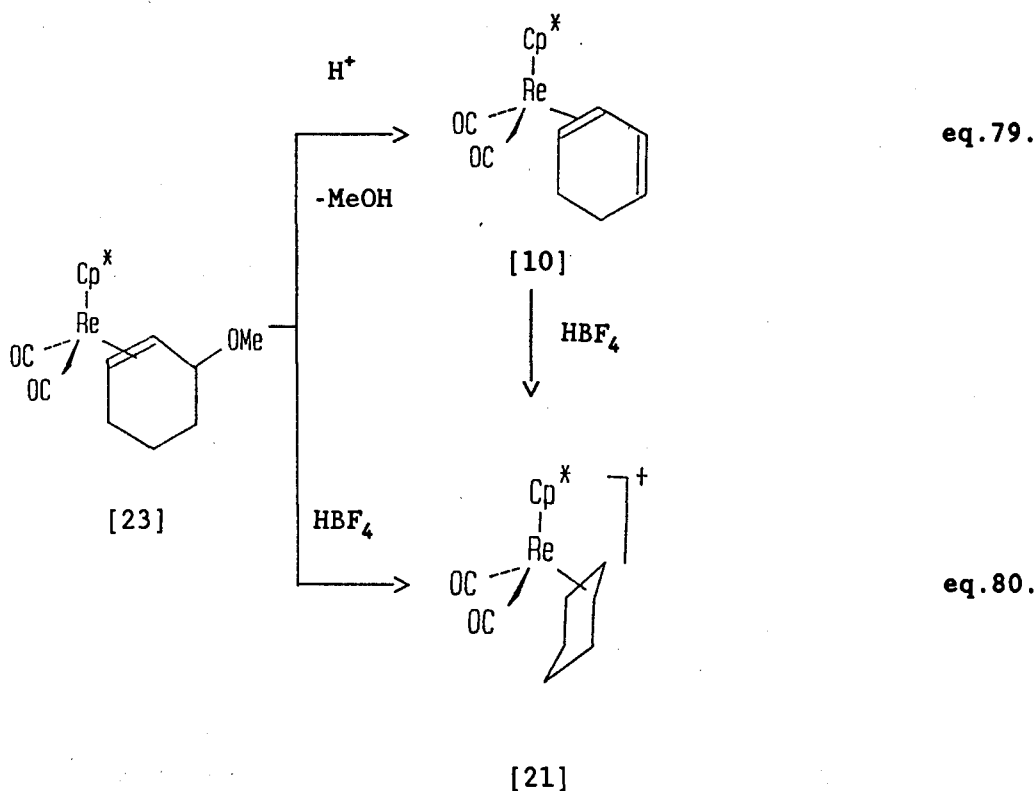
The spectral properties of the two derivatives [22] and [23] are completely consistent with their expected structures. In each case, the IR spectrum shows two strong absorptions corresponding to the dicarbonyl vibrations. The ^1H NMR spectrum

shows the presence of an η^2 -methoxyalkene ligand with no unusual features (Figs. 47, 48). However, the electron-impact mass spectra (Figs. 17(q, r), p.71) show an interesting feature. The molecular ionic fragments of [22] and [23] lose the methoxy (or methanol) group at an early stage of the fragmentation (see Chapter II, Section 2.5.2 for further details), indicating a weak allylic C-OMe bond. This is consistent with the results of chemical reactions (eqs.78-79).

4.4. Chemical Reactions

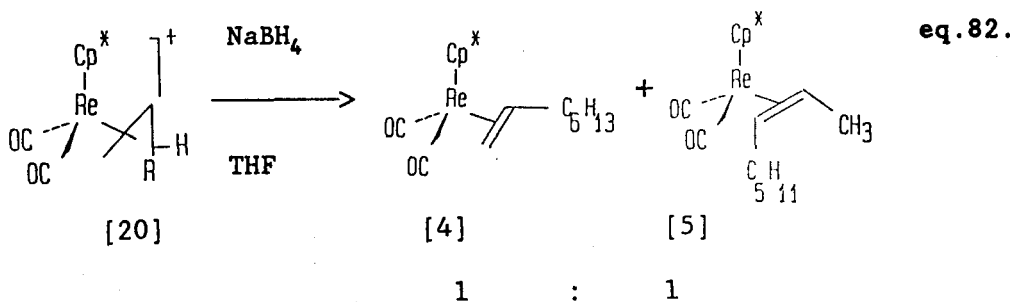
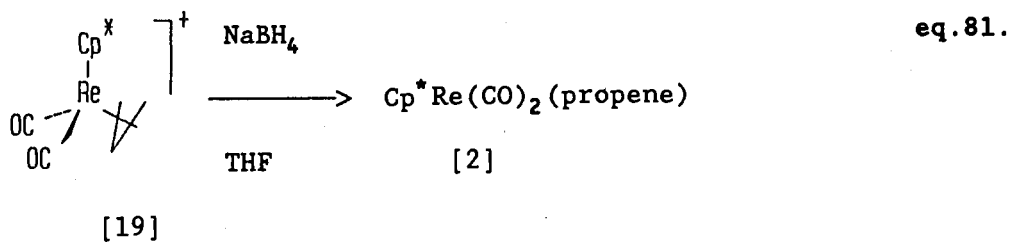
The rhenium η^3 -allyl cationic complexes [19] and [21] can also be formed in the other reactions shown in eqs.77, 78 and 80. These reaction mechanisms are possibly similar to those of the published synthetic routes,^{67a} which presumably involve the protonation of the conjugated diene complexes, or the dehydration of the allylic alcohol complexes, under UV light.^{67a}





(i) Treatment of the η^2 -diene complexes (η^2 -1,3-cyclohexadiene [10] or η^2 -1,4-cyclohexadiene [11]) with HBF₄ in THF at room temperature readily yields the expected η^3 -allyl cationic complex [21] (eq.77).

(ii) The allylic methoxy group is readily removed from the parent ligand in the presence of strong protonic acid to form the corresponding cationic complex (eqs.78, 80). In the second of these two examples, whilst a trace strong protonic acid was present, the η^2 -1,3-cyclohexadiene [10] was formed first, reacting further with the excess HBF₄ to produce the cationic complex [21] (eqs.79-80).

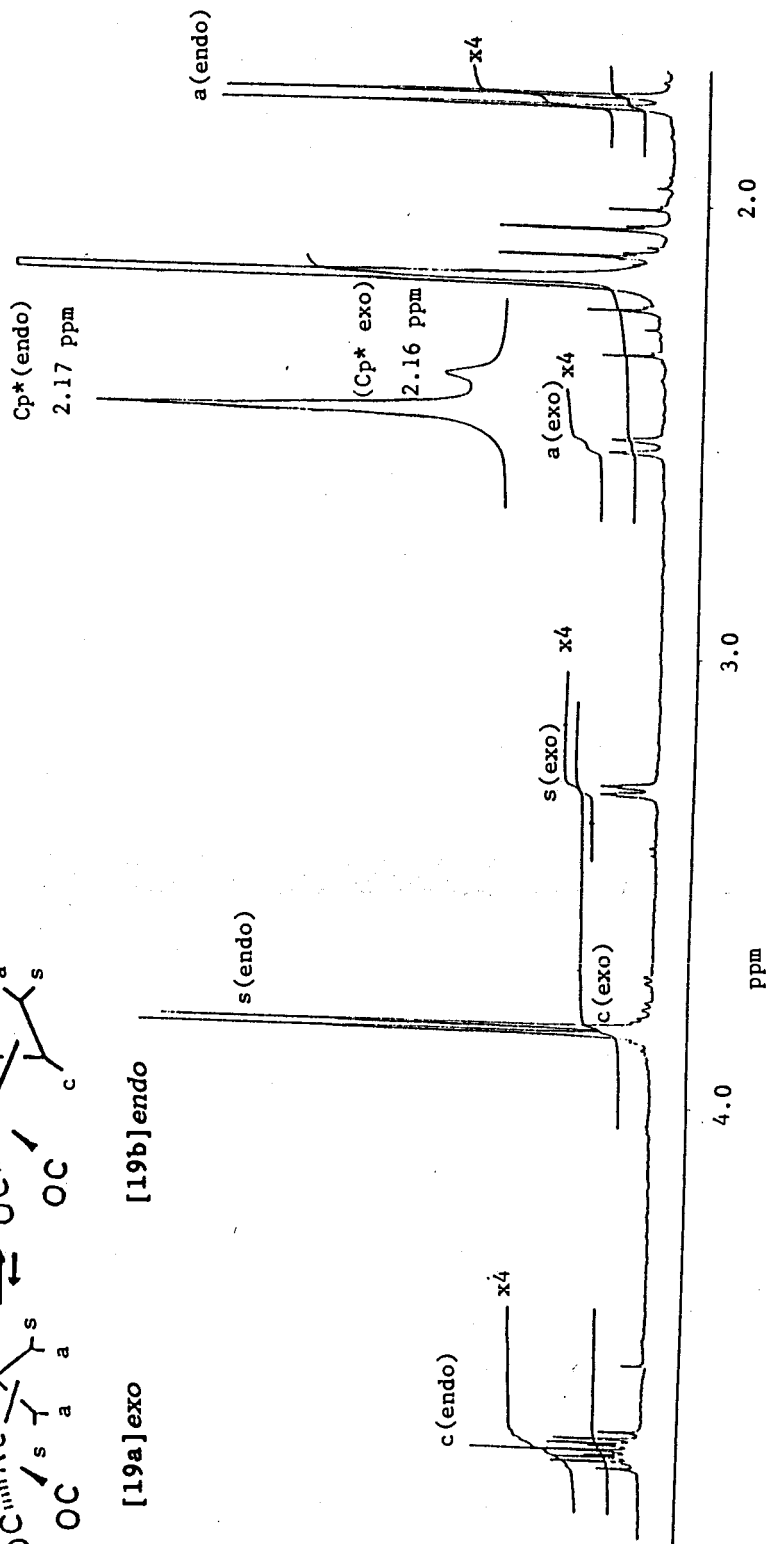
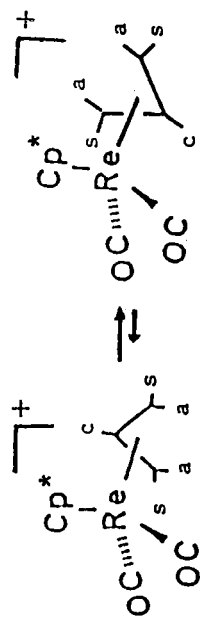


The reactions shown by eqs. 75-76 and 81-82 have been studied to give the following information on the chemical behaviour of the cationic complexes [19]-[21].

(iii) The cationic complexes [19]-[21] react with nucleophilic agents (H^- , MeO^-) in THF at room temperature to undergo preferential attack at the allyl terminus to form the corresponding nucleophilic addition products ([2], [4], [5], [22] and [23]). No product corresponding to attack at the allyl centre or carbonyl was observed. This can be attributed to the positive charge on the allyl terminus.

(iv) Eq. 82 shows that hydride attacks at the allyl terminus without selectivity. Two products [4] and [5] were produced in an approximate ratio of 1:1 as a result. Based on the determination of

Fig. 44. ^1H NMR Spectrum



400MHz ^1H NMR (CD_2Cl_2)

Fig. 45. ^1H NMR Spectrum

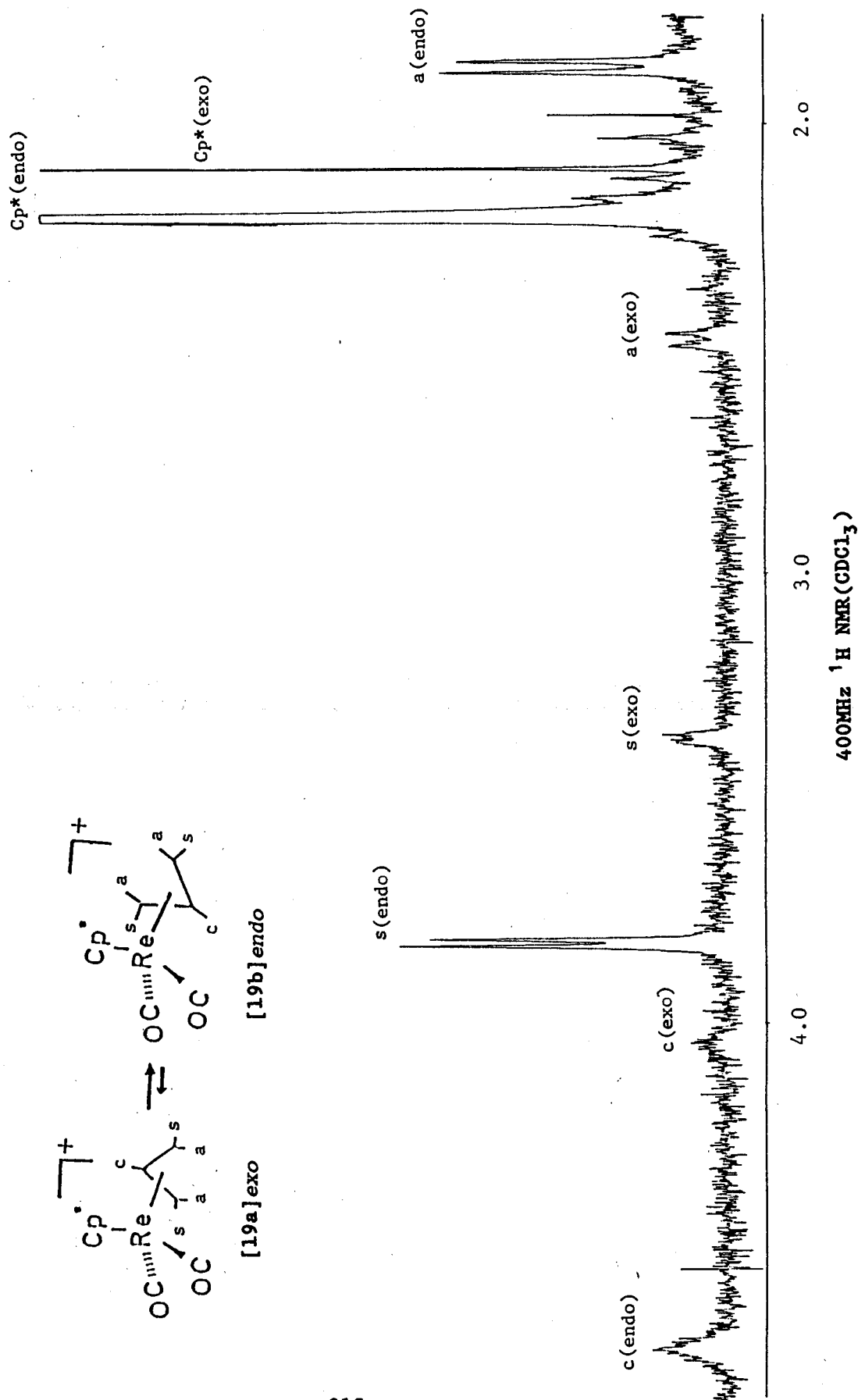


Fig. 46. ^1H NMR Spectrum

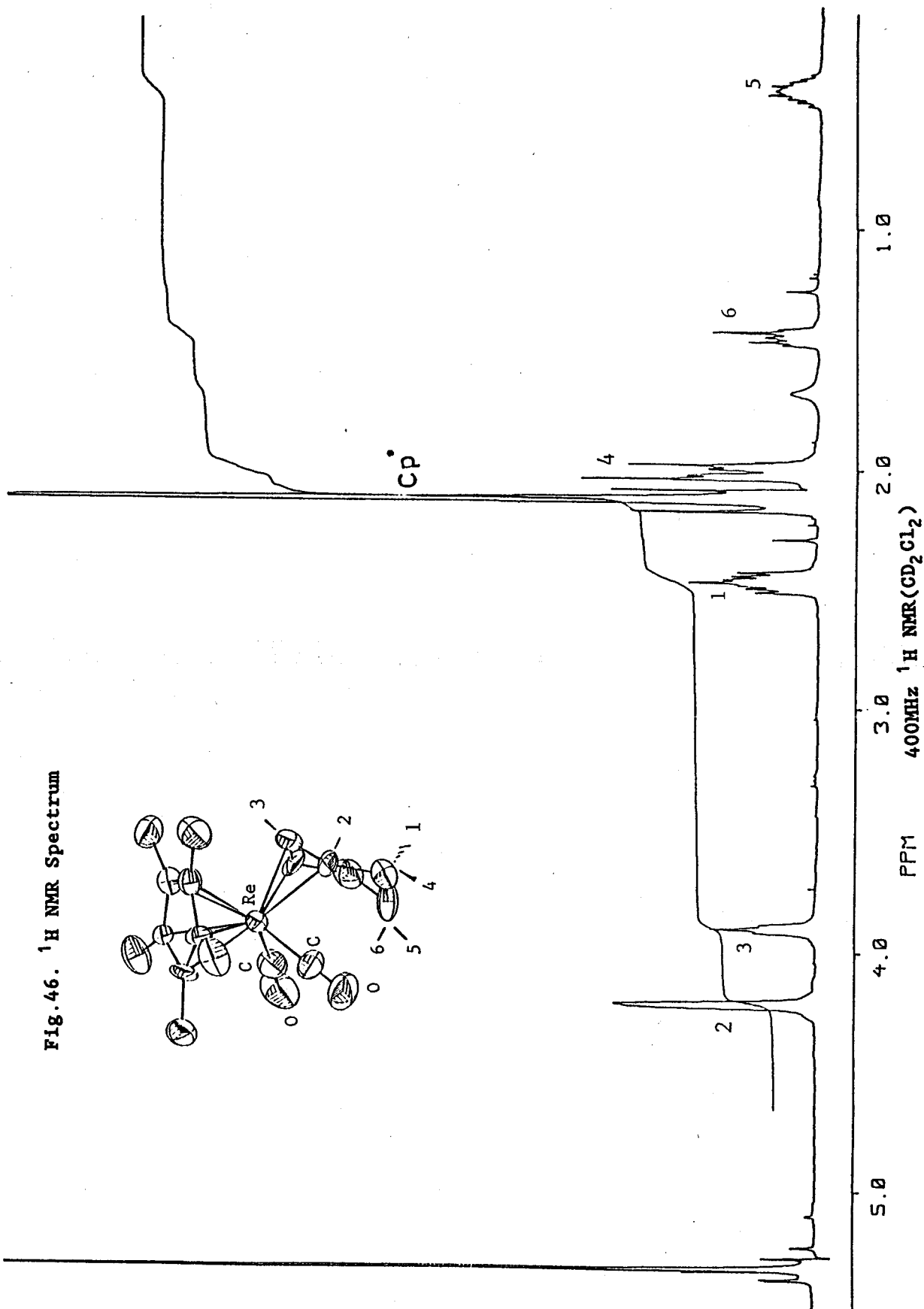
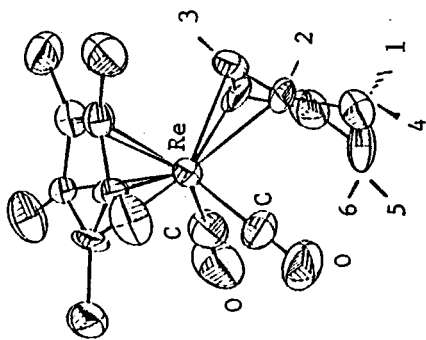
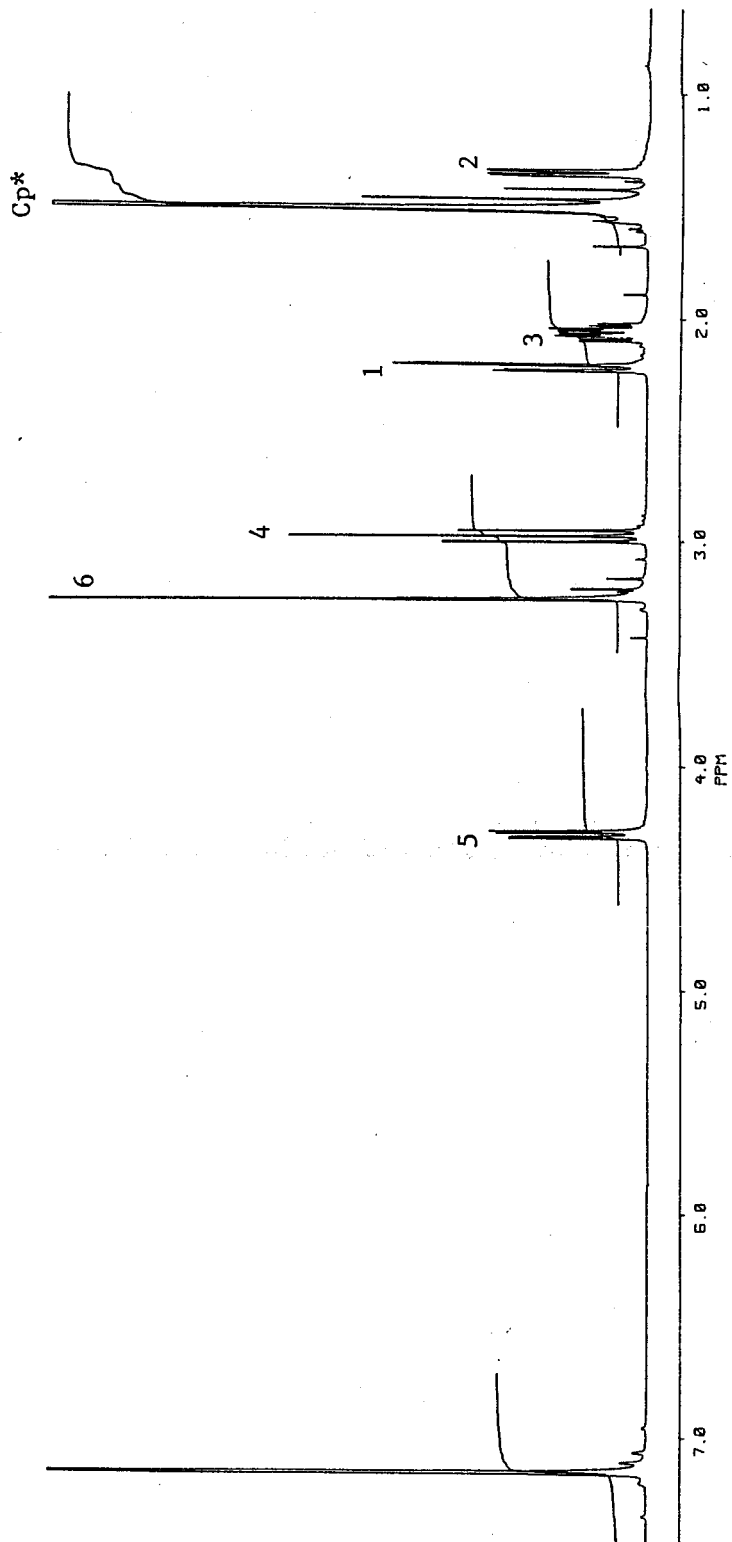
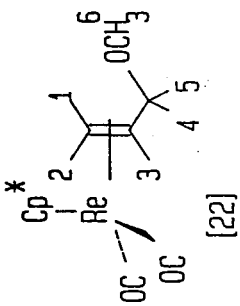
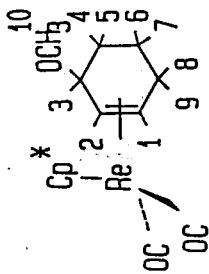


Fig. 47. ^1H NMR Spectrum

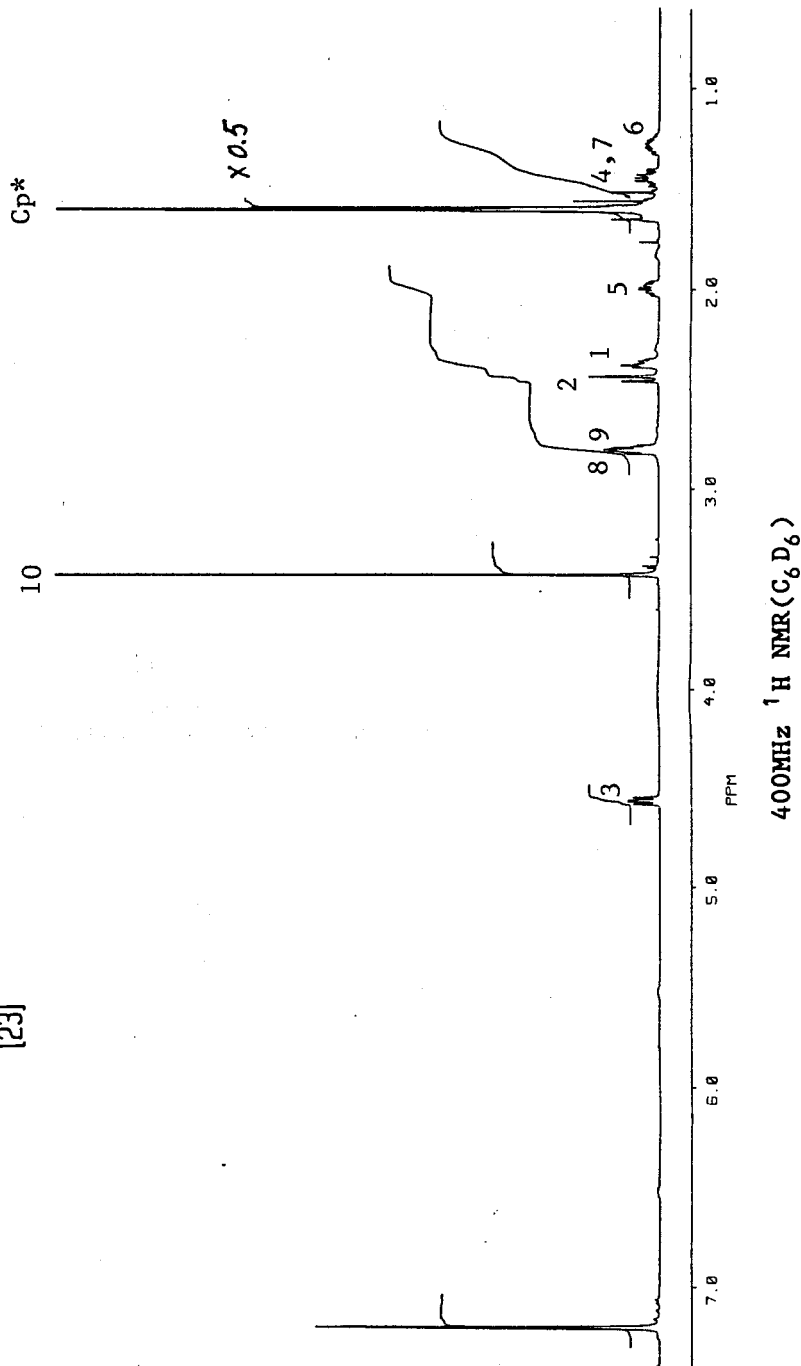


400MHz ^1H NMR(C_6D_6)

Fig. 48. ^1H NMR Spectrum



[23]



the configuration of [5] as the η^2 -*cis*-2-octene by decoupling experiments (see Chapter II), the allylalkane configuration of the cationic complex [20] was thus assigned as the *anti*-substituted one.

(v) Eq.76 offers a convenient route for the synthesis of complex [23]. However, the η^2 -1,3-cyclohexadiene complex [10] was always formed as a by-product in the reaction. The formation of [10] in eq.76 could be minimized by performing the reaction at -78°C .

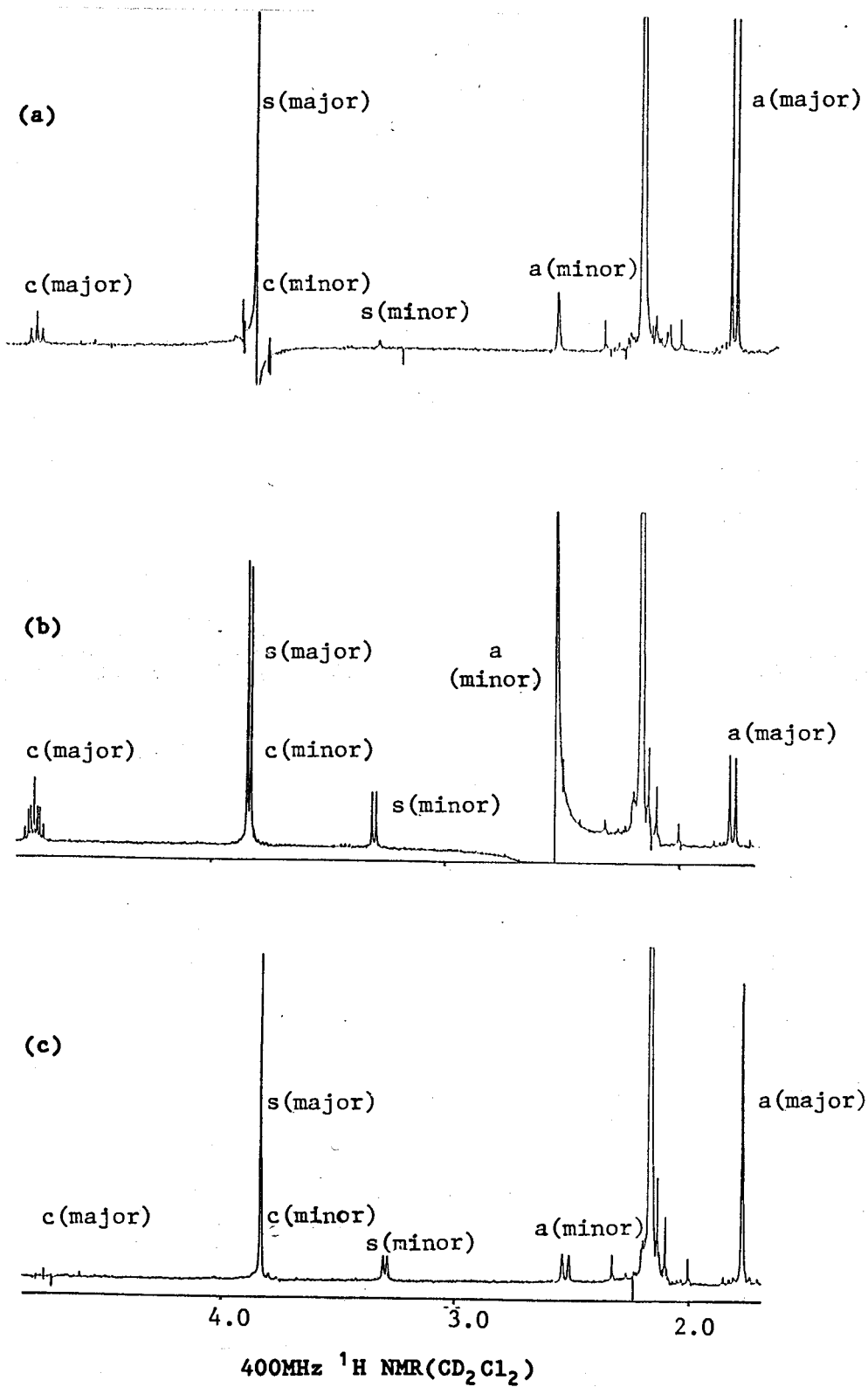
4.5. Discussion

4.5.1. ^1H NMR Spectra

(1) $[\text{Cp}^*\text{Re}(\text{CO})_2(\eta^3\text{-C}_3\text{H}_5)][\text{BF}_4]$ [19]

The room temperature 400MHz ^1H NMR spectrum of [19] (in CD_2Cl_2) exhibits methyl and AMM'XX' allyl resonances for two isomers in approximate ratio 6.4:1 (Fig.44 and Table 17). For the major isomer the multiplet at δ 4.76 is assigned to H_c , and the doublets at δ 3.83 and δ 1.77 are assigned to the *syn* and *anti* protons H_s and H_a respectively. This assignment is in accord with those established for allyl ligands in symmetrical environments, and with the greater separation of the doublet in H_a arising from the larger coupling constant $J_{c,a}$ compared with $J_{c,s}$. For the minor isomer, the

Fig. 49(a-c). Decoupling Experiments on [19]



resonances for H_a and H_s are clearly visible, but the H_c resonance is buried under the H_s signal of the major isomer. This is established by decoupling experiments, by integration, and by the results of saturation transfer experiments. In addition, the 1H NMR spectrum of [19] (Fig.45) in $CDCl_3$ clearly showed that H_c (minor) is at δ 4.06 which is separated from H_s (major) at δ 3.82, although the signal intensities of resonances are weaker due to the poor solubility of [19] in $CDCl_3$.

From the decoupling experiments shown in Figs. 49(a-c), the following observations were obtained:

(a) Irradiation of H_c (minor) and H_s (major) together caused the resonance for H_a (minor) to collapse to a singlet, the resonance for H_c (major) to collapse to a triplet, with a coupling $J_{a,c(major)} = 10.1$ Hz and the resonance for H_s (minor) to collapse to a singlet with a decreased intensity because of the very fast exo-endo exchange causing a magnetization transfer from H_s (major) to H_s (minor) (Fig.49(a)).

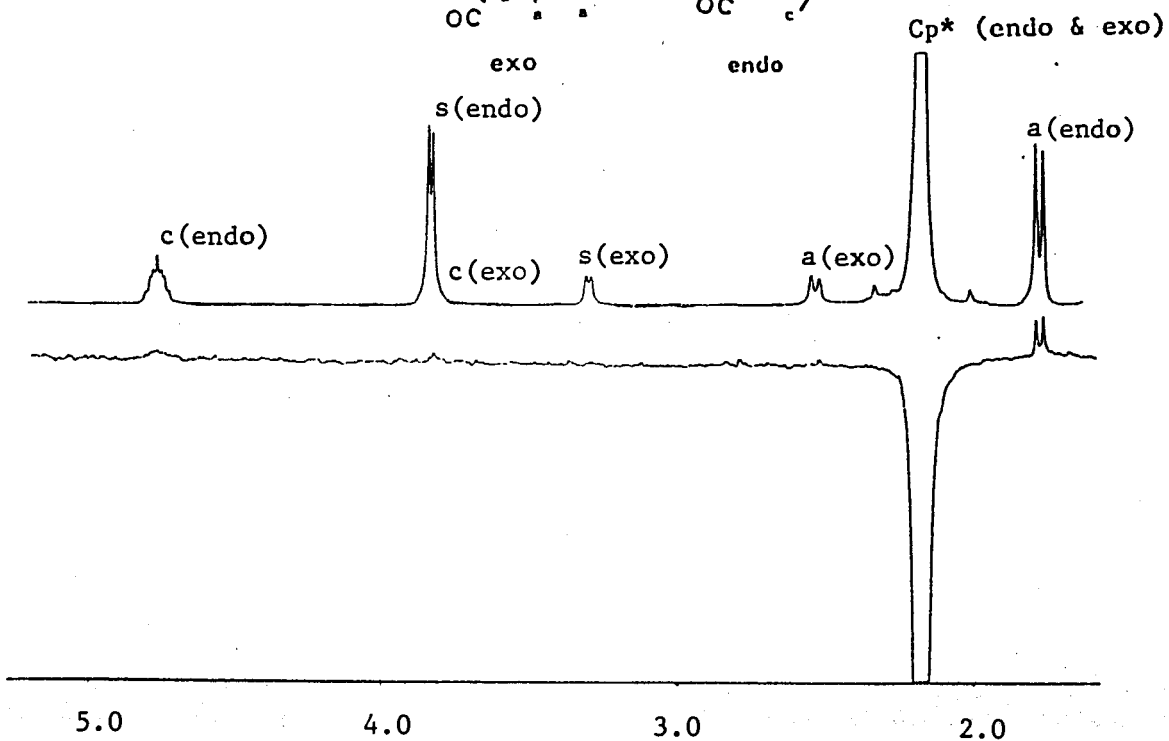
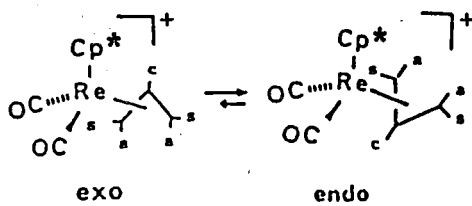
(b) Irradiation of H_a (minor) resulted in a doublet H_a (major) with a decreased intensity due to the magnetization transfer from H_a (minor) to H_a (major) (Fig.49(b)).

(c) Irradiation of H_c (major) caused the two resonances for H_a (major) and H_s (minor) to collapse to singlets (Fig.49(c)).

The observation (a) shows that the H_c (minor) signal is buried under the H_s (major) signal in CD_2Cl_2 .

Fig.50(a-c). NOE Experiments on [19]

(a)



(b)

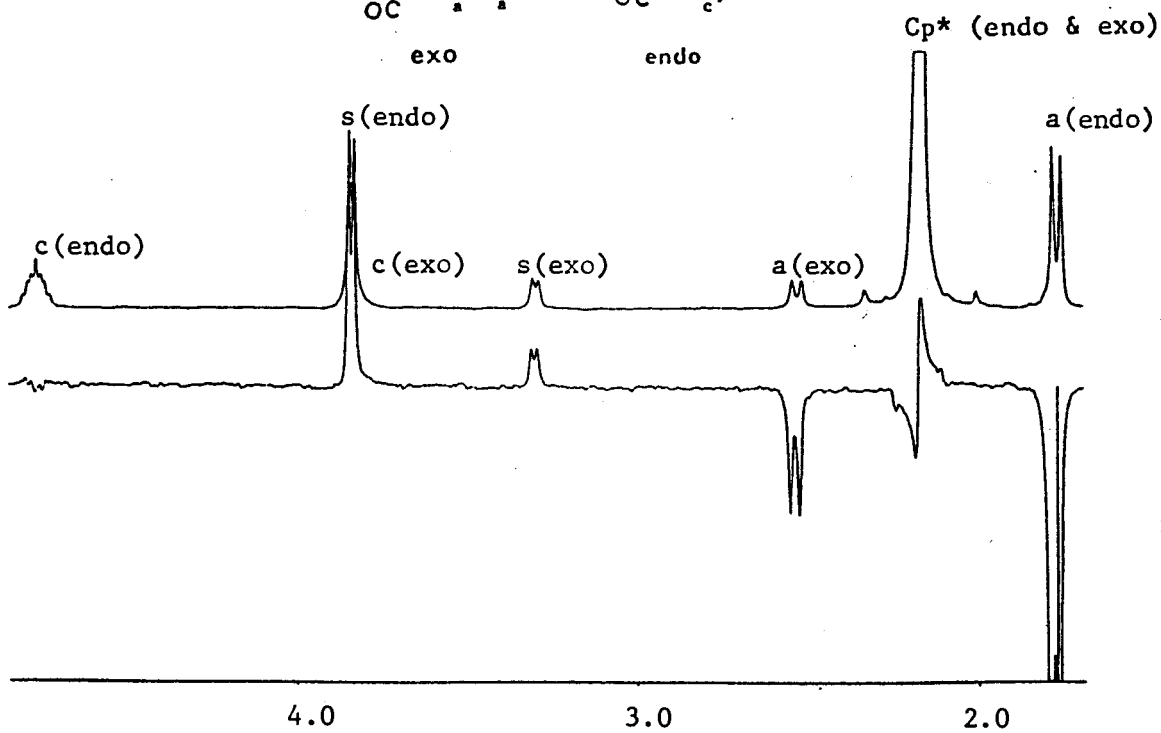
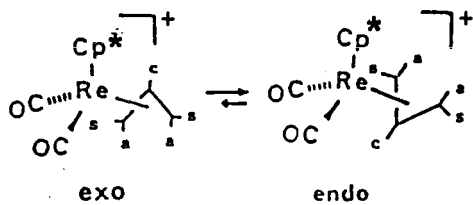
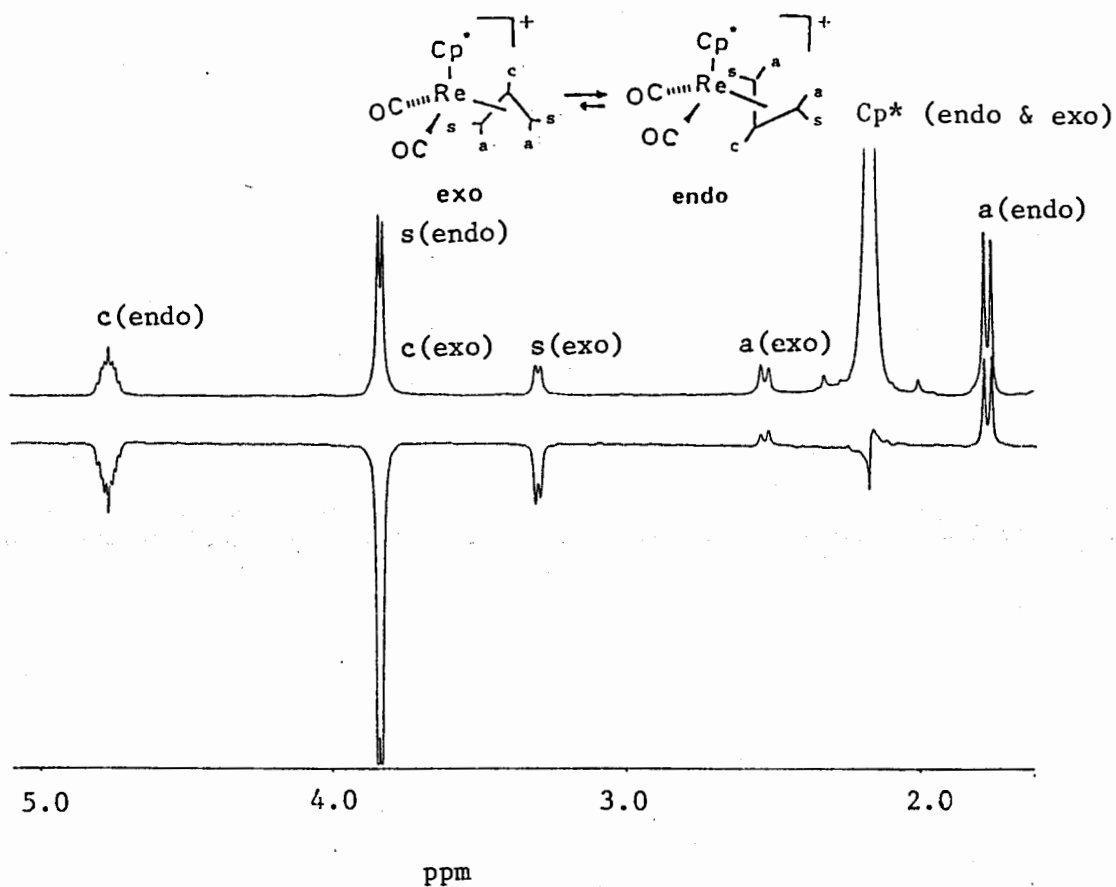


Fig. 50(c).



400MHz ^1H NMR(CD_2Cl_2) at r.t.

The major isomer is assigned as the *endo* isomer from the results of nuclear Overhauser enhancement (NOE) studies. Saturation of the Cp* methyl resonances results in a strong NOE at the δ 1.77 (H_a) signal for the major isomer (Fig.50(a)). In the absence of exchange this would unquestionably establish that this resonance arises from the *endo* isomer since in the *exo* isomer the *anti* protons are remote from the Cp* methyls. However, exchange between *exo* and *endo* isomers is indeed occurring as is evident, for example, from Fig.50(b), where saturation of this resonance results in transfer of magnetization to the signal at δ 2.53, assigned as H_a of the minor isomer. But this does not invalidate the result.

Let us, for the moment, consider the other alternative, that the signal at δ 1.77 is the *anti* resonance of a major *exo* isomer. Enhancement of this resonance cannot arise directly by an NOE from the *exo* isomer's methyls. Could it arise from exchange with the *anti* protons a minor *endo* isomer, which clearly would experience an NOE from the *endo* isomer's methyls? If that were so an enhancement of the *endo* isomer's *anti* protons at δ 2.53 should also be observed and should be relatively as large or larger than the enhancement at δ 1.77 to allow for NOE buildup at this latter position.⁷⁹ No detectable enhancement is observed at δ 2.53 position in Fig.50(a), even though the rate of exchange is clearly significant as judged from the observed saturation transfer in Fig.50(b). On this basis we rule out the second possibility.

Irradiation of the Cp* methyls should also give a NOE to H_c in the minor exo isomer; in agreement a weak but detectable enhancement is observed together with a similarly weak enhancement of H_c(endo) because of exchange. The results of irradiating H_a(endo), Fig.50(b), demonstrate that no syn-anti exchange occurs. There is the expected strong NOE to the endo syn protons, H_s, and a corresponding enhancement of H_s(exo) is also observed because of exchange. However, no transfer of saturation from H_a(endo) to H_s(endo or exo) signals occurs. Comparable results were obtained on irradiating H_s(endo or exo), or H_a(exo). Irradiation at H_s(endo) necessarily results in saturation of H_c(exo) also if, as is proposed, these are coincident. In agreement, a strong inverted signal at H_c(endo) resulted (Fig.50(c)) because saturation is transferred from H_c(exo) to H_c(endo) so confirming the assignment of H_c(exo) to this position. Also, there is a strong NOE from H_s(endo) to H_a(endo) and a magnetization transfer from H_a(endo) to H_a(exo). Transfer of saturation from H_s(endo) to H_s(exo) means that an inverted signal is observed due to fast exo-endo exchange (Fig.50(c)).

The saturation transfer results indicate that the exo-endo interconversion in [19] proceeds by pseudorotation of the allyl group since this mechanism does not scramble the syn and anti protons. Similar exo and endo isomers that also appear to

interconvert by this mechanism are $\text{CpM}(\text{CO})_2(\eta^3\text{-C}_3\text{H}_5)$ ($\text{M} = \text{Mo}, \text{W}$)⁶⁵ and the cations $[\text{CpM}(\text{CO})_2(\eta^3\text{-allyl})]^+$ ($\text{M} = \text{Mn}, \text{Re}$).^{67a} For the neutral Mo and W complexes, the predominant isomer in the mixture is the *exo* form, which becomes destabilized in the methylallyl analogue.⁶⁵ Evidently, the *exo* isomer also predominates in the cationic Mn complex, though the two reports of this compound differ in the resolution achieved between individual resonances for the isomers.⁶⁷ However, the cationic rhenium complex was observed to be predominantly the *endo* isomer^{67a} and we arrive at the same conclusion for the pentamethylcyclopentadienyl analogue [19] here.

One final point about the NMR spectrum of [19] should be made, which is with regard to the relative positions of the resonances for the *exo* and *endo* isomers. These are listed in Table 18 along with literature values for related compounds. Hitherto, for cyclopentadienyl complexes, an empirical generalization has been that the H_a protons of the *exo* isomer resonate most upfield.^{65b} This is not the case for the pentamethylcyclopentadienyl complex [19], where H_a of the *endo* isomer is the most upfield resonance. Unfortunately, the only other pentamethylcyclopentadienyl allyl complex to have been studied, $\text{Cp}^*\text{W}(\text{CO})_2(\eta^3\text{-C}_3\text{H}_5)$, evidently only gave an averaged spectrum in the temperature range examined.⁷⁸

Table 18. ^1H NMR Parameters for $[\text{Cp}^*\text{Re}(\text{CO})_2(\eta^3\text{-C}_3\text{H}_5)][\text{BF}_4]$ [19] and Related Allyl Complexes

Compound	Isomer	$^1\text{H NMR}^a$ (δ)			Solvent	Reference
		H_c	H_s^b	H_a^c		
$[\text{Cp}^*\text{Re}(\text{CO})_2(\eta^3\text{-C}_3\text{H}_5)][\text{BF}_4]$ [19]	endo	4.76m	3.83d[6.7]	1.77d[10.1]	CD_2Cl_2^d	This work
$[\text{Cp}^*\text{Re}(\text{CO})_2(\eta^3\text{-C}_3\text{H}_5)][\text{BF}_4]$ [19]	exo	3.83m	3.29d[7.0]	2.53d[10.9]	CD_2Cl_2^d	This work
$[\text{CpRe}(\text{CO})_2(\eta^3\text{-C}_3\text{H}_5)][\text{BF}_4]$	endo	4.960tt	3.843d[6.1]	3.466d[10.4]	$(\text{CD}_3)_2\text{CO}^e$	67a
$[\text{CpRe}(\text{CO})_2(\eta^3\text{-C}_3\text{H}_5)][\text{BF}_4]$	exo	5.328tt	4.140d[7.0]	2.715d[10.7]	$(\text{CD}_3)_2\text{CO}^e$	67a
$[\text{CpMn}(\text{CO})_2(\eta^3\text{-C}_3\text{H}_5)][\text{BF}_4]$	endo	5.886s	4.736d[6.9]	3.656d[11.2]	$(\text{CD}_3)_2\text{CO}^e$	67a
$[\text{CpMn}(\text{CO})_2(\eta^3\text{-C}_3\text{H}_5)][\text{BF}_4]$	exo	5.840s	4.503d[7.0]	2.416d[11.4]	$(\text{CD}_3)_2\text{CO}^e$	67a
$\text{CpMo}(\text{CO})_2(\eta^3\text{-C}_3\text{H}_5)$	endo	5.10s	2.72d[6.4]	1.76d[10.5]	CDCl_3^g	65
$\text{CpMo}(\text{CO})_2(\eta^3\text{-C}_3\text{H}_5)$	exo	5.10s	2.78d[7.3]	0.88d[10.8]	CDCl_3^g	65
$\text{CpW}(\text{CO})_2(\eta^3\text{-C}_3\text{H}_5)$	endo	5.22s	2.70d[5.6]	1.64d[9.5]	CDCl_3^g	65
$\text{CpW}(\text{CO})_2(\eta^3\text{-C}_3\text{H}_5)$	exo	5.25s	2.73d[6.9]	1.07d[10.4]	CDCl_3^g	65
$\text{CpRu}(\text{CO})_2(\eta^3\text{-C}_3\text{H}_5)$	endo	5.17s	3.03d[6.3]	1.80d[11.0]	CDCl_3^f	76
$\text{CpRu}(\text{CO})_2(\eta^3\text{-C}_3\text{H}_5)$	exo	5.04s	2.92dt[6.9]	1.28dt[10.6]	CDCl_3^f	76

^a Chemical shifts are given in ppm downfield from TMS; Hc, Hs and Ha are the central, syn and anti protons of C_3H_5 ; s, singlet; d, doublet; t, triplet; m, multiplet. All coupling constants are absolute values.

^b J_{HcHs} in brackets.

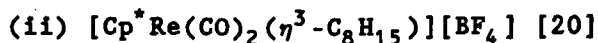
^c J_{HcHa} in brackets.

^d recorded at 400 MHz.

^e recorded at 200 MHz.

^f recorded at 90 MHz.

^g recorded at 100 MHz.



Firstly, the position of the alkyl substituent on the allyl in [20] was assigned to be *anti* to the central proton H(3). This was established by the results of the nucleophilic addition of H^- to the allyl terminus which resulted in the formation of the *cis*-2-octene complex [5] in addition to [4]. Then, the conformation of the allyl group was assigned to be *exo* for steric reasons (obviously, the hindrance of the *anti* alkyl substituent would be much larger in the *endo* conformation). Based on the above assumptions, the proton resonances of [20] were assigned as following. The multiplet at δ 4.62, with a relative intensity one, was assigned to the central proton H(3). The doublet at δ 3.72, with a relative intensity one and a coupling ($J_{2,3} = 6.7$), was assigned to the *syn* proton H(2). The multiplet at δ 2.37, with a relative intensity one, was assigned to the *syn* proton H(4). The broad multiplet at δ 1.95-2.05, with a relative intensity three, was assigned to the *anti* proton H(1) and the methylene protons H(5). The broad multiplet at 1.25-1.43, with a relative intensity six, was assigned to the methylene protons H(6). The triplet at δ 0.92, with a relative intensity three and a coupling ($J_{6,7} = 6.9$), was assigned to the three equivalent methyl protons H(7).

(iii) $[\text{Cp}^*\text{Re}(\text{CO})_2(\eta^3\text{-C}_6\text{H}_9)][\text{BF}_4]$ [21]

The assignments for the complex [21] were determined by decoupling experiments. The broad triplet at δ 3.89, with a relative intensity one and a coupling ($J_{2,3} = 6.0$), was assigned to the central proton H(3) and collapsed to a singlet when irradiating H(2). The broad singlet at δ 4.20, with a relative intensity two, was assigned to the syn protons H(2), as it collapsed to a broad doublet with a coupling ($J_{2,3} = 6.0$) while irradiating H(4). The multiplet at δ 2.47, with a relative intensity two, was assigned to H(1). The multiplet at 2.00, with a relative intensity two, was assigned to H(4). Irradiating H(4) caused the resonance for H(6) to collapse to a doublet of triplets with coupling ($J_{1,6} = 5.5$, $J_{5,6} = 14.5$), and the resonance for H(5) to collapse to a doublet of triplets with couplings ($J_{5,6} = 14.5$, $J_{1,5} = 12.0$). The multiplet at δ 0.42, with a relative intensity one, was assigned to H(5). The multiplet at δ 1.44, with a relative intensity one was assigned to H(6), as this collapsed to a doublet with a coupling ($J_{5,6} = 14.5$) when irradiating H(1). Irradiating H(6) caused the resonance for H(1) to result in a broad doublet of triplets with couplings ($J_{1,4} = 16$, $J_{1,5} = 12.0$).

(iv) $\text{Cp}^*\text{Re}(\text{CO})_2(\eta^2\text{-C}_3\text{H}_5\text{OCH}_3)$ [22]

The resonances for the complex [22] were readily assigned by comparison with those for the propene complex [2], and by chemical shifts, coupling constants and the proton relative intensity (see Table 17). The assignments for the complex [22] were also consistent with the results of decoupling experiments. Irradiating H(1) caused the resonance for H(2) to collapse to a doublet with a coupling ($J_{2,3} = 8.2$). Irradiating H(2) resulted in the resonance for H(1) to collapse to a doublet with a coupling ($J_{1,3} = 10.5$), and the resonance for H(5) to collapse to a doublet of doublets with couplings ($J_{3,5} = 3.5$, $J_{4,5} = 10.5$). Irradiating H(3) resulted in the resonances for H(4) and H(5) collapsing to a broad doublet and a doublet ($J_{4,5} = 10.5$), respectively. Irradiating H(5) caused the resonance for H(4) to collapse to a doublet with a coupling $J_{3,4} = 10.5$.

(v) $\text{Cp}^*\text{Re}(\text{CO})_2(\eta^2\text{-C}_6\text{H}_9\text{OCH}_3)$ [23]

The assignments for the complex [23] were determined by decoupling experiments. The multiplet at δ 2.39, with a relative intensity one, was assigned to H(1). The doublet at δ 2.46, with a relative intensity one and a coupling ($J_{1,2} = 9.3$), was assigned to H(2). The broad triplet at δ 4.56, with a relative intensity one,

was assigned to H(3). The broad multiplet at δ 1.39-1.49, with a relative intensity two, was assigned to H(4,7). The multiplets at δ 2.01 and 1.27, with a relative intensity one each, were assigned to H(5) and H(6) respectively. The multiplet at δ 2.81, with a relative intensity two, was assigned to H(8,9).

Irradiating H(1) and H(2) together caused the resonance for H(3) to appear as a doublet of doublets with couplings ($J_{3,4} = 7.4$, $J_{3,5} = 6.3$). Irradiating H(3) resulted in the resonance for H(1) becoming a doublet of triplets with couplings ($J_{1,2} = 9.3$, $J_{1,8(9)} = 3.5$), and the resonance for H(5) appeared as a doublet of doublets of doublets with couplings ($J_{4,5} = 12.6$, $J_{5,6} = 7.5$, $J_{5,7} = 2.5$). Irradiating H(5) resulted in the resonance for H(3) collapsing to a doublet with a coupling ($J_{3,4} = 7.4$). Irradiating H(6) caused the resonances for H(8,9) to collapse to a broad singlet. Irradiating H(8,9) resulted in the resonance for H(1) appearing as a doublet with a coupling ($J_{1,2} = 9.3$), and the resonance for H(6) becoming a doublet of triplets with couplings ($J_{4,6} = 2.5$, $J_{6,7} = 12.8$).

4.5.2. Syntheses and Reactions

Treatment of η^2 -olefin complexes [2], [4] and [6] with $[\text{Ph}_3\text{C}][\text{BF}_4]$ yielded the corresponding η^3 -allyl cationic complexes [19]-[21] (eq.73). The ^1H NMR of [19] showed the presence of two isomers with a ratio of 6.4/1 = *endo/exo*. But, in the case of [20]

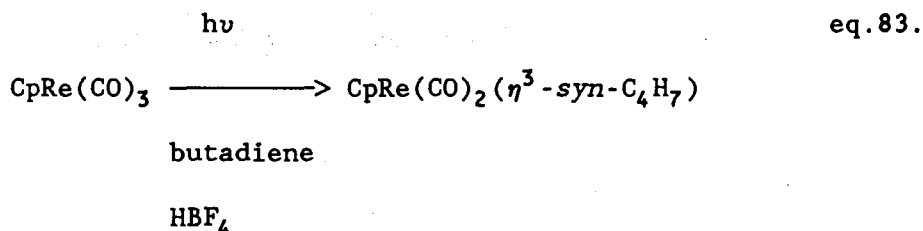
(or [21]), only one isomer [20b]exo (or [21a]exo) was observed as the product. This demonstrated that the cationic complexes [20b]exo and [21a]exo, involving a substituted allyl or a cyclic allyl ligand, differ from the unsubstituted allyl complex [19], where the two isomers undergo a facile *endo-exo* interconversion.

The relevant literature shows that the substituted allyl in cationic complexes can be present in an *anti*-allyl configuration such as $[\text{Fe}(\text{CO})_3(\eta^3\text{-anti-1-methylallyl})]^+$;⁸⁰ or a *syn*-allyl configuration such as $[\text{CpMo}(\text{CO})(\text{NO})(\eta^3\text{-exo-cis-syn-phenylallyl})]^+$; ^{66k} or a mixture of *anti* and *syn* configurations such as $[\text{CpCo}(\text{CO})(\eta^3\text{-1-methylallyl})]^+$.^{67a} Furthermore, some substituted allyl cationic complexes do display *exo-endo* isomerization (e.g., $[\text{CpMo}(\text{CO})(\text{NO})(\eta^3\text{-exo-cis-syn-phenylallyl})]^+$ ^{66k}), and *anti-syn* isomerization (e.g., $[\text{CpCo}(\text{CO})(\eta^3\text{-1-methylallyl})]^+$).^{67a} However, it is noteworthy that the *exo-anti* allyl moiety of [20b]exo is quite stable. We did not observe any evidence for *exo-endo* or *anti-syn* isomerization of the allyl moiety in [20b]exo at room temperature. Similarly, no evidence for the *exo-endo* isomerization of [21a]exo was observed at room temperature. This stability of [20b]exo and [21a]exo could be attributed to the steric hindrance because two bulky groups, Cp* and a pentyl allyl (or a cyclohexyl allyl), are present in [20b]exo (or [21a]exo).

Krivykh reported a general one-stage synthetic route^{67a} to allylcarbonyl cationic complexes, involving the chemical reaction of

an organometallic compound with an allyl alcohol or a conjugated diene in the presence of a strong protonic acid (eqs. 75, 83).

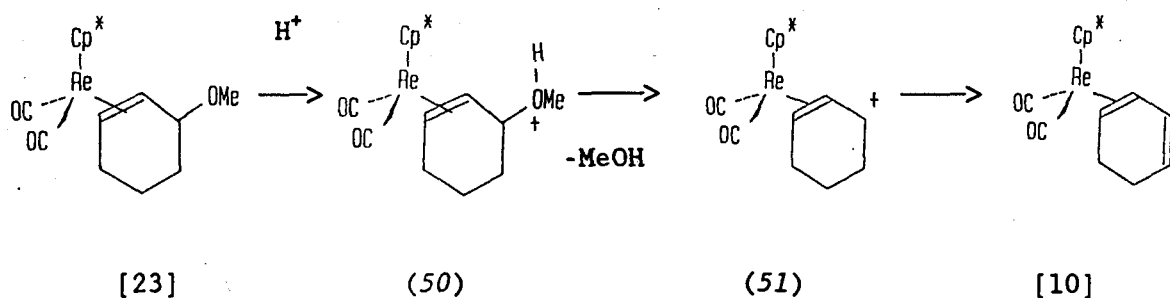
Krivykh supposed that there was primary formation of η^2 -complexes and then subsequent protonation and dehydration to form the allyl cationic complex.^{67a} This proposal is supported by Rosan's⁷⁷ results which show that the cationic complexes $[\text{CpMn}(\text{CO})_2(\eta^3\text{-allyl})]^+$ are made by two convenient synthetic avenues, involving coordination and subsequent dehydration of allylic alcohols. Consistently, our results show that the η^2 -methoxyalkene readily loses the methoxy group in the presence of the strong protonic acid HBF_4 (eq. 78, 80).



However, the complex $\text{Cp}^*\text{Re}(\text{CO})_2(\eta^2\text{-1,3-cyclohexadiene})$ [10] was formed in the reaction in eq. 79, and then the protonation of this complex leads to the formation of the cyclic allyl cationic complex [21]. Note that the complex [10] was readily formed in eq. 79 only in the presence of a trace strong protonic acid. This process of the alcohol loss catalyzed by the proton acid HBF_4 may involve conversion of [23] to (50) and cleavage of (51) to [10] and MeOH

(Scheme 27).

Scheme 27.



Furthermore, the eqs.78-80 agree with the analysis of the mass spectra for [22] and [23] which indicate a weak allylic C-OMe bond. The thermal instability of [23] leads to the formation of the η^2 -1,3-cyclohexadiene complex [10] accompanied by the loss of MeOH. This process will be promoted in the presence of MeO⁻ anion, as illustrated in Scheme 28. In addition, the complex [10] was always present as a by-product in the reaction of the cationic complex [21] with NaOMe (eq.76). Presumably, it resulted from the instability of the product [23] in basic conditions, as described above. However, we could not rule out the possibility that MeO⁻ directly abstracts a proton from the neighboring methylene in the cationic complex [21] (see Fig.51) leading to the formation of [10]. The formation of [10], in eq.76, could be minimized if the reaction was carried out at -78^oC.

Scheme 28.

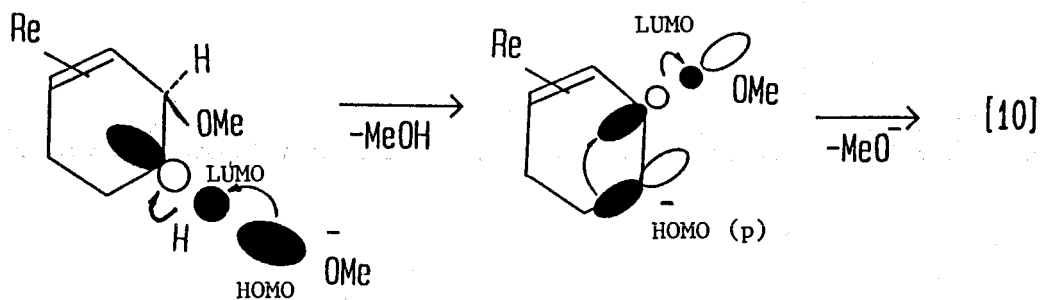
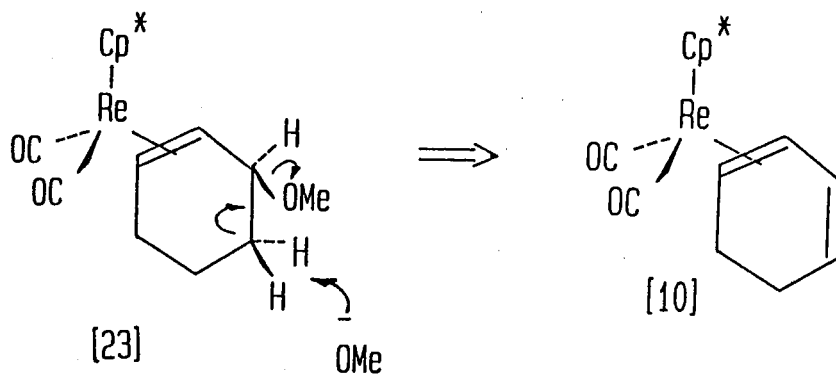
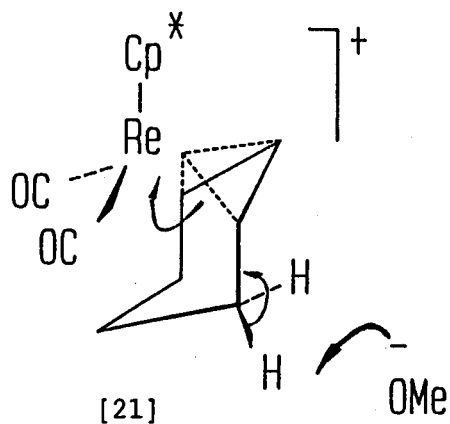


Fig. 51. Proton Abstraction by OMe^-



4.6. Conclusion

The η^3 -allylalkane cationic complexes [19]-[21] were produced by three different routes (eqs.73, 77-80). Nucleophilic addition to these cationic complexes further yielded the related derivatives ([2], [5], [22] and [23]). The ^1H NMR spectrum of [19] showed the presence of two isomers [19a]exo and [19b]endo, which could not be further separated due to the very fast *exo-endo* interconversion even at low temperature (-60°C). The X-ray crystal analysis indicated that [19a]exo was the major isomer in the solid state mixture, while the IR and ^1H NMR spectra showed that [19b]endo was the major isomer in solution. Magnetization transfer results showed that *exo-endo* interconversion occurred with no scrambling of *syn* and *anti* protons, consistent with a pseudorotation mechanism but not a η^3 - η^1 - η^3 mechanism. The cationic complexes [20]-[21] were quite stable without detectable *exo-endo* or *anti-syn* isomerizations. The allyl moiety of [20] was assigned to the *anti*-substituted configuration, based on the formation of *cis*-2-octene complex [5] in the reaction of [20] with NaBH_4 (eq.81). The spectroscopic analysis for [21] showed only one isomer which was further determined to be [21a]exo by X-ray structure determination. Finally, it is worth noting that the MS analysis for [22] and [23] is indicative of a weak allylic C-OMe bond which is consistent with the results of chemical reactions (eqs.78-80).

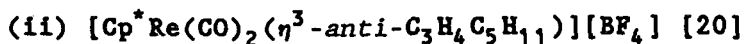
4.7. Experimental Section

Manipulations, solvent purification and spectroscopic measurements were described in Chapter II. FABMS spectra were obtained by Mr. G. Owen on a Hewlett-Packard 5985 GC-MS instrument fitted with a Phrasor Scientific Inc. FAB accessory, using Xe bombardment and samples dispersed in a thioglycerol matrix.

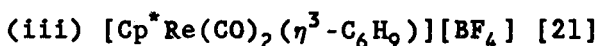
The experimentally observed data for IR and ^1H NMR of the complexes [19]-[23] are listed in Tables 16 and 17.

(i) $[\text{Cp}^*\text{Re}(\text{CO})_2(\eta^3\text{-C}_3\text{H}_5)][\text{BF}_4]$ [19]

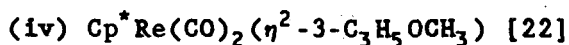
A solution of $[\text{Ph}_3\text{C}][\text{BF}_4]$ (80 mg; 0.24 mmol) in nitromethane (0.5 mL) was added to a solution of $\text{Cp}^*\text{Re}(\text{CO})_2(\eta^2\text{-C}_3\text{H}_6)$ [10] (81 mg; 0.19 mmol) in nitromethane (1 mL) and the solution was heated at 60°C for 5 minutes. The IR spectrum indicated that reaction was complete. The mixture was poured into dry Et_2O (100 mL) and stirred for 20 minutes to ensure removal of trityl fluoroborate, then filtered. The colourless product obtained was recrystallized from CH_2Cl_2 /hexane in yield: 56 mg (0.11 mmol, 57.8%). Anal. Calcd. for $\text{C}_{15}\text{H}_{20}\text{BF}_4\text{O}_2\text{Re}$: C, 35.65; H, 3.99. Found: C, 35.45; H, 4.01. FABMS (thioglycerol, ^{187}Re) m/z 419 [M^+ of cation], 391 [M-CO^+], 377 [$\text{M-C}_3\text{H}_6^+$], 359 [M-2CO-4H], 349 [$\text{M-C}_3\text{H}_6\text{-CO}^+$].



A similar procedure to that used for [19], using $\text{Cp}^*\text{Re}(\text{CO})_2(\eta^2\text{-C}_8\text{H}_{16})$ [4] as a starting material, gave [20] as colourless microcrystals in 90.6% yield. FABMS (thioglycerol, ^{187}Re) m/z 489 [M^+ of cation], 459 [M-CO-2H] $^+$, 429 [M-2CO-4H] $^+$, 377 [$\text{M-C}_8\text{H}_{16}$] $^+$, 348 [$\text{M-C}_8\text{H}_{16}\text{-CO-H}$] $^+$.



Following the procedure of [19], treatment of $\text{Cp}^*\text{Re}(\text{CO})_2(\eta^2\text{-C}_6\text{H}_{10})$ [6] in nitromethane with $[\text{Ph}_3\text{C}][\text{BF}_4]$ gave [21] as colourless microcrystals in 69.3% yield. Anal. Calcd. for [21]: C, 39.64; H, 4.44. Found: C, 39.38; H, 4.51. FABMS (thioglycerol, ^{187}Re) m/z 459 [M^+ of cation], 431 [M-CO] $^+$, 399 [M-2CO-4H] $^+$, 377 [$\text{M-C}_6\text{H}_{10}$] $^+$, 349 [$\text{M-C}_6\text{H}_{10}\text{-CO}$] $^+$, 321 [$\text{M-C}_6\text{H}_{10}\text{-2CO}$] $^+$.



A solution of $[\text{Cp}^*\text{Re}(\text{CO})_2(\eta^3\text{-C}_3\text{H}_5)][\text{BF}_4]$ [19] (30 mg, 0.059 mmol) in 10 ml MeOH was vigorously stirred while solid NaOMe (4 mg, 0.07 mmol) was added stepwise into the reaction solution at room temperature under N_2 . After 2 h, the IR spectrum ($\nu(\text{CO})$, MeOH)

showed the disappearance of two sets of bands for the starting material (2051, 1998 cm^{-1} for [19b]endo; 2035, 1979 cm^{-1} for [19a]exo), and two new bands at 1958, 1883 cm^{-1} for the product [22]. The solvent was removed under vacuum. The residual white solid was washed with hexane (15 ml x 3). The hexane washing solution was collected and filtered through a short Celite column (1 x 1 cm). Removal of hexane gave a white solid in yield: 16 mg (0.036 mmol, 60.3%). Anal. Calcd. for [22]: C, 42.75; H, 5.16. Found: C, 43.10; H, 5.11. MS (EI): m/z 450 $[\text{M}]^+$, 419(weak) $[\text{M-OMe}]^+$, 392 $[\text{M-2CO-2H}]^+$, 376 $[\text{M-C}_3\text{H}_5\text{OMe-2H}]^+$, 362 $[\text{M-OMe-2CO-H}]^+$, 348(base) $[\text{M-C}_3\text{H}_5\text{OMe-CO-2H}]^+$.

(v) $\text{Cp}^*\text{Re}(\text{CO})_2(\eta^2\text{-3-C}_6\text{H}_9\text{OCH}_3)$ [23]

A solution of $[\text{Cp}^*\text{Re}(\text{CO})_2(\eta^3\text{-C}_6\text{H}_9)][\text{BF}_4]$ [21] (30 mg, 0.055 mmol) in 10 ml MeOH was stirred at -78°C while solid MeONa was added stepwise to the solution. The reaction was monitored by IR. All the cationic complex [21] had reacted in 24 h. The IR spectrum ($\nu(\text{CO})$, MeOH) showed the disappearance of bands at 2024, 1962 cm^{-1} for the starting material, and the appearance of two new bands at 1946, 1873 cm^{-1} for the product [23]. Removal of the solvent under vacuum gave a white solid residue, which was washed with hexane (15 ml x 3). The hexane washing solution was collected and filtered through a short

Celite column. Removal of hexane gave a white solid product in yield: 16 mg (0.033 mmol, 60.0%). Anal. Calcd. for [23]: C, 46.61; H, 5.56. Found: C, 46.80; H, 5.51. MS (EI): m/z 490 [M]⁺, 458 [M-MeOH]⁺, 430 [M-MeOH-CO]⁺, 400(base) [M-MeOH-2CO-2H]⁺, 378(weak) [M-C₈H₉OMe]⁺, 376 [M-C₈H₉OMe-2H]⁺, 348 [M-CO-C₈H₉OMe-2H]⁺.

(vi) Reaction of [20] with NaBH₄

A solution of [Cp^{*}Re(CO)₂(η³-C₈H₁₅)] [BF₄] [20] (10 mg, 0.017 mmol) in 5 ml THF was vigorously stirred while the solution of NaBH₄ (1 mg, 0.026 mmol) in 1 ml water was added dropwise at room temperature. After 12 h stirring, the solution was dried under vacuum, then the residual solid was washed with hexane (5 ml x 3). The hexane solution was filtered through a short Celite column and concentrated to about 5 ml by rotary evaporation. The hexane solution was checked by IR(ν(CO)) showing two sets of absorptions at 1960 and 1888 cm⁻¹ for 1-octene complex [4]; and at 1955 and 1883 cm⁻¹ for 2-octene complex[5] with a ratio of 1:1 = 1-octene : 2-octene. Following chromatography on an acidic alumina column, eluting with hexane, the two complexes, 1-octene [4] and 2-octene [5], were isolated. The sample of [5] was further characterized as the *cis*-2-octene configuration by ¹H NMR decoupling experiments. Anal. Calcd. for [5]: C, 49.06; H, 6.38. Found: C, 49.27; H, 6.08.

MS (EI): m/z 490 [M]⁺, 460 [M-CO-2H]⁺, 430(weak) [M-2CO-4H]⁺, 428 [M-2CO-6H]⁺, 378 [M-C₈H₁₆]⁺, 376 [M-C₈H₁₆-2H]⁺, 348(base) [M-CO-C₈H₁₆-2H]⁺.

(vii) Reaction of [19] with NaBH₄

Following the above reaction procedure in (vi), a white solid was isolated from the reaction of [19] with NaBH₄, and was identified by IR(ν (CO)) and MS to be the η^2 -propene complex [2].

(viii) Reaction of [22] with HBF₄

A solution of Cp^{*}Re(CO)₂(η^2 -3-C₃H₅OCH₃) [22] (10 mg, 0.022 mmol) in 10 ml THF was stirred while five drops of aqueous HBF₄ (48-50%) were dropped into the solution. After 30 min. stirring, the solution was pumped to dryness, the residue was washed with ether (5ml x 3), and then extracted with CH₂Cl₂. Removal of CH₂Cl₂ gave a solid which was identified by IR(ν (CO)) and ¹H NMR to be the cationic complex [19].

(ix) Reaction of [23] with HBF₄

One drop of aqueous HBF₄ (48-50%) was added to a solution of Cp^{*}Re(CO)₂(η^2 -3-C₆H₉OCH₃) [23] (8 mg, 0.016 mmol) in 10 ml THF at

room temperature. After 3 h stirring, the solvent was removed at reduced pressure. The residue was washed with hexane (5 ml x 3). Removal of hexane gave a white solid, which was identified by IR($\nu(\text{CO})$) and MS as the η^2 -1,3-cyclohexadiene complex [10]. This solid was dissolved in 5 ml THF again, then two more drops of HBF_4 were dropped into the solution. The solution was continuously stirred until IR($\nu(\text{CO})$, THF) showed two new bands at 2018 and 1954 cm^{-1} attributable to the cationic complex [21]. Removal of solvents gave a solid. The further identifications by IR($\nu(\text{CO})$) and ^1H NMR showed that it had the same properties as the cationic complex [21].

Chapter V

Synthesis and Characterizations of Heterobimetallic, Metal-Metal Bonded Complexes

5.1. Introduction

The homometallic complexes $[\text{Cp}^*\text{M}(\text{CO})_2]_2$ ($\text{M} = \text{Fe}, \text{Ru}, \text{Os}$)⁸¹⁻⁸³ have all been synthesized in recent years, and may be compared with the earlier, and generally better known cyclopentadienyl analogues $[\text{CpM}(\text{CO})_2]_2$. To date, the osmium compound⁸³ has scarcely been studied; however, the ruthenium compound, like its Cp analogue, appears to be a potentially rich source of novel transformations at the diruthenium centre⁸⁴. Currently, there is considerable interest in heterobimetallic complexes,⁸⁵⁻⁸⁷ stimulated in part by the anticipation that these might provide new chemistry not hitherto observed in homometallic compounds, including possible novel catalysis potential⁸⁷.

In this Chapter, we describe the synthesis and structures of heterobimetallic analogues of $[\text{Cp}^*\text{M}(\text{CO})_2]_2$ with iridium-manganese and iridium-rhenium bonds. A related compound with a rhodium-manganese bond is known⁸⁸.

5.2. Synthesis and Characterization

A common procedure for the activation of $\text{Cp}^*\text{Re}(\text{CO})_3$ or $\text{CpRe}(\text{CO})_3$ toward substitution is to generate the substitution-labile THF (or N_2) derivatives $\text{Cp}^*\text{Re}(\text{CO})_2\text{L}$ or $\text{CpRe}(\text{CO})_2\text{L}$ ($\text{L} = \text{THF}, \text{N}_2$). The labile ligand THF (or N_2) can then be replaced by the neutral donor complex system $\text{Cp}^*\text{Ir}(\text{CO})_2$ to form the heterobimetallic, metal-metal bonded complexes (Fig.52) $\text{Cp}^*(\text{CO})\text{Ir}(\mu_2\text{-CO})_2\text{Mn}(\text{CO})\text{Cp}^*$ [24], $\text{Cp}^*(\text{CO})\text{Ir}(\mu_2\text{-CO})_2\text{Re}(\text{CO})\text{Cp}^*$ [25], and $\text{Cp}^*(\text{CO})\text{Ir}(\mu_2\text{-CO})_2\text{Re}(\text{CO})\text{Cp}$ [26] under mild conditions (eq.85).

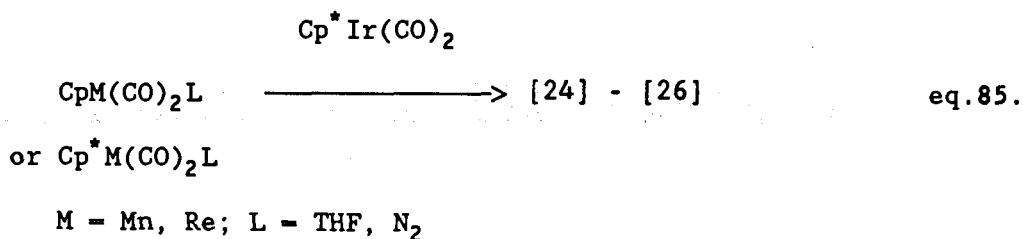
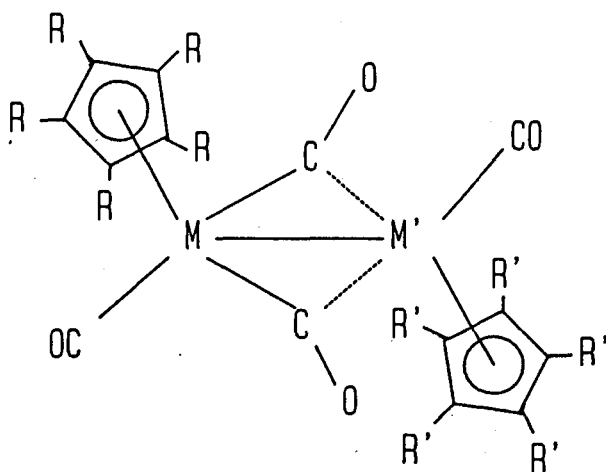


Fig.52. Heterobinuclear Complexes [24]-[26]



[24] $\text{M} = \text{Mn}; \text{M}' = \text{Ir};$

$\text{R} = \text{R}' = \text{CH}_3$

[25] $\text{M} = \text{Re}; \text{M}' = \text{Ir};$

$\text{R} = \text{R}' = \text{CH}_3$

[26] $\text{M} = \text{Re}; \text{M}' = \text{Ir};$

$\text{R} = \text{H}; \text{R}' = \text{CH}_3$

These products were obtained as yellow, or orange-red microcrystalline solids, analytically and spectroscopically pure. The products are somewhat light sensitive (particularly [24]). Further, they are slowly decomposed in benzene, toluene or THF, and quickly decomposed in CH_2Cl_2 or acetone. The solid samples of [24]-[26] are quite stable when stored in the freezer. The compounds [24]-[26] were formulated on the basis of microanalysis and spectroscopy. The IR, NMR and mass spectral data for these complexes [24]-[26] are listed in Tables 19 and 20. The electron-impact mass spectrum (70eV) in each case showed the molecular ion with an isotope abundance pattern in agreement with the calculated pattern. The IR($\nu(\text{CO})$) spectra exhibited a feature common to all three heterobimetallic complexes [24]-[26]: two $\nu(\text{CO})$ absorptions for terminal CO groups above ca 1900 cm^{-1} , and a third, broad weaker absorption near ca 1750 cm^{-1} associated with one or more bridging carbonyl groups. The presence of the ($\eta^5\text{-Cp}^*$) or ($\eta^5\text{-Cp}$) groups was clearly revealed in the ^1H NMR spectra and confirmed by the ^{13}C NMR spectra. In addition, the molecular structure of [26] has been established by X-ray diffraction showing that the Cp^* and Cp groups are oriented *trans* as are the two terminal CO groups. The remaining two semibridging carbonyl groups are primarily bound to the Re atom. The Ir-Re bond length, not corrected for the thermal motion, is $2.8081(6)\text{\AA}$ (Fig.53).

Table 19. Some Spectroscopic Parameters of the Heterobimetallic
Complexes [24]-26]

Cplx	IR(benzene) $\nu(\text{CO}) \text{ cm}^{-1}$	$^1\text{H NMR}(\text{C}_6\text{D}_6)$ $\delta (\text{Cp}^*, \text{Cp})^a \text{ ppm}$	MS(m/z) $\text{M}^+ ; \text{base}$
[24]	1962(m), 1902(vs), 1756(s,br)	1.77, 1.75	630 ^d ; 352
[25]	1954(s), 1898(vs), 1743(m,br)	1.88, 1.81	762 ^e ; 321
[26]	1962(m), 1917(vs), 1739(m,br)	1.83, ^b 4.78 ^c	692 ^e ; 354

Abbreviation: s = strong, vs = very strong, m = middle, br = broad.

^aCp* or Cp was a singlet peak in all cases. ^bfor Cp*. ^cfor Cp. ^dfor ^{193}Ir . ^efor ^{193}Ir and ^{187}Re .

Table 20. ^{13}C NMR Data for the Heterobimetallic
Complexes [24]-[26]

Complex	^{13}C NMR ($\text{C}_6\text{D}_6/\text{C}_6\text{H}_6$ 1:4) δ ppm, J Hz
[24] ^a	8.23, 8.47 (C_5Me_5); 96.69, 101.13 (C_5Me_5); 168.2 (IrCO); 247.9 (μ_2 -CO)
[25] ^b	8.45, 8.90 (C_5Me_5); 98.45, 100.43 (C_5Me_5); 170.32 (IrCO); 203.72 (ReCO); 224.65 (μ_2 -CO)
[26] ^c	9.05 (q, J=129, C_5Me_5); 87.6 (d, J=182, C_5H_5); 100.9 (s, C_5Me_5); 170.6 (IrCO); 200.5 (ReCO); 219.5 (μ_2 -CO)

Abbreviation: s = singlet, d = doublet, q = quartet. ^aAs determined by $^{13}\text{C}(^1\text{H})\text{NMR}$ at 280K. ^bAs determined by $^{13}\text{C}(^1\text{H})\text{NMR}$ at 293K. ^cAs determined at 281K.

Fig.53. Perspective View of the Complex [26]

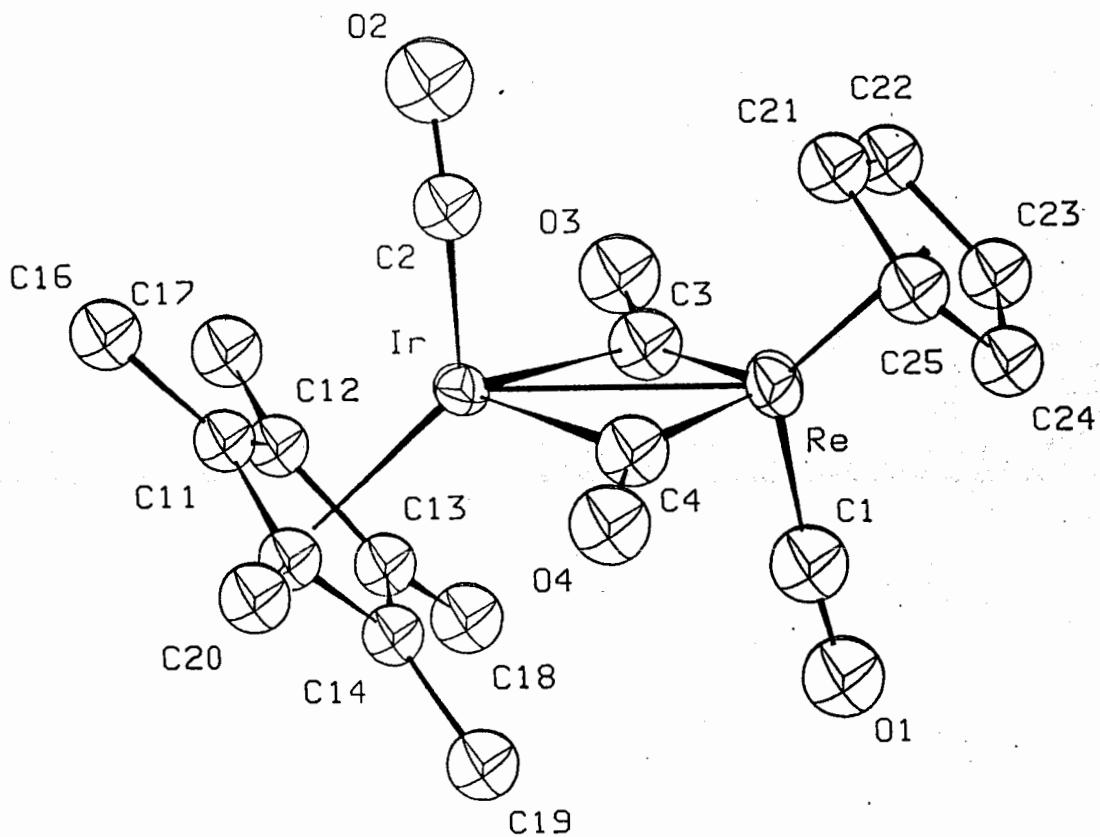
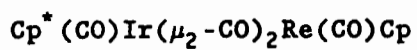


Fig. 54. ^1H NMR (C_6D_6) Spectrum

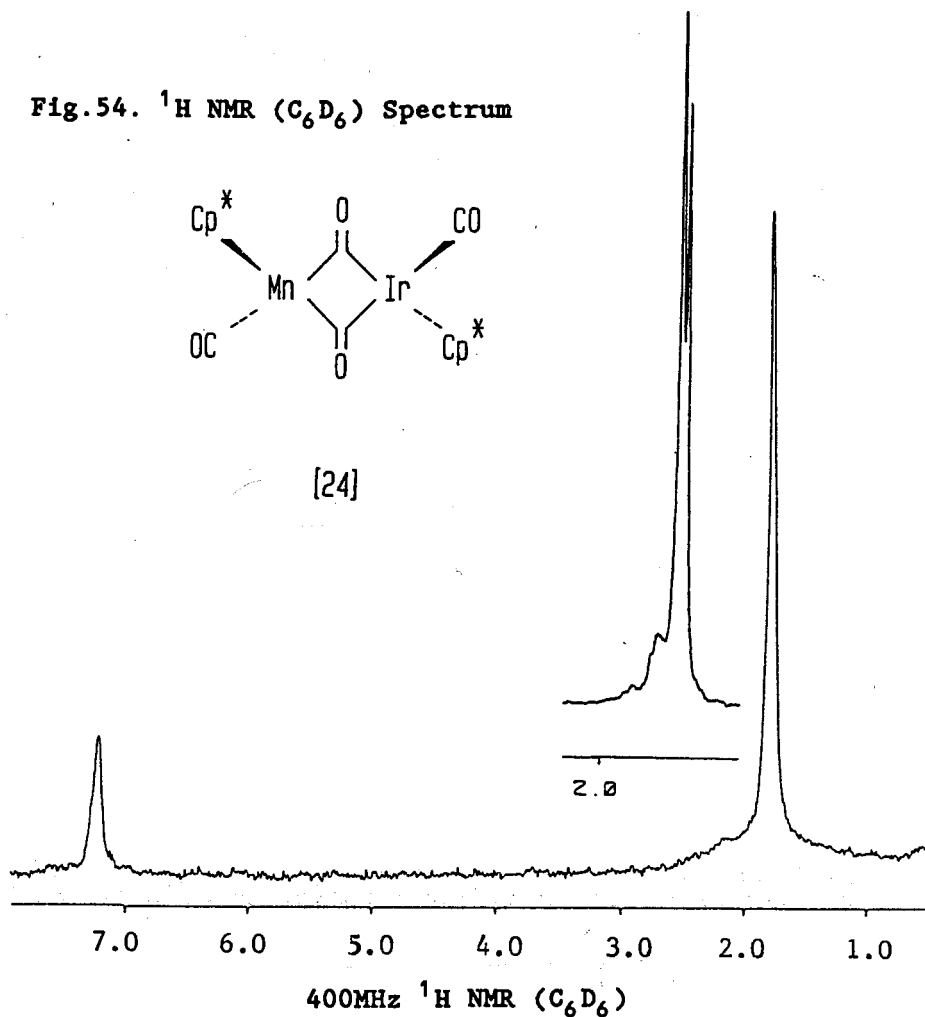


Fig. 55. ^1H NMR Spectrum

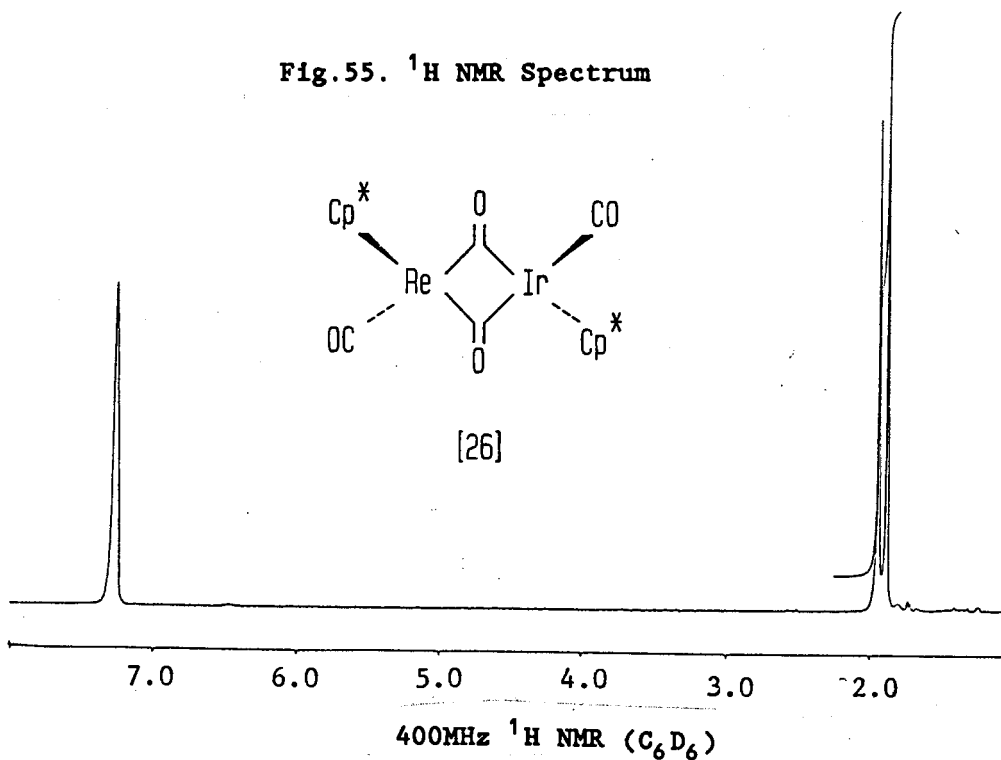
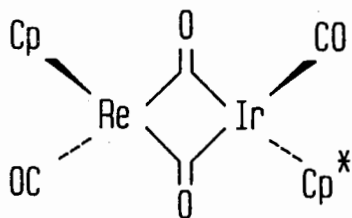
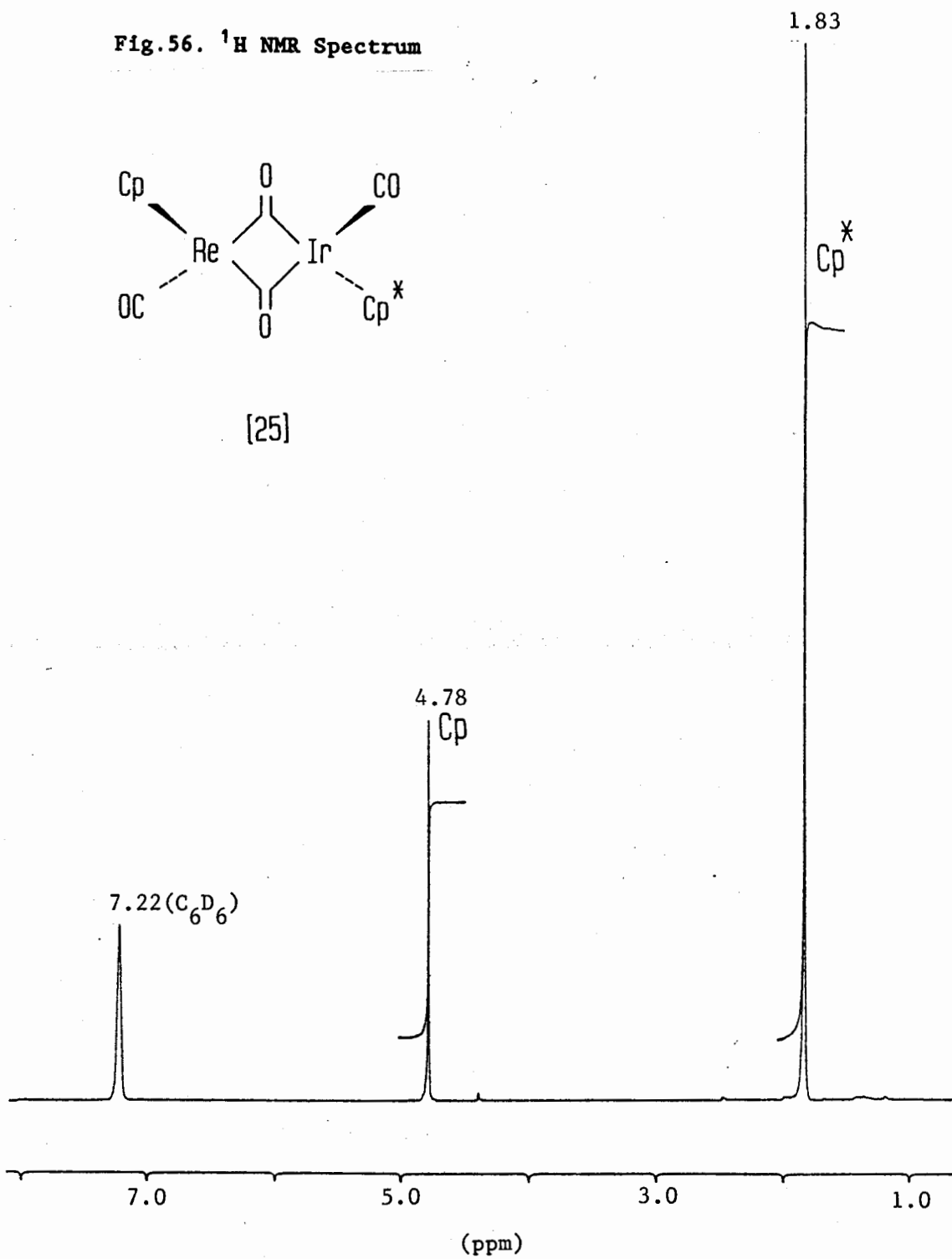


Fig. 56. ^1H NMR Spectrum



[25]



400MHz ^1H NMR(C_6D_6)

5.3. Discussion

5.3.1. Syntheses

The THF complexes $\text{Cp}^*\text{Mn}(\text{CO})_2(\text{THF})$, $\text{Cp}^*\text{Re}(\text{CO})_2(\text{THF})$ and $\text{CpRe}(\text{CO})_2(\text{THF})$, generated by ultraviolet photolysis of the corresponding tricarbonyl complexes in THF, reacted with $\text{Cp}^*\text{Ir}(\text{CO})_2$ with displacement of the labile THF ligand to give moderate yields of the heterobinuclear complexes [24]-[26]. When the syntheses were conducted at room temperature in THF alone, displacement of the THF ligand was inefficient, and reaction times of several hours were required. These reaction times could be shortened considerably at higher temperatures, generally with no decrease in yield (and sometimes a small improvement, particularly where the THF was diluted with cyclohexane). The products are somewhat light sensitive (particularly [24]), so the reactions were best done in the dark. Complex [25] was alternatively synthesized by displacement of the dinitrogen ligand from $\text{Cp}^*\text{Re}(\text{CO})_2(\text{N}_2)$. Although an increased yield was observed by using this procedure, it offers little advantage when the relatively poor conversion⁹¹ of $\text{Cp}^*\text{Re}(\text{CO})_3$ to $\text{Cp}^*\text{Re}(\text{CO})_2(\text{N}_2)$ is taken into account. Several unsuccessful attempts were also made to synthesize the methylcyclopentadienylmanganese analogue of [24] $(\eta^5\text{-MeC}_5\text{H}_4)(\text{CO})\text{Mn}(\mu_2\text{-CO})_2\text{Ir}(\text{CO})(\eta^5\text{-C}_5\text{Me}_5)$ by

analogous procedures, starting from the readily available and inexpensive $(\eta^5\text{-MeC}_5\text{H}_4)\text{Mn}(\text{CO})_3$.

5.3.2. Characterization

The compounds [24]-[26] were characterized on the basis of elemental analysis and spectroscopy. The electron-impact mass spectrum (70eV) in each case gave the parent ion with an isotope abundance pattern in agreement with the calculated pattern. Here, it is worth noting that the isotopic abundance pattern of the molecular ion in each of the cases [25] and [26] has the strongest intensity at m/z $[\text{M}-2]^+$ (Figs.57(a-b)). The reason for this is the relative abundance of the possible combinations of the Ir and Re isotopes. The natural isotopic abundances for Ir and Re are: ^{191}Ir 37.3%, ^{193}Ir 62.7%; and ^{185}Re 37.1%, ^{187}Re 62.9%. Therefore, the one combination corresponding to M^+ is ($^{193}\text{Ir} + ^{187}\text{Re}$) with a probability 39.4%; however, two combinations corresponding to $[\text{M}-2]^+$ are: ($^{193}\text{Ir} + ^{185}\text{Re}$) and ($^{191}\text{Ir} + ^{187}\text{Re}$) with probabilities 23.3% and 23.5% respectively; finally, one combination corresponding to $[\text{M}-4]^+$ is: ($^{191}\text{Ir} + ^{185}\text{Re}$) with a probability 13.8%. The ratio of combination probability is: $[\text{M}]^+ / [\text{M}-2]^+ / [\text{M}-4]^+ = 84.2/100/29.5$, and is very close to the observed data (Figs.58(a-b)). In addition, there is the sequential loss of the four CO groups in each case, and

Fig.57. Mass Spectra for the Complexes [24]-[26]

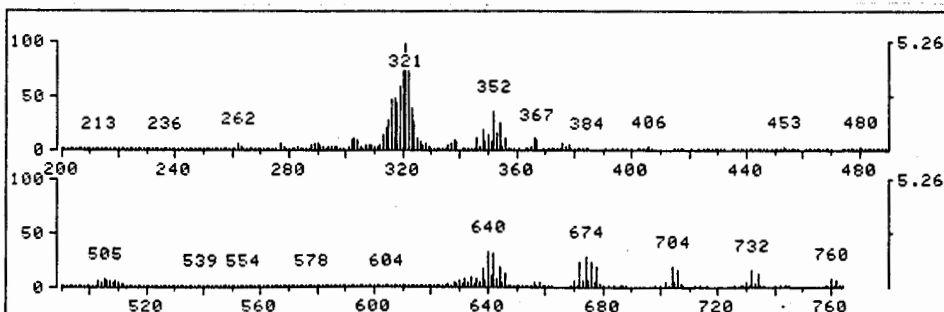
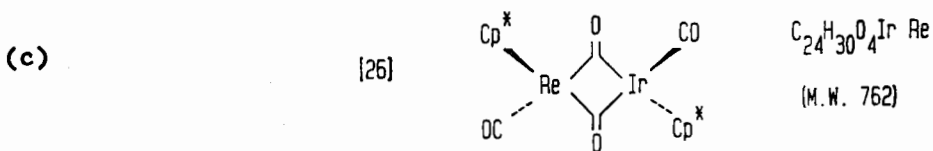
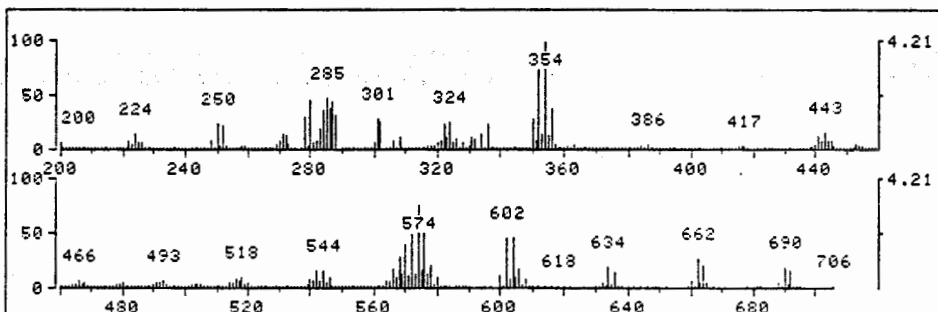
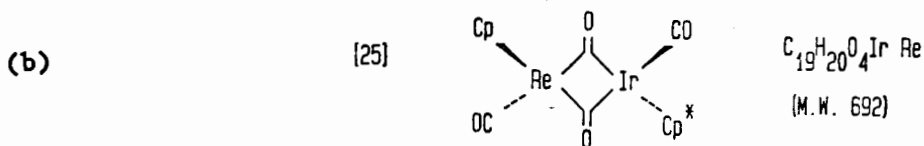
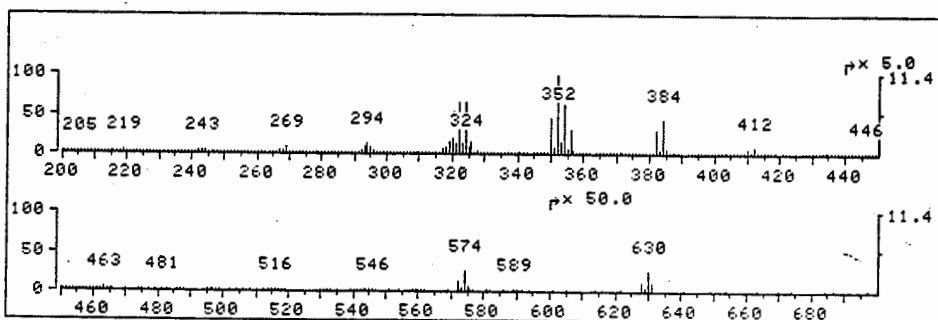
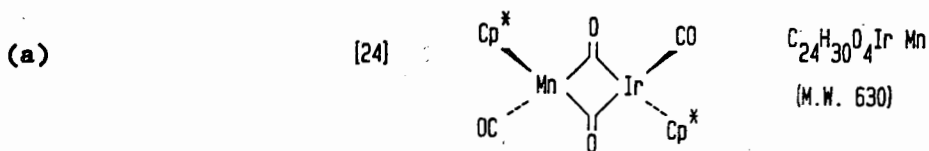


Fig.58. Isotopic Abundance Pattern for [25], [26]

(a) Calculated Isotopic Abundance for M⁺ of [25]

C 19, H 20, O 4, IR 1, RE 1,

MASS	%	REL. INTEN.	
688	11.06	29.33
689	2.40	6.37	...
690	37.68	100.00
691	8.15	21.62
692	32.68	86.74
693	6.98	18.50
694	0.98	2.58
695	0.11	0.28

(b) Observed Isotopic Abundance for M⁺ of [25]

m/z	Rel Abund	Rel %	
688.2	5.8	29.44	_____
689.2	0.7	0.04	_____
690.1	19.7	100.00	_____
691.1	3.2	16.24	_____
692.2	16.0	81.23	_____
693.1	2.5	12.69	_____

(c) Calculated Isotopic Abundance for M⁺ of [26]

MASS	%	REL. INTEN.	
758	10.44	29.21
759	2.87	8.02
760	35.73	100.00
761	9.75	27.27
762	31.36	87.76
763	8.38	23.43
764	1.34	3.73
765	0.17	0.45

the expected loss of H atoms from the Cp* ring, though for [25] and [26] the loss of the final CO group is accompanied by considerable hydrogen loss resulting in a broad envelope of peaks extending below the predicted position. A feature common to all three compounds is the strong appearance of the fragments [Cp*Ir(CO)]⁺ m/z 356, and [(Cp*-2H)Ir(CO)]⁺ m/z 354 indicating that fragmentation of the molecular ion by way of the loss of Cp*Re(CO)₃, CpRe(CO)₃ and Cp*Mn(CO)₃ in [25], [26] and [24] respectively is important. We have observed that these tricarbonyl complexes are predominantly formed also in the solution decompositions of complexes [24]-[26]. Furthermore, this is in accord with the view adopted later on the basis of the crystallography that the structures can be rationalized in terms of a donor metal-metal bond from these fragments to an unsaturated Cp*Ir(CO) moiety. By contrast, the loss of Cp*Ir(CO)₂ is not observed in the mass spectra.

The IR spectra exhibited two $\nu(\text{CO})$ absorptions for terminal CO groups above ca 1900 cm^{-1} , and a third, broad weaker absorption near ca 1750 cm^{-1} associated with one or more bridging carbonyl groups. The presence of the ($\eta^5\text{-C}_5\text{Me}_5$) or ($\eta^5\text{-C}_5\text{H}_5$) groups was clearly revealed in the ¹H NMR spectra and confirmed by the ¹³C NMR spectra. The latter showed, for compound [25] sharp resonances for carbonyl groups at δ 170.32, 203.72 and 224.65 ppm in approximate ratio 1:1:2. The first can be assigned to a CO group terminally

bound to the iridium atom by comparison with $\text{CpIr}(\text{CO})_2$ for which we have measured $\delta(\text{CO})$: 178.0 in C_6D_6 (and with $\text{CpIr}(\text{CO})_2$, $\delta(\text{CO})$: 173.8)⁹²; the second to a CO terminally bound to the Re atom by comparison with $\text{Cp}^*\text{Re}(\text{CO})_3$ for which we have measured $\delta(\text{CO})$: 198.2 in C_6D_6 (and with $\text{CpRe}(\text{CO})_3$, $\delta(\text{CO})$: 195)⁹² and the third to two equivalent bridging CO groups. For the manganese compound [24] the resonance for the terminal $\text{Ir}(\text{CO})$ group was in a similar position (δ 168.2) and the resonance for the bridging CO groups was evident at δ 247.9; however, no resonance could be observed corresponding to the CO group terminally bound to the Mn. This is attributed to quadrupolar broadening of this signal by coupling to the ^{55}Mn nucleus.⁹³ We were able to observe a CO resonance for $\text{Cp}^*\text{Mn}(\text{CO})_3$ in C_6D_6 at δ 227.2.

In the preparation of some of these heterobimetallic complexes, we were kindly assisted by Mr. Ramzi Hader, a summer undergraduate student in our laboratory.

5.3.3. X-ray Structure of Compound [26]

A yellow-orange crystal was selected from a sample of [26] recrystallized from benzene-hexane and the structure was determined by X-ray crystallography, kindly carried out by Dr. R.J. Batchelor in Professor F.W.B. Einstein's laboratory. A perspective view of this complex [26] is shown in Fig.53.

The structure consists of discrete molecules of [26] with no significant intermolecular contacts. In the ordered model presented here, the molecule has no crystallographic symmetry elements. Chemically, however, the molecule has *pseudo-Cs* symmetry, where the mirror plane contains atoms Re, Ir, and the terminal carbonyl groups C(1)-O(1) and C(2)-O(2).

Only two Ir-Re bond distances have been previously reported and are: 2.9117(7)Å for the single covalent bond in $(\text{PCy}_2)(\text{CO})_2\text{Re}(\mu\text{-PCy}_2)_2\text{Ir}(\text{CO})_2(\text{PCy}_2)$, (Cy = cyclohexyl) and 2.6573(5)Å for the formally double bond in $(\text{PCy}_2)_2\text{Re}(\mu\text{-PCy}_2)_2\text{Ir}(\text{PMe}_3)_2$.⁹⁴ These species are chemically rather different to [26]. The Re-Ir distance of 2.8081(6)Å for [26] (not corrected for thermal motion⁹⁵) is more comparable to the Ir-Ir single covalent bond in $[\text{Cp}^*\text{Ir}(\text{CO})_2]_2^+$, (2.8349(12)Å).⁹⁶

The carbonyl groups (C(3)-O(3); C(4)-O(4)) can be described as primarily bound to the Re atom and semibridging to the Ir atom. This is a feature that has been previously observed in the structures of two related molecules of the type $(\text{arene})(\text{CO})\text{M}(\mu_2\text{-CO})_2\text{M}'(\text{CO})(\text{arene}')$, but in each previous case M has been a 3d metal bound to a 4d metal M'. Here we see the same structural feature occurring where both metals are 5d metals. The previous examples are $\text{Cp}(\text{CO})\text{Mn}(\mu_2\text{-CO})\text{Rh}(\text{CO})\text{Cp}^*$,⁸⁸ and $(\eta^6\text{-C}_6\text{H}_6)(\text{CO})\text{Cr}(\mu_2\text{-CO})\text{Rh}(\text{CO})\text{Cp}^*$.^{86h} While the reaction can be envisaged to proceed by displacement of

the weakly bonded THF ligand from $\text{CpRe}(\text{CO})_2(\text{THF})$ by the basic $\text{Cp}^*\text{Ir}(\text{CO})_2$ with the formation of a dative bond from Ir to Re giving $\text{Cp}(\text{CO})_2\text{Re}\leftarrow\text{Ir}(\text{CO})_2\text{Cp}^*$. Clearly CO rearrangement occurs and the structure of [26] that results may be visualized as being built from a dative bond from an 18-electron $\text{CpRe}(\text{CO})_3$ moiety to the 16-electron fragment $\text{Cp}^*\text{Ir}(\text{CO})$, assisted by return of electron density from Ir via the semibridging CO groups in order to mitigate the charge imbalance, as proposed by Cotton for the similar situation in $\text{Cp}_2\text{V}_2(\text{CO})_3(\mu_2\text{-CO})_2$.⁹⁷ Since this structural pattern is now so well established for this type of binuclear complex, there is every reason to expect that complexes [24] and [25] also are structurally analogous to [26], and also possess semibridging CO groups as illustrated. In fact, complex [25] was also investigated by single crystal X-ray diffraction, but the structure solution was abandoned at a point where it was clear that there was severe disorder between the rhenium and iridium atom positions, and their associated carbonyl and $\eta^5\text{-C}_5\text{Me}_5$ groups, in a molecular structure similar to that of [26].

Thus, these structures may be compared directly with the structures of the corresponding homometallic analogues $[\text{Cp}^*\text{M}(\text{CO})_2]_2$ (M = Fe, Ru, Os). Although no crystallographic determinations appear to have been reported for these, the IR spectrum in each case displays a single $\nu(\text{CO})$ absorption at $1908\text{-}1922\text{ cm}^{-1}$ for terminal

carbonyls and a single $\nu(\text{CO})$ absorption at 1707-1745 cm^{-1} for bridging carbonyls. Such a simple spectrum is consistent with a symmetrical *trans* structure of C_{2h} symmetry, with both terminal and bridging CO groups.

5.4. Experimental Section

Reactions and manipulation of products were carried out by using standard Schlenk techniques in an atmosphere of dry nitrogen. The purification of solvents and spectroscopic measurements were performed as described in Chapter II. $\text{Cp}^*\text{Ir}(\text{CO})_2^{89}$, $\text{Cp}^*\text{Re}(\text{CO})_3^{51}$, $\text{Cp}^*\text{Mn}(\text{CO})_3^{90}$ and $\text{Cp}^*\text{Re}(\text{CO})_2(\text{N}_2)^{91}$ were synthesized as described elsewhere. Infrared spectra were run on either a Perkin-Elmer Model 983G spectrophotometer or a Bomem Michelson-120 FTIR instrument. Electron-impact mass spectral data (m/z) are reported based on the more abundant isotopes: ^{193}Ir , ^{187}Re .

The experimentally observed data for IR, ^1H NMR and ^{13}C NMR of the complexes [24]-[26] are listed in Tables 19 and 20.

(1) $\text{Cp}^*(\text{CO})\text{Mn}(\mu_2\text{-CO})_2\text{Ir}(\text{CO})\text{Cp}^*$ [24]

Method 1. A solution of $\text{Cp}^*\text{Mn}(\text{CO})_3$ (80 mg; 0.292 mmol) in freshly distilled THF (100 mL) was irradiated for ca 20 min. at 0°C

with a nitrogen purge, until the IR absorptions of the tricarbonyl complex ($\nu(\text{CO})$: 2003, 1916 cm^{-1}) were almost completely replaced by those of $\text{Cp}^*\text{Mn}(\text{CO})_2(\text{THF})$ ($\nu(\text{CO})$: 1906, 1833 cm^{-1}). Then $\text{Cp}^*\text{Ir}(\text{CO})_2$ (50 mg; 0.130 mmol) was added as a solid in the dark, and the solution stirred for 36h at room temperature with no further irradiation. The IR spectrum now showed the almost complete consumption of the THF complex, and the presence of new $\nu(\text{CO})$ absorptions at 1963, 1905 and 1759 cm^{-1} from the product. The THF was removed under vacuum, and the resulting orange-red solid was washed with hexane. It was then extracted into benzene to give an orange-red solution, from which the product was obtained as orange-red microcrystals by removal of the solvent in a vacuum: yield 60% (based on iridium); mp, decomposed above 140°C. Anal. Calcd for $\text{C}_{24}\text{H}_{30}\text{IrMnO}_4$: C, 45.78; H, 4.80. Found: C, 45.60; H, 4.78. MS(EI, 70ev): m/z 630 $[\text{M}]^+$, 574 $[\text{M}-2\text{CO}]^+$, 546 $[\text{M}-3\text{CO}]^+$, 516 $[\text{M}-4\text{CO}-2\text{H}]^+$.

Method 2. In a modification of the above method, a THF solution of $\text{Cp}^*\text{Mn}(\text{CO})_2(\text{THF})$, prepared as before, was treated with $\text{Cp}^*\text{Ir}(\text{CO})_2$ dissolved in cyclohexane (10 mL) and the mixture was heated to ca 70°C under N_2 for two hours in the dark (the flask was aluminum foil wrapped). The solvent was removed in a vacuum, the remaining red-brown solid was washed with hexane, then dissolved in benzene and passed through a short column of Celite. Removal of the

benzene in a vacuum gave the product in 80% yield (based on iridium).

(ii) $\text{Cp}^*(\text{CO})\text{Re}(\mu_2\text{-CO})_2\text{Ir}(\text{CO})\text{Cp}^*$ [25]

Method 1. A solution of $\text{Cp}^*\text{Re}(\text{CO})_3$ (80 mg, 0.197 mmol) in freshly distilled THF (50mL) was irradiated at 0°C in a quartz reactor for 1.5 h with a slow nitrogen purge until about 70% of the rhenium complex had converted to $\text{Cp}^*\text{Re}(\text{CO})_2(\text{THF})$ ($\nu(\text{CO})$: 1892, 1822 cm^{-1}) as judged by IR spectroscopy. To the light brown solution was then added $\text{Cp}^*\text{Ir}(\text{CO})_2$ (40 mg, 0.104 mmol) dissolved in cyclohexane (15 mL). The apparatus was wrapped in aluminum foil and the solution was heated at 60-65°C for 3.5 hours. The solvent was removed in a vacuum and the remaining dark solid was washed three times with large portions of hexane to remove residual $\text{Cp}^*\text{Re}(\text{CO})_3$ and $\text{Cp}^*\text{Ir}(\text{CO})_2$. The solid was then dissolved in benzene, and twice passed through a short column of Celite to give a bright yellow solution. Removal of the benzene in a vacuum gave the product as a yellow powder in 13% yield. A similar reaction, in which solid $\text{Cp}^*\text{Ir}(\text{CO})_2$ was added directly to the THF solution of the rhenium THF complex, and the solution stirred at room temperature for three days, gave a similar yield of the product after an analogous work-up. Anal. Calcd for $\text{C}_{24}\text{H}_{30}\text{IrO}_4\text{Re}$: C, 37.88; H, 3.97. Found: C, 37.69; H, 3.99. MS(EI, 70 eV): m/z 762 $[\text{M}]^+$, 734 $[\text{M-CO}]^+$, 706 $[\text{M-}$

2CO]⁺, 678 [M-3CO]⁺, 676 [M-3CO-2H]⁺, 674 [M-3CO-4H]⁺.

Method 2. An alternative synthesis was conducted by stirring Cp^{*}Re(CO)₂(N₂) (20 mg, 0.049 mmol) and Cp^{*}Ir(CO)₂ (20 mg, 0.052 mmol) in hexane (10 mL) at 60-65°C for one hour in the dark. A yellow-brown solid precipitated which was purified as above to give the golden-yellow product (21.7 mg, 58%).

(iii) Cp(CO)Re(μ₂-CO)₂Ir(CO)Cp^{*} [26]

A solution of CpRe(CO)₃ (100 mg, 0.298 mmol) in THF (70 mL) was irradiated in a quartz reactor at 0°C under a purge of N₂ for ca 60 min., when it was almost completely converted to CpRe(CO)₂(THF) (ν(CO): 1911, 1837 cm⁻¹) as determined by IR. To this solution was added Cp^{*}Ir(CO)₂ (40 mg, 0.104 mmol) and the mixture was stirred at room temperature in the dark for ten days. The solvent was removed in a vacuum and the resulting brown solid was redissolved in diethyl ether, then chromatographed on a 6 cm column of neutral alumina. Removal of the solvent in a vacuum gave the product as a yellow powder (yield: 21 mg, 29.2%). This procedure was preferred over washing with hexane, in which the product is significantly soluble. Anal. Calcd for C₁₉H₂₀IrO₄Re: C, 33.04; H, 2.92. Found: C, 33.08; H, 2.93. MS(EI, 70eV): m/z 693 [M]⁺, 665 [M-CO]⁺, 637 [M-2CO]⁺, 607 [M-3CO-2H]⁺, 605 [M-3CO-4H]⁺.

References

- [1] Streitwieser, A; Heathcock, C.H. *Introduction to Organic Chemistry*, MacMillan Publ. Co. Inc. New York, 1981, 2nd Ed., p.1194.
- [2] Bergman, R.G. *Science*, 1984, 902-908.
- [3] Hill; C.L. *Activation and Functionalization of Alkanes*, Wiley, 1989.
- [4] (a) Ryabov, A.D. *Chem.Rev.*, 1990, 90, 403-424.
(b) Shinomoto, R.S.; Desrosiers, P.J.; Harper, T.G.P.; Flood, T.C. *J.Am.Chem.Soc.*, 1990, 112, 704.
- [5] Crabtree, R.H. *Chem.Rev.*, 1985, 85, 245-269.
- [6] (a) Kemmitt, R.D.W. *J.Organomet.Chem.* 1981, 211, 279.
(b) Kemmitt, R.D.W.; Russell, D.R. *J.Organomet.Chem.* 1982, 230, 1.
(c) Mague, J.T. *J.Organomet.Chem.* 1983, 242, 241.
(d) Lichtenberger, D.L.; Calabro, D.C.; Kellogg, G.E. *Organometallics*, 1984, 3, 1623-1630.
(e) Saillard, J-Y.; Hoffmann, R. *J.Am.Chem.Soc.*, 1984, 106, 2006.
- [7] (a) Halpern, J. *Inorg.Chim.Acta*, 1985, 100, 41-48.
(b) Nolan, S.P.; Hoff, C.D.; Stoutland, P.O.; Newman, L.J.; Buchanan, J.M.; Bergman, R.G. *J.Am.Chem.Soc.*, 1987, 109, 3143-3145.
- [8] (a) Bergman, R.G.; Janowicz, A.H. *J.Am.Chem.Soc.*, 1983, 105,

4856.

- (b) Jones, W.D.; Feher, F.J. *J. Am. Chem. Soc.*, 1984, 106, 1650.
- [9] Klahn-Oliva, A.H.; Singer, R.D.; Sutton, D. *J. Am. Chem. Soc.*, 1986, 108, 3107.
- [10] Ozin, G.A.; McCaffrey, J.G.; McIntosh, D.F. *Pure & Appl. Chem.*, 1984, 56, 111-128.
- [11] Lichtenberger, D.L.; Blevins, C.H.; Ortega, R.B. *Organometallics*, 1984, 3, 1614-1622.
- [12] (a) Crabtree, R.H.; Holt, E.M.; Lavin, M.; Morehouse, S.M. *Inorg. Chem.* 1985, 24, 1986-1992.
- (b) Ziegler, T.; Tschinke, V.; Fan, L.; Becke, A.D. *J. Am. Chem. Soc.*, 1989, 111, 9177.
- [13] (a) Bergman, R.G.; Seidler, P.F.; Wenzel, T.T. *J. Am. Chem. Soc.*, 1985, 107, 4358.
- (b) Bergman, R.G.; Wenzel, T.T. *J. Am. Chem. Soc.*, 1986, 108, 4856-4867.
- [14] Chatt, J.; Davidson, J.M. *J. Chem. Soc.*, 1965, 843.
- [15] Parshall, G.W. *Acc. Chem. Res.*, 1970, 3, 139.
- [16] Parshall, G.W. *Acc. Chem. Res.*, 1975, 8, 113.
- [17] Webster, D.E. *Adv. Organomet. Chem.*, 1977, 15, 147.
- [18] Kliman, J.P.; Dubeck, M. *J. Am. Chem. Soc.*, 1963, 85, 1544.
- [19] Tolman, C.A.; Ittel, S.D.; Jesson, J.P. *J. Am. Chem. Soc.*, 1978, 100, 4081.
- [20] (a) Giannotti, C.; Green, M.L.H., *J. Chem. Soc., Chem. Commun.*, 1972, 1114.

- (b) Green, M.L.H. *J.Chem.Soc., Dalton Trans.*, 1979, 1157.
- [21] Crabtree, R.H.; Mihelcic, J.M.; Quirk, J.M. *J.Am.Chem.Soc.*, 1979, 101, 7738.
- [22] Janowicz, A.H.; Bergman, R.G. *J.Am.Chem.Soc.*, 1982, 104, 352.
- [23] Hoyano, K.; Graham, W.A. *J.Am.Chem.Soc.*, 1982, 104, 3722.
- [24] (a) Janowicz, A.H.; Bergman, R.G. *J.Am.Chem.Soc.* 1983, 105, 3927-3939.
- (b) Wax, M.J.; Stryker, J.M.; Buchanan, J.M.; Kovac, C.A.; Bergman, R.G. *J.Am.Chem.Soc.*, 1984, 106, 1121-1122.
- [25] (a) Periana, R.A.; Bergman, R.G. *Organometallics*, 1984, 3, 508.
- (b) Periana, R.A.; Bergman, R.G. *J.Am.Chem.Soc.*, 1984, 106, 7272.
- [26] (a) Stoutland P.O.; Bergman, R.G. *J.Am.Chem.Soc.* 1988, 110, 5732-5744.
- (b) Jones, W.D.; Feher, F.J. *Acc.Chem.Res.* 1989, 22, 91.
- (c) Jones, W.D.; Feher, F.J. *J.Am.Chem.Soc.* 1982, 104, 4240.
- [27] (a) Chang, C.K.; Juo, M.S. *J.Am.Chem.Soc.*, 1979, 101, 3413.
- (b) Hill, C.L.; Schardt, B.C. *J.Am.Chem.Soc.* 1980, 102, 6374,
- [28] (a) Sakakura, T.; Tanaka, M. *Chem.Lett.* 1987, 249-252.
- (b) Sakakura, T.; Tanaka, M. *J.Chem.Soc., Chem.Commun.*, 1987, 758 and references therein.
- (c) Sakakura, T.; Tanaka, M. *Chem.Lett.* 1988, 263.
- (d) Tanaka, M.; Sakakura, T. *Pure & Appl. Chem.*, 1990, Vol.62, No.6, 1147.
- [29] McGhee, W.D.; Bergman, R.G. *J.Am.Chem.Soc.*, 1988, 110,

4246.

- [30] Crabtree, R.H.; Mellea, M.F.; Mihelcic, J.M.; Quirk, J.M.
J. Am. Chem. Soc., 1982, 104, 107.
- [31] (a) Hoyano, J.K.; McMaster, A.D.; Graham, W.A.G. *J. Am. Chem. Soc.*, 1983, 105, 7190.
(b) Rest, A.J.; Whitwell, I.; Graham, W.A.G.; Hoyano, J.K.; McMaster, A.D. *J. Chem. Soc., Chem. Commun.*, 1984, 624.
- [32] Ephritikhine, M.; Green, M.L.H.; MacKenzie, R.E. *J. Chem. Soc., Chem. Commun.*, 1976, 619.
- [33] Green, M.L.H.; Wilkinson, G. *J. Chem. Soc.*, 1958, 4314.
- [34] (a) Einstein, F.W.B.; Jones, R.H.; Klahn-Oliva, A.H.; Sutton, D. *Organometallics*, 1986, 5, 2476-2480.
(b) Klahn-Oliva, A.H. *Ph.D Thesis*, Chem. Dept. S.F.U., 1986.
- [35] (a) Angelici, R.J.; Loewen, W. *Inorg. Chem.* 1967, 6, 682.
(b) Gifford, M.; Dixneuf, P. *J. Organomet. Chem.* 1975, 85, C26.
- [36] (a) King, R.B.; Treichel, P.M.; Stone, F.G.A. *J. Am. Chem. Soc.*, 1961, 83, 3593.
(b) Moseley, K.; Maitlis, P.M. *J. Chem. Soc. (A)*, 1970, 2884.
(c) Kreiter, C.G.; Wenz, M.; Bell, P. *J. Organomet. Chem.* 1990, 387, 175.
- [37] Hoyano, J.K.; Graham, W.A.G. *J. Chem. Soc., Chem. Commun.*, 1982, 27.
- [38] Furniss, B.S.; Hannaford, A.J.; Rogers, V.; Smith, P.W.G.
Vogel's Textbooks of Practical Organic Chemistry including Qualitative Organic Analysis, Longman Inc., New York, 1978,

p.1285.

- [39] Johnson, B.F.G.; Lewis, J.; Yarrow, D.J. *J.Chem.Soc., Dalton Trans.* 1972, 2084.
- [40] Arthurs, M.; Sloan, M.; Drew, M.G.B.; Nelson, S.M. *J.Chem. Soc., Dalton Trans.* 1975, 1794.
- [41] (a) Foxman, B.; Marten, D.; Rosan, A.; Raghu, S.; Rosenblum, M.; *J.Am.Chem.Soc.*, 1977, 99, 2160.
(b) Vrieze, K.; Volger, H.C.; Praat, A.P. *J.Organomet.Chem.* 1970, 21, 467.
- [42] Jackman, L.M.; Cotton, F.A. "Dynamic Nuclear Magnetic Resonance Spectroscopy"; Academic Press: New York, 1975, p.51.
- [43] Fleming, I.; Williams, D.H. "Spectroscopic Methods in Organic Chemistry"; McGraw-Hill Publ. Co., Inc. New York, 1966, p.131.
- [44] Hermann, W.A.; Serrano, R.; Rock, H. *Angew.Chem.Int.Ed.Engl.*, 1984, 23, 383.
- [45] (a) Cloke, F.G.N.; Day, J.P.; Greenway, A.M.; Seddon, K.P.; Shimran A.A.; Swain, A.C. *J.Organomet.Chem.* 1989, 372, 231.
(b) Asker, K.A.; Greenway, A.M.; Seddon, K.R.; Shimran, A.A. *J.Organomet.Chem.* 1988, 354, 257.
- [46] Mass spectra were obtained on a Hewlett-Packard Model 5985 instrument equipped with an electron impact (EI) source operating at 70 ev and ion source temperature at 200⁰C.
- [47] (a) Lyatifov, I.R.; Gulieva, G.I.; Mysov, E.I.; Babin, V.N.; Materikova, R.B. *J.Organomet.Chem.* 1986, 326, 83.
(b) Lyatifov, I.R.; Gulieva, G.I.; Mysov, E.I.; Babin, V.N.;

- Materikova, R.B. *J.Organomet.Chem.* 1986, 326, 89.
- [48] Beynon, J.H.; Saunders, R.A.; Williams, A.E. "*The Mass Spectra of Organic Molecules*"; Elsevier Publ. Co., New York, 1968, p.123.
- [49] Otsuka, S.; Tani, K.; Yamagata, T. *J.Chem.Soc., Dalton Trans.* 1973, 2491.
- [50] Patton, A.T.; Strouse, C.E.; Knobler, C.B.; Gladysz, J.A. *J. Am.Chem.Soc.*, 1983, 105, 5804.
- [51] Klahn-Oliva, A.H.; Sutton, D. *Organometallics*, 1989, 198.
- [52] (a) Crabtree, R.H. *The Organometallic Chemistry of the Transition Metals*; Wiley-Interscience: New York, 1988; pp 188-190.
- (b) Davies, S.G. *Organotransition Metal Chemistry: Applications to Organic Synthesis*; Pergamon Press: Oxford, 1982; Chapter 7.
- (c) Collman, J.P.; Hegedus, L.S.; Norton, J.R.; Finke, R.G. *Principles and Applications of Organotransition Metal Chemistry*; University Science Books; Mill Valley, CA, 1987; p 175.
- (d) Parshall, G.W. *Homogeneous Catalysis*; Wiley: New York, 1980; Chapter 3.
- [53] (a) Tulip, T.H.; Ibers, J.A. *J.Am.Chem.Soc.* 1979, 101, 4201.
- (b) Tulip, T.H.; Ibers, J.A. *J.Am.Chem.Soc.* 1978, 100, 3252.
- [54] (a) Sherman, E.O.; Olson, M. *J.Organomet.Chem.* 1979, 172, C13-C19.

- (b) Sherman, E.O.; Schreiner, P.R. *J.Chem.Soc., Chem.Commun.* 1978, 223.
- [55] McGhee, W.S.; Bergman, R.G. *J.Am.Chem.Soc.* 1985, 107, 3388.
- [56] Baudry, C.; Boydell, P.; Ephritikhine, M.; Felkin, H.; Guilhem, J.; Pascard, C.; Dau, E.T.H. *J.Chem.Soc., Chem. Commun.* 1985, 670.
- [57] Baudry, C.; Cormier, J.M.; Ephritikhine, M.; Felkin, H.; J. *Organomet.Chem.* 1984, 227, 99.
- [58] Thorn, D.L. *Organometallics* 1982, 1, 879.
- [59] Chaudret, B.N.; Cole-Hamilton, D.J.; Wilkinson, G. *J.Chem. Soc., Dalton Trans.* 1978, 1739.
- [60] Byrne, J.W.; Blaser, H.U.; Osborn, J.A. *J.Am.Chem.Soc.* 1975, 97, 3871.
- [61] Siedle, A.R.; Newmark, R.A.; Brown-Wensley, K.A.; Skarjune, R.P.; Haddad, L.C. *Organometallics* 1988, 7, 2078.
- [62] (a) Howarth, O.W.; McAteer, C.H.; Moore, P.; Morris, G.E. *J.Chem.Soc., Chem. Commun.* 1981, 506.
- (b) Bonnemann, H. *Angew.Chem., Int.Ed.Engl.* 1983, 22, 246.
- (c) Tanke, R.S.; Crabtree, R.H. *J.Inorg.Chem.*, 1989, 28, 3444.
- [63] Batchelor, R.J.; Einstein, F.W.B.; Jones, R.H.; Zhuang, J.M.; Sutton, D. *J.Am.Chem.Soc.* 1989, 111, 3468.
- [64] An unpublished synthesis of $\text{CpRe(H)(CO)(}\eta^3\text{-C}_3\text{H}_5\text{)}$ has also been done in Professor W.A.G. Graham's laboratory at the University of Alberta: Graham, W.A.G., private communication.
- [65] (a) Faller, J.W.; Incorvia, M.J. *J.Inorg.Chem.*, 1968, 7, 840.

- (b) Faller, J.W.; Chen, C.C.; Mattina, M.J.; Jakubowski, A. J. *Organomet. Chem.*, 1973, 52, 361.
- (c) Faller, J.W.; Johnson, B.V.; Dryja, T.P.; *J.Organomet. Chem.* 1974, 65, 395.
- (d) Faller, J.W.; Rosan, A.M. *J.Am.Chem.Soc.* 1976, 98, 3388.
- [66] (a) Vanarsdale, W.E.; Kochi, J.K. *J.Organomet.Chem.* 1986, 317, 215.
- (b) Faller, J.W.; Chao, K.H.; *Organometallics* 1984, 3, 927.
- (c) Carre, F.; Colomer, E.; Corriu, R.J.P.; Vioux, A. *Organometallics* 1984, 3, 970.
- (d) Faller, J.W.; Murray, H.H.; White, D.L.; Chao, K.; *Organometallics* 1983, 2, 400.
- (e) Faller, J.W.; Shvo, Y.; Chao, K.; Murray, H.H. *J. Organomet.Chem.* 1982, 226, 251.
- (f) Faller, J.W.; Chodosh, D.F.; Katahira, D. *J.Organomet. Chem.* 1980, 187, 227.
- (g) Greenhough, T.J.; Legzdins, P.; Martin, D.T.; Trotter, J. *Inorg.Chem.* 1979, 18, 3268.
- (h) Hsu, L.-Y.; Nordman, C.E.; Gibson, D. H.; Hsu, W.-L. *Organomet.Chem.* 1989, 8, 241.
- (i) Gibson, D.H.; Hsu, W.-L.; Steinmetz, A.L.; Johnson, B.V., *J.Organomet.Chem.*, 1981, 208, 89.
- (j) Fish, R.W.; Johnson, B.V.; Dryja, T.P. *J.Organomet.Chem.*, 1976, 105, 101.
- (k) Faller, J.W.; Lambert, C.; Mazziere, M.R. *J.Organomet.*

- Chem.*, 1990, 383, 161.
- [67] (a) Krivykh, V.V.; Gusev, O.V.; Petrovskii, P.V.; Rybinskaya, M.I. *J.Organomet.Chem.* 1989, 366, 129.
- (b) Clark, H.C.; H.-Smith, M.J.; Ruegger H. *Organometallics* 1988, 7, 2085.
- [68] Noggle, J.H.; Schirmer, R.E. *The Nuclear Overhauser Effect. Chemical Applications*; Academic Press Inc., New York, 1971.
- [69] Clarke, E.L. *J.Organomet.Chem.* 1974, 80, 155.
- [70] Numata, S.; Okawara, R.; Kurosawa, H. *J.Inorg.Chem.* 1977, 16, 1737.
- [71] Foust, A.S.; Hoyano, J.K.; Graham, W.A.G. *J.Organomet.Chem.* 1971, 32, C65-C66.
- [72] Heijden, H.; Orpen, A.G.; Pasman, P. *J.Chem.Soc., Chem. Commun.*, 1985, 1576.
- [73] Chang, B.H.; Grubbs, R.H.; Brubaker, JR. C.H. *J.Organomet.Chem.* 1979, 172, 81-89.
- [74] (a) Silverman, G.S.; Strickland, S.; Nicholas, K.M. *Organometallics*, 1986, 5, 2117.
- (b) Schilling, B.E.R.; Hoffmann, R.; Faller, J.W. *J.Am.Chem.Soc.*, 1979, 101, 592.
- (c) Ozawa, F. Son, T.; Osakada, K.; Yamamoto, A. *J.Chem.Soc., Chem.Commun.*, 1989, 1067.
- [75] (a) Curtis, M.D.; Eisenstein, O. *Organometallics* 1984, 3, 887.
- (b) Adams, R.D.; Chodosh, D.F.; Rosan, A.M. *J.Am.Chem.Soc.*, 1979, 101, 2570.

- [76] Rosan, A.M. *J.Chem.Soc., Chem.Commun.*, 1981, 311.
- [77] Rosan, A.M.; Romano, D.M. *Organometallics* 1990, 9, 1048.
- [78] Alt, H.G.; Engelhardt, H.E.; Wrackmeyer, B.; Rogers, R.D. *J. Organomet.Chem.*, 1989, 379, 289.
- [79] Saunders, J.K.; Bell, R.A. *Canad.J.Chem.*, 1970, 48, 512.
- [80] Brookhart, M.; Harris, D.L. *Inorg.Chem.*, 1974, 13, 1540.
- [81] King, R.B.; Efraty, A. *J.Am.Chem.Soc.*, 1986 93, 4950.
- [82] King, R.B.; Iqbal, M.Z.; King, A.D. Jr. *J.Organomet.Chem.*, 1979 171 53.
- [83] (a) Weber, L.; Bungardt, D., *J.Organomet.Chem.*, 1986 311, 269.
(b) Hoyano, J.K.; May, C.J.; Graham, W.A.G., *Inorg.Chem.* 1982, 21, 3095.
- [84] Forrow, N.J.; Knox, S.A.R. *J.Chem.Soc. Chem.Commun.* 1984, 679.
- [85] Geoffroy, G.L.; Roberts, D.A., In *Comprehensive Organometallic Chemistry*: Wilkinson, G.; Stone, F.G.A.; Abel, E.W.; Eds.; Pergamon Press: Oxford 1982, Vol. 6, p.763.
- [86] (a) Usón, R.; Forniés, J.; Espinet, P.; Fortuno, C.; Tomas, M.; Welch, A.J., *J.Chem.Soc., Dalton Trans*, 1988 3005.
(b) Dey, K.; Werner, H., *Chem.Ber.* 1979 112, 823.
(c) Werner, H.; Feser, R.; Büchuer, W. *Chem.Ber.* 1979, 112, 834.
(d) Nowell, I.W.; Russell, D.R., *J.Chem.Soc., Dalton Trans.* 1972, 2393.
(e) Dey, K.; Werner, H. *J.Organomet.Chem.* 1977, 137, C28.
(f) Connelly, N.G.; Lucy, A.R.; Payne, J.D.; Galas, A.M.R.;

Geiger, W.E. *J.Chem.Soc. Dalton Trans* 1982, 1309.

(g) Werner, H.; Juthani, B. *J.Organomet.Chem.* 1981, 209, 211.

(h) Barr, R.D.; Green, M.; Marsden, K.; Stone, F.G.A.;

Woodward, P., *J.Chem.Soc., Dalton Trans.* 1983, 507.

(i) Einstein, F.W.B.; Pomeroy, R.K.; Rushman, P., Willis, A.C., *Organometallics* 1985 4, 250.

(j) Del Paggio, A.M.; Muetterties, E.L.; Heinekey, D.M.; Day, V.W.; Day, C.S., *Organometallics* 1986, 5, 575.

(k) Green, M.; Mills, R.M.; Pain, G.N.; Stone, F.G.A.;

Woodward, P., *J.Chem. Soc., Dalton Trans.*, 1982, 1309.

(l) Davis, H.B.; Einstein, F.W.B.; Glavina, P.G.; Jones, T.;

Pomeroy, R.K.; Rushman, P., *Organometallics* 1989, 8, 1030, and references therein.

[87] Recent articles with extensive literature citations are:

(a) Zheng, P.Y.; Nadasdi, T.T.; Stephan, D.W. *Organometallics*, 1989, 8, 1393.

(b) Gelmini, L.; Stephan, D.W. *Organometallics*, 1988, 7, 849.

(c) Sartain, W.J.; Selegue, J.P. *Organometallics* 1989, 8, 2153

(d) Stephan, D.W. *Coord.Chem.Rev.* 1989, 95, 41.

[88] Aldridge, H.L.; Green, M.; Howard, J.A.K.; Pain, G.N.; Porter, S.; Stone, F.G.A.; Woodward, P. *J.Chem.Soc., Dalton Trans.*, 1982, 1333.

[89] Kang, J.W.; Moseley, K.; Maitlis, P.M. *J.Am.Chem.Soc.*, 1969, 91, 5970.

[90] Fernal, I.; Korp, J.D.; Herrmann, W.A.; Serrano, R., *Chem.Ber*

- 1984, 117, 434. The sample used in this work was kindly synthesized by Dr. R.D. Sharma of this department.
- [91] Einstein, F.W.B.; Klahn-Oliva, A.H.; Sutton, D.; Tyers, K.G. *Organometallics*, 1986, 5, 53.
- [92] Mann, B.E.; Taylor, B.F., ¹³C NMR Data for Organometallic Compounds; Academic Press: London, 1981; p.180.
- [93] Ref. 92, p.3.
- [94] Baker, R.T.; Calabrese, J.C.; Glassman, T.E., *Organometallics* 1988, 7, 1889.
- [95] The upper and lower limit corrected bond lengths are 2.855Å and 2.817Å; Johnson, C.K. *Crystallographic Computing*, F.R. Ahmed; Ed. Munksgaard 1970, 220.
- [96] Einstein, F.W.B.; Jones, R.H.; Zhang, X.; Yan, X.; Nagelkerke, R.; Sutton, D., *J.Chem.Soc. Chem. Commun.*, 1989, 1424.
- [97] (a) Cotton, F.A., *Prog.Inorg.Chem.* 1976, 21, 1.
(b) Crabtree, R.H.; Lavin, M., *Inorg.Chem.* 1986, 25, 805.
(c) Sargent, A.L.; Hall, M.B. *J.Am.Chem.Soc.* 1989, 111, 1563.